# I. DEVELOPMENT OF NOVEL SILICON PRECURSORS FOR RAPID AND EFFICIENT RADIOFLUORINATION REACTIONS: SYNTHESIS AND BIOLOGICAL EVALUATION OF A $^{18}$F-LABELLED ESTROGEN DENDRIMER CONJUGATE

# II. OTHER STUDIES ON $^{18}$F-LABELLED ESTROGENS

BY

VINCENT M. CARROLL

DISSERTATION

Submitted in partial fulfillment of the requirements
for the degree of Doctor of Philosophy in Chemistry
in the Graduate College of the
University of Illinois at Urbana-Champaign, 2012

Urbana, Illinois

Doctoral Committee:

Professor John A. Katzenellenbogen, Chair
Professor Paul J. Hergenrother
Professor Benita S. Katzenellenbogen
Professor Scott K. Silverman

## ABSTRACT

Molecular imaging (MI) has revolutionized the visualization of complex biochemical processes in normal physiology and diseased states. Although still in its infancy, the data generated from MI studies aids in identifying sites of pathological involvement and provides key insight into the mechanisms that lead to the onset and progression of disease. Consequently, these techniques hold tremendous potential in the areas of diagnostics, therapy assessment, and drug development in the coming years.

Amongst MI techniques, Positron Emission Tomography (PET) separates itself from the rest of the field with its exceptional sensitivity, near limitless depth of penetration and its ability to quantify metabolic processes in living patients. With the ability to visualize and quantify on an individualized basis, PET imaging has received considerable attention recently because of its potential for contributing to personalized medicine. Through better diagnosis, rational selection of targeted therapies, and individualization of therapy regimens for each patient, personalized medicine holds the promise of greatly improving patient outcomes as well as safeguarding against the use of unnecessary, harmful medical procedures.

Given the current status of the PET field and the impact it has on many fields, significant effort is being made to expand the existing repertoire of imaging agents capable of further detailing pathophysiological processes beyond the most commonly used PET tracer, [$^{18}$F]fluorodeoxyglucose, including the use of large, sensitive biomolecules such as peptides and antibodies, which may be of considerable clinical importance. However, the available methodology associated with PET isotope incorporation, specifically fluorine-18, involves rather harsh conditions that are incompatible with sensitive substrates, which restricts the availability of these agents and their subsequent clinical evaluation. Thus, there remains a tremendous need for rapid, mild and efficient methodology that can be used to label these previously inaccessible substrates in a direct, late-stage fashion.

Chapter 1 presents a brief introduction into molecular imaging and the techniques available for use in the preclinical and clinical setting as well as in drug development. Additionally, the basics of PET principles and radiochemistry are introduced, with a significant focus on the synthetic difficulties involved in working with the most commonly used PET isotope, fluorine-18, and why there is a need for improved methodology for its incorporation into new radiopharmaceutical agents, especially sensitive ones.

Chapter 2 details the development of methodology that targets the shortcomings of C-$^{18}$F strategies through Si-$^{18}$F bond formation approaches. We have developed a simple and straightforward strategy in radiofluorinating complex substrates at a late stage, at room temperature, or in an aqueous environment in high radiochemical yields and specific activities through a reactive silyl acetate moiety. The utility and versatility of the approach is showcased in three main areas of research: small adaptor molecules, small molecules, and peptides.

We have applied this Si-$^{18}$F labeling strategy (Chapter 3) to prepare a fluorine-18 labeled version of 17α-ethynylestradiol conjugated PAMAM dendrimer that can be used for *in vivo* distribution studies of this novel hormone-polymer conjugate. Through biodistribution studies, we have found that the EDC, a dendrimer-bound estrogen that provides selective cardiovascular protection without classical stimulation of uterus and mammary tissues, also shows selective, ER-mediated uptake and retention by the vascular target tissues, heart and aorta, but not the classical target, the uterus. These findings suggest that the selective cardiovascular protective effect of EDC is the result of two factors, one mechanistic (selective stimulation of the extra-nuclear pathway of ER action) and one pharmacokinetic (selective accumulation of EDC in vascular targets). This points to a new dimension for extending the selective, potentially beneficial actions of estrogens.

Chapter 4 details the synthetic approaches towards the radiosynthesis a promising ER imaging agent, 2-[$^{18}$F]fluoroestradiol, and illustrates the most well-known difficulty encountered in fluorine-18 chemistry, specifically the radiofluorination of electron-rich aromatic rings. Efforts have focused on the use of diaryliodonium salts which has afforded synthetically useful radiochemical yields of the desired compound and is currently being scaled up, in terms of radioactivity, for evaluation in animal studies.

**ACKNOWLEDGMENTS**

First and foremost, I am forever indebted to Dr. K for giving me the chance to work in his laboratory. It seems like only yesterday I was still trying to convince him to accept me as one of his last graduate students. When I first joined the lab, I was, and still am today, in awe of his brilliant scientific mind and how quickly he can grasp any chemistry or biology-related topic. He has been an amazing role model, showing me the proper way of approaching problems, analyzing data, and most of all, asking the right questions, and as our relationship grew, I thought of Dr. K not only as my boss, but as a good friend. I am truly appreciative of everything he has done for me as a chemist and as a person and I will always cherish our time together.

I have also been fortunate to work with Dr. Michael Welch of Washington University, who has recently passed on. It was always interesting working in St. Louis, especially since I was going from the calm, soft-spoken personality of Dr. K to a rather unique personality of Dr. Welch. It is an understatement that Dr. Welch liked to speak his mind and I could never stop laughing being in his presence because of it. I will always remember the one day I was complaining about the possibility of getting a high hand dose the one month and in his typical quick wit, responded in saying that he has been injected with over 20 radiopharmaceuticals and look how he turned out. But there was so much more to his humor, he was a great scientist, a great person and the world has lost a great man. He may be gone from us but his memories will live on forever.

Great things happen because of great people and I am truly grateful for the group of colleagues that I have had a chance to work with. First and foremost, I will never forget the times with my good friend, Dr. Sung Hoon Kim. He is a remarkably driven and smart chemist and his strong work ethic has always been something for me to model off of. He has been there through the good times and the bad times, but his support for me and our projects never strayed and anything that was needed, I always knew I could rely on him. I thank him for everything that he has done for me. Norio Yasui has been a great lab mate for many years now and has always been there to help out whenever I needed him. I am grateful for Dr. Dong Zhou at Wash U for teaching the ins and outs of being a radiochemist and the proper way of not contaminating myself with radioactivity. And although it's only been a short time, I appreciate Dr. Julie Pollock for being a good friend and trivia buddy. A great deal of thanks goes to other previous members that had an influence on my graduate career including Dr. Terry Moore, Dr. John Comninos, Dr. Davis Oldham, Dr. Chris Mayne, and Dr. Alex Parent. A special thanks also goes to Kathy

Carlson and Kathleen Myerscough for everything they have done for me and always having an open ear to talk to.

I appreciate the efforts of my thesis committee, Dr. Paul Hergenrother, Dr. Benita Katzenellenbogen, Dr. Scott Silverman, and formerly, Dr. Anne Baranger. I am thankful for all their advice and suggestions during the process.

Finally, I would not be here today if it wasn't for the constant and unyielding support of my family and friends. My parents have always been there for me and gave me everything I needed to succeed in the world and words can't describe how thankful I am to have them in my life. Mark and Jill Knafl have been the best friends I could ever ask for and I will miss them dearly when I move away. I owe my biggest debt of gratitude to my wife, Mary, who has supported me through all these years. She is the most sincere and compassionate person I have ever met and although I may not have always expressed it during my time here, I wouldn't have wanted anyone but her by my side.

## TABLE OF CONTENTS

## LIST OF ABBREVIATIONS

| | |
|---|---|
| cAMP | Cyclic Adenosine Monophosphate |
| Ci | Curies |
| CT | Computed Tomography |
| DFT | Density Functional Theory |
| EDC | Estrogen Dendrimer Conjugate |
| $E_2$ | 17β-estradiol |
| $EE_2$ | Ethynyl Estradiol |
| ER | Estrogen Receptor |
| ERE | Estrogen Response Element |
| ERK | Extracellular Signal-Regulated Kinase |
| [$^{18}$F]FBA | 4-[$^{18}$F]Fluorobenzaldehyde |
| [$^{18}$F]FDG | [$^{18}$F]Fluorodeoxyglucose |
| [$^{18}$F]FDOPA | [$^{18}$F]Fluoro-L-DOPA |
| [$^{18}$F]FES | 16α-[$^{18}$F]Fluoroestradiol |
| [$^{18}$F]FETos | 2-[$^{18}$F]Fluoroethyl-tosylate |
| [$^{18}$F]FPB | 4-[$^{18}$F]Fluorophenacyl Bromide |
| [$^{18}$F]FT | [$^{18}$F]Fluorotyrosine |
| GMP | Good Manufacturing Practice |
| HDL | High-Density Lipoprotein |
| HPLC | High Pressure Liquid Chromatography |
| $K_{222}$ | 4,7,13,16,21,24-Hexaoxa-1,10-diazabicyclo[8.8.8]hexacosane |
| LDL | Low-Density Lipoprotein |
| mCi | milliCuries |
| MPS | Mononuclear Phagocyte System |
| MRI | Magnetic Resonance Imaging |
| NHS | *N*-Hydroxysuccimide |
| NO | Nitric Oxide |
| NODA | 1,4,7-Triazacyclononane-1,4-diacetate |
| OFI | Optical Fluorescence Imaging |
| PAMAM | Poly(amido)amine |
| PBS | Phosphate Buffered Saline |
| PEG | Polyethylene Glycol |
| PET | Positron Emission Tomography |
| QC | Quality Control |
| Radio-TLC | Radioactive Thin Layer Chromatography |
| RBA | Relative Binding Affinity |
| RCP | Radiochemical Purity |
| RCY | Radiochemical Yield |
| RGD | Arginine-Glycine-Aspartate |
| SA | Specific Activity |

| | |
|---|---|
| SERM | Selective Estrogen Receptor Modulator |
| [$^{18}$F]SFB | *N*-Succinimidyl-4-[$^{18}$F]fluorobenzoate |
| SPECT | Single Photon Emission Computed Tomography |
| TBAF | Tetrabutylammonium Fluoride |
| TEG | Tetraethylene Glycol |
| TEMPO | 2,2,6,6-Tetramethyl-1-piperidinyloxy |
| TMR | Tetramethylrhodamine |
| US | Ultrasound |

CHAPTER 1

# INTRODUCTION

## I. MOLECULAR IMAGING BACKGROUND

### *A. Background*

Advances in minimally invasive imaging technologies have opened up endless opportunities for molecular diagnostic and therapeutic regimens.[1] Traditionally, the primary role of molecular imaging has been to assist medical diagnosis as a confirmation tool of diseased states through the *in vivo* visualization of the presence and extent of pathologies. More recently, the functional information of diseased states elucidated through imaging techniques has significantly transformed medical diagnosis from a mere identification tool towards the ability to characterize the molecular processes involved with disease progression.[2] Consequently, this will have a tremendous impact on patient care and treatment in the coming years, especially in the development of personalized medicine, in addition to becoming an indispensable research tool for drug development.[3,4]

### *B. Molecular Imaging and Personalized Medicine*

Molecular imaging enables the visualization, characterization, and measurement of *in vivo* biological processes in living systems through the use of specific imaging probes. It comprises a range of techniques (Table 1.1), but the premise is basically the same throughout: an optimally designed tissue- or receptor-specific compound provides an analytical signal (e.g., positrons, gamma rays) that is detected by a given detector, which after using complex computational algorithms, yields a two- or three-dimensional detailed image of the targeted structure or biological process under study.[5] The proper choice among the available imaging techniques ultimately depends on the particular biological process to be visualized and the data that is needed from the study.[6]

| Modality | Spatial Resolution | Sensitivity | Safety Profile | Used Clinically | Quantification |
|---|---|---|---|---|---|
| Computed Tomography (CT) | 0.5-1 mm | Not Determined | Ionizing Radiation | Yes | - |
| Magnetic Resonance Imaging (MRI) | 1 mm | $10^{-3}$-$10^{-5}$ M | No Ionizing Radiation | Yes | Fair |
| Positron Emission Tomography (PET) | 2`-7 mm | $10^{-11}$-$10^{-12}$ M | Ionizing Radiation | Yes | Very Good |
| Single Photon Emission Computed Tomography (SPECT) | 8-10 mm | $10^{-10}$-$10^{-11}$ M | Ionizing Radiation | Yes | Good |
| Ultrasound (US) | 1-2 mm | $10^{-12}$ M | Good Safety Profile | Yes | Poor |
| Optical Fluorescence Imaging (OFI) | 2-3 mm | $10^{-9}$-$10^{-12}$ M | Good Safety Profile | Emerging | Poor to Fair |

**Table 1.1** Comparison of the different molecular imaging techniques available.

Molecular imaging has played a key role in translational biomedical research and diagnostic clinical studies. Imaging the presence and functionality of a given diseased state provides tremendous insight into the mechanisms leading to disease onset and progression. Although similar information in certain cases can be obtained through tumor biopsies and subsequent histopathological evaluations, it is difficult and risky to obtain biopsies from some tumor sites, such as those present in the brain; so, less invasive approaches are needed. Additionally, tumor heterogeneity,[7,8] biopsy sampling errors,[9] and varying expression profiles between primary and metastatic sites[10,11] further complicate matters and thus may not yield a true representation of the diseased state. Advances in medical imaging, however, can provide detailed biochemical information at the earliest stages of disease onset, often before any observable symptoms are seen in the patient. Early detection before the disease has progressed can improve the prognosis and also can allow for the customization of appropriate therapeutic regimens to the individual patient. Such advances hold tremendous potential for accelerating appropriately designed targeted therapy through personalized medicine that not only can serve to reduce high medical care costs but more importantly, safeguards against the use of unnecessary, harmful medical procedures.

Our group has utilized a similar PET imaging strategy to understand the molecular characteristics of a breast tumor before starting treatment in order to establish the most appropriate therapy for patients with advanced $ER^+$ breast cancer. Specifically, the levels of estrogen receptor in a breast tumor have been shown to be important prognostic indicators for the progression of the disease, and the presence of the receptor is used to guide the treatment regimen. Tumor uptake using the most promising high affinity ER agent to date, 16α-[$^{18}$F]fluoroestradiol (Figure 1.1., [$^{18}$F]FES, **1**), as measured by PET imaging, aids in the confirmation of ER expression in the tumor (more accurately than from standard immunohistochemical studies) and thus serves as a strong predictor for the success of hormone therapy.[12,13] Although these studies can confirm the presence of ER in tumors, they do not establish that this ER is functional, and thus uncertainty remains as to whether hormone therapy will be beneficial. The functionality of the receptor can be assessed by an additional hormone challenge test that uses [$^{18}$F]FDG-PET (**2**) to monitor a metabolic flare in terms of enhanced uptake after a 1-day estradiol treatment in breast patients in which tumor ER is functional.[14] Taken together, both approaches aid in the selection of patients that will most likely benefit from ER-targeted therapies and such strategies have already been implemented within the clinic.[15-17] Thus, in this instance, confirmation of the presence and function of ER through FES- and FDG-PET imaging studies enables selected patients to undergo less toxic endocrine therapies instead of the more costly and morbid cytotoxic therapy. By individualizing treatment plans such as this one, the expectation is that patient outcomes will be greatly improved.

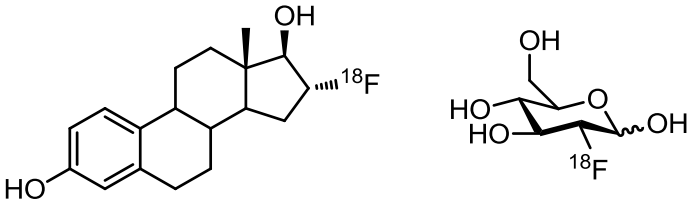


[$^{18}$F]FES, **1** [$^{18}$F]FDG, **2**

**Figure 1.1.** Structures of 16α-[$^{18}$F]fluoroestradiol (FES, **1**) and 2-[$^{18}$F]fluoro-2-deoxyglucose (FDG, **2**).

*C. Impact of Molecular Imaging on Drug Development*

Beyond clinical applications, molecular imaging has become an important component in the drug development process.[18,19] The cost of bringing a drug onto the market has been steadily rising and is expected to continue to rise in the coming years, with the average cost estimated around 1 billion dollars.[20,21] Therefore, the development of more cost-effective strategies aimed at accelerating the drug development process are highly desired. Molecular

imaging is now anticipated to play a key role in this process. After optimization of a radiotracer's *in vivo* behavior, it is possible to determine the occupancy of the drug candidate at the target site through kinetic modeling studies in addition to the duration of target engagement.[22,23] Such studies are aimed at investigating the relationship between receptor occupancy levels of the drug in order to establish dose selection and to observe any pharmacological effects at a given dose. This data not only enables a better understanding of the *in vivo* pharmacokinetics of the drug and the required drug levels needed to obtain pharmacological effects, but more importantly, it provides invaluable insight into potential toxicity or side effects associated with the drug. This in turn facilitates the opportunity for drug companies to halt lead drug candidates that fail to exhibit the desired *in vivo* behavior or may possess unanticipated toxicity that otherwise would have not been discovered until potentially the costly Phase 3 trials. This leads to an enormous cost savings aimed at circumventing the failure of drug candidates in late stages of clinical trials, while at the same time, allowing for the acceleration of those that appear promising.

## II. POSITRON EMISSION TOMOGRAPHY

### *A. Background*

Positron Emission Tomography (PET) is a powerful, minimally invasive imaging technique that is used to visualize and characterize human physiology. Unlike Magnetic Resonance Imaging (MRI) and Computed Tomography (CT), which provide detailed anatomical images associated with structural abnormalities related to pathologies, PET separates itself from the rest of the field with its exceptional sensitivity towards positron detection and its ability to measure metabolic processes in living patients. By monitoring the biodistribution and uptake of a positron emitting radiotracer in the body over a given time period, PET enables researchers to quantitate important physiological and biochemical information about the onset and progression of diseased states.[24]

### *B. PET Imaging of Disease*

PET has a tremendous impact as both a medical and research tool.[25] By far, the most commonly used PET tracer for medical imaging is [$^{18}$F]fluorodeoxyglucose ([$^{18}$F]FDG, **2**).[26] [$^{18}$F]FDG-PET exploits the upregulated glucose transport and glycolysis pathway of tumors, where, after undergoing an initial phosphorylation, the labeled agent becomes irreversibly entrapped in tumor tissues. The subsequent elevated accumulation leads to an imaging contrast between cancerous and normal tissues.[27] As a result, [$^{18}$F]FDG has been extensively used as a

biomarker in oncology, including the detection of breast, lung, and colorectal cancers.[28] In neurology, PET has proved useful for the imaging and characterization of early onset neurodegenerative disorders, such as Alzheimer's[29,30] and Parkinson's diseases.[31,32] The extensive use of PET in neuroimaging is most likely due to the inability of accessing brain tissue except through autopsies, and thus enables diagnosis in living patients. PET has also been extensively utilized in cardiology as a myocardial imaging tool to characterize coronary heart disease.[33]

Given the current status of PET and the impact and potential that it has on various fields of medicine, there is a significant effort among researchers to expand the existing repertoire of imaging agents capable of further detailing pathophysiological processes that may be of considerable clinical importance. Because of this, there is immense interest of the development of more specific imaging probes that can potentially provide additional biological information than what is currently already known for tracers such as FDG.

*C. Principles of PET*

PET imaging probes are radiolabeled with positron-emitting radionuclides which decay by the emission of a positively charged particle called the positron, the antimatter of an electron, which has identical mass but contains a positive charge. Schematically, the decay process for this nuclear transformation is shown below (Figure 1.2):

$$ {}_{a}X^{m} \rightarrow {}_{a-1}Y^{m} + \beta^{+} + \nu $$

a = Atomic Number
m = Mass Number
X = Parent Nuclide
Y = Daughter Nuclide
$\beta^{+}$ = Positron
$\nu$ = Neutrino

**Figure 1.2.** The decay process for positron-emitting radionuclides.

All positron emitters contain nuclei that are proton-rich and emit excess protons in an attempt to reach nuclear stability through two different processes: positron emission and electron capture. Positron emission tends to occur in lower atomic weight nuclei (e.g., $^{18}F$, $^{11}C$), while the predominant mode of decay in higher atomic weight nuclei (e.g., $^{123}I$) is electron capture.

As the radionuclide undergoes positron-emission decay, the emitted positron, being highly interactive, is not detected directly but traverses a short distance (typically 0.5-2.0 mm depending on radionuclide and positron energy) and, due to interactions with the surrounding

medium, decelerates to an energy minimum where it then interacts with an electron. The collision produces an annihilation event from which the two particles yield two gamma photons of 511 keV, which are emitted at approximately 180$^{o}$ to each other (Figure 1.3). It is the simultaneous detection of the two emitted gamma photons along a line of coincidence that enables statistical analysis to reconstruct the location of the annihilation event. The resulting image details the approximate accumulation of the PET radiotracer within a given tissue, and interpretation can facilitate patient diagnosis and possible therapeutic regimen.[34]

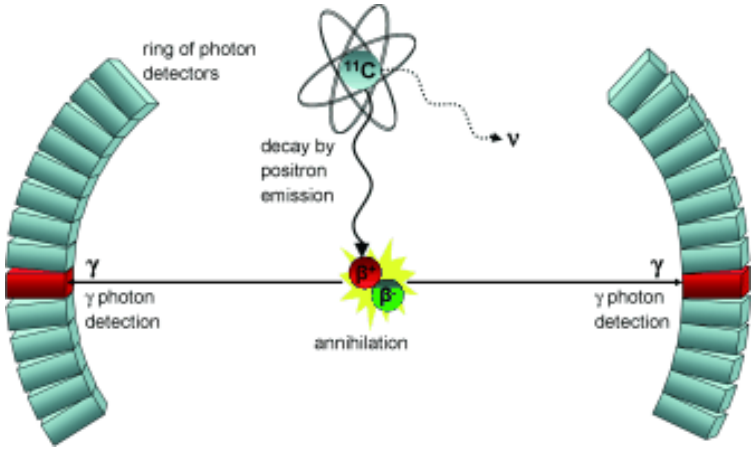


**Figure 1.3.** Schematic representation of a positron decay and the annihilation event that result in a PET image. The $^{11}C$ (blue dot) nucleus emits a positron (red ball) which interacts with an electron (green ball) to produce two gamma photons that are detected by the PET instrument (red blocks).[35]

## III. RADIOSYNTHESIS WITH SHORT-LIVED PET ISOTOPES

### *A. Available Positron Emitters and Synthetic Aspects*

One of the more attractive features of PET is its use of radionuclides (Table 1.2) that are isotopes of the main elements found in biomolecules (e.g., C, N, and O). This enables the radiosynthesis of labeled probes to be chemically indistinguishable from their nonradioactive counterparts and thus to function without altering the *in vivo* biological properties of the original compound. Fluorine is normally not found naturally in biomolecules, but the exchange of a hydrogen or an oxygen atom for a fluorine is one of the more commonly applied bioisoteric replacements, especially in drug development,[36] and at times, this substitution can exhibit improved *in vivo* behavior when compared to their non-fluorinated analogues.[37]

| Radionuclide | Half-Life (min) | Maximum Energy (MeV) | Mode of Decay | Decay Product |
|---|---|---|---|---|
| $^{11}C$ | 20 | 0.97 | $\beta^+$(99%) | $^{11}B$ |
| $^{13}N$ | 10 | 1.20 | $\beta^+$(100%) | $^{13}C$ |
| $^{15}O$ | 2 | 1.74 | $\beta^+$(100%) | $^{15}N$ |
| $^{18}F$ | 110 | 0.64 | $\beta^+$(97%)<br>EC (3%) | $^{18}O$ |

**Table 1.2.** Nuclear properties of commonly used positron-emitting radionuclides.

The incorporation of short-lived radioisotopes into tracers for PET imaging, however, is not a trivial task: the labeled probe must be synthesized, purified, characterized, and reformulated for human injection, all within two or three half-lives of the PET isotope in use. This demands rapid synthetic sequences, with the isotope being introduced as late as possible into the scheme. Typically, a large excess of precursor (often, $10^3$-$10^4$-fold higher than the concentration of the isotope) is used to effectively drive the reaction to completion within the short time frame. To further complicate matters, the presence of ionizing radiation emitted from the radionuclides poses serious health concerns, and because of this, radiosynthesis differs significantly from mainstream organic chemistry. First, all chemical transformations are performed in lead-lined fume hoods called hot cells. These cells are relatively bulky and difficult to work in because they obstruct optimal access to the reaction vessel and require specific handling procedures. Second, standard workup and purification practices in bench top chemistry are unsuitable to the radiochemist. The dangerous radiation necessitates maintaining adequate distances from the radionuclide to limit the absorbed dose; thus, one cannot touch anything inside the hot cell where the isotope is present. Lastly, the production of radioisotopes typically yields only picomolar to nanomolar amounts of activity. Radiochemists often refer to this chemistry as working on tracer levels due to the miniscule amounts of the isotope present. One would imagine that the vast stoichiometric excess of starting material used would only serve to benefit the radiosynthesis. Unfortunately, working at tracer levels can differ significantly from cold chemistry and often involves considerable manipulation of reaction conditions to obtain any successful incorporation.

*B. Radiochemical Yields*

Radiochemical yields (RCYs) can be reported two ways: decay-corrected and non-decay corrected yields. Decay corrected yields, which are calculated back from the end of bombardment of the target, are indicative of the success of the radiochemical reaction and are most often cited in the development of new methodology. Non-decay corrected yields are much

more useful and informative in the preparative potential of a synthetic scheme, and they aid in determining the amount of activity of a radiotracer after purification.

*C. Specific Activity*

A key component associated with PET imaging is the calculated specific activity of the radiotracer. The term specific activity (SA) denotes the amount of radioactivity per mass of compound (both labeled and unlabeled) and is typically expressed in Ci/mmol or GBq/μmol. Radiochemists strive for high SA radiotracers, which contain mainly the desired isotope with minimal non-radioactive nuclide contamination in the desired material. This is critical, especially with receptor-based PET imaging, because of the low physiological concentrations of receptors present within the body and thus, the limited availability of binding sites that can be occupied by the radioligand. Low specific activity material, which contains significant amounts of unlabeled mass as compared to the radiotracer itself, can lead to saturation of these binding sites at low activity levels, resulting in a reduction of signal-to-noise ratios and essentially no image contrast. Moreover, the additional injected mass may be at high enough concentrations to cause pharmacological or toxic side effects. Typically, SA values over 1000 Ci/mmol are deemed suitable for PET imaging studies.

Specific activities can also be defined as effective specific activities. This is the specific activity of a radiotracer that has been determined by a biological assay. Additional mass may be present in the final radiotracer preparation which contains similar biological properties to that of the desired radiopharmaceutical and is taken into account for this calculation.

Several factors contribute to the SA values of labeled compounds. First, these values are directly dependent on the radionuclide's half-life, with the shorter the half-life having higher theoretical specific activities. Second, the ubiquitous presence of nonradioactive nuclides present in glassware, solvents etc., which can also be incorporated into the radiotracer, can significantly reduce activity levels. Lastly, the vast excess of starting materials needed to drive the reaction to completion can complicate purification efforts, and difficulties in fully separating the radiolabelled product from abundant quantities of the unlabeled precursor or other reaction products can also have a detrimental effects, especially if they are able to compete with the labeled radiotracer for the target site of imaging.

## IV. CHEMISTRY OF [$^{18}$F]FLUORIDE ION

*A. Background*

Of all the available positron nuclides employed in PET, fluorine-18 is often considered the isotope of choice for PET imaging because of its ideal nuclear properties. Its sufficiently long half-life (110 min) allows for complex, multi-step syntheses, extended *in vivo* imaging studies, and from a practical point of view, commercial distribution to satellite clinical PET centers that lack F-18 production facilities. Furthermore, the clean decay properties (97% $\beta^+$) and relatively low positron energy results in PET images of the highest quality. Moreover, the low abundance of fluorine-19 in the environment enables the synthesis of F-18 labeled compounds in high specific activity, a perquisite for receptor-based imaging.

However, despite these positive and laudable properties of F-18, the radiochemistry associated with its introduction is far from ideal, especially in the context of direct labeling of sensitive biomolecules such as peptides and proteins. The variety of synthetic methods by which F-18 can be introduced is rather limited and can be divided into two distinct areas: an electrophilic method utilizing [$^{18}$F]$F_2$ directly or less reactive electrophilic reagents derived from the gas itself, and a nucleophilic [$^{18}$F]fluoride anion derived from an aqueous target.

*B. Electrophilic [$^{18}$F]Fluorinations*

Although a majority of F-18 radiochemistry in PET relies on nucleophilic [$^{18}$F]fluoride anion, electrophilic fluorinating agents have played a key role in the development of clinically relevant $^{18}$F-radiopharmaceuticals. For instance, [$^{18}$F]$F_2$ gas was used in the initial synthesis of [$^{18}$F]fluorodeoxyglucose ([$^{18}$F]FDG, **2**, Scheme 1.1) because its regioselective addition to one face of the double bond afforded the required configuration in the $^{18}$F-labelled sugar product.[38] Due to its high reactivity, [$^{18}$F]$F_2$ is typically converted to less reactive and more selective reagents, such as acetyl hypofluorite ($CH_3CO_2$[$^{18}$F]F),[39] xenon difluoride (Xe[$^{18}$F]$F_2$)[40] and fluorosulfonamides (R-$SO_2$-NR[$^{18}$F]F),[41] which are commonly utilized in direct electrophilic substitutions with electron-rich substrates (e.g., alkenes, aryl groups).

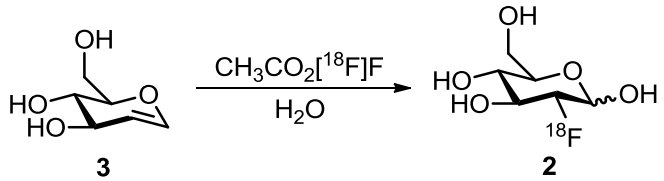


**3** **2**

**Scheme 1.1.** Radiosynthesis of **2** with electrophilic [$^{18}$F]fluoride ion.[38]

The most obvious shortcoming of the electrophilic method is the low specific activities of the [$^{18}$F]fluorinated products. The issue stems from how [$^{18}$F]$F_2$ gas is produced. Two of the more common strategies involve the nuclear reactions, $^{20}$Ne(d,α)$^{18}$F or $^{18}$O(p,n)$^{18}$F, and in order to prevent the [$^{18}$F]fluoride ion from being fully adsorbed on the target walls, $^{19}$F gas (0.1-2%) is added, diluting the original high specific activity [$^{18}$F]fluoride anion with now carrier added $^{19}$F to afford the $^{18}$F-$^{19}$F gas. Thus, in reactions involving the $^{18}$F-$^{19}$F gas, the maximum radiochemical yield (RCY) is 50% since only one [$^{18}$F]fluoride can be incorporated into the desired product, but in practice, specific activities are very low because of the large excess of [$^{19}$F]$F_2$ gas needed in production of the [$^{18}$F]$F_2$ gas. Even with the monofluorinated agents, such as acetyl hypofluorite ($CH_3CO_2$[$^{18}$F]F) where the theoretical RCY can be 100%, these agents are also prepared from the $^{18}$F-$^{19}$F gas; so, the maximum RCY is still at most 50% in these instances. Specific activity values from all of these electrophilic fluorination methods are typically less than 10 Ci/mmol, thereby rendering the corresponding [$^{18}$F]fluoroproducts unsuitable for PET studies involving saturable receptors.

Despite these shortcomings, the electrophilic method still possesses tremendous clinical value in those applications that do not require high specific activity. Currently, it remains the preferred method, due to the synthetic ease over multi-step nucleophilic syntheses, for the routine syntheses of common radiopharmaceuticals for patient use, including [$^{18}$F]fluoro-L-dopa[42] ([$^{18}$F]FDOPA, **5**, Scheme 1.2) and [$^{18}$F]fluorotyrosine ([$^{18}$F]FT).

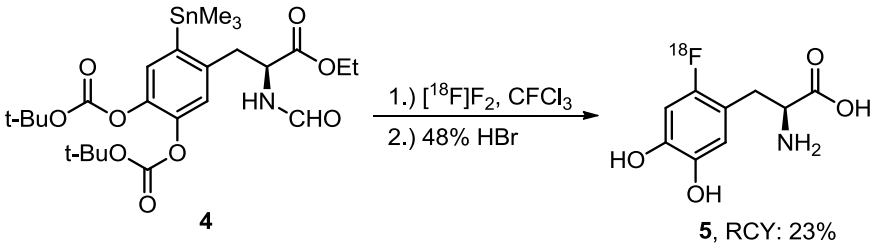


**Scheme 1.2.** Radiosynthesis of [$^{18}$F]FDOPA (**5**) from organotin precursor (**4**) by direct fluorination with [$^{18}$F]$F_2$.[42]

Recently, two influential studies have been reported to address the specific activity issues of [$^{18}$F]$F_2$ gas, and both hold promise for the use of electrophilic F-18 as a viable synthetic alternative. In the context of improving the specific activity of [$^{18}$F]$F_2$ gas, significant improvements have been achieved through the use of [$^{18}$F]fluoromethane, prepared from no-carrier-added [$^{18}$F]fluoride anion and $H_2$[$^{18}$O]O as the target, where, after electrical discharge in

the presence of miniscule amounts of $^{19}F_2$ gas, affords [$^{18}$F]$F_2$ gas in high specific activity (1500 Ci/mmol).[43] In comparison, the previously highest reported SA was 55 Ci/mmol.[44]

Ritter and coworkers reported[45] the first electrophilic [$^{18}$F]fluorination reagent (Scheme 1.3), an *in situ* generated [$^{18}$F]fluoropalladium (IV) species (**7**), prepared from no-carrier-added, high specific activity [$^{18}$F]fluoride anion. The chemistry works exceptionally well in late-stage [$^{18}$F]fluorination of complex substrates, including efficient reactions with electron-rich aromatic rings (**9**), in satisfactory RCYs. The generation of such electrophilic species from the widely available [$^{18}$F]fluoride anion, as opposed to the less accessible [$^{18}$F]$F_2$ gas, affords synthetically useful electrophilic $^{18}$F equivalents in a facile and concise manner with sufficiently high reactivity under mild conditions of late-stage, complex substrates. Consequently, access to conventionally unavailable radiotracers through this method will greatly expand potential PET applications.

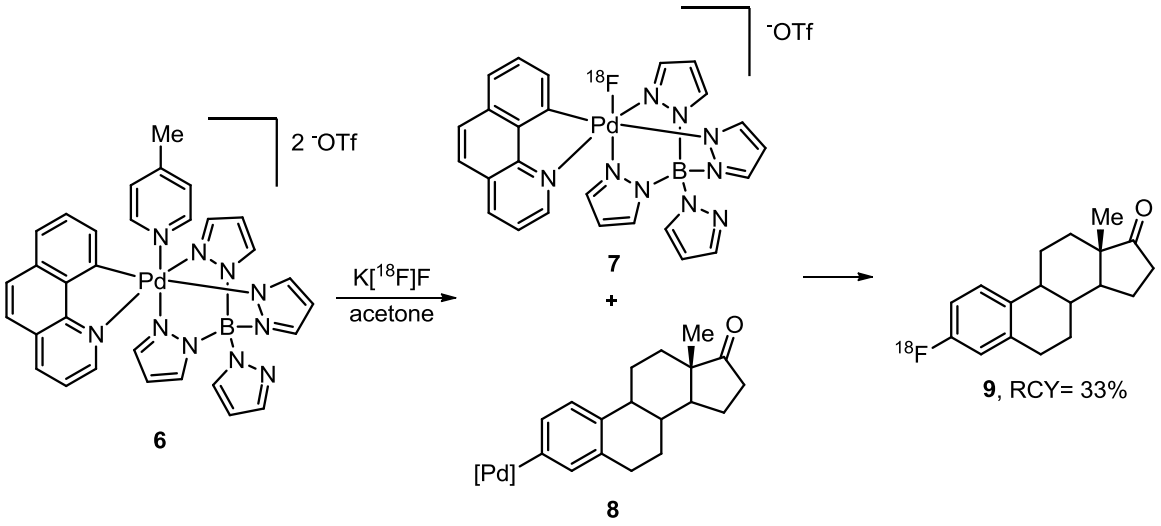


**Scheme 1.3.** Late-stage [$^{18}$]fluorination of complex substrates with electrophilic [$^{18}$F]fluoride (**7**).[45]

*C. Nucleophilic Chemistry*

The nucleophilic method is the method of choice for the radiosynthesis of $^{18}$F-labelled tracers in high specific activity. [$^{18}$F]Fluoride anion may be produced by several methods,[46] but by far, the most common is through proton irradiation of $^{18}$O-enriched water.[47] An enrichment of >95% $H_2$[$^{18}$O]O (occurs naturally in ~0.2%) is required because $^{16}$O can also undergo a nuclear reaction within the target to produce nitrogen-13 ($t_{1/2}$ = 9.96 min), although the byproduct has essentially no effect on the chemistry itself. Overall, this nuclear reaction, $^{18}$O(p,n)$^{18}$F, is intrinsically high yielding from small, compact cyclotrons, with several Curies (Ci) of activity being routinely produced in about an hour. Moreover, the method of production involves no

carrier addition, enabling the production of [$^{18}$F]fluoride ion at high specific activities. This factor alone explains its clear preference over electrophilic methods as it enables production of PET probes that can be used for receptor-based imaging studies. Also, the resulting [$^{18}$F]fluoride ion is obtained as an aqueous solution, affording a product that is considerably easier to handle and work with as compared to [$^{18}$F]$F_2$ gas.

However, the aqueous [$^{18}$F]fluoride obtained is a poor nucleophile because of its tightly bound hydration sphere, and thus one must undertake a tedious, time-consuming drying step in order to produce a sufficiently anhydrous [$^{18}$F]fluoride ion for nucleophilic substitution reactions to proceed. Key to this step is the addition of an appropriate base to afford a reactive, organic soluble fluoride source. Traditionally, slightly soluble inorganic fluoride sources such as K[$^{18}$F]F were utilized, but the slow and inefficient reactions were hampered by the low solubility of the potassium salts. More recently, activation of the [$^{18}$F]fluoride ion through the use of cryptands[48] has significantly enhanced fluoride solubility and in turn, has greatly improved radiochemical yields. By far, the most popular method employs the aminopolyether, 4,7,13,16,21,24-hexaoxa-1,10-diazabicyclo[8.8.8]hexacosane (Figure 1.4, $K_{222}$, **10**), that can effectively complex the potassium counter ion in K[$^{18}$F]F to produce a highly nucleophilic, organic soluble "naked" fluoride anion. Other alkali metals (i.e., Cs, Rb) or quaternary ammonium fluoride salts, obtained from their respective carbonates, bicarbonates, or hydroxides, have also been utilized with varying success. Overall, the choice of cation often plays a critical role in the success of radiofluorination reactions, but definitive guidelines for correctly choosing any of the available options do not exist and more often, one must screen the reaction to find the optimal base.

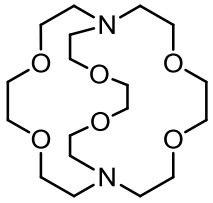


**10**

**Figure 1.4.** Structure of 4,7,13,16,21,24-hexaoxa-1,10-diazabicyclo[8.8.8]hexacosane ($K_{222}$).

In a typical drying step (Scheme 1.4), the water is removed by repeated azeotropic distillation in the presence of acetonitrile, base (e.g., $K_2CO_3$) and phase-transfer catalyst under a stream of nitrogen and thermal drying at temperatures between 80-110 $^{o}$C (left side). More recently, the use of anion-exchange cartridge chemistry[49] (right side) has become more popular, due to the cost effectiveness in recycling the [$^{18}$O]$H_2O$ for future F-18 production. Technically

speaking, the drying step is not vigorous enough to remove all waters of hydration, and as a result, a truly anhydrous [$^{18}$F]fluoride ion source (**12**) has never been achieved. Consequently, this can directly affect the reactivity of the [$^{18}$F]fluoride anion, and RCYs can suffer dramatically. Also, the addition of base, required to prevent the release of [$^{18}$F]HF during the drying, can further complicate matters with base-sensitive precursors. Nevertheless, this is the standard protocol for the vast majority of $^{18}$F-labelling methods, and at this point, the dried [$^{18}$F]fluoride source is ready for use (**12**).

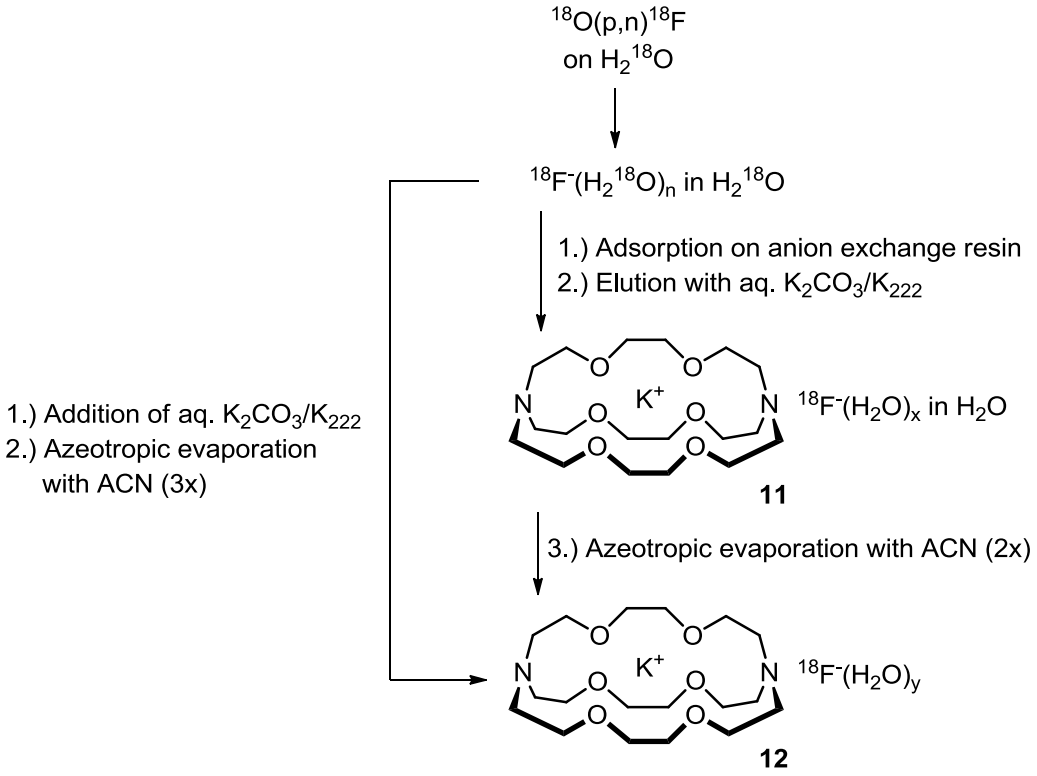


**Scheme 1.4.** Schematic of drying step from time of bombardment to a dried [$^{18}$F]fluoride source (**12**); x = fully hydrated [$^{18}$F]fluoride ion; y = amount of hydration (less than x).

The vast majority of $^{18}$F-labelling strategies involve two methods: nucleophilic substitution on aliphatic and on electron-deficient aromatic systems. In the aliphatic series, substitution is typically performed on halogenated derivatives or sulfonates (i.e., tosylates, mesylates, triflates, or nosylates), with the radiosynthesis of [$^{18}$F]FDG being the most well-known example (Scheme 1.5).[50] The main drawback of this method is the competing elimination reaction to afford the undesired alkene. However, recent studies have found the addition of *tert*-butanol can significantly suppress the elimination pathway and greatly improve radiochemical yields.[51,52]

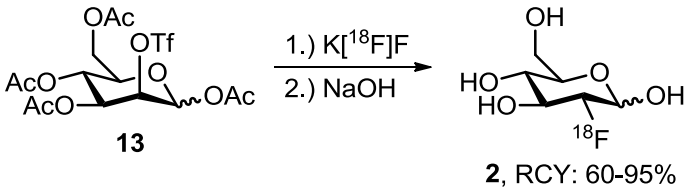


**13** **2**, RCY: 60-95%

**Scheme 1.5.** Radiosynthesis of [$^{18}$F]FDG (**2**) with [$^{18}$F]fluoride anion.[50]

Direct nucleophilic aromatic substitution reactions provide an expedient entry into complex systems in a one-step process. However, the reaction is only feasible if the aryl system is sufficiently electron deficient. Strong electron-withdrawing substituents such as -CN, -CHO, -COR, and -$CF_3$ in the ortho and para positions have been commonly utilized, and the leaving groups are typically nitro and trimethylammonium groups. Other heteroaromatic systems such as the electron-poor pyridine series (**14**), however, do not require activation, and as a result, the simplicity of the method has led to its popularity, especially for the preparation of neurological imaging tracers (Scheme 1.6).[53]

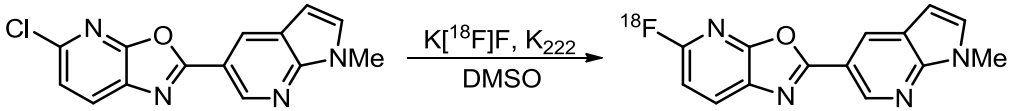


**14** **15**, RCY: 14%

**Scheme 1.6.** Nucleophilic aromatic substitution using an electron-poor pyridine substrate (**14**).[53]

As highlighted previously, nucleophilic aromatic substitutions proceed smoothly on electron-deficient arenes. Unfortunately, similar high-yielding strategies for electron-rich systems are lacking. Thus, the efficient radiofluorination of electron-rich species represents a significant methodological gap within PET chemistry. To date, the use of diaryliodonium salts represents the lone method that can be used for radiofluorination of electron-rich aryl rings in sufficiently high RCYs and specific activities. First reported by Pike,[54] the use of these salts has enabled reliable $^{18}$F-labelling of both unactivated or electron-rich [$^{18}$F]fluoroaromatic compounds, although most have been relatively simple substrates.[55,56] An interesting feature of these compounds is the regioselectivity of the reaction, where fluorinations tend to favor ortho-substituted phenyl groups (aka the “ortho effect”) (Scheme 1.7, left side, **16**).[55] In the absence of an ortho substituent, fluorination favors the least electron-rich ring. Consequently, the use of unsymmetrical diaryliodonium salts where one aryl group is an electron-rich *p*-methoxyphenyl or 2-thiophene group results in selective fluorination to the other, less electronically rich arene (Scheme 1.7, right side, **18**).[57,58]

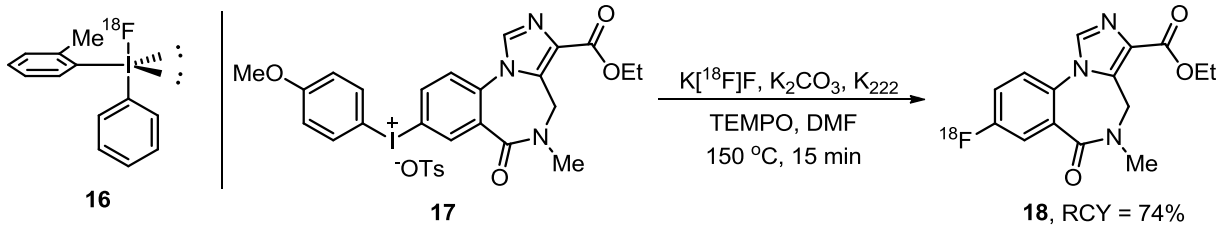


**Scheme 1.7.** Left Side: Transition state in the radiofluorination of diaryliodonium salts that favors [$^{18}$F]fluoride incorporation on the aryl ring bearing an ortho substituent; Right side: Use of unsymmetrical diaryliodonium salts where [$^{18}$F]fluorination prefers the less electronically rich ring.[58]

The short half-lives of positron-emitting nuclides requires concise radiosynthetic sequences involving as few steps as possible to isolate high activity levels of the purified radiotracer. In addition to the large excess of unlabeled precursor as mentioned previously, reaction temperatures typically vary from 120-150 $^{o}$C and can exceed 190 $^{o}$C in order to rapidly drive the reaction to completion. Consequently, direct [$^{18}$F]fluorination strategies are not universally suitable for all $^{18}$F-applications, especially with those containing sensitive organic functionality, because of these harsh reaction conditions (i.e., high temperatures, highly basic media). More often, milder, indirect methods have been employed with $^{18}$F-labelled small organic compounds, commonly referred to as prosthetic groups. Standard protocols generally involve first direct incorporation of the [$^{18}$F]fluoride anion into a more structurally robust prosthetic group, which is then appended to the biomolecule of interest through alkylation, acylation, amination, photochemical or click reactions. A variety of [$^{18}$F]fluorinated precursors are now well established (Figure 1.5) and includes 2-[$^{18}$F]fluoroethyl-tosylate ([$^{18}$F]FETos, (**19**)),[59] *N*-succinimidyl-4-[$^{18}$F]fluorobenzoate ([$^{18}$F]SFB (**20**)),[60] 4-[$^{18}$F]fluorobenzaldehyde ([$^{18}$F]FBA (**21**)),[61] and 4-[$^{18}$F]fluorophenacyl bromide ([$^{18}$F]FPB, (**22**)).[62] The main shortcomings of prosthetic groups are the relatively complex, multistep synthetic sequences needed for their radiosyntheses, and quite often, the radiolabel is incorporated within the first step, which can be methodologically awkward. Ideally, short-lived isotopes should always be incorporated as late as possible in the sequence.

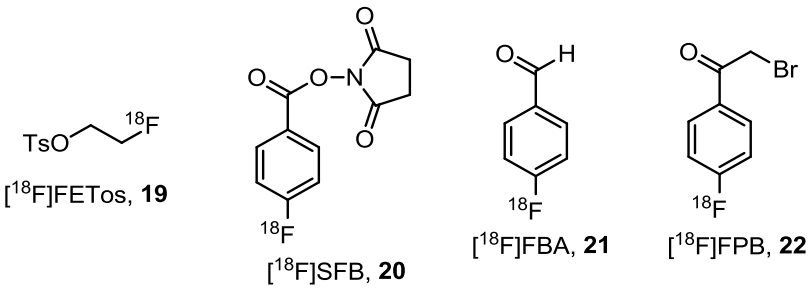


**Figure 1.5.** Structures of $^{18}$F-labelled prosthetic groups used for coupling to biomolecules.

## V. CONCLUDING INTRODUCTORY REMARKS

Although the development of PET radiopharmaceuticals has been ongoing for decades, many of these agents reside in the preclinical stage, with only a handful of them actually being used in the clinic. Of these, almost 90% of all PET scans conducted worldwide involve a single radiotracer, [$^{18}$F]FDG.[63] Despite its popularity, the use of [$^{18}$F]FDG is not without its flaws: it has nonselective uptake in noncancerous conditions (i.e., infection, inflammation),[64] low uptake in certain cancers (i.e., bronchoalveolar cancer),[65,66] and low contrast ratios in several areas of imaging including the brain. Consequently, this can often lead to difficulty in correctly assessing (or staging) a particular diseased state. By improving the specificity and sensitivity beyond what [$^{18}$F]FDG affords, beneficial outcomes will be two-fold: the improved characterization of the diseased state will significantly increase the overall diagnostic accuracy while also giving rise to the possibility of tailoring therapeutic regimens to the individual.

Of the three components that comprise the translational PET imaging process, target discovery and software/hardware development significantly outpace the advancement of novel imaging probes. The key to advancing translational PET is overcoming the barrier that has impeded the field: the lack of synthetic approaches for late-stage radiofluorination of complex substrates in a mild and efficient manner. Mainstream organic chemistry is inundated with chemical building blocks and synthetic methods that have enabled almost any imaginable molecule to be constructed, yet radiochemists are restricted to a single, low-reactivity nucleophilic [$^{18}$F]fluoride salt. Moreover, the harsh conditions (i.e., high temperatures, basic conditions) associated with existing C-$^{18}$F approaches are incompatible with sensitive substrates, including large biomolecules. This then necessitates time-consuming, multi-step strategies, which further limit the practicality of the approach, especially when working with short-lived isotopes. To satisfy the growing demand for novel PET tracers (including peptides and proteins), there is a tremendous need for rapid and efficient methodology in an ideal one-

step, aqueous approach that is amenable to virtually any potential substrate in a late-stage context. Al-$^{18}$F, B-$^{18}$F, and Si-$^{18}$F bonds are intriguing possibilities in this area.

## VI. REFERENCES


(1) Cassidy, P. J.; Radda, G. K. Molecular imaging perspectives. *J. R. Soc. Interface* **2005**, *2*, 133.

(2) Massoud, T. F.; Gambhir, S. S. Molecular imaging in living subjects: seeing fundamental biological processes in a new light. *Genes Dev.* **2003**, *17*, 545.

(3) Willmann, J. K.; van, B. N.; Dinkelborg, L. M.; Gambhir, S. S. Molecular imaging in drug development. *Nat. Rev. Drug Discovery* **2008**, *7*, 591.

(4) de, V. E. G. E.; Oude, M. T. H.; van, V. M. A. T. M.; Nagengast, W. B. Toward molecular imaging-driven drug development in oncology. *Cancer Discov.* **2011**, *1*, 25.

(5) Marik, J.; Bohorquez, S. M. S.; Williams, S.-P.; van, B. N. New imaging paradigms in drug development: the PET imaging approach. *Drug Discovery Today: Technol.* **2011**, *8*, e63.

(6) James, M. L.; Gambhir, S. S. A molecular imaging primer: modalities, imaging agents, and applications. *Physiol. Rev.* **2012**, *92*, 897.

(7) Polyak, K. Heterogeneity in breast cancer. *J. Clin. Invest.* **2011**, *121*, 3786.

(8) Li, J.; Wang, K.; Jensen, T. D.; Li, S.; Bolund, L.; Wiuf, C. Tumor heterogeneity in neoplasms of breast, colon, and skin. *BMC Res. Notes* **2010**, *3*, 321.

(9) Regev, A.; Berho, M.; Jeffers, L. J.; Milikowski, C.; Molina, E. G.; Pyrsopoulos, N. T.; Feng, Z.-Z.; Reddy, K. R.; Schiff, E. R. Sampling error and intraobserver variation in liver biopsy in patients with chronic HCV infection. *Am. J. Gastroenterol.* **2002**, *97*, 2614.

(10) Chandran, U. R.; Ma, C.; Dhir, R.; Bisceglia, M.; Lyons-Weiler, M.; Liang, W.; Michalopoulos, G.; Becich, M.; Monzon, F. A. Gene expression profiles of prostate cancer reveal involvement of multiple molecular pathways in the metastatic process. *BMC Cancer* **2007**, *7*, 25.

(11) Weigelt, B.; Peterse, J. L.; van't, V. L. J. Breast cancer metastasis: markers and models. *Nat. Rev. Cancer* **2005**, *5*, 591.

(12) McGuire, A. H.; Dehdashti, F.; Siegel, B. A.; Lyss, A. P.; Brodack, J. W.; Mathias, C. J.; Mintun, M. A.; Katzenellenbogen, J. A.; Welch, M. J. Positron tomographic assessment of 16 alpha-[$^{18}$F]fluoro-17-beta-estradiol uptake in metastatic breast carcinoma. *J. Nucl. Med.* **1991**, *32*, 1526.

(13) Dehdashti, F.; Mortimer, J. E.; Siegel, B. A.; Griffeth, L. K.; Bonasera, T. J.; Fusselman, M. J.; Detert, D. D.; Cutler, P. D.; Katzenellenbogen, J. A.; Welch, M. J. Positron tomographic assessment of estrogen receptors in breast cancer: comparison with FDG-PET and in vitro receptor assays. *J. Nucl. Med.* **1995**, *36*, 1766.

(14) Dehdashti, F.; Mortimer, J. E.; Trinkaus, K.; Naughton, M. J.; Ellis, M.; Katzenellenbogen, J. A.; Welch, M. J.; Siegel, B. A. PET-based estradiol challenge as a

predictive biomarker of response to endocrine therapy in women with estrogen-receptor-positive breast cancer. *Breast Cancer Res. Treat.* **2009**, *113*, 509.

(15) Mortimer, J. E.; Dehdashti, F.; Siegel, B. A.; Katzenellenbogen, J. A.; Fracasso, P.; Welch, M. J. Positron emission tomography with 2-[$^{18}$F]fluoro-2-deoxy-D-glucose and 16α-[$^{18}$F]fluoro-17β-estradiol in breast cancer: Correlation with estrogen receptor status and response to systemic therapy. *Clin. Cancer Res.* **1996**, *2*, 933.

(16) Dehdashti, F.; Flanagan, F. L.; Mortimer, J. E.; Katzenellenbogen, J. A.; Welch, M. J.; Siegel, B. A. Positron emission tomographic assessment of "metabolic flare" to predict response of metastatic breast cancer to antiestrogen therapy. *Eur. J. Nucl. Med.* **1999**, *26*, 51.

(17) Mortimer, J. E.; Dehdashti, F.; Siegel, B. A.; Trinkaus, K.; Katzenellenbogen, J. A.; Welch, M. J. Metabolic flare: indicator of hormone responsiveness in advanced breast cancer. *J. Clin. Oncol.* **2001**, *19*, 2797.

(18) Bergstrom, M.; Grahnen, A.; Langstrom, B. Positron emission tomography microdosing: a new concept with application in tracer and early clinical drug development. *Eur. J. Clin. Pharmacol.* **2003**, *59*, 357.

(19) Eckelman, W. C.; Rohatagi, S.; Krohn, K. A.; Vera, D. R. Are there lessons to be learned from drug development that will accelerate the use of molecular imaging probes in the clinic? *Nucl. Med. Biol.* **2005**, *32*, 657.

(20) DiMasi, J. A.; Hansen, R. W.; Grabowski, H. G. The price of innovation: new estimates of drug development costs. *J. Health Econ.* **2003**, *22*, 151.

(21) Adams, C. P.; Brantner, V. V. Spending on new drug development. *Health Econ.* **2010**, *19*, 130.

(22) Ichise, M.; Meyer, J. H.; Yonekura, Y. An introduction to PET and SPECT neuroreceptor quantification models. *J. Nucl. Med.* **2001**, *42*, 755.

(23) Laruelle, M.; Slifstein, M.; Huang, Y. Relationships between radiotracer properties and image quality in molecular imaging of the brain with positron emission tomography. *Mol. Imaging Biol.* **2003**, *5*, 363.

(24) Basu, S.; Kwee, T. C.; Surti, S.; Akin, E. A.; Yoo, D.; Alavi, A. Fundamentals of PET and PET/CT imaging. *Ann. N. Y. Acad. Sci.* **2011**, *1228*, 1.

(25) Ametamey, S. M.; Honer, M.; Schubiger, P. A. Molecular Imaging with PET. *Chem. Rev.* **2008**, *108*, 1501.

(26) Couturier, O.; Luxen, A.; Chatal, J.-F.; Vuillez, J.-P.; Rigo, P.; Hustinx, R. Fluorinated tracers for imaging cancer with positron emission tomography. *Eur. J. Nucl. Med. Mol. Imaging* **2004**, *31*, 1182.

(27) Wadsak, W.; Mitterhauser, M. Basics and principles of radiopharmaceuticals for PET/CT. *Eur. J. Radiol.* **2010**, *73*, 461.

(28) Fletcher, J. W.; Djulbegovic, B.; Soares, H. P.; Siegel, B. A.; Lowe, V. J.; Lyman, G. H.; Coleman, R. E.; Wahl, R.; Paschold, J. C.; Avril, N.; Einhorn, L. H.; Suh, W. W.;

Samson, D.; Delbeke, D.; Gorman, M.; Shields, A. F. Recommendations on the use of $^{18}$F-FDG PET in oncology. *J. Nucl. Med.* **2008**, *49*, 480.

(29) Wang, Y.; Klunk, W. E.; Debnath, M. L.; Huang, G.-F.; Holt, D. P.; Li, S.; Mathis, C. A. Development of a PET/SPECT agent for amyloid imaging in Alzheimer's disease. *J. Mol. Neurosci.* **2004**, *24*, 55.

(30) Klunk, W. E.; Engler, H.; Nordberg, A.; Wang, Y.; Blomqvist, G.; Holt, D. P.; Bergstrom, M.; Savitcheva, I.; Huang, G.-f.; Estrada, S.; Ausen, B.; Debnath, M. L.; Barletta, J.; Price, J. C.; Sandell, J.; Lopresti, B. J.; Wall, A.; Koivisto, P.; Antoni, G.; Mathis, C. A.; Langstrom, B. Imaging brain amyloid in Alzheimer's disease with Pittsburgh compound-B. *Ann. Neurol.* **2004**, *55*, 306.

(31) Pavese, N.; Brooks, D. J. Imaging neurodegeneration in Parkinson's disease. *Biochim. Biophys. Acta, Mol. Basis Dis.* **2009**, *1792*, 722.

(32) Stoessl, A. J. Neuroimaging in Parkinson's disease. *Neurotherapeutics* **2011**, *8*, 72.

(33) Handley, M. G.; Medina, R. A.; Nagel, E.; Blower, P. J.; Southworth, R. PET imaging of cardiac hypoxia: Opportunities and challenges. *J. Mol. Cell. Cardiol.* **2011**, *51*, 640.

(34) Levin, C. S. Primer on molecular imaging technology. *Eur. J. Nucl. Med. Mol. Imaging* **2005**, *32*, S325.

(35) Miller, P. W.; Long, N. J.; Vilar, R.; Gee, A. D. Synthesis of $^{11}$C, $^{18}$F, $^{15}$O, and $^{13}$N radiolabels for positron emission tomography. *Angew. Chem., Int. Ed.* **2008**, *47*, 8998.

(36) Mueller, K.; Faeh, C.; Diederich, F. Fluorine in Pharmaceuticals: Looking Beyond Intuition. *Science* **2007**, *317*, 1881.

(37) Zhang, W.; Koehler, K. F.; Harris, B.; Skolnick, P.; Cook, J. M. Synthesis of benzo-fused benzodiazepines employed as probes of the agonist pharmacophore of benzodiazepine receptors. *J. Med. Chem.* **1994**, *37*, 745.

(38) Ido, T.; Wan, C. N.; Casella, V.; Fowler, J. S.; Wolf, A. P.; Reivich, M.; Kuhl, D. E. Labeled 2-deoxy-D-glucose analogs. Fluorine-18-labelled 2-deoxy-2-fluoro-D-glucose, 2-deoxy-2-fluoro-D-mannose and $^{14}$C-2-deoxy-2-fluoro-D-glucose. *J. Labelled Compd. Radiopharm.* **1978**, *14*, 175.

(39) Ogawa, M.; Hatano, K.; Oishi, S.; Kawasumi, Y.; Fujii, N.; Kawaguchi, M.; Doi, R.; Imamura, M.; Yamamoto, M.; Ajito, K.; Mukai, T.; Saji, H.; Ito, K. Direct electrophilic radiofluorination of a cyclic RGD peptide for in vivo $alpha_2beta_3$ integrin related tumor imaging. *Nucl. Med. Biol.* **2003**, *30*, 1.

(40) Constantinou, M.; Aigbirhio, F. I.; Smith, R. G.; Ramsden, C. A.; Pike, V. W. Xenon Difluoride Exchanges Fluoride under Mild Conditions: A Simple Preparation of [$^{18}$F]Xenon Difluoride for PET and Mechanistic Studies. *J. Am. Chem. Soc.* **2001**, *123*, 1780.

(41) Satyamurthy, N.; Bida, G. T.; Phelps, M. E.; Barrio, J. R. Fluorine-18 labeled N-[$^{18}$F]fluoro-N-alkylsulfonamides: novel reagents for mild and regioselective radiofluorination. *Appl. Radiat. Isot.* **1990**, *41*, 733.

(42) Namavari, M.; Bishop, A.; Satyamurthy, N.; Bida, G.; Barrio, J. R. Regioselective radiofluorodestannylation with fluorine-18 and [$^{18}$F] acetyl hypofluorite: a high yield synthesis of 6-[$^{18}$F]fluoro-L-dopa. *Appl. Radiat. Isot.* **1992**, *43*, 989.

(43) Bergman, J.; Solin, O. Fluorine-18-labeled fluorine gas for synthesis of tracer molecules. *Nucl. Med. Biol.* **1997**, *24*, 677.

(44) Bishop, A.; Satyamurthy, N.; Bida, G.; Phelps, M.; Barrio, J. R. Production of [$^{18}$F]$F_2$ using the $^{16}$O($^{3}$He,p)$^{18}$F reaction. *Nucl. Med. Biol.* **1996**, *23*, 385.

(45) Lee, E.; Kamlet, A. S.; Powers, D. C.; Neumann, C. N.; Boursalian, G. B.; Furuya, T.; Choi, D. C.; Hooker, J. M.; Ritter, T. A Fluoride-Derived Electrophilic Late-Stage Fluorination Reagent for PET Imaging. *Science* **2011**, *334*, 639.

(46) Guillaume, M.; Luxen, A.; Nebeling, B.; Argentini, M.; Clark, J. C.; Pike, V. W. Recommendations for fluorine-18 production. *Appl. Radiat. Isot.* **1991**, *42*, 749.

(47) Ruth, T. J.; Wolf, A. P. Absolute cross sections for the production of fluorine-18 via the $^{18}$O(p,n)$^{18}$F reaction. *Radiochim. Acta* **1979**, *26*, 21.

(48) Hamacher, K.; Coenen, H. H.; Stoecklin, G. Efficient stereospecific synthesis of no-carrier-added 2-[$^{18}$F]-fluoro-2-deoxy-D-glucose using aminopolyether supported nucleophilic substitution. *J. Nucl. Med.* **1986**, *27*, 235.

(49) Seo, J. W.; Lee, B. S.; Lee, S. J.; Oh, S. J.; Chi, D. Y. Fast and easy drying method for the preparation of activated [$^{18}$F]fluoride using polymer cartridge. *Bull. Korean Chem. Soc.* **2011**, *32*, 71.

(50) Coenen, H. H.; Pike, V. W.; Stoecklin, G.; Wagner, R. Recommendation for a practical production of [2-$^{18}$F]fluoro-2-deoxy-D-glucose. *Appl. Radiat. Isot.* **1987**, *38*, 605.

(51) Kim, D. W.; Ahn, D.-S.; Oh, Y.-H.; Lee, S.; Kil, H. S.; Oh, S. J.; Lee, S. J.; Kim, J. S.; Ryu, J. S.; Moon, D. H.; Chi, D. Y. A New Class of $SN_2$ Reactions Catalyzed by Protic Solvents: Facile Fluorination for Isotopic Labeling of Diagnostic Molecules. *J. Am. Chem. Soc.* **2006**, *128*, 16394.

(52) Kim, D. W.; Jeong, H.-J.; Lim, S. T.; Sohn, M.-H.; Katzenellenbogen, J. A.; Chi, D. Y. Facile Nucleophilic Fluorination Reactions Using *tert*-Alcohols as a Reaction Medium: Significantly Enhanced Reactivity of Alkali Metal Fluorides and Improved Selectivity. *J. Org. Chem.* **2008**, *73*, 957.

(53) Harrison, S. T.; Mulhearn, J.; Wolkenberg, S. E.; Miller, P. J.; O'Malley, S. S.; Zeng, Z.; Williams, D. L.; Hostetler, E. D.; Sanabria-Bohorquez, S.; Gammage, L.; Fan, H.; Sur, C.; Culberson, J. C.; Hargreaves, R. J.; Cook, J. J.; Hartman, G. D.; Barrow, J. C. Synthesis and Evaluation of 5-Fluoro-2-aryloxazolo[5,4-b]pyridines as β-Amyloid PET Ligands and Identification of MK-3328. *ACS Med. Chem. Lett.* **2011**, *2*, 498.

(54) Pike, V. W.; Aigbirhio, F. I. Reactions of cyclotron-produced [$^{18}$F]fluoride with diaryliodonium salts - a novel single-step route to no-carrier-added [$^{18}$F]fluoroarenes. *J. Chem. Soc., Chem. Commun.* **1995**, 2215.

(55) Chun, J.-H.; Lu, S.; Lee, Y.-S.; Pike, V. W. Fast and High-Yield Microreactor Syntheses of ortho-Substituted [$^{18}$F]Fluoroarenes from Reactions of [$^{18}$F]Fluoride Ion with Diaryliodonium Salts. *J. Org. Chem.* **2010**, *75*, 3332.

(56) Chun, J.-H.; Lu, S.; Pike, V. W. Rapid and Efficient Radiosyntheses of meta-Substituted [$^{18}$F]Fluoroarenes from [$^{18}$F]Fluoride Ion and Diaryliodonium Tosylates within a Microreactor. *Eur. J. Org. Chem.* **2011**, *2011*, 4439.

(57) Ross, T. L.; Ermert, J.; Hocke, C.; Coenen, H. H. Nucleophilic $^{18}$F-Fluorination of Heteroaromatic Iodonium Salts with No-Carrier-Added [$^{18}$F]Fluoride. *J. Am. Chem. Soc.* **2007**, *129*, 8018.

(58) Moon, B. S.; Kil, H. S.; Park, J. H.; Kim, J. S.; Park, J.; Chi, D. Y.; Lee, B. C.; Kim, S. E. Facile aromatic radiofluorination of [$^{18}$F]flumazenil from diaryliodonium salts with evaluation of their stability and selectivity. *Org. Biomol. Chem.* **2011**, *9*, 8346.

(59) Sun, T.; Tang, G.; Tian, H.; Wang, X.; Chen, X.; Chen, Z.; Wang, S. Radiosynthesis of 1-[$^{18}$F]fluoroethyl-L-tryptophan as a novel potential amino acid PET tracer. *Appl. Radiat. Isot.* **2012**, *70*, 676.

(60) Svensson, F.; Kniess, T.; Bergmann, R.; Pietzsch, J.; Wuest, F. Synthesis of an $^{18}$F-labeled cyclin-dependent kinase-2 inhibitor. *J. Labelled Compd. Radiopharm.* **2011**, *54*, 769.

(61) Kuegler, F.; Sihver, W.; Ermert, J.; Huebner, H.; Gmeiner, P.; Prante, O.; Coenen, H. H. Evaluation of $^{18}$F-Labelled Benzodioxine Piperazine-Based Dopamine D4 Receptor Ligands: Lipophilicity as a Determinate of Nonspecific Binding. *J. Med. Chem.* **2011**, *54*, 8343.

(62) Muehlhausen, U.; Ermert, J.; Herth, M. M.; Coenen, H. H. Synthesis, radiofluorination and first evaluation of (±)-[$^{18}$F]MDL 100907 as serotonin 5-HT2A receptor antagonist for PET. *J. Labelled Compd. Radiopharm.* **2009**, *52*, 6.

(63) Scott, A. M. Current status of positron emission tomography in oncology. *Australas Radiol.* **2002**, *46*, 154.

(64) Zhuang, H.; Alavi, A. 18-fluorodeoxyglucose positron emission tomographic imaging in the detection and monitoring of infection and inflammation. *Semin. Nucl. Med.* **2002**, *32*, 47.

(65) Kim, B. T.; Kim, Y.; Lee, K. S.; Yoon, S. B.; Cheon, E. M.; Kwon, O. J.; Rhee, C. H.; Han, J.; Shin, M. H. Localized form of bronchioloalveolar carcinoma: FDG PET findings. *AJR Am. J. Roentgenol.* **1998**, *170*, 935.

(66) Higashi, K.; Ueda, Y.; Sakurai, A.; Ming, X.; Xu, L.; Murakami, M.; Seki, H.; Oguchi, M.; Taki, S.; Nambu, Y.; Tonami, H.; Katsuda, S.; Yamamoto, I. Correlation of Glut-1 glucose transporter expression with [$^{18}$F]FDG uptake in non-small cell lung cancer. *Eur. J. Nucl. Med.* **2000**, *27*, 1778.

CHAPTER 2

# DEVELOPMENT OF NOVEL SILICON PRECURSORS FOR RAPID AND EFFICIENT RADIOFLUORINATION REACTIONS

## I. INTRODUCTION

### *A. Background*

By far, the most widely utilized radiotracer in clinical PET imaging is the glucose analogue, [$^{18}$F]fluorodeoxyglucose ([$^{18}$F]FDG).[1] Many would agree that the development of the field would have not been possible without the discovery of [$^{18}$F]FDG. Its widespread applications in oncology have justified the installation of the expensive production and imaging infrastructure needed within hospitals, and as a result, [$^{18}$F]fluoride ion is now readily available, even from commercial suppliers. With the proper infrastructure in place, clinical research has focused primarily on other small molecules as potential imaging agents to address the limitations of PET imaging with [$^{18}$F]FDG.[2-4] More recently, however, the radiolabeling of large biomolecules, such as peptides, proteins, and antibodies, has also been proposed to expand imaging applications well beyond [$^{18}$F]FDG.[5,6] What has impeded and still remains a significant challenge in accessing these new applications are the mild and efficient radiofluorination reactions that are needed for radiolabeling these sensitive, polyfunctional substrates. Unfortunately, current labeling conditions restrict the use of the more desirable one-step strategy in favor of the multi-step, indirect prosthetic group labeling approach. Consequently, the additional steps required add a further level of synthetic difficulty and increase the absorbed dose by the radiochemist, in addition to raising the problem of overconjugation of the biomolecule with prosthetic group, all of which conspire to severely limit the practicality of this approach.

The synthetic problems associated with the radiolabeling of sensitive biomolecules using [$^{18}$F]fluoride ion are in stark contrast to other isotopic labeling methods, especially those using Cu-64. Despite the less than ideal nuclear properties (i.e., multiple decay processes, isotopic impurities,[7] undesirable transchelation of $^{63}$Cu/$^{64}$Cu *in vivo*[8]), Cu-64 is becoming an attractive alternative in recent years due to the ease of isotopic incorporation. Typically, Cu-64 radiolabeling methods involve a simple and straightforward one-step, wash-in protocol where an aqueous solution of [$^{64}$Cu]-cupric ion is incorporated into chelators appended on biomolecules (i.e., NOTA, DOTA) in high RCYs under mild conditions (Scheme 2.1).[9,10] The use of aqueous conditions without the need for a time-consuming, basic drying step, elevated temperatures or

organic solvents is highly attractive, especially when working with water-soluble proteins and antibodies. At present, analogous approaches with [$^{18}$F]fluoride ion are underdeveloped, but strategies conceptually similar to those used for $^{64}$Cu-labelling are currently being investigated for F-18 using fluorophilic elements (i.e., Al, B, Si).

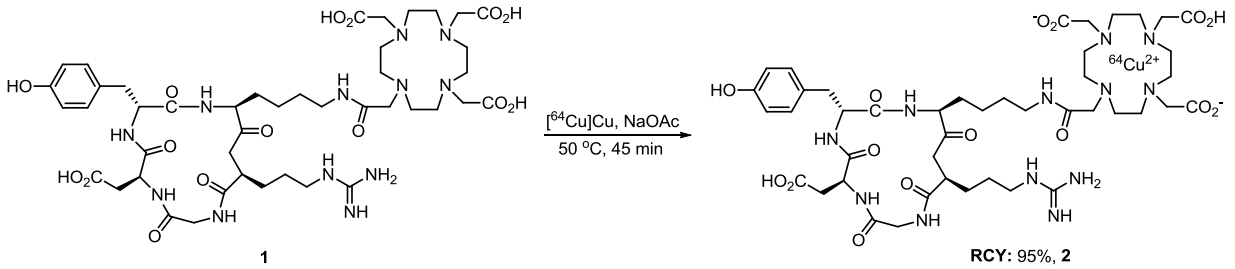


**Scheme 2.1.** Incorporation of [$^{64}$Cu]-cupric ion into complex peptide (**2**) in a mild, one-step process.[9]

*B. Al-$^{18}$F Strategies*

Following the literature precedent of the chelation of radiometals as an effective strategy for radiolabeling peptides, an analogous approach, focused on targeting the high affinity of some metals for fluoride ion, has been achieved through aluminum-[$^{18}$F]fluoride peptide complexes.[11,12] The novel pentadentate bifunctional chelator, 1,4,7-triazacyclononane-1,4-diacetate (NODA), to coordinate $Al^{3+}$ ion provided an effective scaffold to capture aqueous [$^{18}$F]fluoride anion in a single, high yielding step (55-89%) within 15 minutes at 110 °C, and more importantly, the corresponding bioconjugates (**4**) exhibited exceptional stability, with no defluorination observed for 4 hours in human serum at 37 °C (Scheme 2.2).[12] This technically simple labeling procedure has led to the development of labeling kits,[13] similar to those used with $^{99m}$Tc, that will aid in streamlining reactions and facilitate product purification and isolation.[14] As a result, this has enabled rapid and reproducible labelings of peptides in high RCYs and specific activities through a simple, one-step process to afford $^{18}$F-labelled products that are compliable with good manufacturing practices (GMPs) and ready for patient injection within 30 minutes. Of these three new strategies, the Al-$^{18}$F approach is the most recently introduced and while still in its infancy within the development process, possesses the greatest likelihood of benchtop-to-patient translation, especially with their kit formulations.

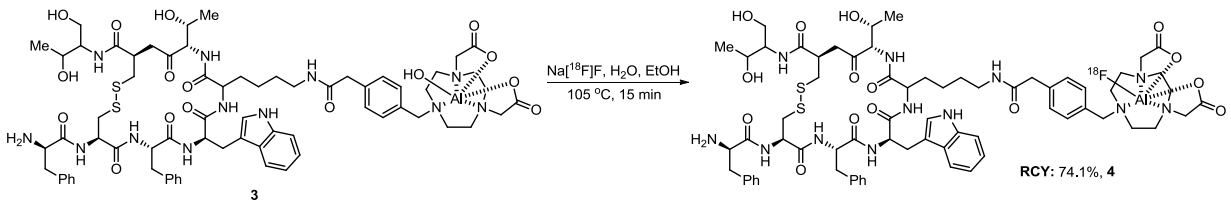


3

**Scheme 2.2.** One-step chelation of aqueous [$^{18}$F]fluoride anion with $Al^{3+}$-NODA.[12]

*C. B-$^{18}$F Strategies*

Trivalent organoboranes, particularly alkyl- and alkynylboranes, exhibit poor stability under atmospheric conditions, thereby making handling of these reagents extremely difficult. The 1960s discovery and subsequent development, most notably by Molander, of potassium organotrifluoroborates as superior alternatives to their trivalent counterparts, however, has transformed the field.[15,16] These reagents exhibit exceptional stabilities towards nucleophiles, air and water, and can be handled on the benchtop without special precautions, all without altering their high reactivity, particularly in palladium-catalyzed cross coupling reactions.[17] The translation into tracer level chemistry with F-18, however, has only recently been realized.

Ting and coworkers were the first to report the $^{18}$F-labelling of aryl boronic esters, under carrier added conditions ($KH^{19}F_2$) to afford [$^{18}$F]-aryltrifluoroborates.[18] Similar to the aluminum chemistry described previously, the attractiveness of the method resides in the simple, one-step protocol, performed under aqueous conditions, which is ideally compatible with water-soluble biomolecules and also alleviates the need for the time-consuming drying step. The initial practicality of the approach was validated through the radiosynthesis of a biotinylated [$^{18}$F]-*p*-aminophenyltrifluoroborate (**6**, Scheme 2.3) and has since led to the development of additional boronic ester bioconjugates, including peptides and nucleic acids, and bifunctional linkers for other potential applications of this chemistry.[19] Additionally, the reported *in vivo* evaluations to date have revealed no skeletal uptake of radioactivity, demonstrating the exceptional stability of the B-$^{18}$F bond.[20]

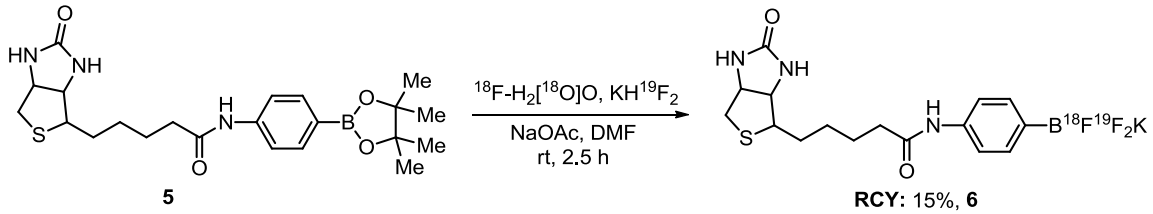


5

**RCY:** 15%, **6**

**Scheme 2.3.** Formation of [$^{18}$F]-aryltrifluoroborates (**6**) from aqueous [$^{18}$F]fluoride ion.[18]

Despite the attractiveness of the simple, aqueous radiochemistry and high *in vivo* stability of the corresponding radiotracers, this approach still suffers from two glaring weaknesses which must be overcome before routine production is possible. First, the reaction with [$^{18}$F]fluoride ion (and KH$^{19}F_2$) is inherently slow (~2-3 hours), and attempts to address this issue with higher concentrations of reagents and small reaction volumes (~10 µl) only further impede the practicality of this method. Second, any carrier-added radiosyntheses are inherently limited to low specific activities. Unfortunately, in this case, the addition of cold [$^{19}$F]fluoride ion is required to achieve moderate RCYs of the desired R-B$^{18}F^{19}F_2K$ (**6**) salt; thus, further design of suitable precursors and optimization of reaction conditions without carrier added are needed to realize the full potential of this method.

*D. Si-$^{18}$F Strategies*

For decades, chemists have exploited the silicon-fluoride bond as a facile method for the deprotection of silyl ethers to the corresponding alcohols.[21] Interestingly, radiochemists have only recently been able to develop similar silyl-based methods to incorporate [$^{18}$F]fluoride ion. Rosenthal reported[22] the first Si-$^{18}$F bond with [$^{18}$F]fluorotrimethylsilane, but preliminary *in vivo* experiments in rats revealed significant bone accumulation, demonstrating the low stability of the Si-$^{18}$F bond in the body and the need for sterically hindered substituents around the silicon atom to prevent hydrolysis. In addition to their B-$^{18}$F work, Ting[18] also investigated the potential of tetrafluorosilcates (**8**, Scheme 2.4) as imaging agents, but the need for carrier added (KH$^{19}F_2$) and moderate stabilities of the corresponding [$^{18}$F]fluoroproducts severely limit the practicality of this approach and call for further experimental and precursor design.

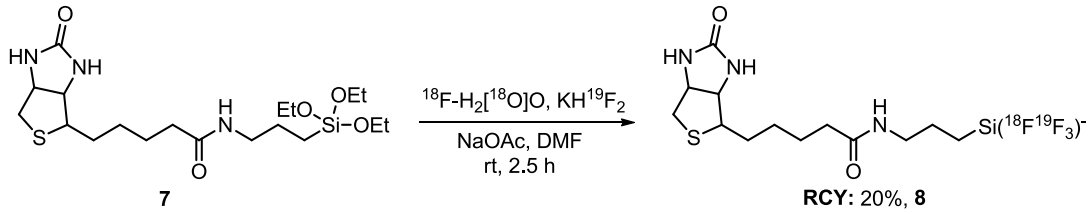


**Scheme 2.4.** Formation of [$^{18}$F]-aryltrifluorosilicates (**8**) from aqueous [$^{18}$F]fluoride ion.[18]

In an attempt to gain better insight into the stabilities of Si-$^{18}$F bonds, Hohne and coworkers utilized density functional theory (DFT) models to estimate the hydrolytic stability of appropriately designed silyl-based precursors; their work revealed the need for at least two *tert*-butyl groups ($t_{1/2}$ of Si-F bond = >300 h) or two isopropyl groups flanked by two methyl groups ($t_{1/2}$ of Si-F bond = >300 h) in order to provide adequate stabilization.[23] This approach was pursued further through the use of bifunctional triorganosilanes (**9**), based on alkoxy, hydroxy,

and hydride leaving groups. Initial studies yielded conversion rates of up to 96% for [$^{18}$F]fluoride incorporation into relatively simple substrates within 20 minutes in DMSO with catalytic amounts of acetic acid (Scheme 2.5).[24,25] Additional investigations into the hydrolytic stabilities of the corresponding [$^{18}$F]fluorosilane products (**10**) showed strong correlations with the previous computational data, suggesting that the presence of more sterically demanding substituents (e.g., tBu) generates [$^{18}$F]fluoroproducts that are more hydrolytically resistant under physiological conditions.

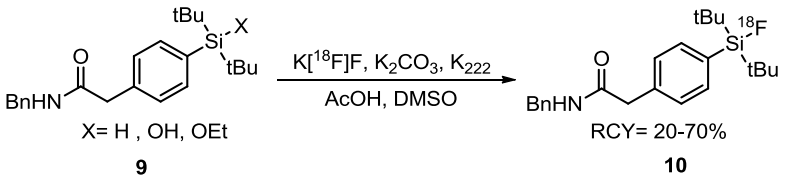


**Scheme 2.5.** Acid-promoted formation of Si-$^{18}$F bonds.[24]

Application of this approach to more structurally complex substrates, such as peptides (**11**, Scheme 2.6), yielded synthetically useful RCYs (~50%) after 15 minutes and in sufficiently high specific activities (1600 Ci/mmol). Although the chemistry cannot be performed with aqueous [$^{18}$F]fluoride as in previous cases (therefore requiring a drying step), the most significant shortcoming of this strategy is the issue of effective specific activity. Specifically, with large, complex substrates such as **11**, the conservative exchange of a hydrogen (**11**) for a [$^{18}$F]fluorine atom (**12**) does not provide sufficiently high structural and electronic differences between starting material and product that would enable effective separation during HPLC purification. As a result, the large excess of starting material (at times, up to 5 mg needed) will most likely not be fully separated from the [$^{18}$F]fluorosilane product. Thus, there will be considerable contamination of the final radiotracer (**12**) with starting material (**11**). Because the starting material is structurally related to the tracer and will most likely compete with the tracer for binding to a receptor target, this will greatly reduce the “effective” specific activity of the labeled material, which could compromise its usefulness in PET imaging of limited capacity targets.

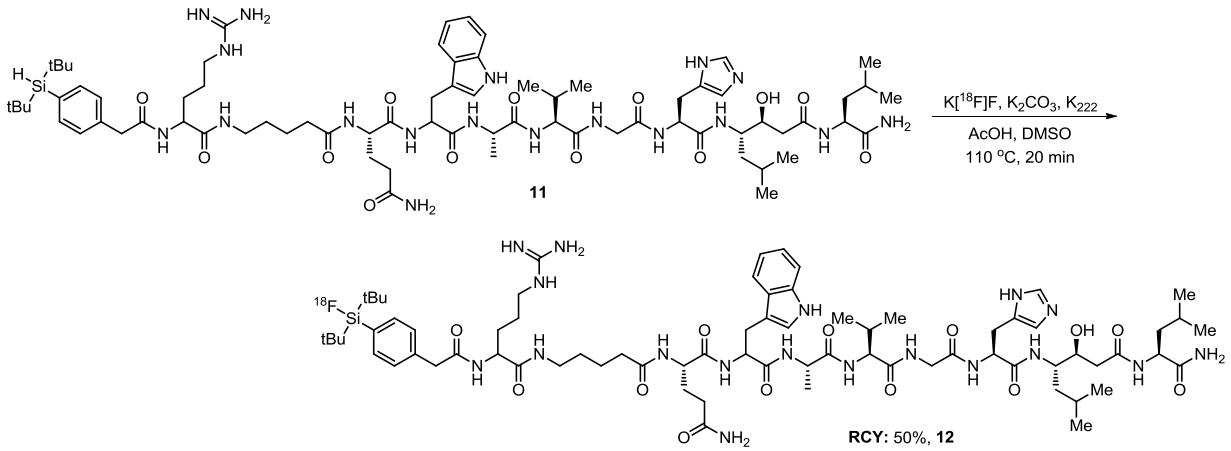


**Scheme 2.6.** Acid-promoted formation of a complex $^{18}$F-labelled peptide (**12**) through a direct, one-step process.[25]

A highly promising Si-$^{18}$F variant method, developed by Schirrmacher and coworkers,[26-30] relies on the facile isotopic exchange between [$^{18}$F]fluorine ion and trialkyl-[$^{19}$F]fluorosilane precursors (Scheme 2.7). The exchange process is surprisingly efficient, with nanomole quantities of starting material (**13**), proceeding rapidly at room temperature in high RCYs (>90%) within 15 minutes.[26] Unfortunately, the method is inherently limited to low specific activities because of the inability to separate the [$^{18}$F]fluorosilane product from the chemically identical [$^{19}$F]fluorosilane starting material, which is in large excess in order to achieve high RCYs. The chemistry works best in a two-step approach to label biomolecules through the use of bifunctional triorgano-[$^{18}$F]fluorosilane derivatives (**15**), each containing a range of coupling functionality, including aldehydes, thiols, amines, alcohols, isothiocyanates, carboxylic acids, and maleimides.

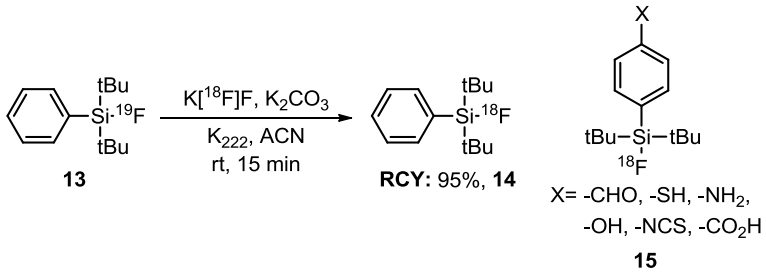


**Scheme 2.7.** Left side: isotopic exchange of [$^{18}$F]fluoride ion with Ar-(tBu)$_2$-Si-$^{19}$F precursor (**13**); Right Side: different [$^{18}$F]fluorosilane products exhibiting a range of coupling functionality.[26]

However, in the presence of complex, polyfunctional biomolecules such as peptides (**16**, Scheme 2.8), RCYs suffer significantly in direct, one-step processes, and any appreciable gain in yields can only be achieved through the use of additional amounts of [$^{19}$F]-starting material

(**16**). Consequently, specific activities of the [$^{18}$F]fluorosilane product (**17**) are extremely low (<100 Ci/mmol), well below the threshold for receptor-based imaging studies, and as a result, isotopic exchange has limited applicability within this area.[26]

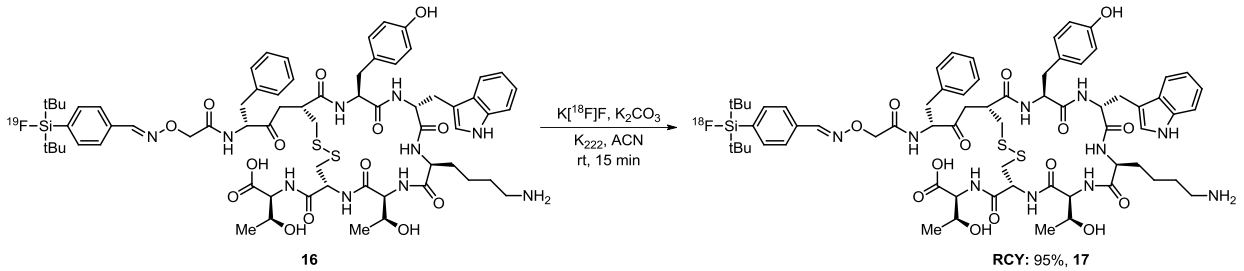


**Scheme 2.8.** Isotopic exchange of [$^{18}$F]fluoride ion into a complex, polyfunctional peptide (**17**).[26]

## II. CONCLUDING INTRODUCTORY REMARKS

In coordination with our group's goal of developing ER PET imaging agents, we were intrigued by the advantages of the Si-$^{18}$F chemistry over the aluminum and boron strategies mainly because it appeared to us that the bulky appended chelator, $Al^{3+}$-NODA, designed to capture aqueous [$^{18}$F]fluoride, in addition to the negative charges associated with the Al-$^{18}$F and B-$^{18}$F complexes would most likely have minimal, if any, affinity for the nuclear ERs. Furthermore, the formation of Si-$^{18}$F bonds has been reported to be extremely rapid and efficient, proceeding in high radiochemical yields at room temperature, and can even be conducted in an aqueous environment. The Si-$^{18}$F labeling methods used so far, however, have disadvantages. Although the exchange is facile with Ar-$(tBu)_2$-Si-$^{19}$F precursors, an excess of $^{19}$F-starting materials is often needed, especially with radiolabeling peptides, and this restricts access to high specific activity $^{18}$F-labelled products. An alternative approach involving reaction of [$^{18}$F]fluoride ion with hydrosilanes, $Ar(R)_2$Si-H, required a troublesome optimization process for each reaction and was slow and relatively inefficient, with remaining precursor difficult to separate from the product. In an attempt to improve on the existing methods, we sought the use of silyl acetates as exceptional alternatives for Si-$^{18}$F radiochemistry.

Herein, we describe a vastly improved version of Si-$^{18}$F bond formation through our silyl acetate moiety, and we demonstrate its utility and flexibility in small molecules and large, polyfunctional biomolecules. These precursors have proven to be extremely reactive to [$^{18}$F]fluoride ion and tolerant of protic functionality and water to provide an ideal one-step approach to functionally complex substrates in a late-stage fashion in high radiochemical yields and specific activities.

## III. RESULTS

*Portions of the synthesis work, notably preparation of the precursors [**22**-**26**, **29**, **30**, **38**-**44**, **46**-**51**, **52-59**, **61**] were done by Dr. Sung Hoon Kim. All of the radiolabeling work was done by the author of this thesis.

### *A. Small Adaptor Si-$^{18}$F Molecules*

The practicality of F-18 methodology for labeling PET agents relies heavily on simple and straightforward approaches that are needed to incorporate the isotope. Thus, the direct, one-step approach is much preferred over multi-step syntheses. More often, however, the incompatibility of certain sensitive substrates to F-18 labeling conditions or the low yields associated with a direct, one-step methods complicates production of the desired tracer and as a result, the multi-step approach is typically favored, especially for large biomolecules. Unfortunately, the complexity of these radiosyntheses complicates transition to clinical production and thus restricts their availability and evaluation in patients.

As discussed previously, the strategy involves initial incorporation of the isotope into small adaptor precursors, which are then readily appended to large, sensitive biomolecules through a variety of methods. Of those reported, the most commonly used adaptor molecule is *N*-succinimidyl 4-[$^{18}$F]fluorobenzoate, (**21**, [$^{18}$F]-SFB), and its use nicely exemplifies the deficiencies in this approach. First, the radiosynthesis of [$^{18}$F]-SFB (**21**) alone involves three steps (Scheme 2.9), with an additional step needed to append **21** to the biomolecule of interest, for a total of at least four steps to access the desired tracer.[31]

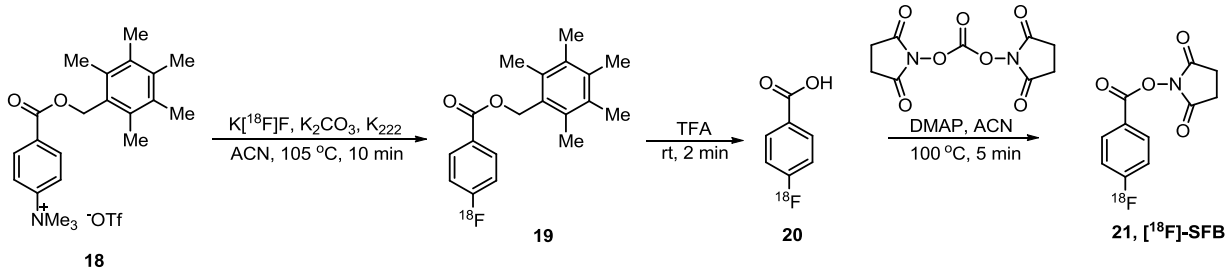


**Scheme 2.9.** Radiosynthesis of *N*-succinimidyl-[$^{18}$F]fluorobenzoate (**21**) for conjugation to biomolecules through a multi-step approach.[31]

Moreover, the isotope is incorporated in the first step of the sequence (**19**), and the additional manipulations restrict access to extremely high activities of **21**, which are required in the clinic. Finally, the multi-step sequence is technically challenging to perform (Figure 2.1). Although high yielding, each step is rather involved and requires purification either using a filter,

cartridge, or extraction from the previous step, leading to undesired absorbed hand and body doses and extreme difficulty in translating the chemistry to automated modules for clinical production. A typical [$^{18}$F]-SFB production protocol is given below.

> $^{18}$F-Fluoride solution (300–400 μL) was transferred to the first reaction vial, without trapping on an anion exchange cartridge, followed by the addition of $K_2CO_3$ (8.63 mg/mL, 5 mmol) and Kryptofix 2.2.2 (4.5 mg, 12 mmol) in 10% water:acetonitrile solution. Then, water and acetonitrile were azeotropically evaporated by heating the reactor to 120 $^{o}$C under a stream of argon followed by a vacuum. Further azeotropic drying was accomplished by the addition of 0.5 mL of acetonitrile. The dried K$^{18}$F • Kryptofix 2.2.2 complex was then dissolved in 400 mL of acetonitrile containing 5 mg (14.7 mmol) of pentamethylbenzyl 4-(*N,N,N*-trimethylammonium)benzoate trifluoromethanesulfonate. The reactor was sealed and heated to 105 $^{o}$C for 10 min, to yield 4-$^{18}$F-fluorobenzoic acid pentamethylphenylmethyl ester. Then, the reactor was cooled to 10 $^{o}$C and 0.8 mL of diethyl ether was added. The crude 4-$^{18}$F-fluorobenzoic acid pentamethylphenylmethyl ester solution was then transferred through the silica cartridge to the second reaction vial. The first reaction vial and silica cartridge were washed with an additional 0.8-mL portion of diethyl ether. The diethyl ether was evaporated for 5 min at 35 $^{o}$C under a stream of argon. Then the reaction vial was cooled to 25 $^{o}$C, and 0.15 mL of 99.9% trifluoroacetic acid (TFA) was added. The pentamethylbenzyl deprotection proceeded for 2 min to yield 4-$^{18}$F-fluoro-benzoic acid ($^{18}$F-FBA). Thereafter, the reaction vial was cooled to 4 $^{o}$C, and TFA was evaporated under a stream of argon, followed by the addition of 3 mg of 4-(dimethylamino)pyridine and 5.2 mg of *N,N*-disuccinimidyl carbonate. The reactor was sealed and heated to 100 $^{o}$C for 5 min. The reaction vial was then cooled to 30 $^{o}$C, and the crude $^{18}$F-SFB was diluted with 20 mL of water and passed through an activated C18 cartridge. The cartridge was washed with 10 mL of water and 1.8 mL of petroleum ether. Finally, the $^{18}$F-SFB was eluted from the cartridge with 1 mL of dichloromethane. The solvent was removed by a stream of argon at 25 $^{o}$C.

**Figure 2.1** Reported method detailing the difficulty in the radiosynthesis of *N*-succinimidyl-[$^{18}$F]fluorobenzoate (**21**).[31]

In an effort to simplify existing labeling chemistries, we sought to address the deficiencies in C-$^{18}$F approaches through the use of our silyl acetate precursors (**28**, Scheme 2.11). As shown in Scheme 2.10, the initial preparation of the desired silyl acetates **28** commenced with lithiation of bromide **22**, followed by condensation with di-*tert*-butylchlorosilane, to provide hydrosilane **23**. Hydrolysis of acetal **23** and subsequent Jones oxidation afforded acid **25**, which readily underwent ester formation (**26**) under DCC-mediated conditions. The corresponding hydrosilanes (**24** and **26**) were converted to the desired silyl acetates (**28**) in high yields through a Pd-mediated process (Scheme 2.11).

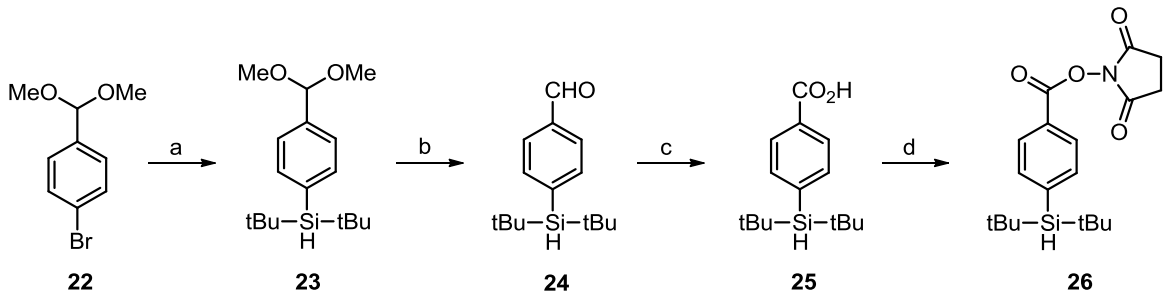


**22** **23** **24** **25** **26**

**Scheme 2.10.** Synthesis of hydrosilane precursors for silyl acetate products. (a) (i) *n*BuLi, THF, -78 $^{o}$C; (ii) $(tBu)_2$-SiH-Cl, TEA, THF, -78 $^{o}$C→rt; (b) $SiO_2$, rt; (c) Jones reagent, acetone, 0 $^{o}$C; (d) DCC, DMAP, DCM, 0 $^{o}$C.

The silyl acetate products have proven to be quite useful. First, the silyl acetates can be rapidly accessed, and the flexibility of the preparative sequence enables the generation of products that exhibit a wide range of different coupling functionality that would be utilized in a two-step labeling approach. Moreover, the production method can be used to incorporate other coupling functionality (i.e., alkynes for click chemistry), depending on the particular need. Secondly, the silyl acetates are extremely bench-stable, and they tolerate exposure to air and water, and silica gel purifications. Traditionally, Si-Cl bonds epitomized reactive silyl functionality, but their sensitivity towards hydrolysis to the unreactive silanol limits their utility in our [$^{18}$F]fluorination conditions. Likewise, Si-Cl precursors would need to be purified by distillation, since they are unstable on silica gel; thus, they would be limited to relatively small substrates and would require multi-step [$^{18}$F]fluorination approaches. However, the exceptional stability of the Si-OAc bond enables silica gel purification, which expands their applicability for the preparation of a wide variety of potential substrates, including complex, polyfunctional peptides, by direct [$^{18}$F]fluorinations. Even with this elevated stability of the starting material, **28** reacted rapidly with cold fluoride anion at room temperature within 5 minutes, with benzene being the optimal solvent (Scheme 2.11). More importantly, the fluorination of silyl acetates had minimal effect on the sensitive coupling functionality (i.e., NHS ester). This was key, since in previous methods, sensitive ester functionality was incompatible with the conditions required for radiofluorination. In addition, our interest in amine-reactive functionality was rooted in our desire to label a poly(amido)amine (PAMAM) dendrimer to understand the biodistribution of this interesting ER-targeted biopolymer. The NHS ester, in this case, was found to be the superior functionality over other potential strategies (i.e., reductive amination with CHO derivative), in terms of efficiency and reactivity, for this transformation.

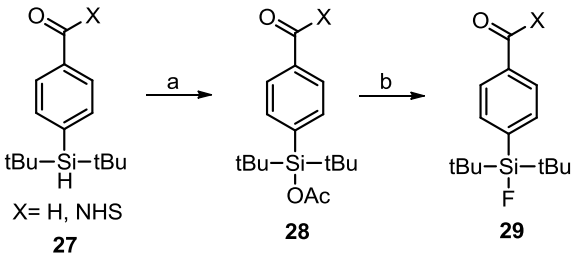


**Scheme 2.11.** Pd-mediated synthesis of silyl acetates (**28**) and cold fluorination with TBAF. (a) $Pd(OAc)_2$, AcOH, PhH, reflux; (b) TBAF, PhH, rt.

The translation of the fluorination chemistry in Scheme 2.11 to tracer-level chemistry with [$^{18}$F]fluoride anion proved to be challenging. First and foremost, the initial re-solubilization of the fluoride salt, TBA$^{18}$F (from TBA[$HCO_3$]), which was found to be the best fluoride source in our original cold fluoride screen, was far from ideal (Scheme 2.12). Initially, this remained a significant limitation of our approach, since most of the expensive [$^{18}$F]fluoride isotope would be stuck to the reaction vial and therefore, unreactive, and eventually would be discarded as waste. Resolubilization is a fairly standard problem after the drying step is completed, and one of the main reasons that radiochemists prefer polar aprotic solvents (i.e., ACN, DMF, DMSO) is because of their ability to successfully re-dissolve the [$^{18}$F]fluoride source from the glass surface. However, our cold chemistry screen of solvents with TBA$^{19}$F revealed far superior yields with less polar solvents, with benzene being the optimal solvent. Unfortunately, these non-polar aprotic solvents were not efficient for re-dissolving the dried TBA$^{18}$F, although the low levels of activity that were solubilized did provide promising yields of the desired compound, especially with PhH and DCM. Thus, we began to investigate other strategies in an attempt to discover a more organic-soluble [$^{18}$F]fluoride source.

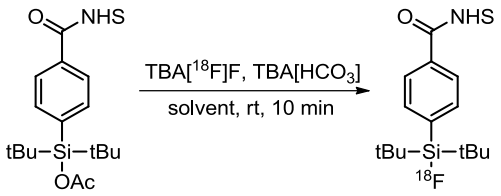


**30** **31**

| Solvent | Total Activity of TBA[$^{18}$F]F (mCi) | TBA[$^{18}$F]F in Solution (mCi) | TBA[$^{18}$F]F on Vial (mCi) | % in Solution | RCY |
|---|---|---|---|---|---|
| Benzene | 5.34 | 1.32 | 4.02 | 24.7 | 61 |
| DCM | 5.18 | 2.75 | 2.43 | 53.1 | 72 |
| Isoamyl Alcohol | 5.62 | 0.18 | 5.44 | 3.20 | 32 |
| Diethyl Ether | 4.97 | 0.36 | 4.61 | 7.24 | 46 |

**Scheme 2.12.** Evaluation of the solubility and reaction with **30** of TBA[$^{18}$F]F in various organic solvents.

Of the commonly used [$^{18}$F]fluoride sources (i.e., TBA[$^{18}$F]F, Cs[$^{18}$F]F, Rb[$^{18}$F]F), by far the most widely used is the K[$^{18}$F]F-$K_{222}$ complex. Initial attempts to replicate previous protocols ($K_2CO_3$ (1 mg) and $K_{222}$ (7 mg)) afforded a highly soluble [$^{18}$F]fluoride source in PhH (70-80% of activity in solution), but the excess base proved detrimental to the stability of the product **31**. As shown in Figure 2.2, the crude radio-HPLC revealed multiple $^{18}$F-products, with the desired product (**31**) being retained at 4.15 minutes. After continued analysis over a 30 minute time period, **31** completely decomposed with a subsequent increase in the radio-peak to the right (4.66 minutes). This was not too surprising since the reaction is conducted under basic conditions in the presence of a base-sensitive NHS ester functionality, and it was assumed that the increase of the radio-peak at 4.66 minutes was the carboxylic acid derivative. However, synthesis of the cold fluorine standard of the acid and co-injection with the reaction mixture revealed elution of the acid to the left of the product peak. Identification of the product to the right of **31** still remains undetermined.

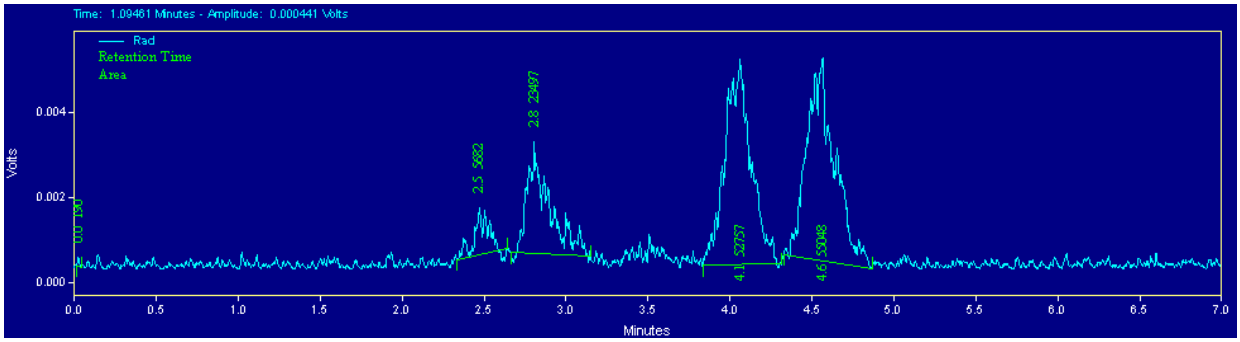


**Figure 2.2.** Radio-HPLC of the [$^{18}$F]fluorination of **30** with K[$^{18}$F]F-$K_{222}$ showing the base sensitivity of **31** and the formation of multiple side [$^{18}$F]fluoroproducts. Product elutes at 4.15 minutes with the remaining other [$^{18}$F]fluoroproducts being undetermined.

The initial investigations in the radiofluorination of **30** led to two main conclusions: low solubility of TBA[$^{18}$F]F in the preferred solvent, PhH, and sensitivity of the NHS ester to the added base. The simple solution to these problems would be to essentially eliminate TBA[$^{18}$F]F, PhH, and added base from being factors in the success of the reaction. Unfortunately, there was little precedent in the literature for this approach to work since almost every [$^{18}$F]fluorination reaction involves a drying step, a [$^{18}$F]fluoride salt, and an organic solvent under scrupulously dry conditions. However, our anticipated reaction conditions would be the exact opposite of how classical C-$^{18}$F strategies are performed: no drying step or [$^{18}$F]fluoride salts, and a reaction to be conducted in an aqueous environment.

Preliminary investigations revealed a critical dependence of the reaction temperature to afford high RCYs, starting from the cyclotron-produced aqueous [$^{18}$F]fluoride source without any added base or a drying step (Scheme 2.13). The attractiveness of targeting silicon with [$^{18}$F]fluoride is due to the mildness of the reaction conditions and the hope that they would be compatible with the efficient radiolabeling of sensitive substrates that had proved to be incompatible with conventional C-$^{18}$F labeling approaches. Unfortunately, attempts to successfully [$^{18}$F]fluorinate **30** at room temperature afforded no conversion to the desired product, but when the reaction was heated to 105 $^{o}$C, excellent yields could be obtained.

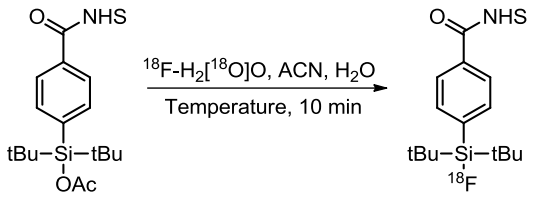


**30** **31**

| Temperature | 5% $H_2O$-ACN | 10% $H_2O$-ACN | 20% $H_2O$-ACN |
|---|---|---|---|
| rt | 0% | 0% | 0% |
| 88 $^oC$ | 33.7% | 60.1% | 65.9% |
| 105 $^oC$ | 63.2% | 75.3% | 92.1% |

**Scheme 2.13.** Screening of the optimal water concentration and temperature for the radiofluorination of **30**.

Nevertheless, the radiofluorination of **30** is highly attractive because of its simplicity. The labeling is rapid and efficient, producing the $^{18}$F-labelled product in high radiochemical purity, with only one major F-18 product being formed, as shown in the radio-HPLC of the crude reaction mixture (Figure 2.3). This is one of the first reported cases in which the cyclotron-produced $^{18}$F-aqueous solution could be used directly as an off-the-bench reagent, without the need for the tedious drying step; this significantly reduces precious reaction time and drastically improves the reliability of the [$^{18}$F]fluorination. To date, this reaction has been performed over 10 times without a single RCY under 90%. Also, in stark contrast to [$^{18}$F]-SFB (**26**), the radiosynthesis is technically simple: the aqueous [$^{18}$F]fluoride is placed in a glass vial, an ACN solution with dissolved **30** is added, heated to 105 $^o$C for 10 minutes, and injected directly into the HPLC for purification. Overall, we can rapidly access 35-40 mCi of **31**, starting from only 50-55 mCi of aqueous [$^{18}$F]fluoride within 1 hour after HPLC purification.

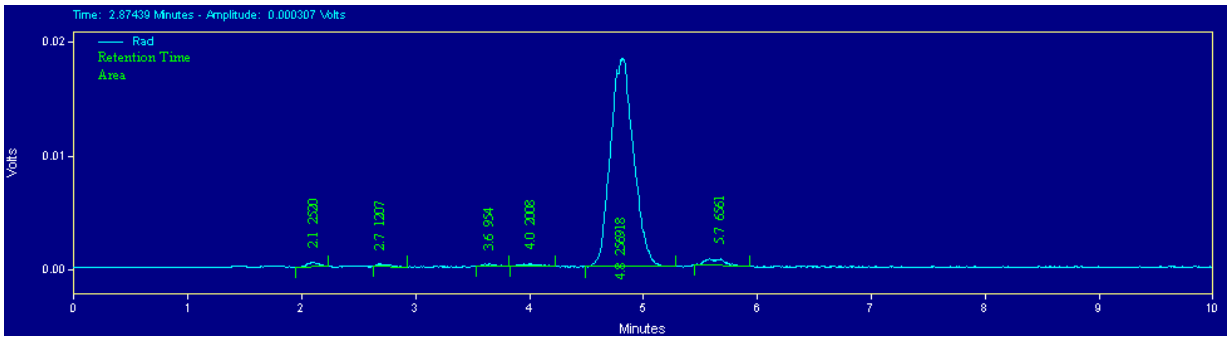


**Figure 2.3.** Crude radio-HPLC trace of the [$^{18}$F]fluorination of **30** (retention time = 4.82 minutes) under aqueous conditions.

The original objective of the project was to develop mild and efficient methodology through Si-$^{18}$F bond formation to address the shortcomings of C-$^{18}$F strategies. Although the base-free, 105 $^{o}$C reaction can be considered a milder alternative to the exceedingly harsh temperatures (in excess of 130 $^{o}$C) and basic conditions (pH ~9) required for the C-$^{18}$F approaches, our present reaction was still far from the ideal room temperature reactions we had initially envisioned. We began to re-investigate this possibility through two strategies. First, we drastically reduced the amount of added base in the drying step, which had originally caused extensive decomposition, such that only 0.1 mg and 1 mg of $K_2CO_3$ and $K_{222}$ respectively were used. Secondly, to improve the re-solubilization of the [$^{18}$F]fluoride salt with PhH, we switched the glass vial for a plastic one, since it was hypothesized that the anion would have less affinity for the plastic and therefore might be more readily redissolved into the PhH solution.

In the midst of finding the best vial for this purpose, we initially chose an unknown, clear plastic vial that maintained full integrity of the vessel wall during the drying step (ACN, 105 $^{o}$C, 0.1 mg $K_2CO_3$ and 1 mg $K_{222}$). Upon addition of the precursor in PhH, however, portions of the vessel wall appeared to dissolve, and it was belatedly realized that the unknown vial was polystyrene-based. Quite surprisingly though, in the presence of miniscule amounts of dissolved polystyrene, RCYs were high (in excess of >90%), with a significant reduction in side product formation, as determined by the radio-HPLC trace. After considerable screening of amounts and other polymers (i.e., $PEG_{2000}$), we found that 25-50 µg of polystyrene was sufficient to maintain high RCYs (Scheme 2.14), albeit in slightly longer reaction times (15 minutes); this amount was also sufficient to inhibit the undesired decomposition previously seen (Figure 2.2) and to afford high radiochemical purity (Scheme 2.14, bottom) in the crude radio-HPLC trace.

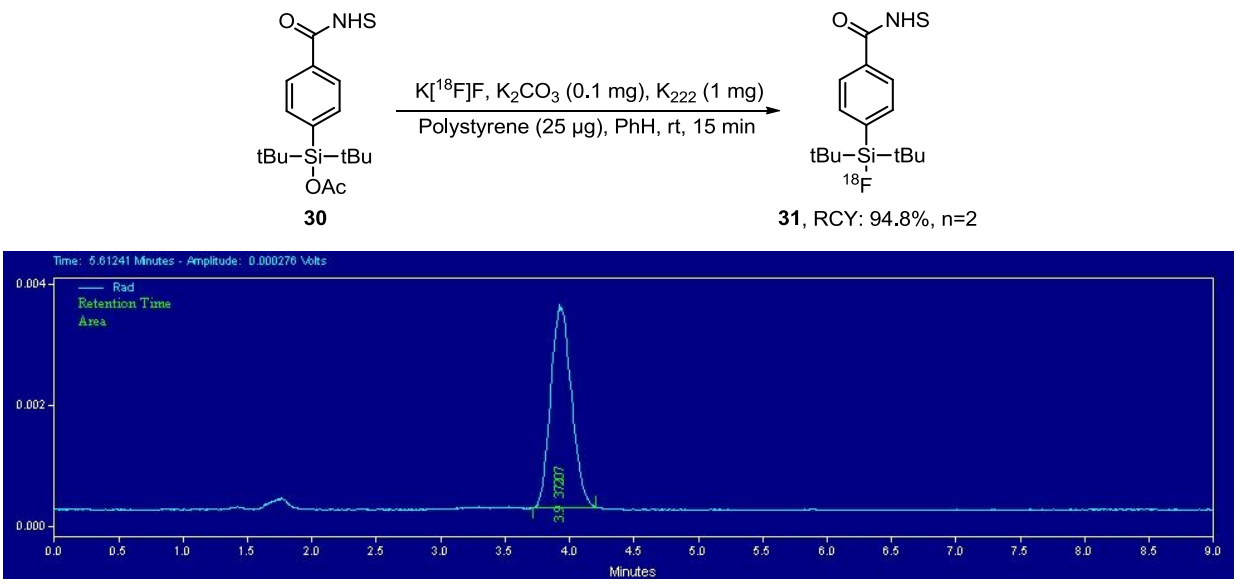


**30** **31**, RCY: 94.8%, n=2

**Scheme 2.14.** Room temperature [$^{18}$F]fluorination of **30** in the presence of lowered base and polystyrene. Bottom: Crude radio-HPLC of the [$^{18}$F]fluorination showing an efficient formation of a single desired $^{18}$F-compound (Retention time = 3.93 minutes).

Overall, we have established a superior method in the realm of Si-$^{18}$F bond formation strategies through the use of silyl acetates, which have proven to stable yet extremely reactive to [$^{18}$F]fluoride anion, through two approaches to afford rapid and efficient formation of the desired [$^{18}$F]fluorosilane products in high RCYs (>90%) and specific activities (3500-3800 Ci/mmol). To demonstrate the utility of this approach, we prepared a $^{18}$F-labelled version of an estrogen dendrimer conjugate (EDC, **32**) to evaluate its *in vivo* biodistribution in the context of the cardiovasculature (Scheme 2.15).[32-34] A simple dilution of the $^{18}$F-$H_2$[$^{18}$O]O water with acetonitrile and dissolved NHS-silyl acetate (**6**) and heating at 105 $^{o}$C for 10 minutes yielded **31** in high RCY. After cooling to room temperature, the reaction mixture, without any extraction, is injected directly into the HPLC to afford **7** in high radiochemical purity (>99%) and specific activity. The purified [$^{18}$F]fluorosilane product can be readily appended to EDC (**32**) within 10 minutes, albeit in somewhat varying RCYs of **33** (60-98%). The attractiveness of the approach lies heavily in the efficiency of the radiofluorination reaction: beginning with 50 mCi, the reaction sequence can reliably afford 15 mCi of the desired compound (**33**) after 2 hours. This is a highly attractive feature, especially when conducting time-sensitive animal studies that are dependent on sufficient amounts of activity of the radiotracer at a specified time.

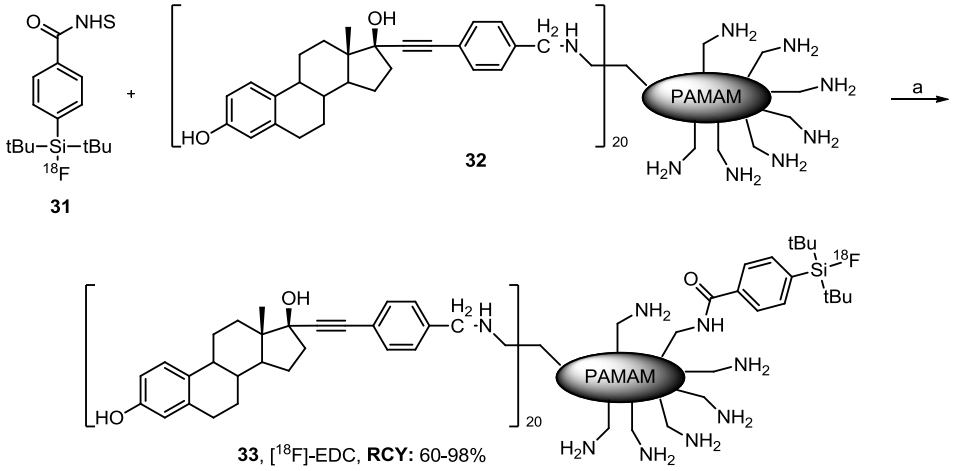


**Scheme 2.15.** Radiosynthesis of [$^{18}$F]EDC through the Si-$^{18}$F approach. (a) MeOH, rt.

Of the necessary steps for radiotracer production, the HPLC purification step is by far the most time-consuming. The process involves exceedingly long retention times (20-30 minutes), especially for short-lived isotope work, which is generally needed to effectively separate the large excess of precursor from the [$^{18}$F]fluoroproduct. Most HPLC purifications involve reverse phase conditions, and therefore, the collected fractions of the radiotracer are present in varying concentrations of acetonitrile and water. The volume of the liquid can be quite high (~10 mL), and because the amount of organic solvent present is not compatible with animal work, it must be removed. The standard procedure typically involves dilution of the collection activity with water to a total volume of 50 mL which is then passed through an intricate array of Teflon tubing to capture the radiotracer on a C18 cartridge. After additional washings with water, drying over a stream of nitrogen and elution of the labeled organic species with ethanol, this step alone consumes 30 minutes. Moreover, the dilution step causes loss of activity from precipitation on the vial wall, and at times, the C18 cartridge is not fully effective at capturing the radiotracer. Overall, both complicated steps involve at least 45-60 minutes of effort, which equates to approximately a quarter of the activity being lost from decay processes alone, in addition to the losses within the tubings and vials. Thus, a more efficient protocol is needed to maximize retrieval of the desired radiotracer.

In an attempt to circumvent these shortcomings and bypass this HPLC purification process altogether, we have modified our original silyl acetate moiety with acid units that are either tethered to beads or chromatographically distinct (made extremely polar with polyethylene glycol chains) (Scheme 2.16). Because reaction of the silicon atom with [$^{18}$F]fluoride ion will release the labeled [$^{18}$F]fluorosilane, any remaining precursor should be easily separable by

solid-phase extraction in the case of polar esters or removed by simple filtration in the case of the beads. In fact, the bead technology could be adapted to precursor cartridges, where the fluoride ion is introduced by flow, and only labeled product emerges from the cartridge. If successful, this will enable kit-like protocols that will streamline reactions and facilitate rapid product isolation and purification.

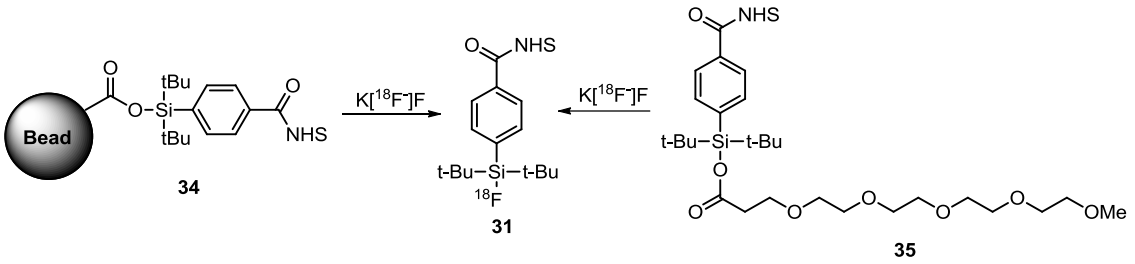


**Scheme 2.16.** Proposed HPLC-free strategy for the synthesis of **31** through the use of polar PEG chains or a bead system.

To date, this technology is still under development, but promising results have already been obtained. As shown in Figure 2.4, [$^{18}$F]fluorination of the original silyl acetate NHS derivative (Scheme 2.13) yielded a HPLC UV chromatogram showing significant amounts of mass, including starting material and other decomposition products, that must be removed before the next conjugation step can be performed. However, when the PEG-based derivative (**35**) was utilized (Scheme 2.17), there is a tremendous reduction of mass in the UV trace with only two peaks present: solvent front (1.5 min) and residual PhH (2.5 min). Radiochemical yields (50-70%) and specific activities appear promising, with the radiochemical purity being the only limiting factor to date (~85%). Nevertheless, in the event of high radiochemical purity, this highly encouraging approach would be a significant advancement for the field since [$^{18}$F]fluorosilane products could be rapidly accessed within minutes, devoid of the time-consuming HPLC purification process, and used directly in the next conjugation step. In the case of the EDC labeling procedure (Scheme 2.15), where total production time is 2 hours, application of the PEG-based strategy could significantly reduce the whole process down to 20 minutes. Further investigations into the factors contributing to the undesired decomposition of **31** are needed for this goal to be realized.

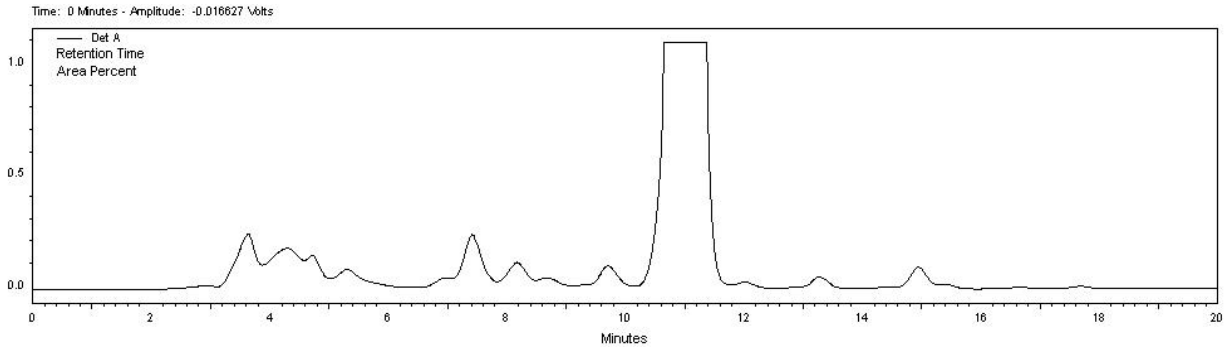


**Figure 2.4.** UV trace of the radiofluorination of **30** using the aqueous [$^{18}$F]fluoride method showing significant mass with the product present at 16 minutes.

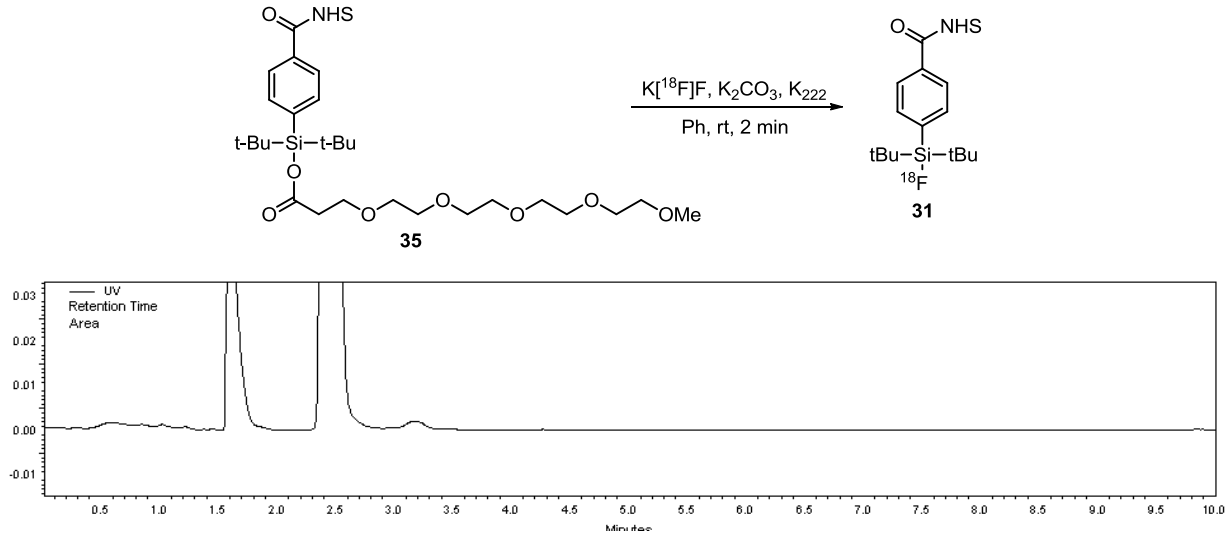


**Scheme 2.17.** UV trace of the radiofluorination of **35** showing negligible mass peaks of other products.

*B. Si-$^{18}$F Small Molecules*

A significant portion of PET agent development involves small-molecule research. The approach is largely conducted through nucleophilic alkyl chain displacement, aromatic substitution or diaryliodonium salt C-$^{18}$F bond formation strategies; however, besides the problems associated with the high temperatures and basicity seen previously, these approaches also necessitate the use of protecting groups, which can potentially complicate efforts. A typical nucleophilic aromatic substitution reaction is shown in Scheme 2.18 (unpublished work), showing the minimum 2-step sequence with the isotope being introduced early in the sequence and a final deprotection step. Consequently, this approach restricts access to the more desirable one-step, late-stage [$^{18}$F]fluorination strategies that would be optimum for short-lived isotope work.

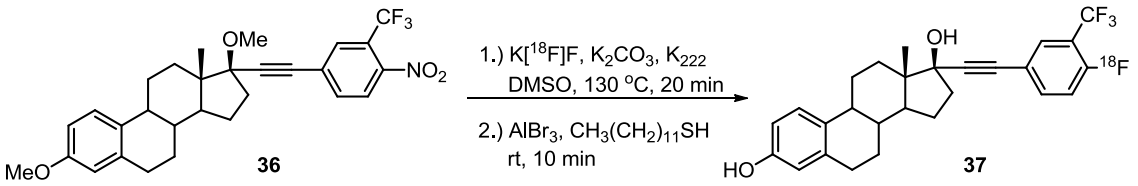


**Scheme 2.18.** Example of a required two-step approach for nucleophilic aromatic substitution.

Moreover in this sequence, the conditions ($AlBr_3$, dodecanethiol) needed for removal of the methyl ethers caused complete decomposition of the substrate. Attempts to perform the reaction in the absence of protecting groups were also unsuccessful, leading only to the formation of undesired [$^{18}$F]fluoroproducts. Switching to a more acid-labile tetrahydropyran (THP) group afforded a simple solution to this problem; however, similar solutions are restricted to relatively simple small molecule substrates. These synthetic issues become more complicated with complex, polyfunctional substrates since the flexibility and available protection/deprotection synthetic options become rather limited, and ultimately this leads to additional steps or harsh conditions that are most likely incompatible with these substrates. Protecting group-free strategies would render these problems obsolete and access substrates in a rapid, late-stage fashion. The use of Si-$^{18}$F bonds provides an intriguing solution to this problem.

In an effort to develop silicon-based ER PET imaging agents, we focused on appending the $(tBu)_2$-Si-OAc moiety at the 17α position of estradiol since this position is known to tolerate large substitution and produce ligands that still retain high affinity for the estrogen receptor.[35] Beginning with alkylation of the iodophenol (**39**) with the Boc-protected bromide (**38**), acid hydrolysis of the Boc group, followed by a Sonogashira reaction with commercially available ethynyl estradiol (**42**), afforded the requisite amine **43**, which reacted readily with the NHS ester **30** to yield the desired precursor (**44**) for [$^{18}$F]fluorination (Scheme 2.19).

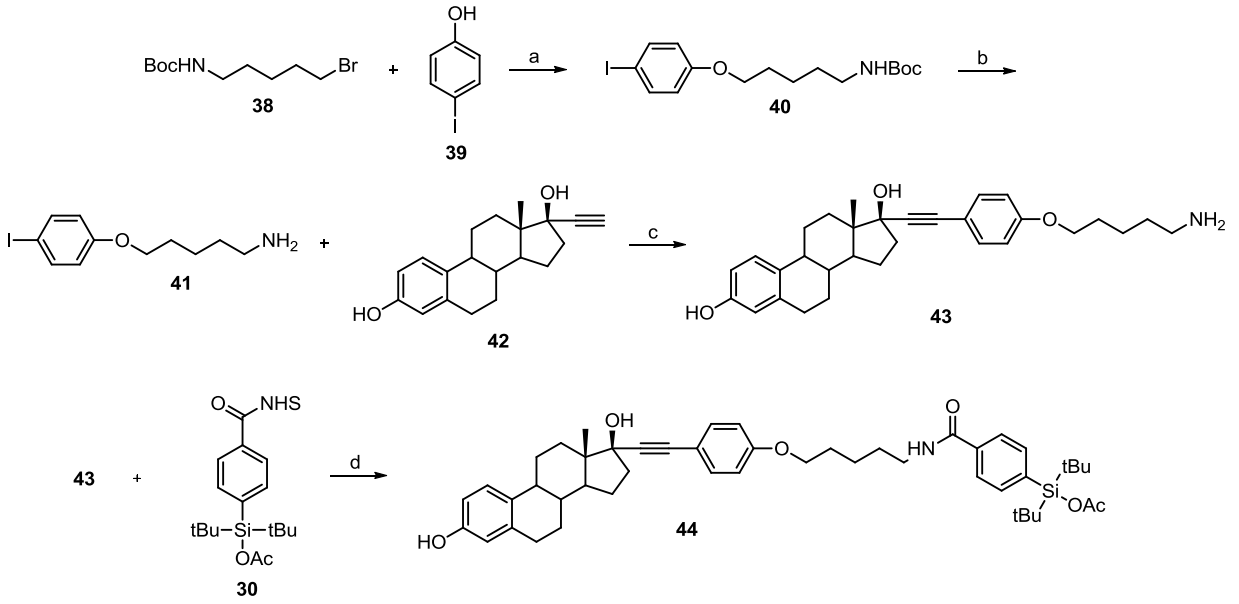


**Scheme 2.19.** Synthesis of the small molecule [$^{18}$F]fluorination precursor for Si-$^{18}$F-based ER PET imaging agents. (a) $K_2CO_3$, DMF, 55 $^{o}$C; (b) $SiO_2$, rt; (c) piperidine, CuI, $PdCl_2(PPh_3)_4$, ACN, 55 $^{o}$C; (d) **30**, TEA, DMF, rt.

Similar to the radiosynthesis of **30**, we subjected silyl acetate **44** to the two originally discovered conditions, and in both instances, high radiochemical yields and specific activities were obtained (Scheme 2.20). Under the aqueous [$^{18}$F]fluoride method, **44** reacted rapidly in near quantitative yield with only a single [$^{18}$F]fluorinated product being formed, as shown in the radio-HPLC of the crude reaction product (Scheme 2.20, bottom). The efficiency of this protecting group-, drying step-, and base-free reaction is exemplified by the preparative recovery of **45**, where over 60% (non-decay corrected) of the starting activity is present in the desired compound. In contrast to the protecting group strategies, the silyl acetate moiety enables a direct, one-step [$^{18}$F]fluorination into a complex substrate in the presence of acidic functionality in a highly efficient (one [$^{18}$F]fluorinated product, only 45 minutes total), late-stage fashion.

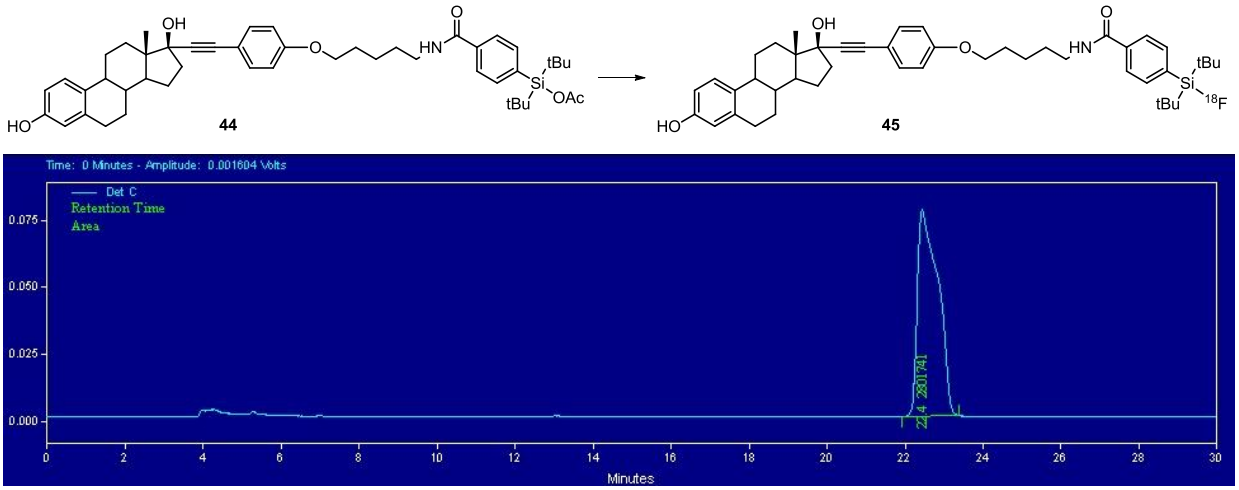


**Scheme 2.20.** Radiosynthesis of Si-$^{18}$F-based ER small molecule (**45**). Top: Method A- K[$^{18}$F]F, $K_2CO_3$, $K_{222}$, DMSO, rt, 10 min, RCY: 86.8% (n=2); Method B: $^{18}$F-$H_2$[$^{18}$O]O, ACN, 105 $^{o}$C, 10 min, RCY: 94.4% (n=2); SA = 2300-2500 Ci/mmol. Bottom: crude radio-HPLC of the reaction showing only a single $^{18}$F-product being formed (Retention time = 22.4 minutes).

The only difference from the original conditions was the use of DMSO rather than PhH in the room temperature method. Use of PhH was initially attempted, and a quantitative conversion to a [$^{18}$F]fluorinated product was observed by radio-TLC; however, co-injection with the cold standard revealed a different and still unidentified product. Switching the solvent to DMSO, however, afforded the desired compound in high radiochemical yields.

*C. Masking the High Lipophilicity of the (tBu)$_2$-Si-$^{18}$F Group with PEG Chains*

From a chemical perspective, the silyl acetates have proven to be ideal substrates: easily prepared and bench stable, yet highly reactive to [$^{18}$F]fluoride ion and able to give labeled products in exceptional RCYs and SAs, even in the presence of water and protic functionality. Despite these merits, a major shortcoming of this approach is the high lipophilicity of the corresponding products, which can significantly alter the *in vivo* behavior of a tracer, especially for compounds of low molecular weight. Previous investigations of similar [$^{18}$F]fluorosilane products showed poor biodistributions, with high accumulation in the liver and excessive nonspecific binding to nontarget tissue.[36] Moreover, the presence of the two bulky *tert*-butyl substituents significantly reduces the likelihood of receptor tolerance, and binding affinities can suffer considerably.

However, modification of the original *tert*-butyl design with smaller substituents (e.g., methyl groups) revealed significant hydrolysis, indicating that the *tert*-butyl groups are required

for engendering high *in vivo* stability of the Si-$^{18}$F bond. Attempts to counter the lipophilicity of the group with more polar PEG chains, carbohydrates, or quaternary ammonium salts have afforded only minor improvements in the behavior of these agents.[37,38] Therefore, strategies aimed at masking the high lipophilicity of the $(tBu)_2$-Si-$^{18}$F moiety to improve the *in vivo* pharmacokinetics and biodistributions of these agents are needed.

Our original attempt to develop silicon-based ER imaging agents (Scheme 2.20) yielded potential tracers with negligible affinity for the receptor (RBA: ERα, ERβ = <0.1%) and thus were of little utility to us. To improve binding affinities for ER, we became interested in a common nonsteroidal motif, based on a 1,1-diarylethylene unit, that is well-known to afford potent estrogens having high affinity for the receptor.[39] For our purpose, we focused on the adamantane derivative, which is a minor modification of the well-known nonsteroidal estrogen, cyclofenil (Figure 2.4).[40] To provide an attachment point for our silyl acetate moiety, we appended ethylene glycol chains of varying length bearing a reactive terminal amine group for reaction with the NHS ester **27**, and we evaluated their relative ligand binding affinities for the estrogen receptor in competitive radioligand binding assays using [$^3$H]-17β-estradiol ($E_2$) as a tracer and full-length human estrogen receptors, ERα and ERβ. The results, as shown in Figure 2.5, are expressed as relative binding affinities (RBAs) and are referenced to the affinity of $E_2$, which is set to 100%. The hydrosilane derivatives (**47**, **49**, and **51**) were used in these studies due to their ease of preparation, handling and enhanced stability during the assay itself. Due to the similar nature of the hydrosilanes, it is hypothesized that the fluorine derivatives will have comparable values.

Modification of the original high affinity compound (**46**) with the silane moiety, $(tBu)_2$-Si-H (**47**), resulted in a significant reduction in the affinity for the receptor. Extension of the amine side chain with a single tetraethylene glycol (TEG) linkage (**49**) afforded minor improvements in affinity, albeit still considerably less than the underivatized compound (**48**). Only when an additional TEG chain was attached could sufficiently high binding affinity be obtained (**51**). A possible reason for the tolerance of the bulky silane moiety and subsequent increase in RBA in the presence of the di-TEG moiety is the result of the ability of this moiety to enwrap the hydrophobic silane group, removing it from the unfavorable aqueous environment and ensconcing it in a more organic-friendly environment as a result of multiple oxyethylene group interactions between the cyclofenil and glycol chain. Such possibilities were confirmed through 2-dimensional NMR studies.

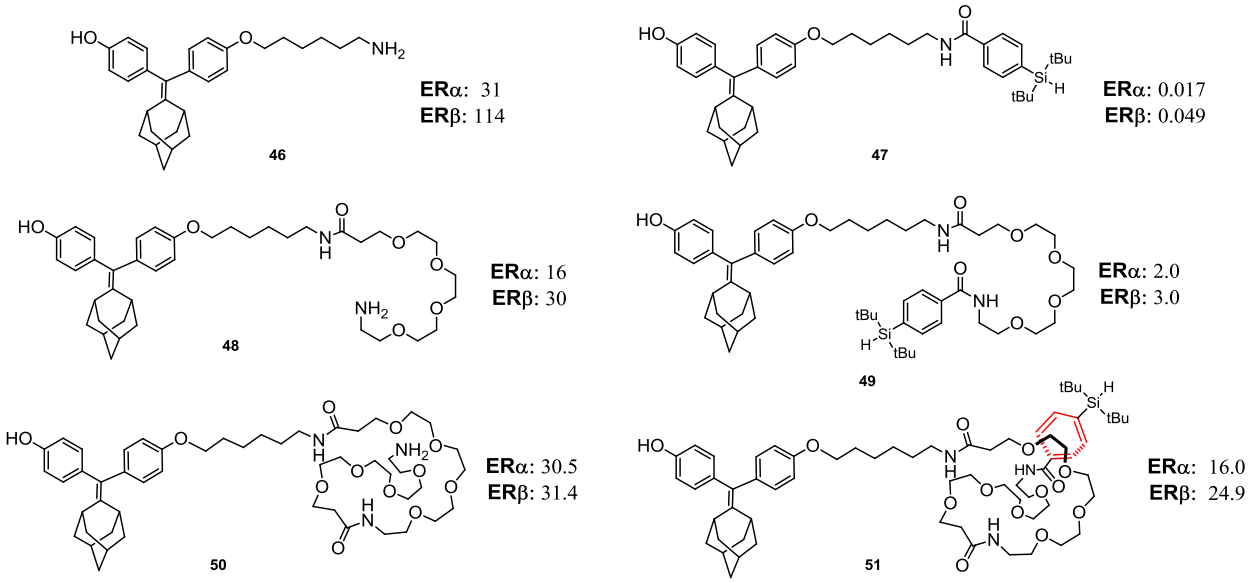


**Figure 2.5.** RBAs of various silyl-based adamantane compounds showing the needed for a diTEG linkage to obtain high affinity estrogens.

The preparation of diTEG silyl acetate **59** commenced from mesylate **52** (Scheme 2.21). The formation of phthalimide **54**, followed by selective mono-alkylation of diphenol **55** and acid deprotection, afforded amine **57** in high yield. An iterative double amidation/deprotection sequence afforded the requisite free amine **58** from which the silyl acetate **30** could be appended.

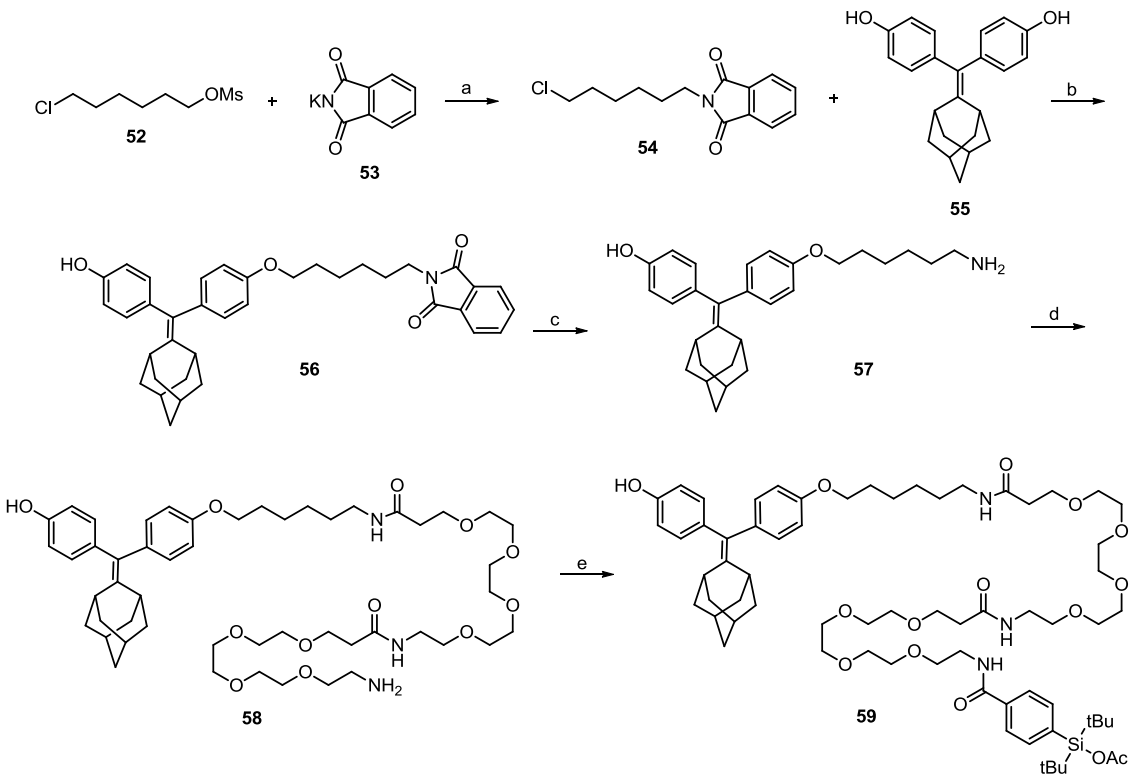

**Scheme 2.21.** Synthesis of the diTEG-adamantane compound (**59**). (a) DMF, 50 $^{o}$C; (b) $K_2CO_3$, DMF, 75 $^{o}$C; (c) $H_2NNH_2$, MeOH, rt; (d) NHSCO-diTEG-NHBoc, TEA, DMF, rt; TFA, DCM, rt; (e) **30**, TEA, DMF, rt.

Application of the aqueous [$^{18}$F]fluoride method afforded exceptional RCYs (Scheme 2.22). Key to the success of this approach was effective separation of starting material (**59**) from the [$^{18}$F]fluorosilane product **60**. Since these are relatively high molecular weight compounds and the reaction involves only a minor substitution for [$^{18}$F]fluoride ion, it is critical to obtain clean separation of the two in order to reach high effective specific activities. Additional investigations are still needed to find the optimal HPLC conditions for this important separation. The promise of this strategy as a viable masking approach to counter the high lipophilicity of the [$^{18}$F]fluorosilane moiety is still currently being evaluated in animal models.

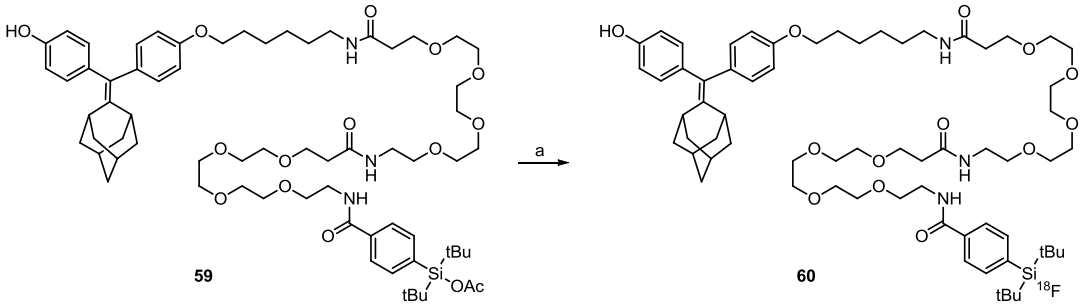

**Scheme 2.22.** Radiosynthesis of **51**. (a) $^{18}$F-$H_2$[$^{18}$O]O, ACN, 105 $^{o}$C, 10 min, RCY: 91.6% (n=2).

*D. Direct, One-Step Labeling of Peptides Through Si-$^{18}$F Bonds*

[$^{18}$F]Fluorinated peptides have been a focal point of a great deal of research in recent years in an attempt to improve and expand on the successes of [$^{18}$F]FDG. Their tremendous potential has been demonstrated in imaging several diseases, especially cancers, due to their favorable pharmacokinetics, metabolic stabilities and higher tolerance towards bulky substitutions.[41] However, progress in the area has been exceedingly slow: Only a few $^{18}$F-labelled peptides have been evaluated in humans,[42-44] and this has been largely attributed to the lack of efficient methodology to access these agents for clinical use.

To demonstrate the versatility of the silyl acetate moiety for radiolabeling peptides and to improve on the existing methodology,[25,26] we became interested in the direct radiofluorination of an RGD peptide. Cyclic RGD pentapeptides are well-known to have high binding affinity and selectivity for the most well-known member of the integrin family, $\alpha_v\beta_3$.[45,46] Studied mainly for its role in tumor growth, progression, and angiogenesis, $\alpha_v\beta_3$ is a target for radiotracers that has the potential for early detection of metastatic tumors, and for monitoring tumor growth, metastasis and therapeutic response by PET imaging.[47,48]

Application of the $(tBu)_2$-Si-OAc moiety for peptide labeling commenced with NHS ester **30** being coupled to the free $-NH_2$ of the lysine residue of commercially available cRGD to afford the desired [$^{18}$F]fluorination precursor (**61**, Scheme 2.23). The initial difficulty in assessing the success of the radiofluorination reaction was due to the inability of the [$^{18}$F]fluorosilane product (**62**) to move on a silica gel TLC plate. Due to the safety hazards of working with positron emitters, radiochemists are rather limited by the availability of analytical instruments that can be utilized for product detection. The setups for traditional analytical instruments (NMR, UV-Vis, IR, and MS (unless coupled to a HPLC)) are incompatible with the specific safety and handling procedures that are demanded by PET isotopes. As a result, radio-TLCs and –HPLCs are two of the most common instruments available to radiochemists for product analysis.

A radio-TLC is a straightforward method for analyzing the conversion of [$^{18}$F]fluoride ion into [$^{18}$F]fluoroproducts. Key to this is the fact that unreacted [$^{18}$F]fluoride ion remains at the baseline of a silica gel TLC plate, while any F-18 organic products will move with the solvent front as is typical for traditional TLC development. After development, the plate is then placed on a TLC scanner, which can detect the activities along the path length (Figure 2.6). Since the resolution between unreacted and reacted $^{18}$F-peaks is not ideal (peaks are generally very broad), TLC development often involves very polar solvent conditions, such as 100% EtOAc or

5%MeOH/DCM. Consequently, a single peak may comprise of multiple [$^{18}$F]fluoroproducts. Thus, radio-TLCs are only useful for determining conversion rates, and the corresponding yields are not representative of the true radiochemical yields of the desired compound or radiochemical purities. Injection of the reaction mixture into the HPLC and analysis of the trace is a better indicator of both RCY and RCP, since it allows for better resolution of the [$^{18}$F]fluorinated products.

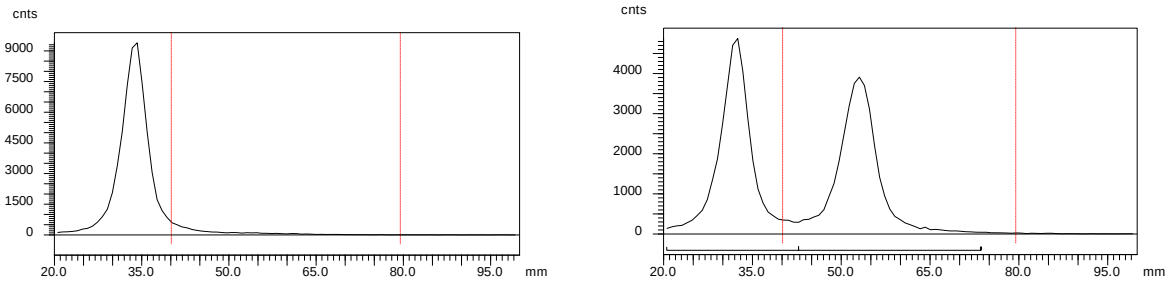


**Figure 2.6.** Depiction of a radio-TLC analysis. Left: peak remains at the baseline and is indicative of unreactive [$^{18}$F]fluoride (35 mm). Right: reaction analysis showing unreacted [$^{18}$F]fluoride (35 mm) and [$^{18}$F]fluoroproduct (55 mm).

In the case of the radiofluorination of cRGD (**61**, Scheme 2.23), the corresponding product (**62**) did not move on the TLC plate, possibility indicating no conversion to **62**. However, injection of the cold standard with the reaction mixture revealed co-elution with a single radioactive peak in the radio-HPLC, suggesting product formation. Since the product did not move on the TLC plate, it was also difficult to ascertain incorporation yields. After extensive screening of elution solvents and TLC plates, we were able to find conditions (C18 plate, 80% ACN, 20% $H_2O$, 0.1% TFA) that could be used to analyze the reaction, albeit in low but workable resolution.

Similar to the [$^{18}$F]fluorination of the small-molecule example (Scheme 2.20), DMSO was the preferred solvent for **61** (Scheme 2.23) and resulted in excellent yields of **62** within 15 minutes, giving a product in high radiochemical purity before further purification. The reaction times were slightly longer than the previous examples, and this is most likely attributed to the nature of the peptide, but further analysis of the reaction revealed high RCYs (in excess of 60%) within 5 minutes with only a slight increase in the yield with an additional 10 minutes.

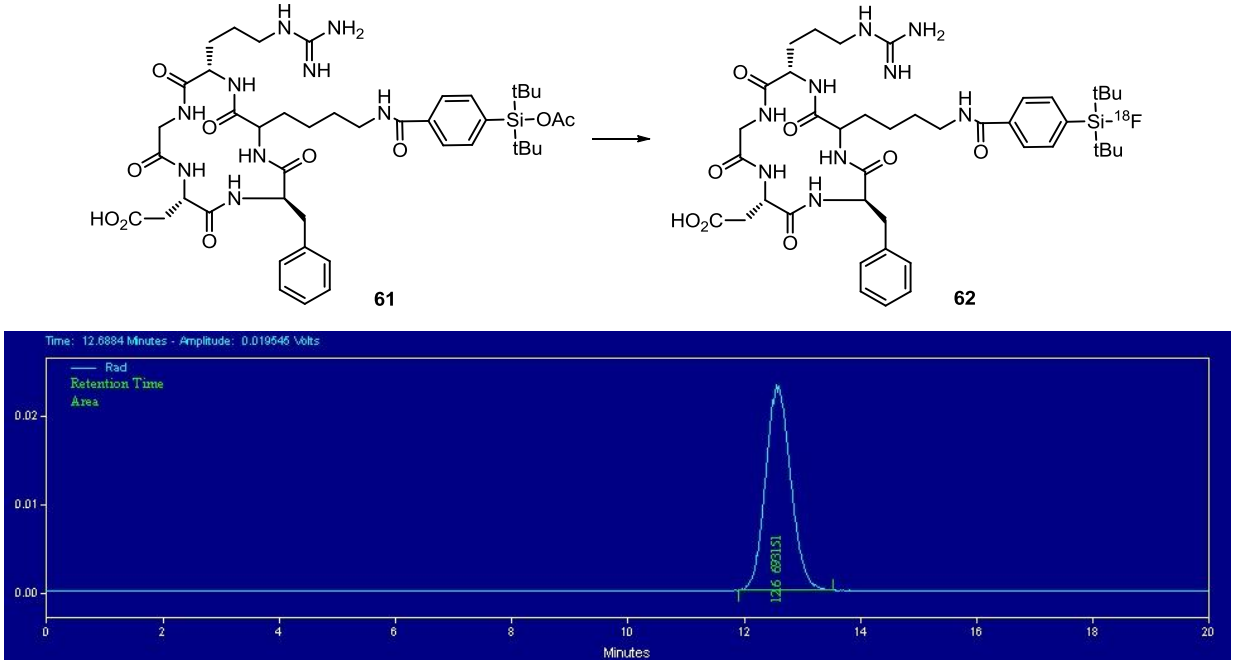


**Scheme 2.23.** Direct, one-step radiosynthesis of a complex peptide **62**. Method A: $^{18}F$-$H_2[^{18}O]O$, ACN, MeOH, 105 $^{o}C$, 10 minutes, RCY: 81.1% (n=2); Method B: $K[^{18}F]F$, $K_2CO_3$, $K_{222}$, DMSO, rt, 15 minutes, RCY: 85.7% (n=2). Bottom: radiochemical purity after purification of **62** (retention time = 12.6 minutes).

The aqueous [$^{18}$F]fluoride protocol required a minor modification, the addition of MeOH as a cosolvent, since the original conditions could not fully solubilize the peptide. Nevertheless, **61** reacted rapidly in high RCY within 10 minutes, with a single [$^{18}$F]fluorinated product being formed. Even with the rather harsh, elevated temperature (105 $^{o}$C), no decomposition of the sensitive peptide substrate was observed, most likely the result of the short reaction time. Upon cooling to room temperature, the crude reaction mixture can be injected directly into the HPLC without the need for any additional purification, and the peak activity is collected on a C18 cartridge and eluted with ethanol, ready for animal injection in less than 1 hour.

The recovery yields were not exceedingly high or representative of the radio-TLC and -HPLC analysis. Although yields were in excess of 80% with a single product being formed, only 4 mCi were obtained from 20 mCi of starting activity. The most likely source of loss in this case was in the HPLC column. After injection and recovery of **62**, subsequent counting of the HPLC column with a Geiger counter revealed significant amount of activity stuck in the column. It seems as though the product precipitates within the HPLC column after removal of the DMSO from elution and mixing with the HPLC eluent (ACN/$H_2O$/TFA solution). This is a difficult problem to solve, and switching to a more polar solvent is not the simple solution. Since there is

a large excess of starting material, typical HPLC retention times are deliberately long (20-30 minutes) to provide sufficient separation of the two materials and often involve more aqueous-based reverse phase conditions. Switching to a more organic-based condition will decrease retention times, hamper separation, and ultimately result in contamination of the [$^{18}$F]fluoroproduct with starting material. When working with high molecular weight substrates such as this, long retention times are essential for separation since the structural and electronic differences are exceedingly small. Attempts at varying the HPLC conditions resulted in lower specific activities, and the original conditions are currently the best available for this application.

## IV. DISCUSSION

The potential impact of PET imaging on the fields of medical care and drug development is undeniable. In the clinic, the functional information of diseased states obtained through PET imaging techniques has significantly transformed medical diagnosis from a mere identification tool towards characterizing the molecular processes involved with disease progression.[49] The ability to characterize disease at the molecular level through imaging provides an indispensable clinical tool that can aid in the diagnosis, prognosis, and the design of proper therapeutic regimens for a particular diseased state.[50,51] As a result, PET imaging has received significant attention recently due to the possibility of developing medicine that is personalized for each patient.[51] By individualizing treatment plans, the expectation is that patient outcomes will be greatly improved through better diagnosis and targeted therapies, as well as safeguarding against the use of unnecessary, harmful medical procedures. This enticing possibility, however, relies on the clinical availability of well-designed radiotracers for specific biomarkers or diseased states that can yield the desired information for personalized medicine to develop. Unfortunately, the availability of such agents are lacking, and the field continues to be dominated by a single, nonspecific agent, [$^{18}$F]FDG.[1]

Of the multiple components that encompass the PET imaging process, target discovery and software/hardware development significantly outpace the advancement of novel imaging probes. A significant impediment to the field is the lack of synthetic approaches that can access these desired probes in a mild and efficient manner that is demanded by the sensitivity of many of these substrates. Consequently, the lack of compatible and efficient methodology restricts their clinical evaluation and development. Mainstream organic chemistry is dominated by an innumerable amount of synthetic building blocks and methodology that has enabled the

construction of almost any imaginable structure. However, the $^{18}$F-labelling chemistry, reactions are limited to a single entity, [$^{18}$F]fluoride anion, and incorporation of the isotope is not trivial. Consequently, the available methodology is extremely limited and as a result, tracer development is exceedingly slow.

A significant portion of radiofluorination reactions are predicated on C-$^{18}$F bond formation. Although successfully employed for decades, this approach is not without its issues. First, this approach is only well-established in two areas: $S_n2$ alkyl displacement and nucleophilic aromatic substitution. Access to agents not included in these strategies involves indirect, multi-step approaches that are time-consuming and inefficient, and ultimately limit the practicality of these approaches. Second, the conditions for incorporation of the isotope are often harsh (basic, high temperatures) and require protecting groups. As a result, these conditions restrict the use of most substrates, especially biomolecules, for the ideal, one-step approach and complicate synthetic efforts significantly. Consequently, the incompatibility of complex, polyfunctional biomolecules has necessitated the use of alternative strategies to access these agents in a rapid, late-stage fashion.

Interest in Al-$^{18}$F, B-$^{18}$F, and Si-$^{18}$F bonds has been largely driven by the potential of peptides, proteins, and antibodies as imaging agents and the need for these substrates to be radiolabeled under mild conditions, preferably in an aqueous environment. Our interest in the field was spurred on by the rapid and efficient manner of Si-$^{18}$F bond formation and the most likely compatibility of the corresponding Si-$^{18}$F products (over the Al-$^{18}$F and B-$^{18}$F ones) within the estrogen receptor system. Of the reported conditions, both are inherently limited to low specific activity and have little value in receptor-based PET imaging. Consequently, we sought to improve on the existing methodology through the use of our silyl acetate precursors which have proven to be ideal substrates: easily prepared and bench-stable, yet highly reactive to [$^{18}$F]fluoride ion, giving high radiochemical yields and specific activities. The versatility of the silyl acetate moiety was demonstrated in three main active areas of research: adaptor molecules, small molecules, and peptides.

Although a direct, one-step radiofluorination is highly desirable, the incompatibility of some substrates or the difficulty associated with a one-step approach demand a synthetically simpler indirect, multistep strategy through the use of small adaptor molecules. However, the existing available chemistry is flawed by complex, inefficient sequences that make translation to the clinic exceedingly difficult, especially since the isotope is incorporated very early in the

sequence. Alternatively, our NHS ester **30** reacts rapidly with aqueous [$^{18}$F]fluoride ion without the need for the time-consuming drying step or added base. Exceedingly high levels of activity of **31** (35-40 mCi from starting 50-55 mCi of activity) can be quickly accessed within 45 minutes after HPLC purification. The utility of the method was demonstrated in the radiosynthesis of [$^{18}$F]-EDC where 15 mCi of material can be routinely synthesized from 50 mCi of activity within 2 hours.

To illustrate the utility of the approach for radiolabeling of small molecules, we became interested in developing Si-$^{18}$F–based ER PET imaging agents. The problem with small-molecule radiosyntheses is their multi-step approaches which typically involve deprotection steps and/or functional group manipulations and restricts the use of direct, late-stage [$^{18}$F]fluorinations to rapidly access functionally complex agents. The protection/deprotection sequences are usually amenable to relatively simple small molecules, but this becomes more complicated with complex substrates and only further undermines the practicality of the approach. However, the Si-OAc moiety facilitates a protecting group-free strategy to generate a complex [$^{18}$F]-estrogen (**45**) in high RCYs and preparative yields through a simple, late-stage aqueous [$^{18}$F]fluorination. We also developed a complementary room temperature [$^{18}$F]fluorination method for those substrates that may not be compatible with the higher temperatures required in the previous method. Similarly, the reaction proceeds smoothly, in the presence of protic functionality, with the K[$^{18}$F]F-$K_{222}$ cryptate in high RCYs within 10 minutes.

One of the more active areas of research is the radiolabeling and *in vivo* investigations of peptides. However, despite their attractive *in vivo* properties, $^{18}$F-labelled peptides have had limited success, with only a few being evaluated in humans.[42-44] The dismal success rate has largely been attributed to the lack of methodologies that would enable more convenient and efficient preparation of these agents. Because of this, a majority of the peptides are radiolabeled with a useful “wash-in” of radiometals, especially with Cu-64, despite their less than ideal nuclear properties.[54] The direct, one-step labeling of silyl peptides with [$^{18}$F]fluoride ion has only recently been demonstrated as a viable strategy, albeit in low specific activities in most instances.[26] Application of the silyl acetate chemistry, however, afforded high RCYs of cRGD **62** through both methods and in contrast to those previously reported, in high SAs. This is one of the first reported cases of high RCYs and SAs in a one-step [$^{18}$F]fluorination of peptides and should hold tremendous potential for future applications in this area.

Although the $(tBu)_2$-Si-OAc moiety has proven to be highly efficient at capturing [$^{18}$F]fluoride ion, the required two *tert*-butyl groups that are required to provide high hydrolytic stability to the Si-$^{18}$F bond can also have a tremendous impact on the *in vivo* behavior of the radiotracer, especially those of low molecular weight. Efforts to counter the high lipophilicity with PEG chains, sugars, or ammonium salts have yielded minimal success.[37,38] Our efforts to mask the impact of this group through the use of tetraethylene glycols has afforded extremely potent estrogens which can be readily labeled with F-18. This approach relies on the more polar TEG chains to effectively solvate the hydrophobic silane entity away from the unfavorable aqueous environment and into a more organic-friendly setting. This strategy appears to work best with a diTEG linkage, which provides significant improvements in the binding affinities for the receptor, as compared to the original silyl-estrogen. Unfortunately, high RBAs do not necessarily predict *in vivo* behavior, and further animal studies are still needed to validate this approach as an effective means to counter the problems associated with the $(tBu)_2$-Si-$^{18}$F moiety.

A concern for the majority of radiofluorination reactions is the purification process and specific activities, as the large excess of starting materials needed to drive the reaction to completion often can complicate purification efforts and generate tracers with low SA or effective SA. A notable feature of these silyl acetates is the low amount of precursor needed for the reaction. Traditionally, typical amounts of precursor range from 1-2 mg and can exceed 5 mg, especially when using iodonium salts or the hydrosilane chemistry. Since these reactions usually form nano-to-pico mole amount of [$^{18}$F]fluoroproducts, it is not difficult to see why the purification problem is so severe. However, the silyl acetates in all cases react rapidly in extremely low amounts (NHS ester (**30**, 0.1 mg, 0.28 µmol), $EE_2$ (**44**, 0.3 mg, 0.39 µmol), and peptide (**61**, 0.3 mg, 0.33 µmol)), which facilitates much easier purifications and ultimately is one of the main reasons for our high specific activities. Also, the problem with starting material contamination only serves to validate the PEG- and bead-based approaches as viable strategies, since this would eliminate the HPLC purification process altogether and allow for only the [$^{18}$F]fluorosilane product to be eluted off the cartridge, devoid of any starting material. Further studies are still needed to improve radiochemical purities.

Due to the presence of harmful ionizing radiation, $^{18}$F-labelling demands significantly different handling and tracer production protocols compared to mainstream organic chemistry. Even relatively simple purifications, such as extractions, are extremely difficult to perform, especially in relation to safety considerations. In almost all instances, production in the clinic is performed in automated synthesizers called modules to eliminate human error and maintain

reliable availability of tracers for patient use. These relatively simple machines serve as an all-in-one module for routine production from the end of bombardment to the final HPLC purification step and work especially well for standard procedures such as for [$^{18}$F]FDG, but the transition to more challenging protocols is not as straightforward. The machine functions through an intricate array of lines, filters, pumps, and columns and any additional step such as a simple extraction requires modification of the existing module. Minor modifications (i.e., extraction) can be readily accommodated into the machine, but the number of available options is rather limited, and at times, these modifications can often be a source of production failures. Consequently, the translation into the clinic demands simple and straightforward protocols. The silyl acetate moiety provides just that. A simple dilution of the cyclotron-produced aqueous [$^{18}$F]fluoride source and subsequent heating for 10 minutes enables rapid and efficient fluorination of precursors in high RCYs. After cooling and without any other manipulations, the reaction mixture is injected directly into the HPLC and provides the purified radiotracer within 1 hour. Application of the method, in the event of a suitable Si-$^{18}$F radiotracer, should provide a facile transition into the clinic.

## V. CONCLUSION

In summary, we have developed a rapid and efficient Si-$^{18}$F bond formation protocol based on silyl acetate precursors that is broadly applicable to small molecules and peptides. This method is particularly noteworthy given its experimentally simple, exceptional generality, and high level of functional group tolerance which permits entry to once previously inaccessible sensitive substrates, including complex, polyfunctional biomolecules, in a direct, late-stage approach to radiolabeling with F-18. The corresponding [$^{18}$F]fluorosilane products were obtained in high yields and specific activities, and the utility of the method was demonstrated in labeling a challenging biopolymer, an estrogen dendrimer conjugate (EDC), allowing its *in vivo* evaluation within the cardiovascular system. Current efforts have focused on addressing the high lipophilicity of the $(tBu)_2$-Si-$^{18}$F with ethylene glycol chains and is currently being validated in animal models as a viable approach.

## VI. METHODS

### Materials

All reactions were carried out under a nitrogen atmosphere with dry solvents using anhydrous conditions unless otherwise stated. Solvents used in the reactions were dried in a solvent delivery system (neutral alumina column). Reagents were purchased from Aldrich and used without further purification, unless otherwise stated. Yields refer to chromatographically and spectroscopically ($^1$H NMR) homogeneous materials, unless otherwise stated. Reactions were monitored by thin layer chromatography (TLC) carried out on Merck silica gel 60 F254 precoated plates (0.25 mm) using UV light as the visualizing agent and ceric ammonium molybdate and heat as developing agents. Flash column chromatography was performed on Silica P Flash silica gel (40-64 $\mu$M, 60 Å) from SiliCycle. $^1$H NMR spectra were recorded at 23 $^o$C on a Varian Unity-400, Varian Inova-500 or Varian Unity-500 spectrometer and are reported in ppm using residual protium as the internal standard ($CHCl_3$, δ = 7.26, $CD_2HCN$, δ = 1.94, center line, acetone-$d_6$, δ = 2.05, center line). The following abbreviations were used to denote the multiplicities: s = singlet, d = doublet, dd = doublet of doublets, t = triplet, q = quartet, m = multiplet and b = broad. Proton-decoupled $^{13}$C NMR spectra were recorded on a Varian Unity-500 (126 MHz) spectrometer and are reported in ppm using solvent as an internal standard ($CDCl_3$, δ = 77.16, $CD_3CN$, δ = 1.30, center line, acetone-$d_6$, δ = 29.80, center line). High resolution mass spectra were obtained at the University of Illinois School of Chemical Sciences Mass Spectrometry Laboratory. No-carrier-added [$^{18}$F]fluoride was produced at Washington University Medical School by the $^{18}$O(p,n)$^{18}$F reaction through proton irradiation of enriched (95%) [$^{18}$O]$H_2O$ using a RDS111 cyclotron. Screw-cap test tubes used for drying fluoride and radiolabeling were purchased from Fisher Scientific (Pyrex No. 9825). Radiochemical purification utilized a reverse-phase semi-preparative HPLC column (HPLC: Thermo P2000, Column: Agilent Zorbax SB-C18, 5 µm, 9.4 X 250 mm, Product #: 880975-202, λ = 254 nm, ACN/$H_2O$). For quality control, the radiochemical purity was determined by analytical HPLC (HPLC: P4000, Column: Altima C18, 5 µm, 250 mm, Product #: 88056). C18 Sep-Pak cartridges were purchased from Waters Corporation (Milford, MA, USA). For the thin-layer chromatography (TLC) analyses, EM Science Silica Gel 60 F254 TLC plates were purchased from Fisher Scientific (Pittsburgh, PA, USA). Radio-TLC was accomplished using a Bioscan 200 imaging scanner (Bioscan, Inc., Washington, DC, USA). Radioactivity was counted with a Beckman Gamma 8000 counter containing a NaI crystal (Beckman Instruments, Inc., Irvine, CA, USA).

**Estrogen Receptor Binding Affinity Assays**

Relative binding affinities were determined by a competitive radiometric binding assay using 10 nM [$^3$H]estradiol as tracer (Amersham Biosciences, Piscataway, NJ), and purified full-length human ERα and ERβ (PanVera/Invitrogen, Carlsbad, CA). Compounds were assayed from $10^{-4}$ to $10^{-9}$ M as equivalents of estradiol (20-fold lower than the molar concentration of the dendrimer itself). Incubations were for 18-24 h at 0 °C, and the bound compound-receptor complexes were absorbed onto hydroxyapatite (BioRad, Hercules, CA), and the unbound compound was washed away. The binding affinities are expressed as relative binding affinity (RBA) values, with the RBA of estradiol for both receptors being set at 100. The values given are the average ± range or SD for two or more independent determinations. Estradiol binds to ERα with a $K_d$ of 0.2 nM and to ERβ with a $K_d$ of 0.5 nM.

**4-(Di-tert-butylsilyl)benzaldehyde (24):** To a solution of 4-bromobenzaldehyde dimethyl acetal (1.20 g, 5.20 mmol) in THF (10 mL) at -78 $^o$C was added *n*BuLi (3.20 mL, 5.12 mmol, 1.6 M in hexanes) and left to stir at this temperature for 1 h. Triethylamine (0.86 mL, 6.26 mmol) was added into the reaction mixture before injecting di-*tert*-butylchlorosilane (3.25 g, 18.2 mmol) at -78 $^o$C. The reaction was left to warm to room temperature over 10 h before being quenched with EtOAc (50 mL) and sat. aq. $NH_4Cl$ (50 mL). The crude reaction was further extracted with EtOAc (40 mL), and the combined organic extracts were dried over $MgSO_4$ and concentrated *in vacuo*. Purification by column chromatography (Hex:EtOAc, 1:0→1:1) afforded **24** (0.84 g, 65.0%) as a white solid. Due to air sensitivity, the product was immediately used in the next reaction. $^1$H NMR (500 MHz, $CDCl_3$): δ 10.0 (s, 1H), 7.84 (d, *J* = 8.0 Hz, 2H), 7.77 (d, *J* = 8.0 Hz, 2H), 3.93 (s, 1H), 1.07 (s, 18H); $^{13}$C (126 MHz, $CDCl_3$): δ 192.9, 144.7, 136.8, 136.5, 128.6, 29.1, 19.3.

**4-(Di-*tert*-butylsilyl)benzoic acid (25):** To a solution of **24** (0.49 g, 2.00 mmol) in acetone (10 mL) at 0 $^o$C was added dropwise a freshly prepared Jones reagent until a reddish color remained before being quenched with MeOH (10 mL). The crude reaction was extracted with EtOAc (2 X 50 mL) from water (50 mL), and the combined organic extracts were dried over $MgSO_4$ and concentrated *in vacuo*. Purification by column chromatography (Hex:EtOAc,3:2) afforded **25** (0.45 g, 85.4%) as an off-white solid. $^1$H NMR (500 MHz, $CDCl_3$): δ 12.50 (br, 1H), 8.06 (d, *J* = 8.0 Hz, 2H), 7.69 (d, *J* = 8.0 Hz, 2H), 3.90 (s, 1H), 1.04 (s, 18H); $^{13}$C (126 MHz, $CDCl_3$): δ 172.9, 143.6, 136.1, 129.8, 129.0, 29.0, 19.2; ESI (m/z): 263.1 [M + 1].

**2,5-Dioxopyrrolidin-1-yl 4-(di-tert-butylsilyl)benzoate (26):** To a solution of **25** (0.26 g, 1.0 mmol) in DCM (20 mL) at 0 $^{o}$C was added cat. DMAP (5 mg) and *N,N'*-dicyclohexylcarbodiimide (0.21 g, 1.0 mmol). The resulting mixture was left to stir until the acid disappeared on TLC and quenched upon filtering off the dicyclohexyl urea. Purification by column chromatography (Hex:EtOAc,3:2) afforded **26** (0.35 g, 98.2%) as an off-white solid. $^{1}$H NMR (500 MHz, $CDCl_3$): $\delta$ 8.09 (d, *J* = 8.0 Hz, 2H), 7.74 (d, *J* = 8.0 Hz, 2H), 3.92 (s, 1H), 2.92 (s, 4H), 1.06 (s, 18H); $^{13}$C (126 MHz, $CDCl_3$): $\delta$ 169.5, 145.4, 136.3, 129.3, 125.6, 29.0, 25.9, 19.2; HRMS (ESI) calc'd for $C_{19}H_{28}NO_4Si$ [M + 1] 362.1788; found 362.1788.

**2,5-Dioxopyrrolidin-1-yl 4-(acetoxydi-tert-butylsilyl)benzoate (28):** To a solution of **27** (0.10 g, 0.25 mmol) in PhH (1 mL) at room temperature was added $Pd(OAc)_2$ (34 mg, 0.15 mmol) and acetic acid (15 mg, 0.25 mmol). The resulting black mixture was heated at 85 $^{o}$C before being filtered at room temperature. Purification by column chromatography (Hex:EtOAc,3:2) afforded **28** (85 mg, 82%) as clear oil. $^{1}$H NMR (400 MHz, $CDCl_3$): $\delta$ 8.09 (d, *J* = 8.0 Hz, 2H), 7.72 (d, *J* = 8.0 Hz, 2H), 2.89 (s, 4H), 2.34 (s, 3H), 1.08 (s, 18H); $^{13}$C (100 MHz, $CDCl_3$): $\delta$ 170.1, 169.4, 162.1, 142.6, 135.2, 129.2, 125.9, 28.1, 25.9, 23.2, 20.9; HRMS (ESI) calc'd for $C_{21}H_{30}NO_6Si$ [M + 1] 420.1842; found 420.1840.

**2,5-dioxopyrrolidin-1-yl-4-(di-tert-butylchlorosilyl)benzoate (63):** $Cl_2$(g) was bubbled into $CCl_4$ (20 mL) at -78 $^{o}$C to capture $Cl_2$ (g) and determine the concentration as 3.5 mM. To a solution of **26** (0.36 g, 1.0 mmol) in DCM (0.50 mL) at -78 $^{o}$C was added the $Cl_2$ in $CCl_4$ (0.50 mL, 1.75 mmol). After 5 min, the solvent was evaporated with a stream of $N_2$(g) and then applied onto a $SiO_2$ prep-TLC plate, followed by elution with Hex:EtOAc (3:2) to afford **63** (0.34 g, 85%) as an off-white solid. $^{1}$H NMR (500 MHz, $CDCl_3$): $\delta$ 8.13 (d, *J* = 8 Hz, 2H), 7.92 (d, *J* = 8.0 Hz, 2H), 2.92 (s, 4H), 1.11 (s, 18H); $^{13}$C (126 MHz, $CDCl_3$): $\delta$ 169.4, 162.1, 142.3, 135.5, 129.4, 126.2, 28.1, 25.9, 22.3.

**Di-*tert*-butyl(4-(((2,5-dioxopyrrolidin-1-yl)oxy)carbonyl)phenyl)silyl 2,5,8,11,14-pentaoxaheptadecan-17-oate (35):** To a solution of **63** (40 mg, 0.10 mmol) in EtOAc (1 mL) at room temperature was added TEA (42 µL, 0.30 mmol) and 3-($\omega$-methyl)tetraethylene glycolyl-propionic acid (70 mg, 0.25 mmol). The resulting mixture was left to stir at room temperature for 4 h before being directly applied to a $SiO_2$ prep-TLC plate. $^{1}$H NMR (500 MHz, $CDCl_3$): $\delta$ 8.10 (d, *J* = 8.0 Hz, 2H), 7.75 (d, *J* = 8.0 Hz, 2H), 3.83 (t, *J* = 6.0 Hz, 2H), 3.66-3.61 (m, 10H), 3.56-3.54 (m, 2H), 3.37 (s, 3H), 2.92 (s, 4), 2.79 (t, *J* = 6.0 Hz, 2H), 1.10 (s, 18H); $^{13}$C (126 MHz,

$CDCl_3$): δ 170.7, 169.4, 162.2, 142.5, 135.2, 129.2, 125.9, 72.2, 70.9, 70.8, 70.8, 70.7, 67.2, 59.3, 37.3, 28.2, 25.9, 20.9; ESI-MS [M + 1] 640.3.

**Bead-$(tBu)_2$Si-OAc (34):** To solution of Novasyn-$CO_2H$ resin (0.10 g, 0.03 mmol, Novabiochem, carboxy terminated PEG resin, 0.28 mmol/g) in THF (1 mL) and DCM (1 mL) was added **63** (27 mg, 0.07 mmol) and TEA (5.8 µL, 0.04 mmol). The reaction mixture was left shaking at room temperature for 1 d before being passed through a sintered glass filter and washed with DCM (4 X 10 mL). The resin was dried under vacuum for 1 d and used for reaction.

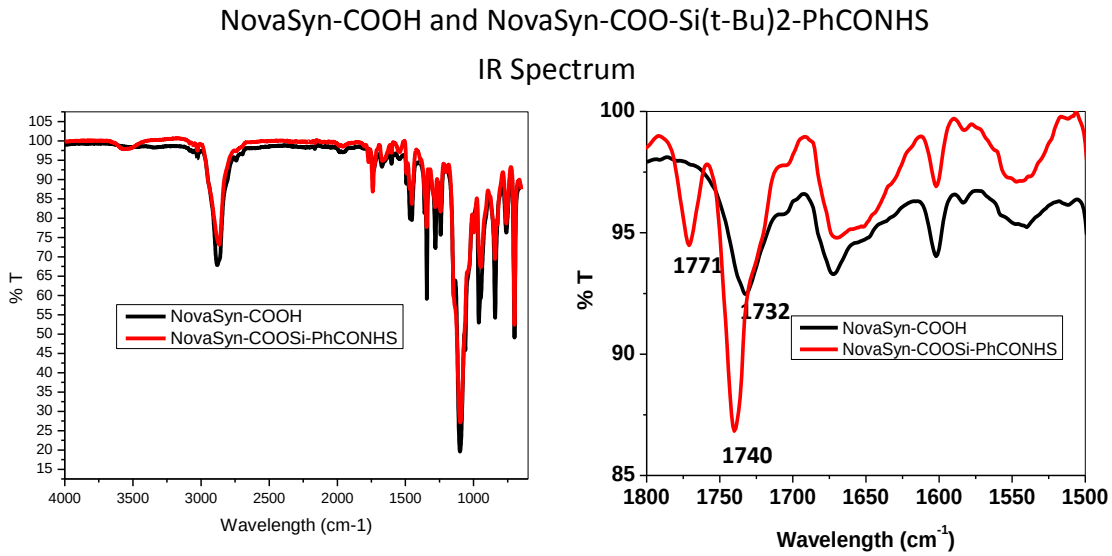


**2,5-Dioxopyrrolidin-1-yl 4-(di-tert-butylfluorosilyl)benzoate (29):** To a solution of **28** (2.0 mg, 4.8 µmol) in DCM (0.20 mL) was added TBAF·$3H_2O$. The resulting mixture was left to stir at room temperature for 5 min before being passed directly through a silica gel plug to afford **29** (1.7 mg, 95%) as a colorless liquid. $^1$H NMR (500 MHz, $CDCl_3$): δ 7.67 (d, *J* = 8.0 Hz, 2H), 7.13 (d, *J* = 8.0 Hz, 2H), 2.93 (s, 4H), 1.07 (s, 18H); $^{13}$C (126 MHz, $CDCl_3$): δ 169.4, 167.6, 143.1, 136.4, 134.5, 129.5, 27.4, 25.9, 20.5; $^{19}$F (470 MHz, $CDCl_3$): δ -188.9; HRMS (ESI) calc'd for $C_{19}H_{27}NO_4SiF$ [M + 1] 380.1693; found 380.1689.

**5-(4-Iodophenoxy)pentan-1-amine (40):** To a solution of 4-iodophenol (0.22 g, 1.0 mmol) in DMF (1 mL) was added $K_2CO_3$ (0.15 g, 1.1 mmol) and 5-*t*-butoxycarbonylamino-pentylbromide (0.32 g, 1.2 mmol). The resulting mixture was left to stir for 1 h at 55 °C before being quenched with sat. $NH_4Cl$ (40 mL). The crude reaction was extracted with EtOAc (2 X 75 mL), and the combined organic extracts were dried over $MgSO_4$ and concentrated *in vacuo*. After evaporation, the crude material was redissolved in TFA-DCM (10 mL, 1:1) and left to stir at rt for

1 h before being quenched with sat. $NaHCO_3$. The crude reaction was extracted with $CHCl_3$ (2 X 75 mL), and the combined organic extracts were dried over $MgSO_4$ and concentrated *in vacuo*. Purification by column chromatography ($CHCl_3$:MeOH (10%)) afforded **40** (0.22 g, 73%) as a white powder. $^1$H NMR (500 MHz, $CDCl_3$ + $CD_3OD$): $\delta$ 7.45 (d, *J* = 8.0 Hz, 2H), 6.58 (d, *J* = 8.0 Hz, 2H), 3.84 (t, *J* = 8.0 Hz, 2H), 2.83 (t, *J* = 8.0 Hz, 2H), 1.72 (q, *J* = 7.0 Hz, 2H), 1.63 (q, *J* = 7.0 Hz, 2H), 1.46 (q, *J* = 7.0 Hz, 2H); $^{13}$C (126 MHz, $CDCl_3$ + $CD_3OD$): $\delta$ 158.9, 138.3, 116.9, 82.8, 67.6, 39.6, 28.6, 27.3, 23.1; HRMS (ESI) calc'd for $C_{11}H_{17}NOI$ [M + 1] 306.0346; found 380.0344.

**(13S,17S)-17-((4-((5-Aminopentyl)oxy)phenyl)ethynyl)-13-methyl-7,8,9,11,12,13,14,15,16, 17-decahydro-6H-cyclopenta[a]phenanthrene-3,17-diol (43):** To a solution of **41** (0.20 g, 0.65 mmol) in ACN (15 mL) at room temperature was added 17α-ethynylestradiol (0.15 g, 0.5 mmol), CuI (10 mg, 0.05 mmol), piperidine (2 mL), and $PdCl_2(PPh_3)_2$ (10 mg, 0.01 mmol). The resulting mixture was stirred for 4 h at 55 $^o$C before being evaporated at room temperature. The crude material was redissolved in EtOAc (2 X 50 mL), washed with brine, and the organic layers were combined and concentrated *in vacuo*. Purification by column chromatography ($CHCl_3$:MeOH (10%)) afford **43** (0.15 g, 65%) as a pale yellow solid. $^1$H NMR (500 MHz, $CDCl_3$ + $CD_3OD$): $\delta$ 7.33 (d, *J* = 8.0 Hz, 2H), 7.10 (d, *J* = 8.0 Hz, 1H), 6.78 (d, *J* = 8.0 Hz, 2H), 6.60 (td, *J* = 8.0, 2.0 Hz, 1H), 6.53 (d, *J* = 2.0 Hz, 1H), 3.90 (t, *J* = 8.0 Hz, 2H), 0.88 (s, 3H); $^{13}$C (126 MHz, $CDCl_3$ + $CD_3OD$): $\delta$ 159.2, 154.6, 138.2, 133.2, 131.9, 126.6, 115.6, 114.6, 113.0, 91.8, 85.7, 80.3, 67.9, 49.9, 47.8, 43.9, 41.7, 39.8, 39.2, 33.3, 32.8, 29.9, 29.1, 27.6, 26.8, 23.5, 23.1, 13.2; HRMS (ESI) calc'd for $C_{31}H_{40}NO_3$ [M + 1] 474.3008; found 474.3017.

**Di-*tert*-butyl(4-((5-(4-(((13*S*,17*S*)-3,17-dihydroxy-13-methyl-7,8,9,11,12,13,14,15,16,17-decahydro-6H-cyclopenta[a]phenanthren-17-yl)ethynyl)phenoxy)pentyl)carbamoyl) phenyl)silyl acetate (44):** To a solution of **43** (20 mg, 0.04 mmol) in DMF (0.10 mL) was added **30** (21 mg, 0.05 mmol) and TEA (7 µL, 0.05 mmol) at room temperature. The resulting mixture was left to stir at this temperature for 1 h before the solvent was removed under a stream of $N_2$ (g). Purification by prep-TLC (Hex:EtOAc, 3:2) afforded **44** (23 mg, 75%) as a white solid. $^1$H NMR (500 MHz, $CDCl_3$): $\delta$ 7.70 (d, *J* = 8.0 Hz, 2H), 7.61 (d, *J* = 8.0 Hz, 2H), 7.33 (d, *J* = 8.0 Hz, 2H), 7.12 (d, *J* = 8.0 Hz, 1H), 6.78 (d, *J* = 8.0 Hz, 2H), 6.62 (dd, *J* = 8.0, 2.0 Hz, 1H), 6.55 (d, *J* = 2.0 Hz, 1H), 3.93 (t, *J* = 8.0 Hz, 2H), 3.46 (q, *J* = 8.0 Hz, 2H), 2.81-2.74 (m, 2H), 2.40-2.29 (m, 2H), 2.22 (s, 3H), 0.89 (s, 3H); $^{13}$C (126 MHz, $CDCl_3$): $\delta$ 170.4, 167.9, 159.2, 153.9, 138.4, 137.5, 135.6, 135.0, 133.3, 132.4, 126.7, 125.8, 115.2, 114.6, 112.9, 91.5, 96.0, 80.6, 67.9,

49.9, 47.8, 43.8, 40.1, 39.7, 39.3, 36.8, 33.3, 29.9, 29.6, 29.0, 28.2, 27.4, 26.7, 23.7, 23.3, 23.1, 20.9, 13.1; HRMS (ESI) calc'd for $C_{48}H_{64}NO_6Si$ [M + 1] 778.4503; found 778.4521.

**4-(Di-tert-butylfluorosilyl)-*N*-(5-(4-(((13S,17S)-3,17-dihydroxy-13-methyl-7,8,9,11,12,13,14, 15,16,17-decahydro-6H-cyclopenta[a]phenanthren-17-yl)ethynyl)phenoxy)pentyl) benzamide (64):** To a solution of **44** (5 mg, 6.4 µmol) in DCM (0.20 mL) was added TBAF·$3H_2O$ at room temperature. The resulting mixture was left to stir at this temperature before being directly applied to a $SiO_2$ prep-TLC plate. Purification (Hex:EtOAc, 3:2) afforded **64** (4.0 mg, 85%) as a white solid. $^1$H NMR (500 MHz, $CDCl_3$): $\delta$ 7.76 (d, *J* = 8.0 Hz, 2H), 7.70 (d, *J* = 8.0 Hz, 2H), 7.38 (d, *J* = 8.0 Hz, 2H), 7.18 (d, *J* = 8.0 Hz, 1H), 6.84 (d, *J* = 8.0Hz, 2H), 6.83 (dd, *J* = 8.0, 2.0 Hz, 1H), 6.58 (d, *J* = 2.0 Hz, 1H), 6.16 (t, *J* = 5.0 Hz, 1H), 3.99 (t, *J* = 8.0 Hz, 2H), 3.53 (q, *J* = 8.0 Hz, 2H), 2.90-2.80 (m, 2H), 2.40-2.29 (m, 2H), 2.22 (s, 3H), 0.95 (s, 3H). HRMS (ESI) calc'd for $C_{46}H_{59}NO_3SiF$ [M + 1] 720.4248; found 720.4250.

**RGD-$(tBu)_2$-Si-OAc (61):** To a solution of RGD peptide (3 mg, 3.9 µmol) in DMF (0.10 mL) was added **30** (2 mg, 4.8 µmol) and TEA (1 µL). The resulting mixture was left to stir at room temperature for 15 min before being quenched upon diethyl ether addition (20 mL). The crude reaction was then centrifuged to afford **61** (2.8 mg) as a colorless solid. HRMS (ESI) calc'd for $C_{44}H_{65}N_9O_{10}Si$ [M + 1] 908.4702; found 908.4709.

**RGD-$(tBu)_2$-Si-F (65):** To a solution of **61** (0.5 mg, 0.6 µmol) in DMSO (0.10 mL) was added TBAF·$3H_2O$. The resulting mixture was left to stir at room temperature for 5 min before being quenched upon diethyl ether addition (20 mL). The crude reaction was then centrifuged to afford **65** as a colorless solid. HRMS (ESI) calc'd for $C_{44}H_{63}N_9O_8SiF$ [M + 1] 868.4553; found 868.4564.

**Radiochemical Syntheses**

**2,5-Dioxopyrrolidin-1-yl-4-(di-tert-butyl-[$^{18}$F]fluorosilyl)benzoate (31):** 51 mCi of [$^{18}$F]fluoride in 200 µL [$^{18}$O]$H_2O$ was eluted into Pyrex vial (No. 9825) and used as is without any drying step or added base. The syringe was rinsed with dry 500 µL ACN, and any residual activity was added to vial. **30** (1 mg, 2.81 µmol) was dissolved in dry 300 µL ACN, added to the reaction vial, the vial was capped firmly and placed in an oil bath at 105 $^o$C for 10 minutes (RCY: 93.5%, n = 3, SA = 3500-3800 Ci/mmol). After 10 minutes, the vial was cooled at room temperature for 2 minutes and the solvent was injected directly into the semi-preparative HPLC. The reaction vial was rinsed with 3 mL of the HPLC eluting solvent (80% ACN/ 20% $H_2O$) and the rinse solvent

was added to the initial reaction mixture before injecting into HPLC. The purification was carried by a semi-preparative HPLC system (Agilent Zorbax SB-C18, 5 µm, 9.4 X 250 mm, Product #: 880975-202), eluting with a gradient (A: 80% ACN 20% $H_2O$ → B: 90% ACN 10% $H_2O$ over 15 min) at a flow rate of 4 mL/min and with the UV detector set at 254 nm. The radioactive peak corresponding to **31** was detected at 14 to 16 min and was collected in a large glass vial. The collected activity was diluted with 30 mL $H_2O$ and passed through a C18 column to capture the activity. The collection vial was rinsed with 3 mL $H_2O$, which was also passed through the C18 column. A nitrogen line was connected to the cartridge to dry as best as possible residual $H_2O$ captured in cartridge. The activity (35.9 mCi) was eluted from the column with $Et_2O$ (0.8 mL), and nitrogen was used to remove the solvent. The desired compound was obtained within 45 minutes and the radiochemical purity was assessed by HPLC and was deemed suitable for the next conjugation step. Non-decay corrected yield = 70.4%. Decay-corrected yield = 93.5%.

**Radio-TLC of the radiofluorination of 30 with [$^{18}$F]fluoride ion after 10 minutes:**

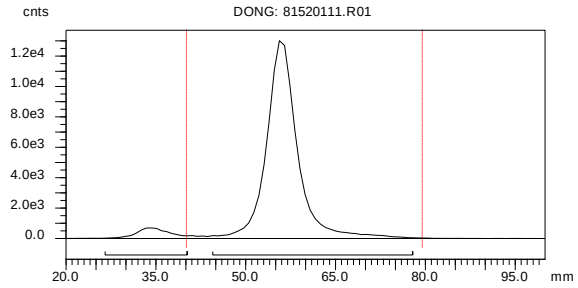


**TLC Eluting Conditions:** 100% EtOAc

**Region 1 (unreacted [$^{18}$F]fluoride; 35 mm):** 5.3%

**Region 2 ([$^{18}$F]fluoroproduct; 55 mm):** 94.7%

**Prep HPLC purification of crude material:**

**Conditions:** A: 80% ACN 20% $H_2O$ → B: 90% ACN 10% $H_2O$ over 15 mins, flow rate = 4 mL/ min, λ = 254 nm

**UV trace:**

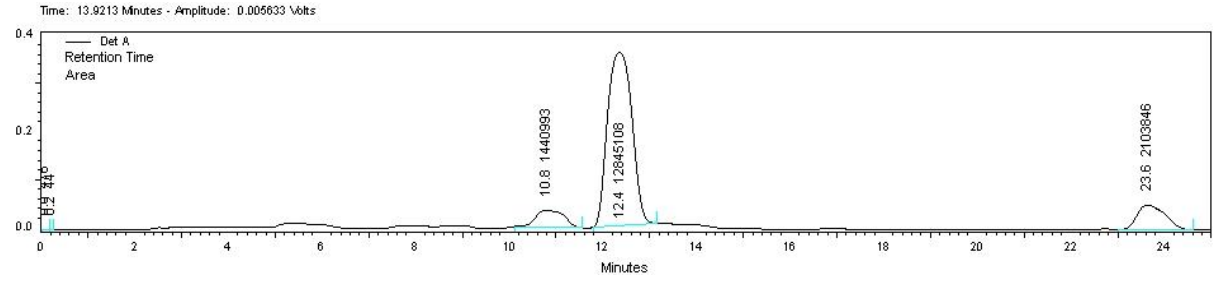

**Radioactivity trace (Product: 15.2 min):**

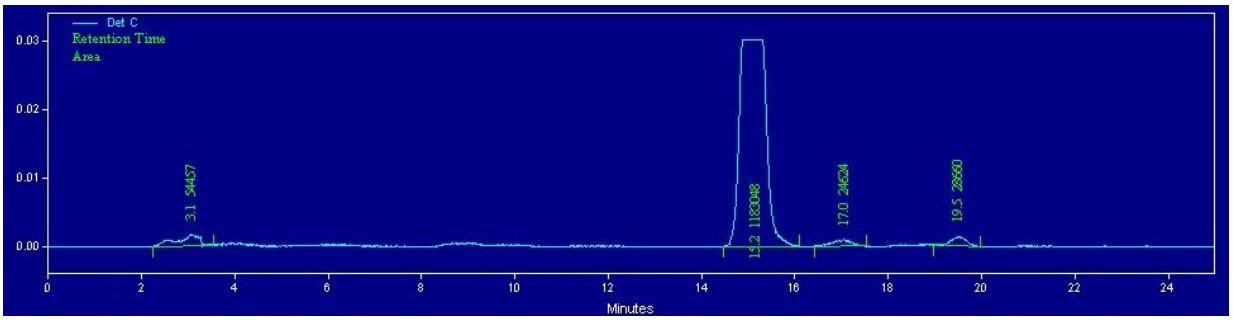


**Quality Control analysis after purification:**

**Conditions:** 80% ACN, 20% $H_2O$ flow rate = 2 mL/ min, λ = 254 nm

**UV trace used for specific activity determination (Product: 4.51 min):**

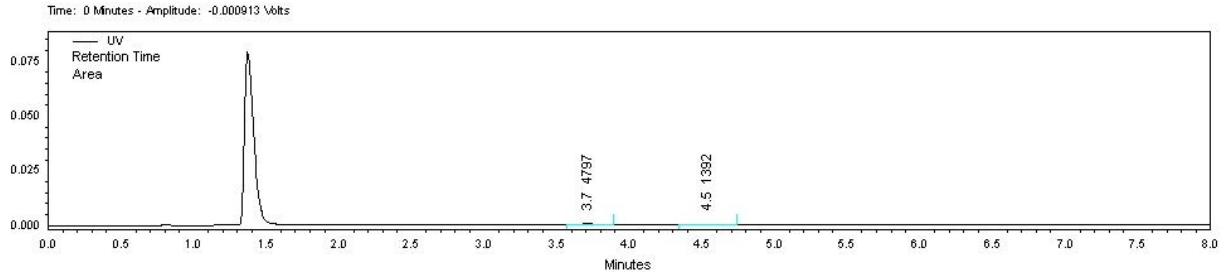


**UV trace of co-injection with cold standard for product (31) confirmation (Product: 4.56 min):**

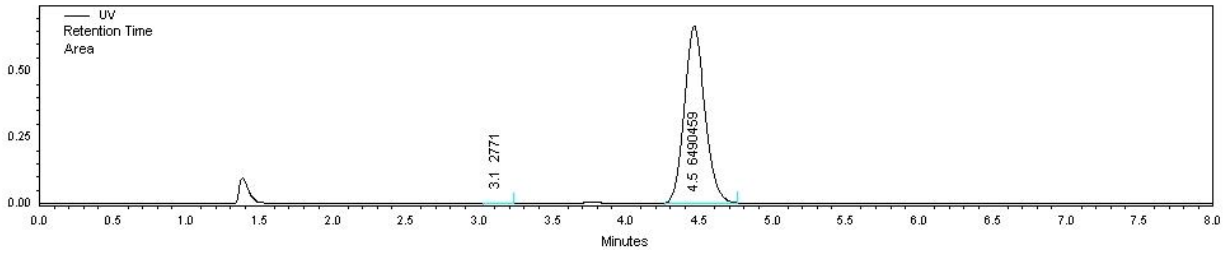

**Radioactivity trace of co-injection with cold standard for product (31) confirmation and radiochemical purity:**

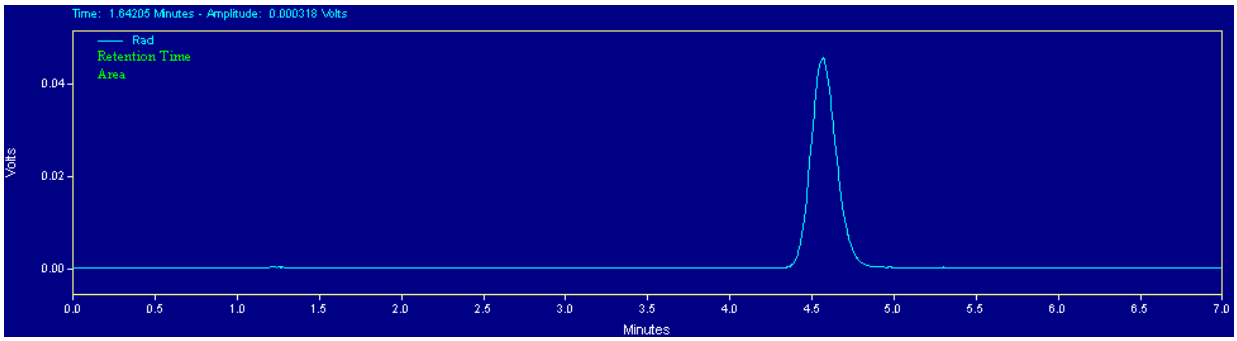


**[$^{18}$F]-EDC (33):** To a dried solution of **31** in 40 µL MeOH was added EDC (**32**, 6 nmol in 10 µL MeOH) at room temperature and left to stir for 10 mins (RCY: 60-98%). The reaction mixture was added directly to a G25 column (PD Minitrap G-25, Sephadex G-25 medium, Product #: 28-9180-07), and **33** was eluted with PBS buffer (~1.5 mL, in 0.5 mL increments) to obtain 15.1 mCi in ca. 80 min from end of bombardment. The isolated yield (without decay correction) was 29.4%, with a radiochemical purity of >99% and specific activity of 2500 mCi/µmol (92.5 GBq/µmol); Decay-corrected yield = 48.6%.

**[$^{18}$F]-EDC purity determined by radio-TLC:**

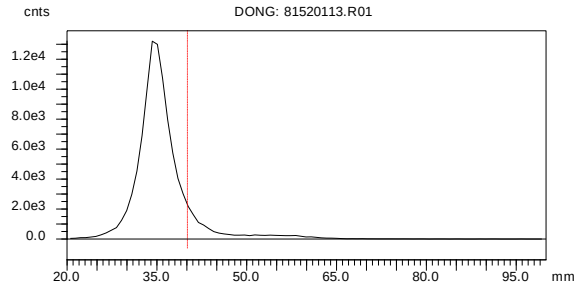


**TLC Eluting Conditions:** 100% MeOH

**Region 1 (35 mm; [$^{18}$F]-EDC):** 100%

**2,5-Dioxopyrrolidin-1-yl-4-(di-tert-butyl-[$^{18}$F]fluorosilyl)benzoate (31):** To a plastic vial was added 5.51 mCi of [$^{18}$F]fluoride in 50 µL [$^{18}$O]$H_2O$, 0.1 mg $K_2CO_3$ (solution: 1 mg/50 µL in $H_2O$), and 1 mg $K_{222}$ (solution: 56 mg/1000 µL in ACN). The vial was placed in an oil bath at 105 $^{o}$C and the water was removed by azeotropic evaporation with ACN (1 mL) using a stream of nitrogen. This was repeated twice more with 1 mL increments of ACN until the [$^{18}$F]fluoride source was deemed dry. The residue containing the [$^{18}$F]F$\cdot K_{222}$ cryptate was redissolved in 0.3 mL PhH (0.289 mCi stuck in vial) and transferred to a glass vial containing **30** (1 mg, 2.81

μmol), 0.025 mg polystyrene, and 0.2 mL PhH. The reaction was maintained at room temperature for 10 minutes and monitored by radio-TLC (RCY: 94.8%, n = 2). Confirmation of product (**31**) and the purity was assessed as above.

**Radio-TLC of the radiofluorination of 30 with [$^{18}$F]fluoride ion after 10 minutes:**

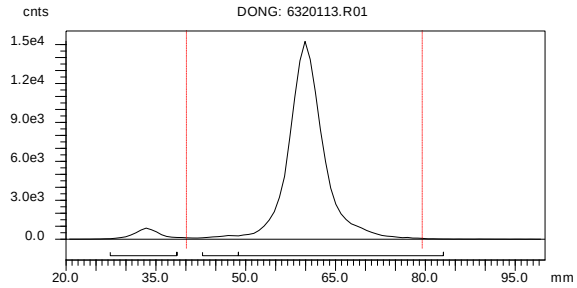


**TLC Eluting Conditions:** 100% EtOAc

**Region 1 (unreacted [$^{18}$F]fluoride; 35 mm):** 3.9%

**Region 2 ([$^{18}$F]fluoroproduct; 60 mm):** 96.1%

**Radioactivity trace (Product: 3.93 min):**

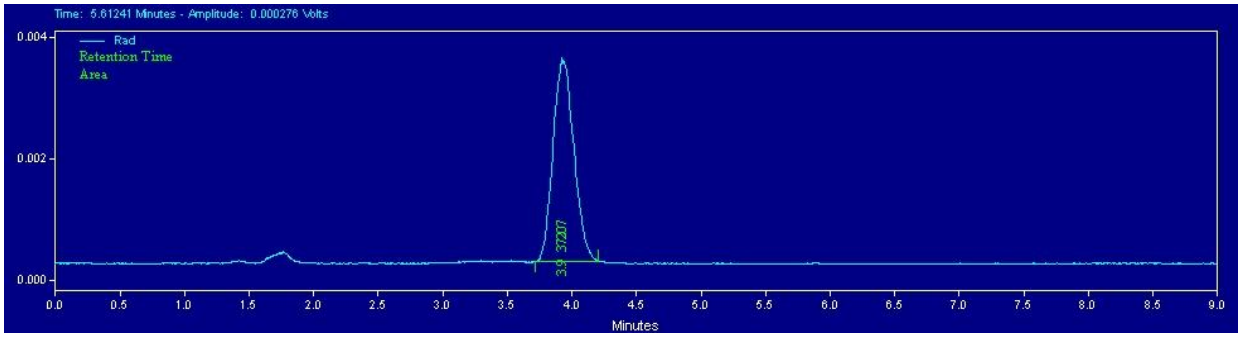


**2,5-Dioxopyrrolidin-1-yl-4-(di-tert-butyl-[$^{18}$F]fluorosilyl)benzoate (31):** To a plastic vial was added 1.036 mCi of [$^{18}$F]fluoride in 25 μL [$^{18}$O]$H_2O$, 0.1 mg $K_2CO_3$ (solution: 1 mg/50 μL in $H_2O$), and 1 mg $K_{222}$ (solution: 56 mg/1000 μL in ACN). The vial was placed in an oil bath at 105 $^{o}$C and the water was removed by azeotropic evaporation with ACN (1 mL) using a stream of nitrogen. This was repeated twice more with 1 mL increments of ACN until the [$^{18}$F]fluoride salt was deemed dry. The residue containing the [$^{18}$F]F$\cdot K_{222}$ cryptate was redissolved in 0.3 mL PhH (0.211 mCi stuck in vial) and transferred to a glass vial containing **35** (1 mg, 1.75 μmol) and 0.2 mL PhH. The reaction was maintained at room temperature for 2 minutes, injected onto and eluted from a silica gel plug (Hexanes:EtOAc, 4:3, 2 mL). Confirmation of product (**31**) and purity was assessed as above.

**Radio-TLC of the radiofluorination of 35 with [$^{18}$F]fluoride ion after 10 minutes (left) and after silica gel purification (right):**

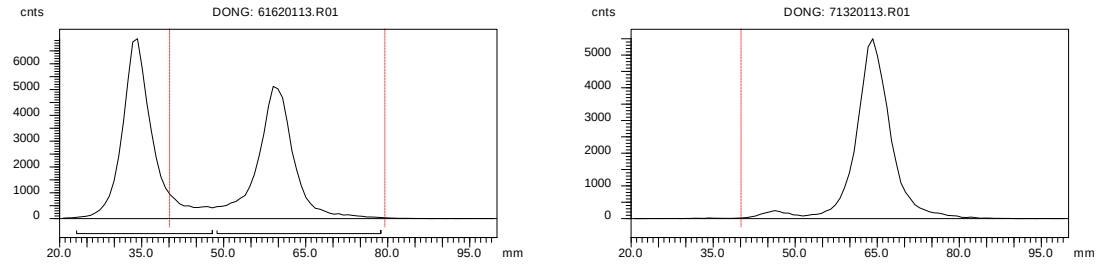


**TLC Eluting Conditions:** 100% EtOAc

**Region 1 (unreacted [$^{18}$F]fluoride; 35 mm):** 53.8%

**Region 2 ([$^{18}$F]fluoroproduct; 55 mm):** 46.2%

**Quality Control analysis after purification:**

**Conditions:** 80% ACN, 20% $H_2O$ flow rate = 2 mL/ min, λ = 254 nm

**UV trace:**

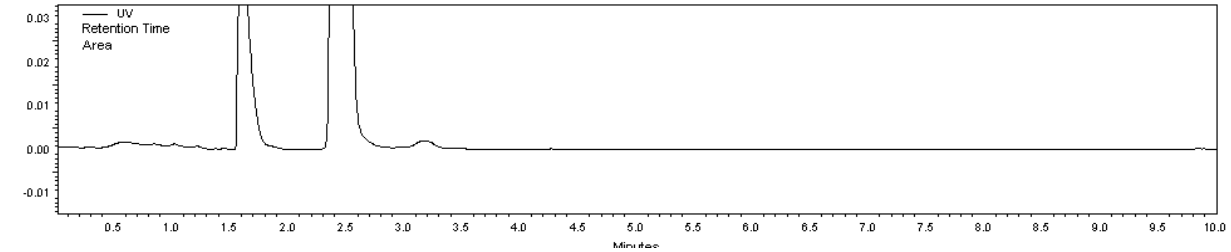


**Radioactivity trace:**

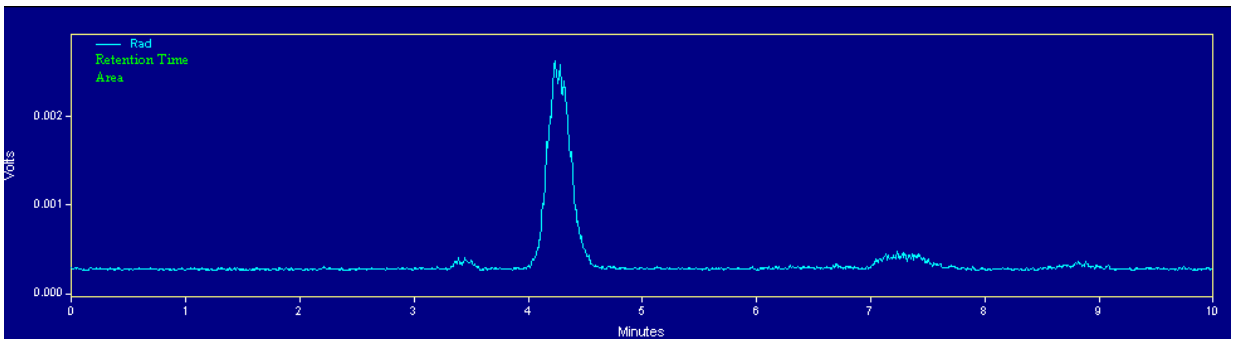


**EE$_2$-(tBu)$_2$-Si-$^{18}$F (45):** 21.8 mCi of [$^{18}$F]fluoride in 100 µL [$^{18}$O]$H_2O$ was eluted into Pyrex vial (No. 9825) and used as is without any drying step or added base. **44** (0.3 mg, 0.3 µmol) was dissolved in dry 400 µL ACN, added to reaction vial, capped firmly and placed in oil bath at 105 $^0$C for 10 minutes (RCY: 94.4%, n = 2, SA = 2300-2500 Ci/mmol). After 10 minutes, the vial was cooled at room temperature for 2 minutes and then injected directly into the semi-preparative

HPLC. The reaction vial was rinsed with 1 mL of the HPLC eluting solvent (80% ACN/ 20% $H_2O$) and added to the initial reaction mixture before injecting into HPLC. The purification was carried by a semi-preparative HPLC system (Agilent Zorbax SB-C18, 5 µm, 9.4 X 250 mm, Product #: 880975-202), eluting with a gradient (80% ACN 20% $H_2O$) at a flow rate of 4 mL/min and the UV detector set at 254 nm. The radioactive peak corresponding to **45** was detected at 22 to 24 min by the radioactivity detector and was collected in a large glass vial. The collected activity was diluted with 40 mL $H_2O$ and passed through a C18 column to capture the activity. The collection vial was rinsed with 3 mL $H_2O$, which was also passed through the C18 column. A nitrogen line was connected to the cartridge to dry as best as possible residual $H_2O$ captured in cartridge. The activity (13.72 mCi) was eluted from the column with 2.0 mL, and nitrogen was used to remove the solvent. The desired compound was obtained within 45 minutes and the radiochemical purity was assessed by the HPLC. Non-decay corrected yield = 62.9%. Decay-corrected yield = 84.0%.

**Radio-TLC of the radiofluorination of 44 with [$^{18}$F]fluoride ion after 10 minutes:**

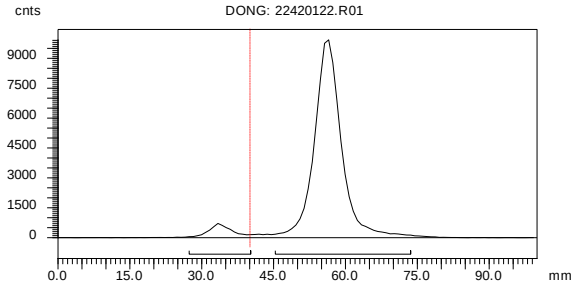


**TLC Eluting Conditions:** 100% EtOAc

**Region 1 (unreacted [$^{18}$F]fluoride; 35 mm):** 5.72%

**Region 2 ([$^{18}$F]fluoroproduct; 55 mm):** 94.28%

**Prep HPLC purification of crude material:**

**Conditions:** 80% ACN 20% $H_2O$, flow rate = 4 mL/ min, λ = 254 nm

**UV trace:**

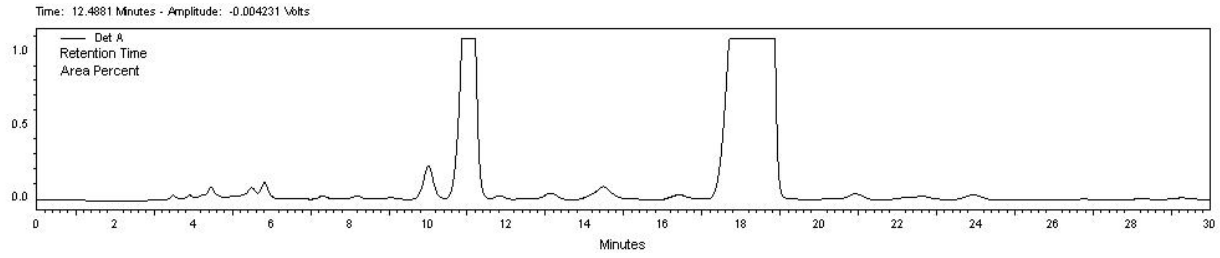


**Radioactivity trace (Product: 22.4 min):**

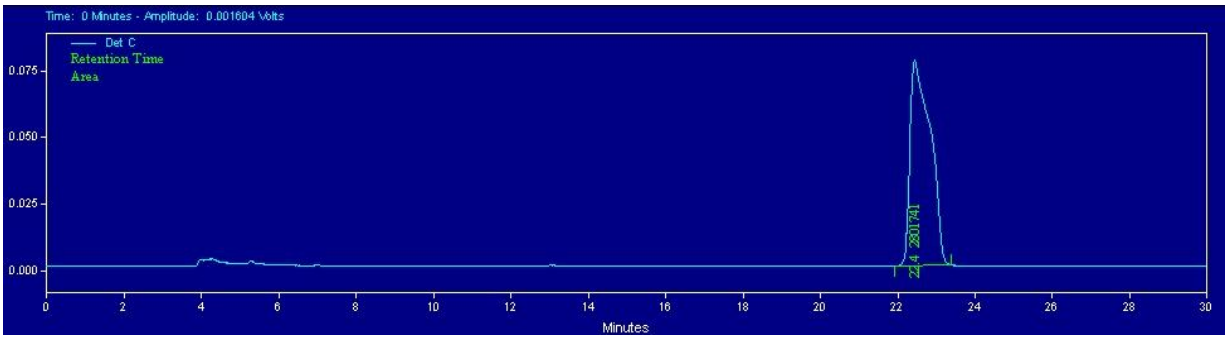


**Quality control analysis after purification:**

**Conditions:** 100% ACN, flow rate = 1.5 mL/ min, λ = 254 nm

**UV trace used for specific activity determination (Product: 5.11 min):**

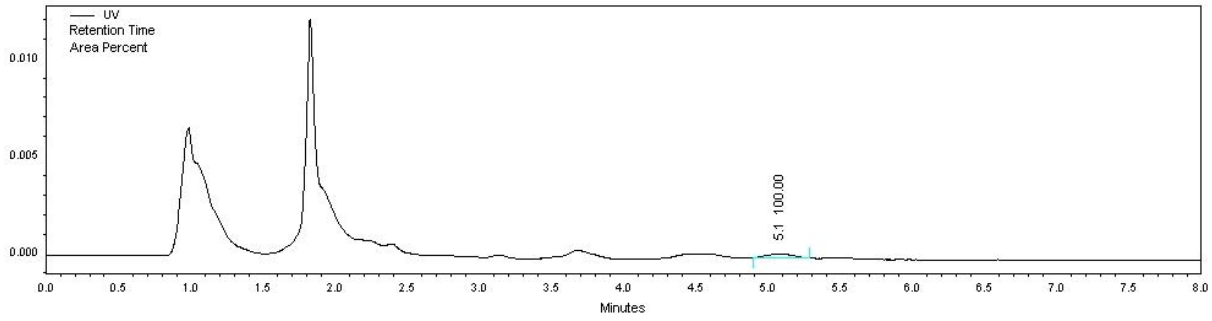

**UV trace of co-injection with cold standard for product (45) confirmation (Product: 5.01 min):**

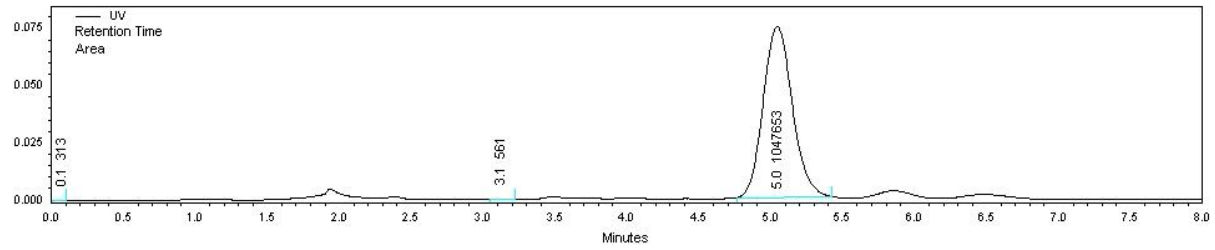


**Radioactivity trace of co-injection with cold standard for product (45) confirmation and radiochemical purity (Product: 5.12 min):**

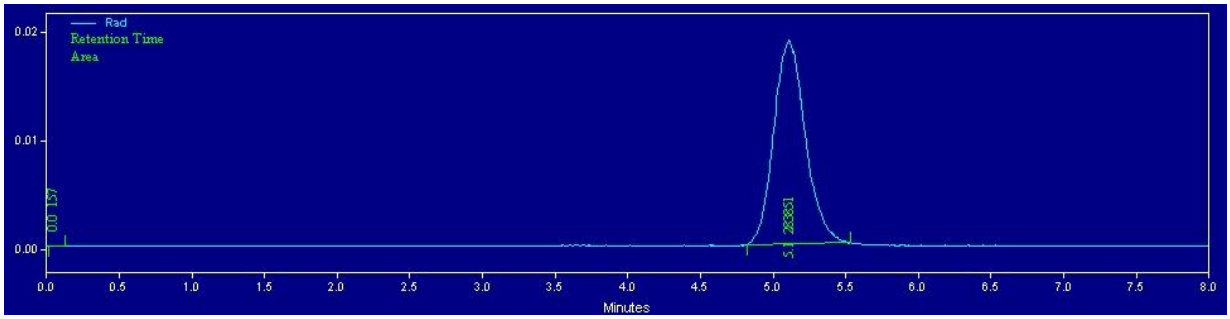


**$EE_2$-$(tBu)_2$-Si-$^{18}$F (45):** To a glass vial was added 4.55 mCi of [$^{18}$F]fluoride in 15 µL [$^{18}$O]$H_2O$, 0.2 mg $K_2CO_3$ (Solution: 1 mg/ 50 µL in $H_2O$), and 2 mg $K_{222}$ (Solution: 56 mg/ 1000 µL in ACN). The vial was placed in an oil bath at 105 $^{o}$C and the water was removed from azeotropic distillation with ACN (1 mL) using a stream of nitrogen. This was repeated twice more with 1 mL increments of ACN until the [$^{18}$F]fluoride source was deemed dry. The residue containing the [$^{18}$F]F$^{-}$$K_{222}$ cryptate was redissolved in 0.3 mL DMSO containing **44** (0.3 mg, 0.39 µmol). The reaction was maintained at room temperature for 10 minutes and monitored by radio-TLC (RCY: 86.8%, n = 2). Confirmation of product (**45**) and purity was assessed as above.

**Radio-TLC of the radiofluorination of 44 with [$^{18}$F]fluoride ion after 10 minutes:**

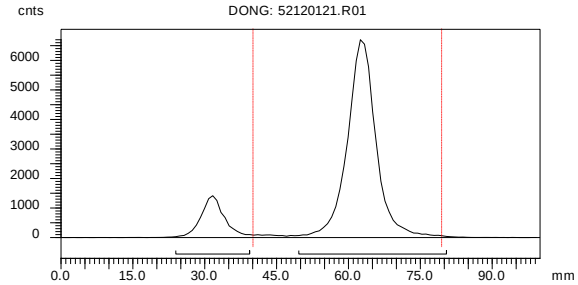


**TLC Eluting Conditions:** 100% EtOAc

**Region 1 (unreacted [$^{18}$F]fluoride; 35 mm):** 14.53%

**Region 2 ([$^{18}$F]fluoroproduct; 65 mm):** 85.47%

**RGD-(tBu)$_2$-Si-$^{18}$F (62):** To a glass vial was added 19.75 mCi of [$^{18}$F]fluoride in 15 µL [$^{18}$O]$H_2O$, 0.1 mg $K_2CO_3$ (Solution: 1 mg/ 50 µL in $H_2O$), and 1 mg $K_{222}$ (Solution: 56 mg/ 1000 µL in ACN). The vial was placed in an oil bath at 105 $^{o}$C and the water was removed by azeotropic distillation with ACN (1 mL) using a stream of nitrogen. This was repeated twice more with 1 mL increments of ACN until the [$^{18}$F]fluoride source was deemed dry. The residue containing the [$^{18}$F]F$\cdot K_{222}$ cryptate was redissolved in 0.3 mL DMSO containing **61** (0.3 mg, 0.33 µmol), left at room temperature for 15 minutes (RCY: 85.7%, n = 2) and then injected directly into the HPLC. The reaction vial was rinsed with 3 mL of the HPLC eluting solvent (45% ACN/ 55% $H_2O$/ 0.1% TFA) and added to the initial reaction mixture before injecting into HPLC. The purification was carried by a semi-preparative HPLC system (Agilent Zorbax SB-C18, 5 µm, 9.4 X 250 mm, Product #: 880975-202), eluting with a gradient (45% ACN/ 55% $H_2O$/ 0.1% TFA) at a flow rate of 4 mL/min and the UV detector set at 254 nm. The radioactive peak corresponding to **62** was detected at 18 to 20 minutes by the radioactivity detector and was collected in a large glass vial. The collected activity was diluted with 30 mL $H_2O$ and passed through a C18 column to capture the activity. The collection vial was rinsed with 3 mL $H_2O$, which was also passed through the C18 column. A nitrogen line was connected to the cartridge to dry as best as possible residual $H_2O$ captured in cartridge. The activity (4.05 mCi) was eluted from the column with 2 mL EtOH, and nitrogen was used to remove the solvent. The desired compound was obtained within 45 minutes and the radiochemical purity was assessed by the HPLC. Non-decay corrected yield = 20.5%. Decay-corrected yield = 27.2%.

**Radio-TLC of the radiofluorination of 61 with [$^{18}$F]fluoride ion after 15 minutes:**

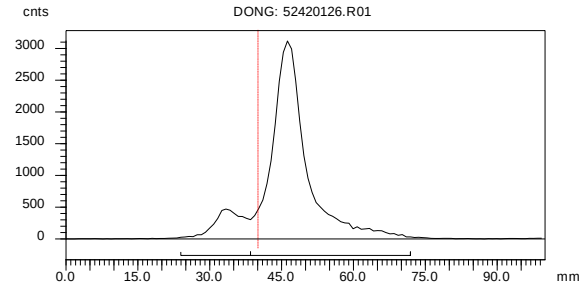


**TLC Eluting Conditions:** 45% ACN/ 55% $H_2O$/ 0.1% TFA; C18 plate

**Region 1 (unreacted [$^{18}$F]fluoride; 35 mm):** 11.65%

**Region 2 ([$^{18}$F]fluoroproduct; 45 mm):** 88.35%

**Prep HPLC purification of crude material:**

**Conditions:** 45% ACN 55% $H_2O$ 0.1% TFA, flow rate = 3 mL/ min, λ = 254 nm

**UV trace (Product: 5.11 min):**

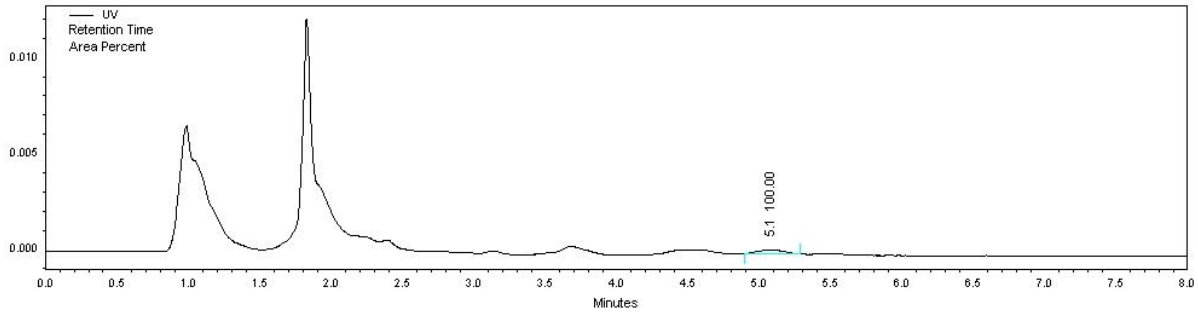


**Radioactivity trace:**

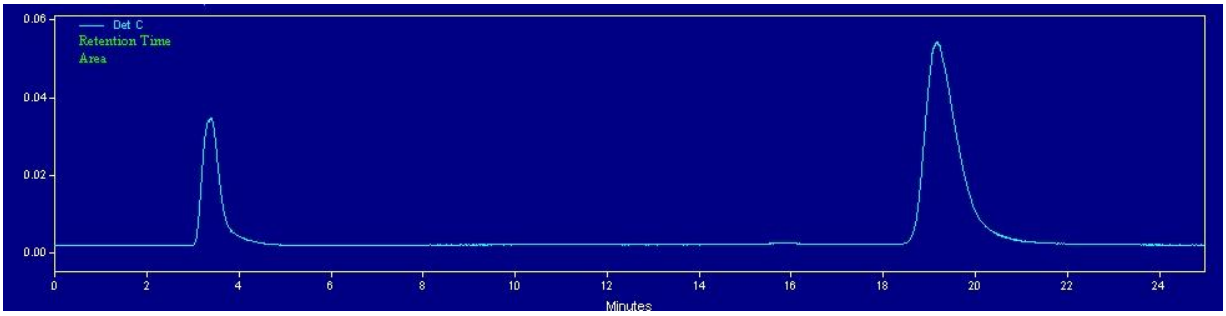


**Quality control analysis after purification:**

**Conditions:** 60% ACN, 40% $H_2O$ flow rate = 1.5 mL/ min, λ = 254 nm

**UV trace used for specific activity determination (Product: 12.5 min):**

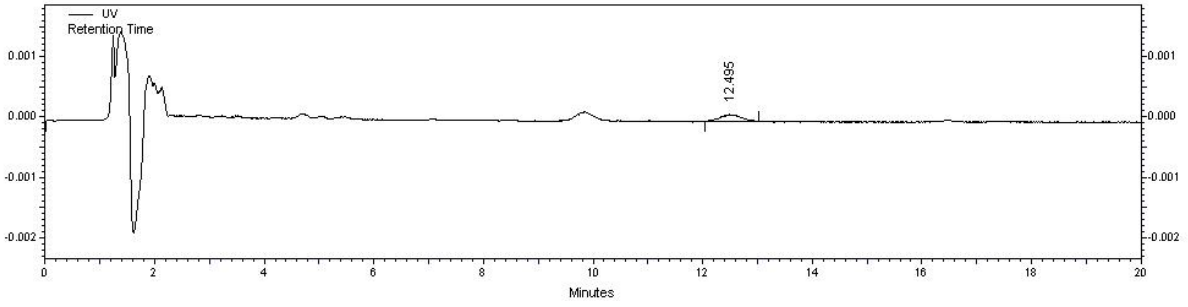

**UV trace of co-injection with cold standard for product (62) confirmation (Product: 4.61 min):**

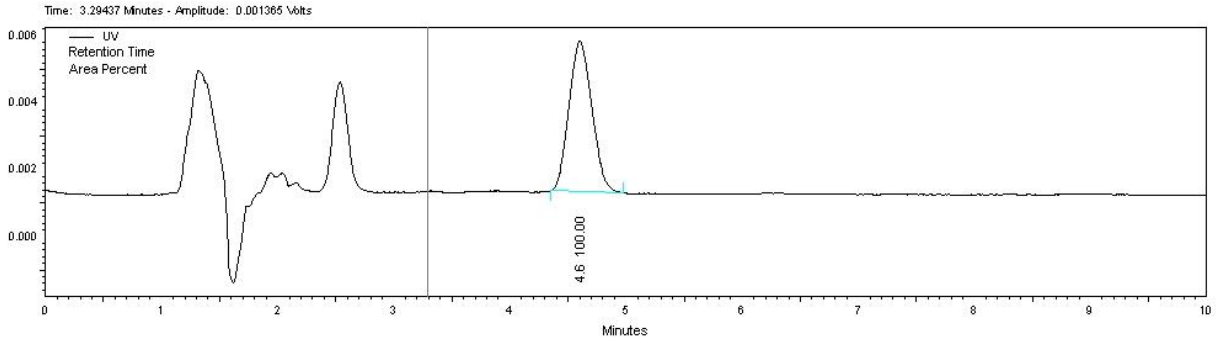


**Radioactivity trace of co-injection with cold standard for product (62) confirmation and radiochemical purity (Product: 4.72 min):**

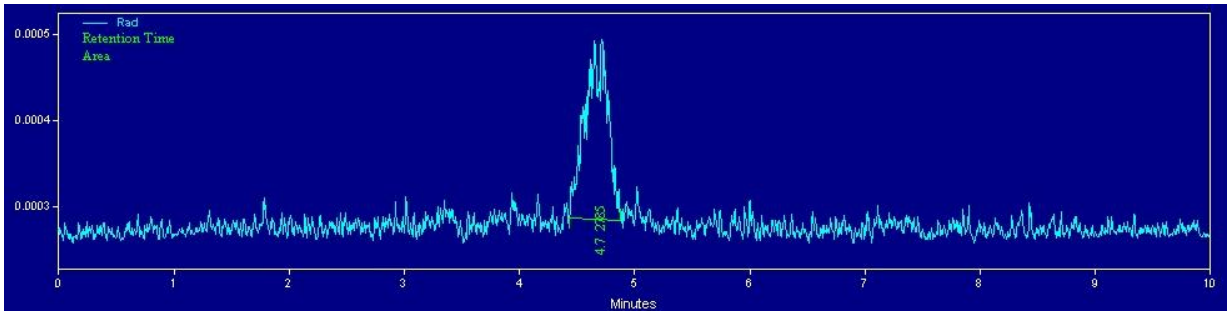


**RGD-(tBu)$_2$-Si-$^{18}$F (62):** 2.31 mCi of [$^{18}$F]fluoride in 20 µL [$^{18}$O]$H_2O$ was eluted into Pyrex vial (No. 9825) and used as is without any drying step or added base. **61** (0.3 mg, 0.33 µmol) was dissolved in dry 200 µL ACN, 200 µL MeOH and 30 µL $H_2O$ added to reaction vial, capped firmly and placed in oil bath at 105 $^{o}$C. The reaction was maintained at this temperature for 10 minutes and monitored by radio-TLC (RCY: 81.1%, n = 2). Confirmation of product (**62**) and purity was assessed as above.

**Radio-TLC of the radiofluorination of 61 with [$^{18}$F]fluoride ion after 10 minutes:**

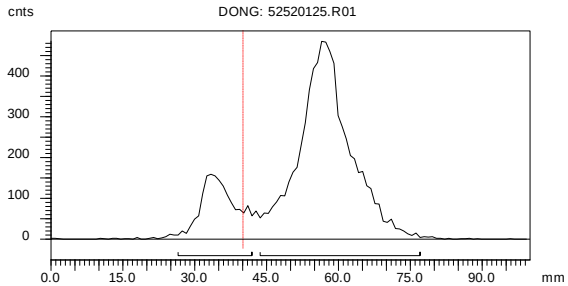


**TLC Eluting Conditions:** 45% ACN/ 55% $H_2O$/ 0.1% TFA; C18 plate

**Region 1 (unreacted [$^{18}$F]fluoride; 35 mm):** 18.19%

**Region 2 ([$^{18}$F]fluoroproduct; 60 mm):** 81.81%

**Radio-TLC of the radiofluorination of 59 with [$^{18}$F]fluoride ion after 10 minutes:**

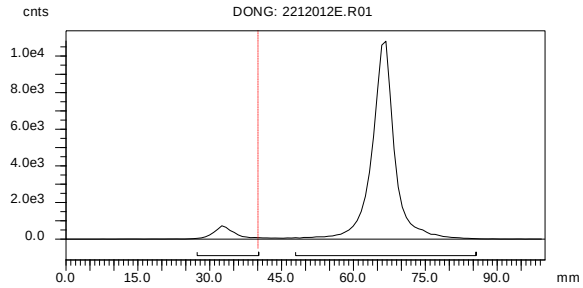


**TLC Eluting Conditions:** 100% EtOAc

**Region 1 (unreacted [$^{18}$F]fluoride; 35 mm):** 5.69%

**Region 2 ([$^{18}$F]fluoroproduct; 65 mm):** 94.31%

## VII. REFERENCES


(1) Couturier, O.; Luxen, A.; Chatal, J.-F.; Vuillez, J.-P.; Rigo, P.; Hustinx, R. Fluorinated tracers for imaging cancer with positron emission tomography. *Eur. J. Nucl. Med. Mol. Imaging* **2004**, *31*, 1182.

(2) Mukherjee, J.; Christian, B. T.; Dunigan, K. A.; Shi, B.; Narayanan, T. K.; Satter, M.; Mantil, J. Brain imaging of 18F-fallypride in normal volunteers: blood analysis, distribution, test-retest studies, and preliminary assessment of sensitivity to aging effects on dopamine D-2/D-3 receptors. *Synapse* **2002**, *46*, 170.

(3) Piert, M.; Machulla, H.-J.; Picchio, M.; Reischl, G.; Ziegler, S.; Kumar, P.; Wester, H.-J.; Beck, R.; McEwan, A. J. B.; Wiebe, L. I.; Schwaiger, M. Hypoxia-specific tumor imaging with $^{18}$F-fluoroazomycin arabinoside. *J. Nucl. Med.* **2005**, *46*, 106.

(4) Hall, L. T.; Struck, A. F.; Perlman, S. B. Clinical molecular imaging with PET agents other than $^{18}$F-FDG. *Curr. Pharm. Biotechnol.* **2010**, *11*, 545.

(5) Been, L. B.; Suurmeijer, A. J. H.; Cobben, D. C. P.; Jager, P. L.; Hoekstra, H. J.; Elsinga, P. H. [$^{18}$F]FLT-PET in oncology: current status and opportunities. *Eur. J. Nucl. Med. Mol. Imaging.* **2004**, *31*, 1659.

(6) Wang, R. E.; Niu, Y.; Wu, H.; Amin, M. N.; Cai, J. Development of NGR peptide-based agents for tumor imaging. *Am. J. Nucl. Med. Mol. Imaging* **2011**, *1*, 36.

(7) Abbas, K.; Kozempel, J.; Bonardi, M.; Groppi, F.; Alfarano, A.; Holzwarth, U.; Simonelli, F.; Hofman, H.; Horstmann, W.; Menapace, E.; Leseticky, L.; Gibson, N. Cyclotron production of $^{64}$Cu by deuteron irradiation of $^{64}$Zn. *Appl. Radiat. Isot.* **2006**, *64*, 1001.

(8) Boswell, C. A.; Sun, X.; Niu, W.; Weisman, G. R.; Wong, E. H.; Rheingold, A. L.; Anderson, C. J. Comparative in Vivo Stability of Copper-64-Labeled Cross-Bridged and Conventional Tetraazamacrocyclic Complexes. *J. Med. Chem.* **2004**, *47*, 1465.

(9) Chen, X.; Hou, Y.; Tohme, M.; Park, R.; Khankaldyyan, V.; Gonzales-Gomez, I.; Bading, J. R.; Laug, W. E.; Conti, P. S. Pegylated Arg-Gly-Asp peptide: $^{64}$Cu labeling and PET imaging of brain tumor $\alpha v\beta_3$-integrin expression. *J. Nucl. Med.* **2004**, *45*, 1776.

(10) Wu, A. M.; Yazaki, P. J.; Tsai, S.-W.; Nguyen, K.; Anderson, A.-L.; McCarthy, D. W.; Welch, M. J.; Shively, J. E.; Williams, L. E.; Raubitschek, A. A.; Wong, J. Y. C.; Toyokuni, T.; Phelps, M. E.; Gambhir, S. S. High-resolution microPET imaging of carcinoembryonic antigen-positive xenografts by using a copper-64-labeled engineered antibody fragment. *Proc. Natl. Acad. Sci. U. S. A.* **2000**, *97*, 8495.

(11) McBride, W. J.; Sharkey, R. M.; Karacay, H.; D'Souza, C. A.; Rossi, E. A.; Laverman, P.; Chang, C.-H.; Boerman, O. C.; Goldenberg, D. M. A novel method of $^{18}$F radiolabeling for PET. *J. Nucl. Med.* **2009**, *50*, 991.

(12) D'Souza, C. A.; McBride, W. J.; Sharkey, R. M.; Todaro, L. J.; Goldenberg, D. M. High-Yielding Aqueous $^{18}$F-Labeling of Peptides via Al$^{18}$F Chelation. *Bioconjugate Chem.* **2011**, *22*, 1793.

(13) Griffiths, G. L.; Goldenberg, D. M.; Jones, A. L.; Hansen, H. J. Radiolabeling of monoclonal antibodies and fragments with technetium and rhenium. *Bioconjugate Chem.* **1992**, *3*, 91.

(14) McBride, W. J.; D'Souza, C. A.; Karacay, H.; Sharkey, R. M.; Goldenberg, D. M. New Lyophilized Kit for Rapid Radiofluorination of Peptides *Bioconjugate Chem.* **2012**, *23*, 538.

(15) Darses, S.; Genet, J.-P. Potassium Organotrifluoroborates: New Perspectives in Organic Synthesis. *Chem. Rev.* **2008**, *108*, 288.

(16) Molander, G. A.; Ellis, N. Organotrifluoroborates: Protected Boronic Acids That Expand the Versatility of the Suzuki Coupling Reaction. *Acc. Chem. Res.* **2007**, *40*, 275.

(17) Darses, S.; Genet, J.-p. Potassium trifluoro(organo)borates: New perspectives in organic chemistry. *Eur. J. Org. Chem.* **2003**, 4313.

(18) Ting, R.; Adam, M. J.; Ruth, T. J.; Perrin, D. M. Arylfluoroborates and Alkylfluorosilicates as Potential PET Imaging Agents: High-Yielding Aqueous Biomolecular $^{18}$F-Labeling *J. Am. Chem. Soc.* **2005**, *127*, 13094.

(19) Smith, G. E.; Sladen, H. L.; Biagini, S. C. G.; Blower, P. J. Inorganic approaches for radiolabelling biomolecules with fluorine-18 for imaging with Positron Emission Tomography. *Dalton Trans.* **2011**, *40*, 6196.

(20) Ting, R.; Harwig, C.; auf, d. K. U.; McCormick, S.; Austin, P.; Overall, C. M.; Adam, M. J.; Ruth, T. J.; Perrin, D. M. Toward [$^{18}$F]-Labeled Aryltrifluoroborate Radiotracers: In Vivo Positron Emission Tomography Imaging of Stable Aryltrifluoroborate Clearance in Mice. *J. Am. Chem. Soc.* **2008**, *130*, 12045.

(21) Corey, E. J.; Venkateswarlu, A. Protection of hydroxyl groups as tert-butyldimethylsilyl derivatives. *J. Amer. Chem. Soc.* **1972**, *94*, 6190.

(22) Rosenthal, M. S.; Bosch, A. L.; Nickles, R. J.; Gatley, S. J. Synthesis and some characteristics of no-carrier added [$^{18}$F]fluorotrimethylsilane. *Int. J. Appl. Radiat. Isot.* **1985**, *36*, 318.

(23) Hohne, A.; Yu, L.; Mu, L.; Reiher, M.; Voigtmann, U.; Klar, U.; Graham, K.; Schubiger, P. A.; Ametamey, S. M. Organofluorosilanes as model compounds for $^{18}$F-labeled silicon-based PET tracers and their hydrolytic stability: experimental data and theoretical calculations (PET = positron emission tomography). *Chem. Eur. J.* **2009**, *15*, 3736.

(24) Mu, L.; Hohne, A.; Schubiger, P. A.; Ametamey, S. M.; Graham, K.; Cyr, J. E.; Dinkelborg, L.; Stellfeld, T.; Srinivasan, A.; Voigtmann, U.; Klar, U. Silicon-based building blocks for one-step $^{18}$F-radiolabeling of peptides for PET imaging. *Angew. Chem., Int. Ed.* **2008**, *47*, 4922.

(25) Hohne, A.; Mu, L.; Honer, M.; Schubiger, P. A.; Ametamey, S. M.; Graham, K.; Stellfeld, T.; Borkowski, S.; Berndorff, D.; Klar, U.; Voigtmann, U.; Cyr, J. E.; Friebe, M.; Dinkelborg, L.; Srinivasan, A. Synthesis, $^{18}$F-Labeling, and in Vitro and in Vivo Studies of Bombesin Peptides Modified with Silicon-Based Building Blocks. *Bioconjugate Chem.* **2008**, *19*, 1871.

(26) Schirrmacher, R.; Bradmoeller, G.; Schirrmacher, E.; Thews, O.; Tillmanns, J.; Siessmeier, T.; Bucholz, H. G.; Bartenstein, P.; Waengler, B.; Niemeyer, C. M.; Jurkschat, K. $^{18}$F-labeling of peptides by means of an organosilicon-based fluoride acceptor. *Angew. Chem., Int. Ed.* **2006**, *45*, 6047.

(27) Schirrmacher, E.; Waengler, B.; Cypryk, M.; Bradtmoeller, G.; Schaefer, M.; Eisenhut, M.; Jurkschat, K.; Schirrmacher, R. Synthesis of p-(Di-tert-butyl[$^{18}$F]fluorosilyl)benzaldehyde ([$^{18}$F]SiFA-A) with High Specific Activity by Isotopic Exchange: A Convenient Labeling Synthon for the $^{18}$F-Labeling of N-amino-oxy Derivatized Peptides. *Bioconjugate Chem.* **2007**, *18*, 2085.

(28) Rosa-Neto, P.; Waengler, B.; Iovkova, L.; Boening, G.; Reader, A.; Jurkschat, K.; Schirrmacher, E. [$^{18}$F]SiFA-isothiocyanate: A New Highly Effective Radioactive Labeling Agent for Lysine-Containing Proteins. *ChemBioChem* **2009**, *10*, 1321.

(29) Iovkova, L.; Wangler, B.; Schirrmacher, E.; Schirrmacher, R.; Quandt, G.; Boening, G.; Schurmann, M.; Jurkschat, K. para-Functionalized aryl-di-tert-butylfluorosilanes as potential labeling synthons for $^{18}$F radiopharmaceuticals. *Chem. Eur. J.* **2009**, *15*, 2140.

(30) Kostikov, A. P.; Chin, J.; Orchowski, K.; Niedermoser, S.; Kovacevic, M. M.; Aliaga, A.; Jurkschat, K.; Wangler, B.; Wangler, C.; Wester, H.-J.; Schirrmacher, R. Oxalic Acid Supported Si-$^{18}$F-Radiofluorination: One-Step Radiosynthesis of N-Succinimidyl 3-(Di-tert-butyl[$^{18}$F]fluorosilyl)benzoate ([$^{18}$F]SiFB) for Protein Labeling. *Bioconjugate Chem.* **2012**, *23*, 106.

(31) Jacobson, O.; Weiss, I. D.; Kiesewetter, D. O.; Farber, J. M.; Chen, X. PET of tumor CXCR4 expression with 4-$^{18}$F-T140. *J. Nucl. Med.* **2010**, *51*, 1796.

(32) Kim, S. H.; Katzenellenbogen, J. A. Hormone-PAMAM dendrimer conjugates: polymer dynamics and tether structure affect ligand access to receptors. *Angew. Chem., Int. Ed.* **2006**, *45*, 7243.

(33) Harrington, W. R.; Kim, S. H.; Funk, C. C.; Madak-Erdogan, Z.; Schiff, R.; Katzenellenbogen, J. A.; Katzenellenbogen, B. S. Estrogen dendrimer conjugates that preferentially activate extranuclear, nongenomic Versus genomic pathways of estrogen action. *Mol. Endocrinol.* **2006**, *20*, 491.

(34) Chambliss, K. L.; Wu, Q.; Oltmann, S.; Konaniah, E. S.; Umetani, M.; Korach, K. S.; Thomas, G. D.; Mineo, C.; Yuhanna, I. S.; Kim, S. H.; Madak-Erdogan, Z.; Maggi, A.; Dineen, S. P.; Roland, C. L.; Hui, D. Y.; Brekken, R. A.; Katzenellenbogen, J. A.; Katzenellenbogen, B. S.; Shaul, P. W. Non-nuclear estrogen receptor α signaling promotes cardiovascular protection but not uterine or breast cancer growth in mice. *J. Clin. Invest.* **2010**, *120*, 2319.

(35) Anstead, G. M.; Carlson, K. E.; Katzenellenbogen, J. A. The estradiol pharmacophore: ligand structure-estrogen receptor binding affinity relationships and a model for the receptor binding site. *Steroids* **1997**, *62*, 268.

(36) Wangler, B.; Quandt, G.; Iovkova, L.; Schirrmacher, E.; Wangler, C.; Boening, G.; Hacker, M.; Schmoeckel, M.; Jurkschat, K.; Bartenstein, P.; Schirrmacher, R. Kit-Like $^{18}$F-Labeling of Proteins: Synthesis of 4-(Di-tert-butyl[$^{18}$F]fluorosilyl)benzenethiol (Si[$^{18}$F]FA-SH) Labeled Rat Serum Albumin for Blood Pool Imaging with PET. *Bioconjugate Chem.* **2009**, *20*, 317.

(37) Waengler, C.; Waser, B.; Alke, A.; Iovkova, L.; Buchholz, H.-G.; Niedermoser, S.; Jurkschat, K.; Fottner, C.; Bartenstein, P.; Schirrmacher, R.; Reubi, J.-C.; Wester, H.-J.; Waengler, B. One-Step $^{18}$F-Labeling of Carbohydrate-Conjugated Octreotate-Derivatives Containing a Silicon-Fluoride-Acceptor (SiFA): In Vitro and in Vivo Evaluation as Tumor Imaging Agents for Positron Emission Tomography (PET). *Bioconjugate Chem.* **2010**, *21*, 2289.

(38) Kostikov, A. P.; Iovkova, L.; Chin, J.; Schirrmacher, E.; Waengler, B.; Waengler, C.; Jurkschat, K.; Cosa, G.; Schirrmacher, R. N-(4-(di-tert-butyl[$^{18}$F]fluorosilyl)benzyl)-2-hydroxy-N,N-dimethylethylammonium bromide ([$^{18}$F]SiFAN+Br-): A novel lead compound for the development of hydrophilic SiFA-based prosthetic groups for $^{18}$F-labeling. *J. Fluorine Chem.* **2011**, *132*, 27.

(39) Muthyala, R. S.; Sheng, S.; Carlson, K. E.; Katzenellenbogen, B. S.; Katzenellenbogen, J. A. Bridged bicyclic cores containing a 1,1-diarylethylene motif are high-affinity subtype-selective ligands for the estrogen receptor. *J. Med. Chem.* **2003**, *46*, 1589.

(40) Lunan, C. B.; Klopper, A. Antiestrogens. *Clin. Endocrinol.* **1975**, *4*, 551.

(41) Schottelius, M.; Wester, H.-J. Molecular imaging targeting peptide receptors. *Methods* **2009**, *48*, 161.

(42) Beer, A. J.; Haubner, R.; Goebel, M.; Luderschmidt, S.; Spilker, M. E.; Wester, H.-J.; Weber, W. A.; Schwaiger, M. Biodistribution and pharmacokinetics of the $\alpha v\beta_3$-selective tracer $^{18}$F-galacto-RGD in cancer patients. *J. Nucl. Med.* **2005**, *46*, 1333.

(43) Haubner, R.; Weber, W. A.; Beer, A. J.; Vabuliene, E.; Reim, D.; Sarbia, M.; Becker, K.-F.; Goebel, M.; Hein, R.; Wester, H.-J.; Kessler, H.; Schwaiger, M. Noninvasive visualization of the activated $\alpha v\beta_3$ integrin in cancer patients by positron emission tomography and [$^{18}$F]Galacto-RGD. *PLoS Med.* **2005**, *2*, 244.

(44) Wester, H. J.; Schottelius, M.; Scheidhauer, K.; Meisetschlaeger, G.; Herz, M.; Rau, F. C.; Reubi, J. C.; Schwaiger, M. PET imaging of somatostatin receptors: design, synthesis and preclinical evaluation of a novel $^{18}$F-labelled, carbohydrated analogue of octreotide. *Eur. J. Nucl. Med. Mol. Imaging* **2003**, *30*, 117.

(45) Pfaff, M.; Tangemann, K.; Mueller, B.; Gurrath, M.; Mueller, G.; Kessler, H.; Timpl, R.; Juergen, E. Selective recognition of cyclic RGD peptides of NMR defined conformation by $\alpha IIb\beta_3$, $\alpha V\beta_3$, and $\alpha_5\beta_1$ integrins. *J. Biol. Chem.* **1994**, *269*, 20233.

(46) Haubner, R.; Gratias, R.; Diefenbach, B.; Goodman, S. L.; Jonczyk, A.; Kessler, H. Structural and Functional Aspects of RGD-Containing Cyclic Pentapeptides as Highly Potent and Selective Integrin $\alpha V\beta_3$ Antagonists. *J. Am. Chem. Soc.* **1996**, *118*, 7461.

(47) Chen, X.; Park, R.; Shahinian, A. H.; Bading, J. R.; Conti, P. S. Pharmacokinetics and tumor retention of $^{125}$I-labeled RGD peptide are improved by PEGylation. *Nucl. Med. Biol.* **2004**, *31*, 11.

(48) Chen, X.; Park, R.; Shahinian, A. H.; Tohme, M.; Khankaldyyan, V.; Bozorgzadeh, M. H.; Bading, J. R.; Moats, R.; Laug, W. E.; Conti, P. S. $^{18}$F-labeled RGD peptide: initial evaluation for imaging brain tumor angiogenesis. *Nucl. Med. Biol.* **2004**, *31*, 179.

(49) Massoud, T. F.; Gambhir, S. S. Molecular imaging in living subjects: seeing fundamental biological processes in a new light. *Genes Dev.* **2003**, *17*, 545.

(50) Grewal, R. K.; Tuttle, R. M.; Fox, J.; Borkar, S.; Chou, J. F.; Gonen, M.; Strauss, H. W.; Larson, S. M.; Schoder, H. The effect of posttherapy $^{131}$I SPECT/CT on risk classification and management of patients with differentiated thyroid cancer. *J. Nucl. Med.* **2010**, *51*, 1361.

(51) Pither, R. PET and the role of in vivo molecular imaging in personalized medicine. *Expert Rev. Mol. Diagn.* **2003**, *3*, 703.

(52) Willmann, J. K.; van, B. N.; Dinkelborg, L. M.; Gambhir, S. S. Molecular imaging in drug development. *Nat. Rev. Drug Discovery* **2008**, *7*, 591.

(53) de, V. E. G. E.; Oude, M. T. H.; van, V. M. A. T. M.; Nagengast, W. B. Toward molecular imaging-driven drug development in oncology. *Cancer Discov.* **2011**, *1*, 25.

(54) Lucignani, G. Labeling peptides with PET radiometals: Vulcan's forge. *Eur. J. Nucl. Med. Mol. Imaging* **2008**, *35*, 209.

CHAPTER 3

# A NEW DIMENSION IN SELECTIVE ESTROGEN ACTION: A VASCULAR-PROTECTING ESTROGEN DENDRIMER CONJUGATE SHOWS SELECTIVE RECEPTOR-MEDIATED UPTAKE IN THE HEART AND VASCULATURE

## I. INTRODUCTION

### *A. Background*

Discrepancies in the incidence of heart disease between males and females, and in pre- vs. postmenopausal women, illustrate the significant beneficial effect of estrogen on the cardiovascular system.[1,2] Until recently, the cardioprotective effects of estrogen were originally attributed to its effects on serum lipid concentrations by modulating the hepatic expression of apoprotein genes.[3] Large, randomized trials have revealed similar conclusions, documenting estrogen's ability to increase the beneficial high-density lipoprotein (HDL) serum concentrations while decreasing harmful low-density lipoprotein (LDL) concentrations.[4] Maintaining a proper balance between the two concentrations have been shown to be critical in preserving vascular health, with subsequent studies revealing that even minor disruptions can offset key signaling pathways within these tissues and eventually lead to the onset of atherosclerosis.[5-7] However, only one-third of the observed clinical benefits of estrogen therapy are attributed to the lipid concentration alterations,[3] suggesting a more direct interaction between estrogen and blood vessels in vascular health maintenance. Consequently, the estrogen receptor (ER) in the vasculature is now considered an important target for the beneficial actions of estrogens.

### *B. Estrogen Receptor Signaling*

The physiological effects of both endogenous and synthetic estrogens are mediated through two estrogen receptors, ERα and ERβ, which are both members of the nuclear receptor superfamily of ligand-regulated transcription factors.[8] The receptors are composed of five domains, each with a specific function including DNA and ligand binding, transcriptional activation and repression, and receptor dimerization.[9] Upon ligand binding, the receptor undergoes major conformational changes to facilitate ER dimerization, binding to estrogen response elements (EREs) on target genes, and recruitment of coregulator proteins, thereby altering the expression of specific genes within the nucleus.[10] ERs can also modulate transcription in the absence of ligand binding through protein-protein interactions with other transcription factors.[11] However, many of the cardioprotective effects attributed to estrogen have

been largely mediated through an extranuclear signaling pathway with membrane-associated ERs.

The estrogen receptor has traditionally been conceived to function exclusively through nuclear activation ("genomic pathway").[12] More recently, emerging data has identified an additional extranuclear role, capable of initiating diverse nongenomic cellular responses via activation of plasma membrane associated ERs ("nongenomic pathway") (Figure 3.1).[13] In contrast to the classical genomic pathway of estrogen action (i.e., several hours to days), these nongenomic responses are often extremely rapid, with biological effects typically observed within seconds to minutes. The rapid nature of this response system assisted in its initial discovery in 1967[14] when cyclic adenosine monophosphate (cAMP) levels were observed to significantly increase within 15 seconds upon intravenous administration of physiological amounts of 17β-estradiol ($E_2$) and was further supported in other studies demonstrating rapid calcium responses to $E_2$ in endometrial cells.[15] Compelling evidence now confirms the existence of the nongenomic pathway: rapid signaling has been identified in many different cell types including oocytes, osteoblasts, osteoclasts, breast cancer cells, adipocytes and endothelial cells, where it mediates ion fluxes, kinase cascades and enzyme activities.[16-22] However, because of the difficulty in selectively activating the nongenomic over the genomic pathway (i.e., traditional estrogens are effective at stimulating both pathways), the extent to which the biological effects of estrogen are attributed to the nongenomic pathway and whether this pathway is operative and biologically relevant *in vivo* have remained unknown. Consequently, the mechanism of action and the cellular functions of these extranuclear ERs are now being defined, and this has since become an active area of investigation.[13]

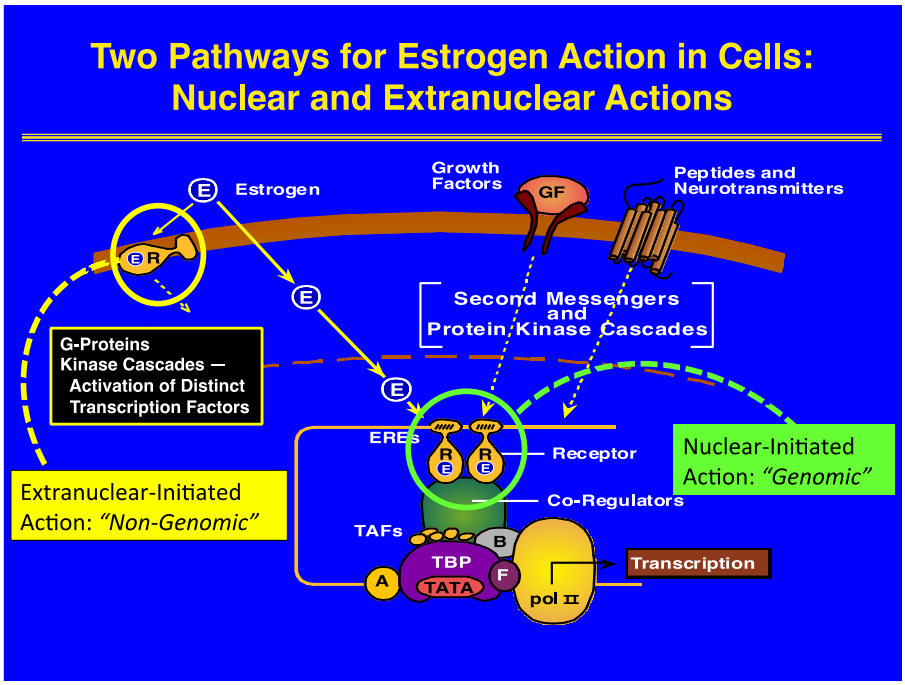


**Figure 3.1.** Schematic depicting two mechanisms of estrogen signaling: nuclear, or genomic, signaling (green) and extranuclear, or nongenomic, signaling (yellow).

*C. Nuclear and Membrane-Associated ERs*

Although it has yet to be sequenced, it appears membrane ERs are structurally very similar to nuclear ERs: immunohistochemistry studies shared the same epitope homology as nuclear ERα[23] and the expression of ERα and ERβ in ER null cells resulted in the detection of both nuclear and membrane-localized pools of ERs.[24] Furthermore, analysis of double knockout ERα/ERβ mice (DERKO) did not reveal a functional ER protein at the cell surface.[25] Moreover, both nuclear and membrane-initiated signaling were eliminated in the presence of either small interfering RNA or antisense oligonucleotides directed against the proteins.[25-27] Lastly, and perhaps the most convincing, membrane-extracted ERs displayed an identical mass to nuclear ERs by mass spectrometry and identical binding affinities for the endogenous ligand, 17β-estradiol.[27]

*D. The Estrogen Receptor and the Cardiovascular System*

The many clinical and basic science investigations have demonstrated estrogen's impact on cardiovascular health. In animal studies, estrogen has been shown to stimulate endothelial cell growth following denudation,[28] inhibit the proliferation of vascular smooth-muscle cells[29,30] and attenuate arterial lesion sizes,[31,32] all of which are key to maintaining the integrity of the blood vessel. Even minor disruptions to the wall can lead to vascular disease.[33] Moreover,

additional investigations in specialized normolipidemic and hypercholesterolemic animal models revealed no effect of estrogen treatment on circulating lipid concentrations, further demonstrating the direct relationship between estrogen and the blood vessel wall.[29,34,35]

Blood vessels are composed of smooth-muscle cells and an endothelial cell lining, with both ER subtypes being identified within each, as well as in myocardial cells.[36] Although the absolute level of expression of ERα and ERβ is not well characterized, it is known that both endothelial and smooth muscle cells bind estrogen with high affinity.[3] Upon binding, the clinical benefits of estrogen are at least partially related to its capacity to enhance the bioavailability of the powerful vasodilator nitric oxide (NO) through stimulation of endothelial nitric oxide synthase (eNOS).[37,38] NO, produced from the conversion of L-arginine to L-citrulline by eNOS, is well-known to provide significant benefits to the vasculature through regulation of blood pressure and platelet aggregation while maintaining the structural integrity of the vessel wall through the promotion of endothelial cell growth and migration, and attenuation of smooth muscle cell growth and migration.[28,39,40]

Cell-based studies have further established the intricate relationship between the estrogen receptor and eNOS. In cultured endothelial cells, physiological concentrations of $E_2$ caused eNOS activation within 15 minutes of exposure to the hormone, which is consistent with studies in arteries, and the response is blunted by ER antagonism, suggesting an ER-mediated process.[41,42] Furthermore, overexpression of ERα within these cells resulted in an enhancement of NO production. In COS-7 cells, which do not constitutively express ERα or eNOS, NO production could only be detected after cotransfection of ERα and eNOS cDNAs.[5]

Vascular benefits of NO production are now well-documented, and it is becoming clear that estrogen binding with membrane-associated ERs and subsequent stimulation of eNOS play a key role in blood vessel health and have since provided the rationale for hormone replacement therapy (HRT) in cardiovascular maintenance.[43]

*E. Estrogen, Heart Disease, and Hormone Replacement Therapy*

Before menopause, the main endogenously derived circulating estrogen is 17β-estradiol, and depending on the age and stage of the menstrual cycle of a female, concentrations of this hormone can vary considerably: serum estradiol concentrations are low in preadolescent girls, ranges from 100 pg/mL in the follicular phase to 600 pg/mL at the time of ovulation in premenopausal women, and after menopause, declines to levels seen in men of similar age (2-5 pg/mL).[44] Correlation of serum estradiol concentrations to the incidence of heart disease in

women is quite striking: the incidence of heart disease is low in premenopausal women, comparable to those seen in men, steadily rises in postmenopausal women, and reverts back to premenopausal levels with estrogen replacement therapy.[44] Such studies have demonstrated the significance of estrogen within the cardiovascular system and the need to maintain optimal serum estrogen concentrations to decrease the risk of developing heart disease.

Unfortunately, a liability associated with estrogen administration for the maintenance of cardiovascular health is the global agonist effects estrogen has on the many and diverse estrogen target tissues. The beneficial effects in the vasculature can come at the expense of overstimulation of other estrogen-sensitive tissues, such as breast and uterus, which increase the risks of cancers in these tissues, as revealed by recent hormone replacement therapy (HRT) studies.[45,46] Much effort has gone into the development of estrogens that have a more favorable profile of beneficial vs. detrimental effects in different target tissues.[47,48] Such compounds, termed selective estrogen receptor modulators (SERMs), have a selectivity based on differential interaction with coregulator proteins that mediate the nuclear action of the ER, and though they represent an therapeutic advance, their desired beneficial agonist effects rarely match those of estradiol itself. The development of estrogens that selectively stimulate the extra-nuclear pathway, in the absence of nuclear activation, would provide intriguing and potentially safer alternatives to the estrogens and SERMs currently used in HRT regimens that non-selectively target both pathways.

*F. The Estrogen Dendrimer Conjugate (EDC)*

Currently, the only successful strategy to achieve selective activation of the extra-nuclear pathway of estrogen action has been to tether estrogens to a large molecule that prevents its nuclear uptake. The most widely used are various commercial preparations of a conjugate between estradiol and bovine serum albumin ($E_2$-BSA)[49-51] or, to a lesser extent, peroxidase ($E_2$-peroxidase).[52-54] Numerous studies in cell culture have shown that $E_2$-BSA is able to activate kinase cascades and other rapid cellular responses that are presumed to be mediated by extra-nuclear ER action. Nevertheless, $E_2$-BSA has proved to be a troublesome reagent: its affinity for ER is limited and instability in the covalent link between estrogen and BSA releases active estrogens;[55] furthermore, the protein nature of BSA makes it unsuitable for *in vivo* work.

Recently, we reengineered such hormone-macromolecule conjugates by designing a more structurally robust system called the estrogen dendrimer conjugate (**1**, EDC, Figure 3.2).[56]

The EDC is constructed through the use of a high affinity estrogen, ethynyl estradiol, derivatized at the 17α-position of the steroid, a position known to tolerate large substitution and still retain high affinity for ER.[57] The estrogen is attached through a short linker, that has been shown not to affect its binding affinity, to a large, positively charged, non-biodegradable generation-6 (G6) poly(amido)amine (PAMAM) dendrimer. Key to the design is the use of hydrolytically stable linkages between the estrogen and PAMAM dendrimer as any release of the estrogen would stimulate the undesired genomic pathway and reduce the selectivity for the preferred nongenomic pathway.

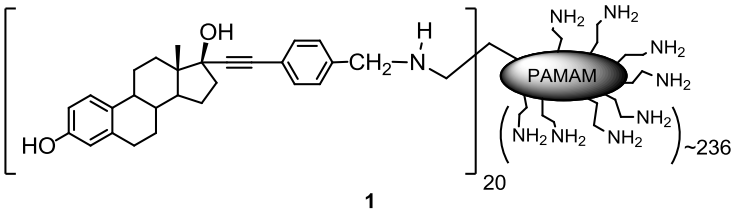


**1**

**Figure 3.2.** Structure of the Estrogen Dendrimer Conjugate (EDC).

The synthesis of EDC is straightforward (Scheme 3.1).[56] The benzaldehyde derivative (**3**) can be rapidly accessed through a Sonogashira reaction between commercially available ethynyl estradiol (**2**) and 4-bromobenzaldehyde and the degree of dendrimer substitution by the estrogen can be controlled simply by adjusting the molar ratios of aldehyde (**3**) to dendrimer (**4**) which in our case, 20 of the free 256 amines present on the PAMAM periphery were utilized for derivatization. In MeOH, imine formation was spontaneous; reduction with borohydride was quantitative, and the reaction could be monitored by aldehyde peak disappearance in the $^{1}$H NMR spectrum. The resulting EDC (**1**) then underwent 5 extensive rounds of rigorous purification to remove any unreacted estrogen, with the final ligand-to-dendrimer being determined by matrix-assisted laser desorption ionization (MALDI) which reflected the reaction stoichiometry.

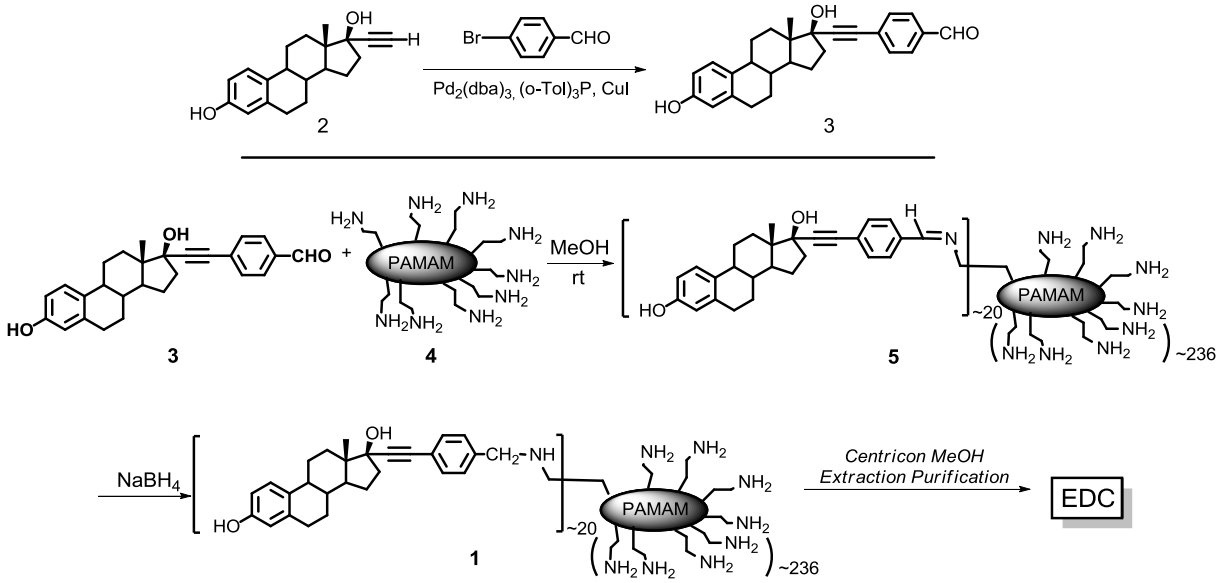


**Scheme 3.1.** Synthesis of EDC (**1**).[56]

An attractive feature of the PAMAM dendrimer system is that its periphery can be further functionalized with fluorophores to follow the cellular distribution of EDC with confocal microscopy (Figure 3.3). In MCF-7 cells, a tetramethylrhodamine-labeled EDC (TMR-EDC) showed bright fluorescent speckles at the plasma membrane with no accumulation in the nuclei, which were stained blue. Replication of the same experiment with a 30-fold excess of estradiol as a blocking agent revealed a marked suppression in cellular fluorescence, suggesting the uptake in the previous experiment was most likely an ER-mediated process.[58]

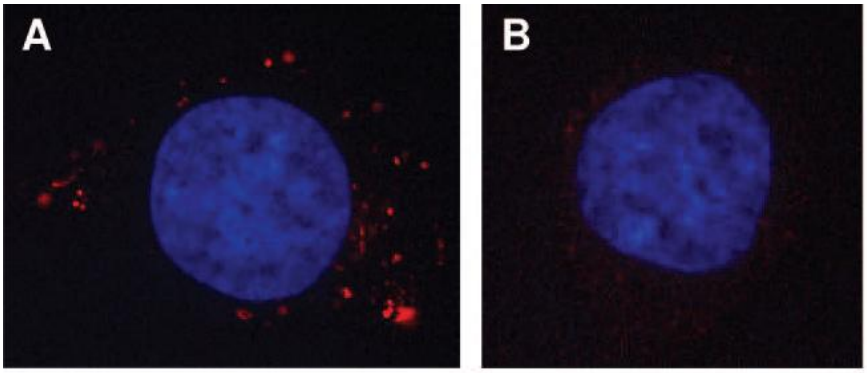


**Figure 3.3.** Fluorescence photomicrographs of MCF-7 cells treated with 100 nM (estrogen equivalents) TMR-EDC (A) or together with a 30-fold excess of $E_2$ (B) after 45 minutes. Red fluorescence is from TMR-EDC; blue staining with 4',6-diamidino-2-phenylindole indicates the nucleus.[58]

A key aspect of these types of estrogens is their ability to selectively activate the nongenomic pathway over the genomic pathway; thus, they can be used to understand the

biological significance of this pathway and to test whether it is a viable target for therapy. From the confocal microscopy studies, one would expect that an ER ligand that remains outside the nucleus, because of its size and charge, would have an attenuated capacity to activate nuclear activities. To assess genomic stimulation (Figure 3.4), the relative potency of $E_2$ and EDC to regulate two known endogenous estrogen responsive genes (pS2 and WISP2)[59] was evaluated in $ER^+$ MCF-7 cells.[58] Dose-response studies revealed a strong and pronounced stimulation by estradiol at very low concentrations ($10^{-11}$-$10^{-12}$ M), while in contrast, stimulation with EDC was only seen at much higher concentrations ($10^{-7}$ M). To investigate the effectiveness of EDC in activating the nongenomic pathway (Figure 3.5), the time course and dose response of extracellular signal-regulated kinase (ERK) was monitored in MCF-7 cells, because this cell line has been shown to exhibit strong nongenomic responses to $E_2$. In the presence of EDC at low concentrations ($10^{-11}$-$10^{-12}$ M), a very robust stimulation in the phosphorylation of ERK was observed, even more so than when compared to estradiol itself.[58] These studies demonstrated the effectiveness of EDC in selectively stimulating the nongenomic pathway, in the absence of nuclear activation, and now serves as an ideal biological tool to probe the complexities of estrogen action in the context of both pathways.

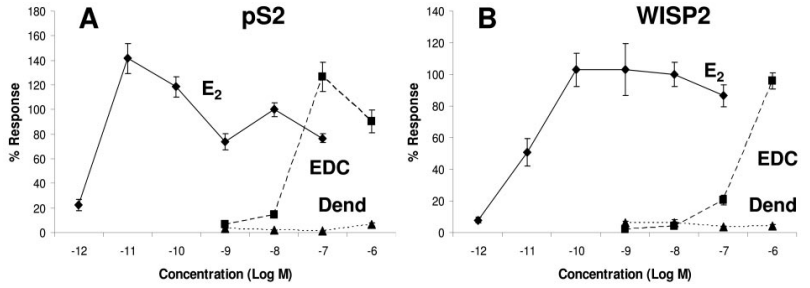


**Figure 3.4.** Regulation of estrogen-responsive genes pS2 (A) and WISP2 (B) in MCF-7/Her 2 cells treated with $E_2$, EDC, or empty dendrimer (Dend) for 8 hours at the indicated concentration.[58]

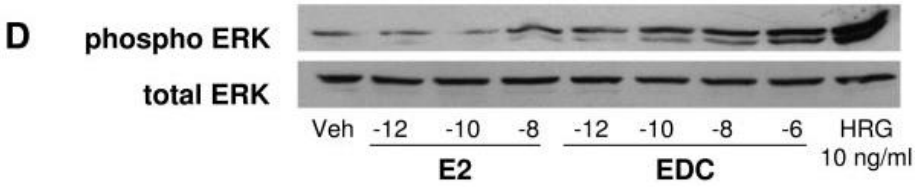


**Figure 3.5.** Stimulation of ERK phosphorylation in MCF-7/Her 2 cells by $E_2$ (10 nM) and EDC (10 nM estrogen equivalents) for 20 minutes.[58]

Although the desired selectivity between the two pathways was obtained, it still remained unknown whether the nongenomic pathway was operative *in vivo*. PAMAM dendrimers are commonly utilized as drug delivery systems[60,61] and EDC would assume a similar role in interrogating the significance of extranuclear estrogen actions *in vivo* within the context of the cardiovascular system. In collaboration with Phil Shaul at UT Southwestern Medical Center,[62] the cardioprotective effects of EDC were assessed in a carotid injury mouse model, in which a mouse carotid artery underwent electric injury and the extent of repair was evaluated after three day treatment with $E_2$ and EDC. Quite strikingly, as shown in Figure 3.6, EDC is nearly as effective at repairing the injury to the arterial wall, as depicted by the decrease in blue color as compared to the controls, vehicle or empty dendrimer.

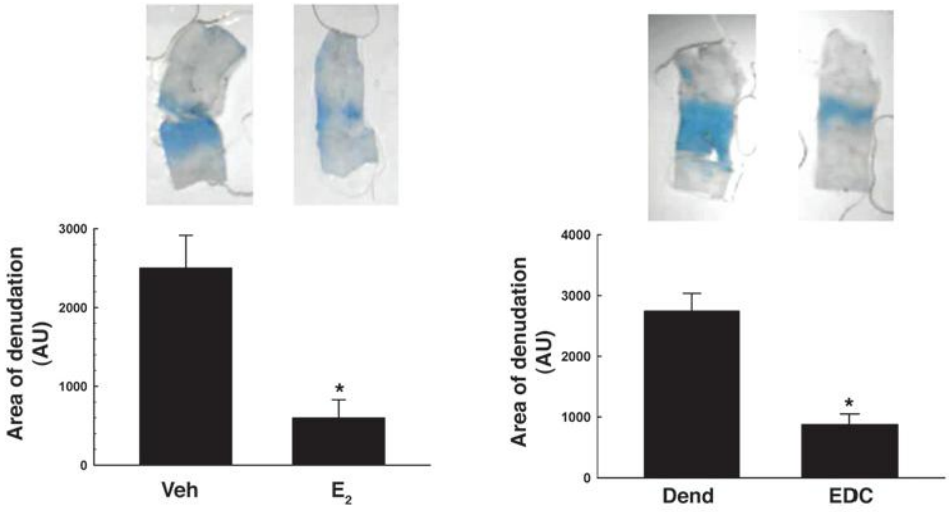


**Figure 3.6.** Non-nuclear ER signaling promotes endothelial monolayer *in vivo* in ovariectomized female mice following perivascular electric injury. Left: Vehicle versus $E_2$ 3 day treatment after injury. Right: Empty dendrimer versus EDC 3 day treatment after injury. Blue color indicates the extent of injury.[62]

However, in order for EDC to possess any clinical value, it would need to retain these exceptional cardioprotective properties while having minimal effect on other estrogen-sensitive tissues (i.e., breast, uterus). This is exactly the problem with traditional HRT and the nonselective nature of the administered estrogens. Since the receptor is widely distributed within both males and females, the beneficial effects in one tissue, such as the vasculature in this case, can come at the expense of overstimulation in others and increase the risks of certain cancers.[45,63] Selective agents for protection of the cardiovasculature, similar to those seen with bone-selective SERMs (i.e., raloxifene) used in the treatment of osteoporosis, are still in need of further development.[64]

Remarkably, EDC possesses exceptional selectivity *in vivo*: investigations in the stimulations of uterotrophic responses and MCF-7 cell breast cancer xenograft growth, which readily responded to $E_2$ through genomic stimulation, revealed no stimulation by EDC (Figure 3.7). As a result, the observed benefits are largely the result of the ability of EDC to selectively stimulate the nongenomic response, which is sufficient to provide protection of the cardiovascular tissue and more importantly, its inability stimulate estrogen sensitive tissues (i.e., breast, uterus) because of its attenuated capacity to activate the genomic pathway. These findings are quite significant and should have a tremendous impact on the development of ER-targeted hormone replacement agents in the future.

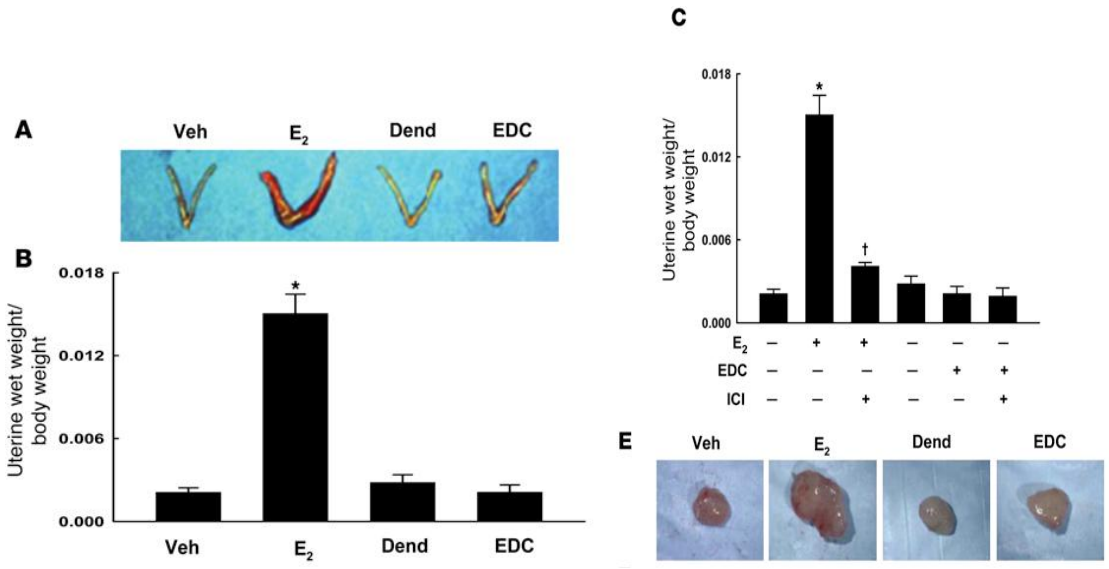


**Figure 3.7.** Non-nuclear ER signaling does not stimulate an uterotrophic response or breast cancer cell tumor growth. (**A**) Uteri from mice treated for 24 days with vehicle, $E_2$, empty dendrimer, or EDC. (**B**) Evaluation of uterine wet weight to body weight ratios**.** (**C**) Extended uterotrophic study with ER antagonism, ICI. (**E**) MCF-7 cell tumor xenografts after 21 day treatment with $E_2$, vehicle, empty dendrimer or EDC.[62]

## II. CONCLUDING INTRODUCTORY REMARKS

Overall, EDC has been found to retain good affinity for ER, but because of its size and charge, it is excluded from the nucleus. Consequently, EDC was found to possess minimal capacity for stimulating genomic activities, but a number of studies from our lab[58,65,66] and others[67-69] have shown that EDC effectively and selectively activates rapid extra-nuclear ER signaling in a variety of cellular response systems. More significantly, recent studies have demonstrated in two *in vivo* animal models that EDC provides cardiovascular protection equivalent to that of estradiol, yet unlike estradiol, does so without stimulating uterine growth or

breast tumor proliferation.[62] These findings established that action only through the extra-nuclear ER pathway, as stimulated by EDC, is sufficient to provide remarkably selective cardiovascular benefit, thereby avoiding undesired effects on other estrogen-responsive tissues.

To investigate further the basis for the remarkable target-tissue selective activity of EDC, we have labeled this conjugate with fluorine-18 (F-18) and examined its biodistribution *in vivo*. We find that [$^{18}$F]-EDC (**8**) is cleared rapidly from blood, and as expected for a particulate species, much activity becomes sequestered in spleen and liver. Nevertheless, significant uptake and retention are found in the heart and aorta, but by contrast, essentially no [$^{18}$F]-EDC is taken up by the uterus. By comparing the uptake of [$^{18}$F]-EDC with that of a structurally related analogue with little affinity for ER ([$^{18}$F]-XDC, **21**), we found that uptake in the heart and aorta appears to depend on the ER binding activity of EDC. These findings suggest that the selective cardiovascular protective effect of EDC is the result of two factors, one mechanistic (selective stimulation of the extra-nuclear pathway of ER action) and one pharmacokinetic (selective accumulation of EDC in vascular targets), and it points to a new dimension for extending the selective, potentially beneficial actions of estrogens.

## III. RESULTS

### *A. Synthesis of [$^{18}$F]-EDC*

EDC (**1**) was prepared as described previously;[56] the degree of $EE_2$ substitution was an average of 18 steroid molecules per dendrimer molecule, with a polydispersity index of 1.02, as determined by MALDI-TOF MS analysis. EDC was radiolabeled with fluorine-18 using two complementary methods based *N*-hydroxysuccinimide ester chemistry with either Si-$^{18}$F or Cu-click approaches. Both approaches utilized an indirect, multi-step sequence where fluorine-18 was first introduced into small adaptor compounds and then appended to EDC through hydrolytically stable amide bonds. A direct approach was not attempted due to the inherent difficulty associated with radiolabeling a large nanoparticle such as EDC in a one-step process.

The Si-$^{18}$F approach has proved to be highly useful (Scheme 3.2). First and foremost, the aqueous [$^{18}$F]fluoride source from the cyclotron can be used as an off-the-bench reagent, without having to resort to the tedious and time-consuming drying step required for classical C-$^{18}$F chemistry and the formation of a dried [$^{18}$F]fluoride salt. A simple dilution of the [$^{18}$F]F-$H_2$[$^{18}$O]O water with acetonitrile, dissolution of the NHS-silyl acetate (**6**), and heating at 105 $^{o}$C for 10 minutes yielded **7** in high RCYs. After cooling to room temperature, the reaction mixture,

without any extraction, is injected directly into the HPLC to afford **7** in high radiochemical purity (>99%) and specific activity (3500-3800 Ci/mmol). The purified [$^{18}$F]fluorosilane product can be readily appended to EDC (**1**) within 10 minutes, albeit in varying RCYs of **8** (60-98%). The sources of this variability have been difficult to ascertain, but appear to be dependent on the amount of $H_2O$ of **7** after purification, pH of the EDC solution, and precipitation issues from overconjugation. Nevertheless, the attractiveness of the approach lies in the high efficiency of the radiofluorination reaction: beginning with 50 milliCuries (mCi), the reaction sequence can reliably afford 15 mCi of the desired compound after 2 hours. This is a highly attractive feature, especially when conducting time-sensitive animal studies that are dependent on obtaining sufficient amounts of activity of the radiotracer at a specified time.

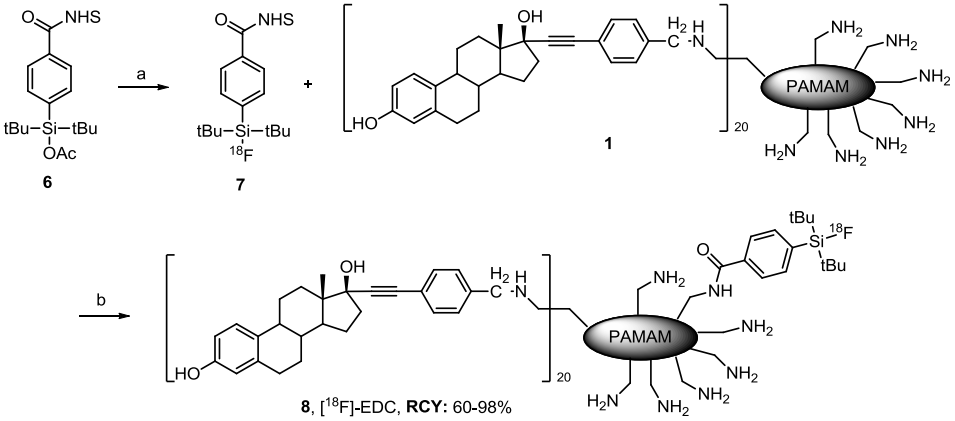


**Scheme 3.2.** Radiosynthesis of [$^{18}$F]-EDC (**8**) with the silyl acetate approach. (a) [$^{18}$F]F-$H_2$[$^{18}$O]O, ACN, 105 $^{o}$C, 10 min; (b) **1**, **7**, MeOH, rt, 10 min.

Of the available "click chemistry," the most commonly used click-reaction is the Cu(I) catalyzed 1,3-dipolar cycloaddition of terminal alkynes with azides, called the Huisgen reaction, yielding 1,4-disubstitued 1,2,3-triazoles under mild conditions.[70] The popularity of the reaction is attributed to its high efficiency, absence of protecting group protocols, chemical inertness of the azides and alkynes towards biological molecules and formation of an extremely stable triazole moiety, and it has since been used in numerous applications,[71] but only recently have application in $^{18}$F-labelling been reported.[72] Our approach takes advantage of the rapid and efficient manner of these reactions through a three-step sequence (Scheme 3.3): displacement of a tosylate to form the [$^{18}$F]fluoroazide (**10**), Cu-mediated click reaction to afford triazole **12**, and a final conjugation to EDC. Although an additional step is needed and lowered purified [$^{18}$F]-EDC-Click (**13**) activities, this approach has its own merits. The sequence still only requires one HPLC purification step, since the [$^{18}$F]fluoroazide **10** can be readily distilled out of the reaction

mixture in high radiochemical purity. Due to the chemoselective nature of the click reaction, the next step can be performed directly, in the presence of other distilled mass from the previous step, without the need for HPLC purification. Consequently, sufficient amounts of **13** can be readily obtained in high SA (800-2600 Ci/mmol).

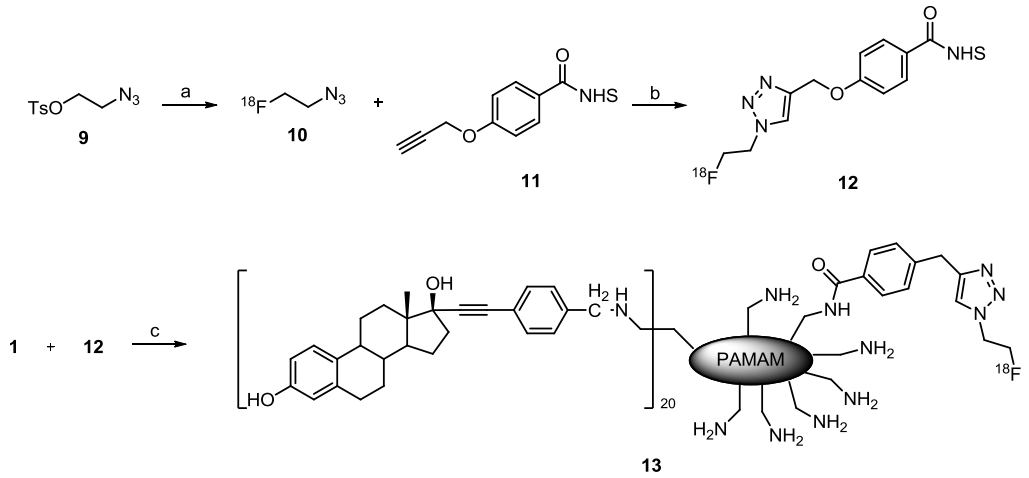


**Scheme 3.3.** Radiosynthesis of [$^{18}$F]-EDC-Click (**13**) with copper click approach. (a) K[$^{18}$F]F, $K_2CO_3$, $K_{222}$, ACN, 88 $^{o}$C, 5 minutes; (b) $CuSO_4$, sodium ascorbate, BPDS, DMF, $H_2O$, rt, 5 minutes; (c) **1**, **12**, MeOH, rt, 10 minutes.

To investigate non ER-mediated uptake of the EDC, we also prepared and radiolabeled an ER non-binding analogue of EDC, termed XDC (**20**, Scheme 3.5), in which the $EE_2$ hormone was replaced by a biphenyl methyl ether analogue. We modified our original high affinity estrogen by blocking the energetically crucial hydrogen bond between A-ring phenol of estradiol and polar residues in the ER ligand binding pocket through methyl ether formation and further by flanking it with two ortho methyl groups. These changes, together with deletion of the B-ring, afforded **18** with very low ER binding affinity (<0.001% relative to estradiol, 100%), and after it was conjugated to the G6 PAMAM dendrimer, we found that XDC had an ER binding affinity that was more than 45-fold less than that of EDC (0.083% for XDC and 3.8% for EDC).

The non-binding estrogen was rapidly accessed through a three-step sequence (Scheme 3.4) involving a Suzuki coupling between boronic acid **14** and bromide **15**, Grignard addition to the ketone **16**, and a Sonogashira reaction to afford the desired compound (**18**). This analogue (1**8**) was designed to be matched with the original estrogen (**7**) in EDC in terms of lipophilicity (Figure 3.8: cLogP$^{o/w}$ 5.98 for **18** vs 5.53 for **19**) to allow comparison of the two particles based solely on the affinity of the attached estrogens for ER and not from the differences in LogP, which can markedly perturb *in vivo* biodistributions.

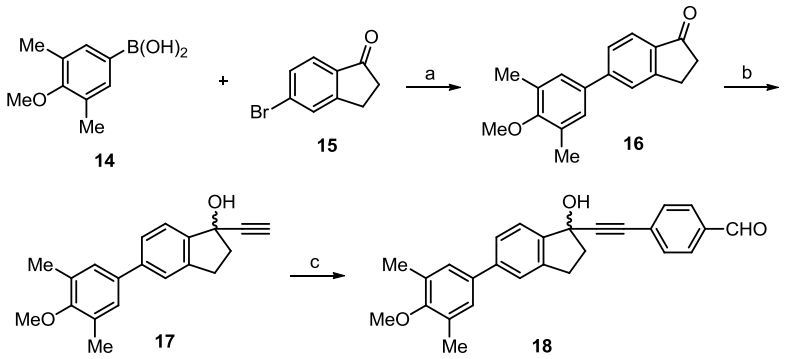


**Scheme 3.4.** Synthesis of a non-binding estrogen (**18**). (a) $Na_2CO_3$, $Pd(PPh_3)_4$, DMF, 80 $^oC$; (b) TMSC≡CMgBr, THF, -78 $^oC$; (c) 4-iodobenzaldehyde, piperidine, CuI, $Pd(Cl_2)(PPh_3)_4$, THF, reflux.

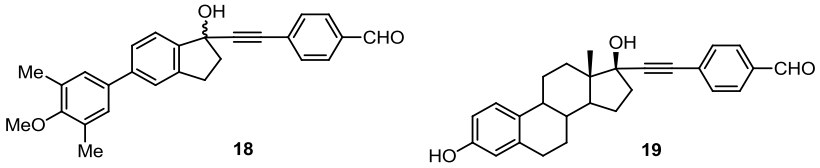


**Figure 3.8.** Structures for $LogP^{o/w}$ determinations: 5.98 for **18** vs 5.53 for **19**.

Under conditions identical to those previously used for [$^{18}$F]-EDC, XDC (Scheme 3.5) was radiolabeled with our [$^{18}$F]fluorosilane system in high radiochemical purity (>99%) and specific activity (1800 mCi/μmol; 67 GBq/μmol). The Si-$^{18}$F approach was re-used in this system after $^{19}$F-NMR studies were inconclusive on the cause of defluorination and since the defluorination did not affect the biodistribution, it was the preferred method of choice since it was technically simpler and afforded EDC in higher specific activities.

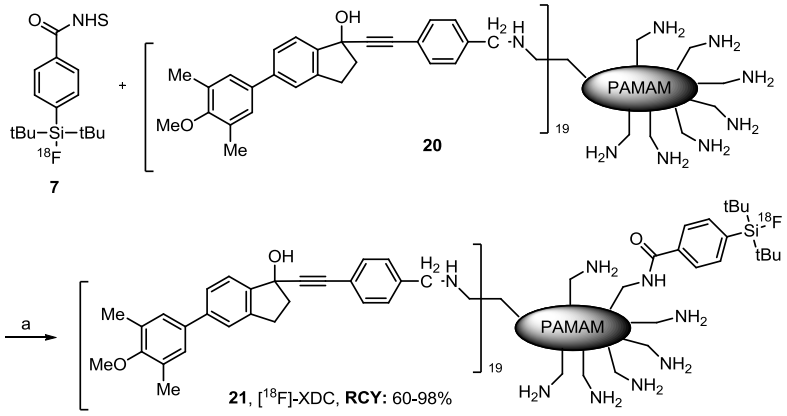


**Scheme 3.5.** Radiochemical synthesis of [$^{18}$F]-XDC (**21**). (a) MeOH, rt, 10 min.

*B. Biodistribution of [$^{18}$F]-EDC*

After IV injection, the tissue distribution of [$^{18}$F]-EDC (**8**) in adult female C57BL6 mice was determined at 30 minutes and 2 hour post injection, and tissue activity, expressed as the percent injected dose per gram of tissue, is shown in Figure 3.9. The highest initial uptake (%ID/g) of [$^{18}$F]-EDC was localized in the spleen, followed by high levels in the liver and lung, consistent with the expected recognition and binding of an unprotected particle by opsonins and subsequent sequestration by the mononuclear phagocyte system (MPS) active in these tissues.[73] In kidney and muscle, [$^{18}$F]-EDC exhibited low uptake, with blood clearance occurring rapidly over the time course of the experiment, as relatively low activity was present at the 30 minutes and clearance was almost complete within 2 hours.

Strikingly, [$^{18}$F]-EDC showed rapid and persistent accumulation in two presumed cardiovascular target tissues, heart and aorta. At 30 minutes, the %ID/g was 19.7 in the heart and 8.15 in the abdominal aorta, and unlike activity in blood, activity in these target tissues persisted at 2 hours with minimal clearance. In contrast to traditional $^{18}$F-labelled estrogens that often exhibit high uterine uptake in mice (10-15 %ID/g),[74] [$^{18}$F]-EDC shows minimal uptake in the uterus, most likely due to its particulate nature, which limits its access to the major pool of ERs in the nucleus. Taken together and outside of uptake in organs with high MPS activity, the tissue biodistribution of [$^{18}$F]-EDC correlates well with the pattern of selective *in vivo* activity that we have reported.[62]

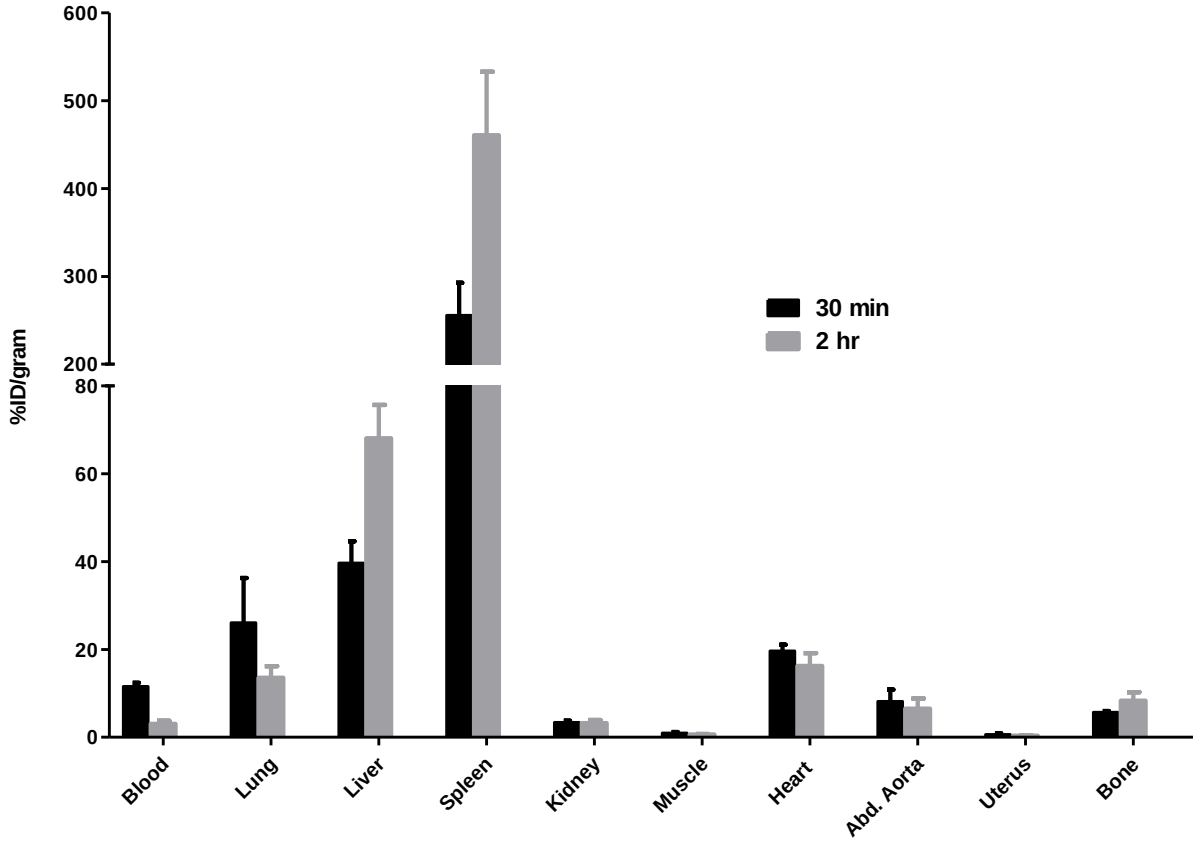


**Figure 3.9.** Biodistribution of [$^{18}$F]-EDC in adult female C57BL6 mice (%ID/g). Mice were injected with 15-20 µCi of [$^{18}$F]-EDC, and tissue distribution, determined at 30 minutes and 2 hours, is expressed as % of injected dose per gram tissue (%ID/g).

Although the EDC clearly is being rapidly sequestered by particle clearance organs, it is notable that even small molecule estrogens are rapidly lost from blood, so the blood clearance and tissue exposure is actually not all that different. The only difference resides in where the tracer becomes concentrated: small molecules typically clear through the liver and kidneys and are eliminated, but the EDCs become sequestered in the lung, liver, and spleen. The only legitimate concern from the initial biodistribution was the possible hydrolysis of the Si-$^{18}$F bond as indicated by the elevated bone uptake (13% and 18% ID/organ at 0.5 and 2 hours, respectively). With the presence of numerous potential nucleophiles on the periphery of the PAMAM, the likelihood of amine attack on the silicon atom is not improbable, but did warrant further investigations with $^{19}$F NMR studies before continuing with this approach and we switched to the Cu-click strategy at this time.

Following the same animal protocol used previously and the radiolabeling method in Scheme 3.2, the Si-$^{18}$F and C-$^{18}$F-labelled (**13**, Figure 3.10) EDCs showed remarkably similar

biodistributions: high uptake in the lung, liver and spleen, low uptake in the kidney, muscle, and uterus, and elevated activities in the cardiovascular tissues, heart and abdominal aorta. However, with the Si-$^{18}$F labeled EDC, bone uptake was 13% and 18% ID/organ in female mice at 0.5 and 2 hours, but was only 2.8% and 2.5%ID/organ with the [$^{18}$F]-EDC-Click material, suggesting that with time the Si-$^{18}$F material is undergoing some progressive defluorination. Besides this unanticipated occurrence, loss of fluoride from the Si-$^{18}$F material was relatively minor and did not perturb the overall distribution. This is not too surprising since the level of substitution from the $^{18}$F-conjugation is at most three appended groups and as a result, one would expect the conjugation not to alter the physical properties of the high molecular weight EDC (MW: 55,000) to any significant extent.

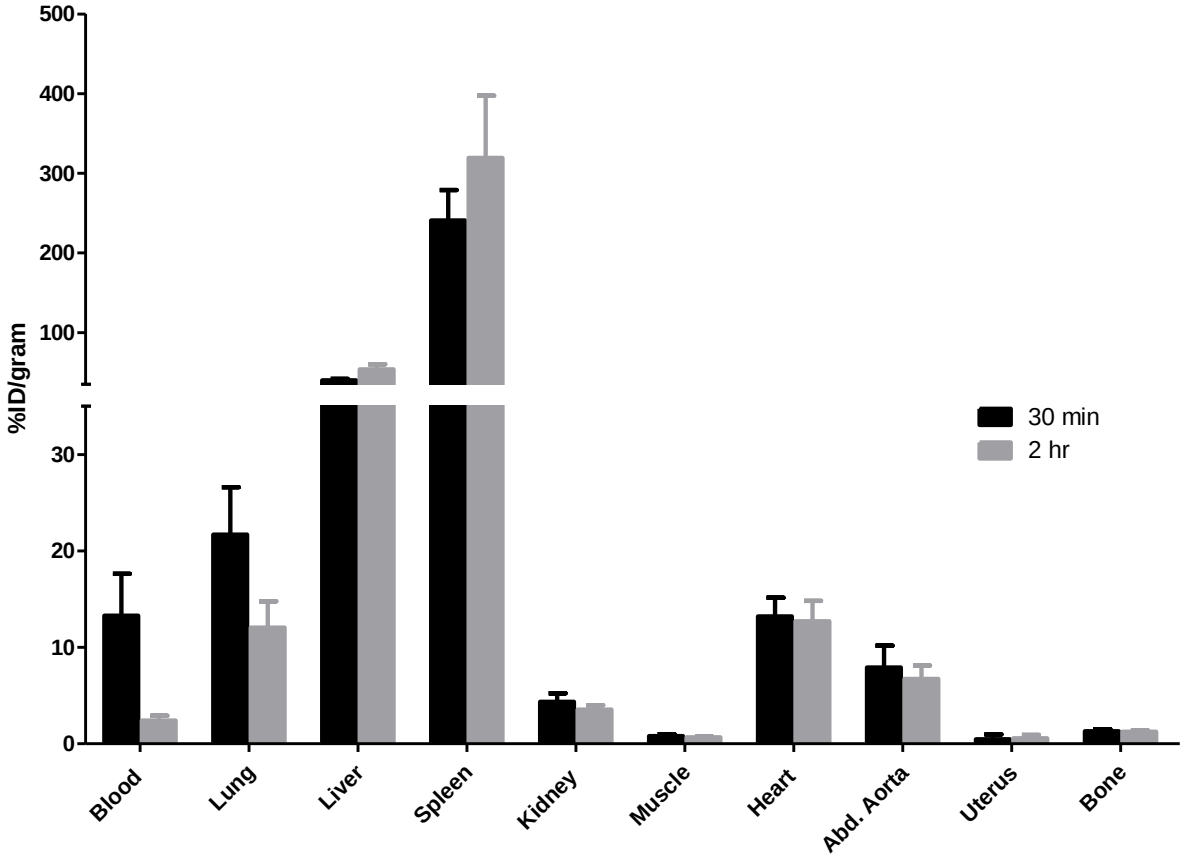


**Figure 3.10.** Biodistribution of [$^{18}$F]-EDC-Click (**13**) in adult female C57BL6 mice (%ID/g). Mice were injected with 15-20 µCi of [$^{18}$F]-EDC-Click, and tissue distribution, determined at 30 minutes and 2 hours, is expressed as % of injected dose per gram tissue (%ID/g).

Blocking studies are often performed to validate receptor-mediated uptake. Typically, these studies involve two sets of injections. The first injection attempts to saturate the receptor binding sites with a large excess of either a chemically identical cold standard (only differs in the

isotope present) or a compound that is known to have high affinity for the receptor (i.e., $E_2$ for ER) and the second injection introduces the radiotracer. Our strategy focused on saturating the available ER binding sites with $E_2$ or unlabeled EDC to impede uptake in the heart and abdominal aorta in an attempt to confirm the observed elevated uptake was indeed ER-mediated.

Initially, we attempted to block the uptake of [$^{18}$F]-EDC-Click (**13**) in the heart and aorta by co-administration of an excess of unlabeled estradiol (20-100-fold excess), but in both cases, the blocking was unsuccessful since high uptake was still seen in the heart and aorta. We believe that the lack of competition by estradiol represents simply its ineffectiveness as a monovalent ligand in competing with the multivalent ligand character of the EDC. Only when we used a 500-fold excess of unlabeled EDC could we effectively block the uptake, as shown in Figure 3.11. This study involved three different animal groups: a high dose, low dose, and EDC block group. The high dose group (30 µCi) served as a standard to confirm a similar biodistribution as the previous two cases and thus enables the blocking study results to be correlated to each study from before. The low dose group (3-5 µCi) was designed to ensure complete blockage of uptake if indeed it is ER-mediated. The EDC block involved a 500-fold excess of EDC, which equates to around 40 µg of material; this dose was injected into the mouse before any of the low dose was injected. At 2 hours post injection (Figure 3.11), the highest doses were concentrated in the liver and spleen but more importantly, when the EDC block was administered against the low dose, there is a significant reduction in EDC uptake within the heart and abdominal aorta, indicating the elevated uptake within these target tissues seen previously (Figure 3.8 and 3.9) was most likely ER-mediated.

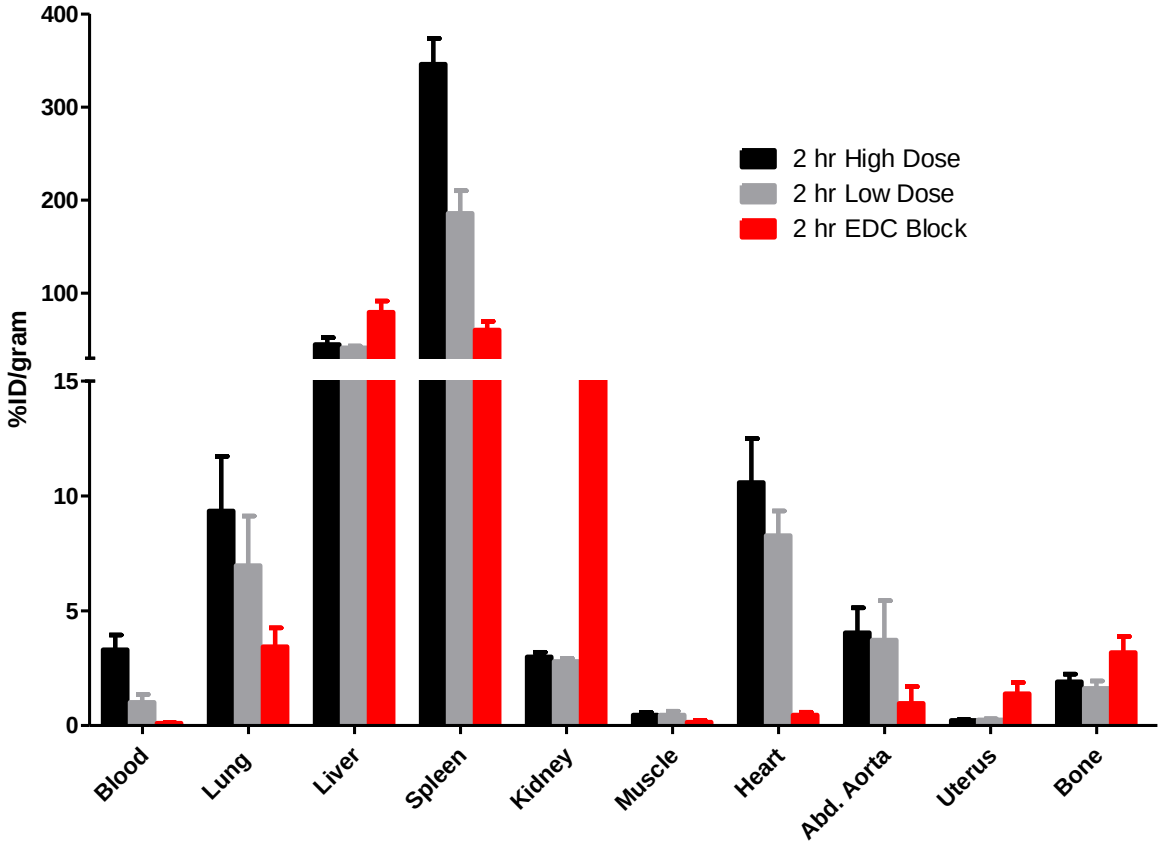


**Figure 3.11.** Biodistribution and blocking study of [$^{18}$F]-EDC-Click (**13**) in adult female C57BL6 mice (%ID/g). Mice were injected with 25-30 µCi of [$^{18}$F]-EDC-Click for the high dose, 3-5 µCi for the low dose and the block involved a 500-fold excess of unlabeled EDC and a 3-5 µCi dose of labeled material. Tissue distribution, determined at 2 hours, is expressed as % of injected dose per gram tissue (%ID/g).

To further investigate whether the selective uptake and retention of [$^{18}$F]-EDC in the heart and aorta was mediated by binding to the ER, a biodistribution was also performed with the non-ER binding EDC analogue, [$^{18}$F]-XDC (**21**); results are shown in Figure 3.12. Again, highest uptake of this particulate tracer was in spleen and liver, but notably, uptake in the heart and aorta at 30 minutes was 20-fold less than that of [$^{18}$F]-EDC. Furthermore, even this reduced heart and aorta uptake of [$^{18}$F]-XDC was essentially cleared by 2 hours, whereas the greater uptake of [$^{18}$F]-EDC in these tissues was essentially unchanged at 2 hours. Thus, as shown in the expansion of the heart and aorta uptake data for the two agents (see Figure 3.12 inset), the non-ER binding [$^{18}$F]-XDC showed much lower and less persistent uptake in the vascular target tissues than the ER binding [$^{18}$F]-EDC, consistent with an ER-binding mediated

process.

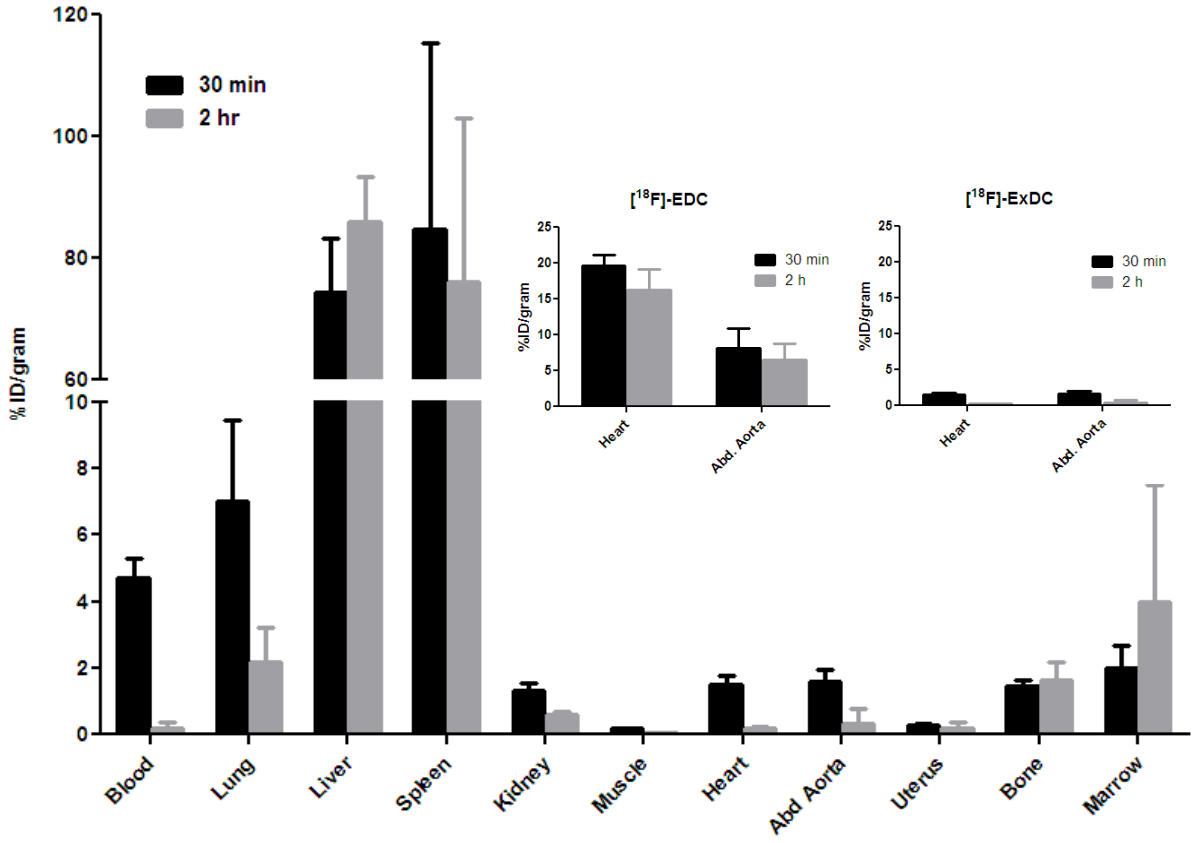


**Figure 3.12.** Biodistribution of [$^{18}$F]-XDC (**21**) in adult female C57BL6 mice (%ID/g). Mice were injected with 15-20 µCi of [$^{18}$F]-XDC, and tissue distribution, determined at 30 minutes and 2 hours, is expressed as % of injected dose per gram tissue (%ID/g). Inset: comparison of uptake in the heart and abd. aorta between [$^{18}$F]EDC (Figure 3.9) and [$^{18}$F]-XDC.

## IV. DISCUSSION

In this study, we have determined the biodistribution of EDC, a conjugate between $EE_2$ and a G6 PAMAM dendrimer, labeled with F-18 using two convenient and efficient methods. As is typical for a particulate species, the bulk of [$^{18}$F]-EDC is rapidly taken up by the spleen and liver, presumably by an MPS-mediated process.[73] The undesired uptake in these nontarget tissues still remains a significant obstacle for targeted-base drug delivery systems using these types of polymeric nanoparticles. The problem arises from their recognition as foreign particles *in vivo* and the defense mechanisms that designed for their removal. Upon injection, particles undergo opsonization, thereby rendering them visible to phagocytic cells and results in their very rapid removal from the bloodstream, typically within minutes.[75] The particle then becomes engulfed through endocytosis by the phagocyte, which begins to secrete enzymes and other

chemical factors (i.e., hydrogen peroxide) to break down the foreign material.[76] In our case, EDC is a non-biodegradable biopolymer and cannot be degraded significantly by this process. As a result, the particle becomes sequestered and stored in MPS organs, which explains the high uptake by the liver and spleen from our biodistributions. Several strategies of camouflaging ("stealth particles") have been developed to bypass recognition and opsonization in an attempt to increase blood retention time and uptake in the desired target tissue, with PEGylation being the most well-known.[77,78] Current efforts to redesign EDC with polyethylene glycol chains to extend blood circulation, minimize the undesired uptake in non-target tissue and increase uptake in the cardiovasculature are currently underway.

Although the [$^{18}$F]-EDC clearly is being rapidly sequestered by particle-clearance organs, it is notable that even small molecule estrogens are rapidly lost from blood, so the blood clearance and tissue exposure is actually not all that different; it is just that the small molecules clear through the liver and kidneys and are eliminated, but [$^{18}$F]-EDC becomes trapped in the lung, liver, and spleen. However, very marked uptake and retention of [$^{18}$F]-EDC is also noted in the heart and abdominal aorta, known target sites of the extra-nuclear action of estrogens. EDC uptake and retention in these sites appears to be ER mediated because a structurally matched, but non-ER binding EDC analogue, XDC, shows little uptake and rapid clearance. The ER-mediated uptake of EDC in heart and aorta appears to be of a different nature than that of small molecule estrogens, which are most avidly taken up by the uterus, but not by heart and aorta; EDC, by contrast, shows no uptake and retention by the uterus.

The negligible amount of activity present in the blood with the EDC block (Figure 3.11) is of interest and suggests that the high dose of EDC might be accelerating clearance processes, but since similar reductions of activity are not seen in other organs, this is most likely not the case; thus, the exact cause for the low blood activity is still unknown. Also, the increased uptake in certain tissues, including the uterus, bone and especially the kidney, is of note. However, the exceedingly high dose of material needed for the EDC block might be sufficient to cause some unanticipated pharmacological effects, which may lead to saturation of MPS organs and an increase uptake in nontarget tissue, although the mechanisms leading to this have yet to be determined. Nonetheless, cold EDC was effective at outcompeting [$^{18}$F]-EDC to block ER-mediated uptake and the unforeseen biodistribution concerns were only observed in the blocking study when EDC was present at much higher concentrations than in the previous studies (Figure 3.9 and 3.10).

It has been a longstanding challenge to develop estrogens that provide an ideal balance between beneficial vs. detrimental health effects in older women. While estrogen agonists like estradiol and conjugated equine estrogens suppress menopausal hot flush and maintain bone strength and cardiovascular health, they increase the risks of breast and endometrial cancers.[79] By contrast, antiestrogens, including SERMs, suppress estrogen-dependent cancers but generally exacerbate hot flush and are not fully protective of bone and vascular health.[80] Thus, our recent report that EDC provided protection against cardiovascular injury equivalent to that of estradiol in two animal models—without stimulation of the uterus or mammary tissue—was a significant finding, because it indicated that pharmacological separation of these desired vs. undesired effects of estrogens could be cleanly achieved.[62]

Mechanistically, this remarkable pharmacological separation appears to arise because in cells the EDC restricts estrogen stimulation only to the extra-nuclear signaling pathway, which appears sufficient to afford vascular protection but insufficient for stimulation of uterine and mammary tissues.[58] The selective stimulation of the extra-nuclear over the nuclear ER signaling pathway appears to result from the unique subcellular distribution of EDC. Using fluorescence microscopy, we have shown that EDC labeled with rhodamine rapidly associates with the plasma membrane of ER-positive breast cancer and vascular endothelial cells, and with time enters the cytoplasm, apparently by endocytosis; however, it is never found in the nucleus, even after 24 hours.[58]

In the animal studies showing vascular protection by EDC,[62] the agent was administered continuously by an osmotic minipump at a dose that maintained blood levels of EDC presenting a concentration of tethered $EE_2$ ligand equivalent to that of a protective dose of estradiol. In this study, the [$^{18}$F]-EDC and [$^{18}$F]-XDC agents were administered by IV injection, which is the route typically used to study the biodistribution of agents labeled with short-lived radionuclides. Remarkably, beyond the expected sequestration of these particulate species by liver and spleen, the [$^{18}$F]-EDC, but not the [$^{18}$F]-XDC, showed selective accumulation and retention in heart and aorta; this uptake appears to be ER mediated, yet there is essentially no accumulation in the uterus. Thus, in addition to selective ER pathway activation, the selective bioactivity of EDC in the vasculature may also originate from its selective biodistribution to these tissues.

The contrast in the ER-mediated biodistribution of EDC (heart, aorta) vs. that of small molecule estrogens, such as the well-studied 16α-[$^{18}$F]fluoroestradiol (FES) (uterus), is striking.

In principle, this difference could derive from access to the different cellular pools of ER, with small molecules like FES being able to access the larger nuclear pool of ER, but the more limited subcellular trafficking of EDC providing access only to the extra-nuclear or membrane fraction of ER. While the distribution of ER in the nuclear vs. extra-nuclear pools of the heart and vascular endothelium is not known, in cell culture extra-nuclear or membrane ER is considered to be a minor component of the total cellular ER (approximately 5-10% of ERα is present at the membrane).[27] Nevertheless, in our studies, it appears to be adequate to mediate selective, ER-dependent uptake and retention of EDC in heart and aorta.

There is increasing interest in the development of pharmaceuticals based on polymeric carriers such the PAMAM dendrimers;[77,81,82] thus, it is conceivable of an agent like EDC that could be developed into a drug for human use. However, it is worthwhile to consider whether there are alternative strategies for developing an estrogen pharmaceutical with EDC-like selective cardiovascular protection without uterus and breast stimulation, whether it might be based on other, smaller polymers or might even be a small molecule that could be orally active. Agents based on estrogens covalently attached to alternative polymers would probably need to share with EDC the subcellular trafficking that restricts the hormonal element from engaging nuclear ER, which might depend on the inherent charge or polymer architecture of the PAMAM dendrimer. Because the extra-nuclear ER signaling pathway involves the engagement of ER with tethering and coregulator components that are distinct from those utilized in the nuclear pathway, it is conceivable that a small molecule estrogen might stabilize an ER conformation that can selectively activate those cofactors necessary for extra-nuclear activity and not those responsible for nuclear activity. Small molecules of this nature have been explored to some extent in other systems (bone),[64] but it is important that any such small molecule, even if it has selective activity itself, not be prone to metabolism to more conventional and non-selective hormonal agents.

In conclusion, through biodistribution studies, we have found that the EDC, a dendrimer-bound estrogen that provides selective cardiovascular protection without classical stimulation of uterus and mammary tissues, also shows selective, ER-mediated uptake and retention by the vascular target tissues, heart and aorta, but not the classical target, uterus. Thus, the favorable cardiovascular-selective activity of EDC may rely not only on its capacity to selectively activate the extra-nuclear pathway of ER signaling, but also from an inherent pharmacokinetically selective, ER-directed biodistribution that favors vascular targets over reproductive targets.

## V. METHODS

### Materials

All reactions were carried out under a nitrogen atmosphere with dry solvents using anhydrous conditions unless otherwise stated. Solvents used in the reactions were dried in a solvent delivery system (neutral alumina column). Reagents were purchased from Aldrich and used without further purification, unless otherwise stated. Yields refer to chromatographically and spectroscopically ($^1$H NMR) homogeneous materials, unless otherwise stated. Reactions were monitored by thin layer chromatography (TLC) carried out on Merck silica gel 60 F254 precoated plates (0.25 mm) using UV light as the visualizing agent and ceric ammonium molybdate and heat as developing agents. Flash column chromatography was performed on Silica P Flash silica gel (40-64 $\mu$M, 60 Å) from SiliCycle. $^1$H NMR spectra were recorded at 23 $^o$C on a Varian Unity-400, Varian Inova-500 or Varian Unity-500 spectrometers and are reported in ppm using residual protium as the internal standard ($CHCl_3$, δ = 7.26, $CD_2HCN$, δ = 1.94, center line, acetone-$d_6$, δ = 2.05, center line). The following abbreviations were used to explain the multiplicities: s = singlet, d = doublet, dd = doublet of doublets, t = triplet, q = quartet, m = multiplet and b = broad. Proton-decoupled $^{13}$C NMR spectra were recorded on a Varian Unity-500 (126 MHz) spectrometer and are reported in ppm using solvent as an internal standard ($CDCl_3$, δ = 77.16, $CD_3CN$, δ = 1.30, center line, acetone-$d_6$, δ = 29.80, center line). High resolution mass spectra were obtained at the University of Illinois Mass Spectrometry Laboratory. No-carrier added [$^{18}$F]fluoride was produced at Washington University Medical School by the $^{18}$O(p,n)$^{18}$F reaction through proton irradiation of enriched (95%) [$^{18}$O]$H_2O$ using a RDS111 cyclotron. Screw-cap test tubes used for drying fluoride and radiolabeling were purchased from Fisher Scientific (Pyrex No. 9825). Radiochemical purification utilized a reversed-phase semi-preparative HPLC column (HPLC: Thermo P2000, Column: Agilent Zorbax SB-C18, 5 µm, 9.4 X 250 mm, Product #: 880975-202, λ = 254 nm, ACN/$H_2O$). For quality control, the radiochemical purity was determined by analytical HPLC (HPLC: P4000, Column: Altima C18, 5 µm, 250 mm, Product #: 88056). C18 Sep-Pak cartridges were purchased from Waters Corporation (Milford, MA, USA). For the thin-layer chromatography (TLC) analyses, EM Science Silica Gel 60 F254 TLC plates were purchased from Fisher Scientific (Pittsburgh, PA, USA). Radio-TLC was accomplished using a Bioscan 200 imaging scanner (Bioscan, Inc., Washington, DC, USA). Radioactivity was counted with a Beckman Gamma 8000 counter containing a NaI crystal (Beckman Instruments, Inc., Irvine, CA, USA).

**Estrogen Receptor Binding Affinity Assays**

Relative binding affinities were determined by a competitive radiometric binding assay using 10 nM [$^{3}$H]estradiol as tracer (Amersham BioSciences, Piscataway, NJ), and purified full-length human ERα and ERβ (PanVera/InVitrogen, Carlsbad, CA). Compounds were assayed from $10^{-4}$ to $10^{-9}$ M as equivalents of estradiol (20-fold lower than the molar concentration of the dendrimer itself). Incubations were for 18-24 h at 0 °C, and the receptor-dendrimer complexes were absorbed onto hydroxyapatite (BioRad, Hercules, CA), and the unbound dendrimer was washed away. The binding affinities are expressed as relative binding affinity (RBA) values, with the RBA of estradiol for both receptors being set at 100. The values given are the average ± range or SD for two or more independent determinations. Estradiol binds to ERα with a $K_d$ of 0.2 nM and to ERβ with a $K_d$ of 0.5 nM.

**Radiochemical Syntheses**

**[$^{18}$F]-EDC (8):** 51 mCi of [$^{18}$F]fluoride in 200 µL [$^{18}$O]$H_2O$ was eluted into Pyrex vial (No. 9825) and used as is without any drying step or added base. The syringe was rinsed with dry 500 µL CAN, and any residual activity was added to vial. **6** (1 mg) was dissolved in dry 300 µL ACN, added to reaction vial, capped firmly and placed in oil bath at 105 $^{o}$C for 10 minutes (RCY: 94.7% by radio-TLC). After 10 minutes, the vial was cooled at room temperature for 2 minutes and then injected directly into the semi-preparative HPLC. The reaction vial was rinsed with 3 mL of the HPLC eluting solvent (80% ACN/ 20% $H_2O$) and added to the initial reaction mixture before injecting into HPLC. The purification was carried by a semi-preparative HPLC system (Agilent Zorbax SB-C18, 5 µm, 9.4 X 250 mm, Product #: 880975-202), eluting with a gradient (A: 80% ACN 20% $H_2O$ → B: 90% ACN 10% $H_2O$ over 15 mins) at a flow rate of 4 mL/min and the UV detector set at 254 nm. The radioactive peak corresponding to **7** was detected at 14 to 16 min by the radioactivity detector and was collected. The collected activity was diluted with 30 mL $H_2O$ and passed through a C18 column to capture the activity. The reaction vial was rinsed with 3 mL $H_2O$, which was also passed through the C18 column. A nitrogen line was connected to the cartridge to dry as best as possible residual $H_2O$ captured in cartridge. The activity (30.9 mCi) was eluted from the column with 0.8 mL $Et_2O$, and nitrogen was used to remove the solvent. To a solution of **7** in 40 µL MeOH was added EDC (**1**, 6 nmol in 10 µL MeOH) at room temperature and left to stir for 10 mins. The reaction mixture was added directly to a G25 column (PD Minitrap G-25, Sephadex G-25 medium, Product #: 28-9180-07), and **8** was eluted with PBS buffer (~1.5 mL, in 0.5 mL increments) to obtain 15.1 mCi in ca. 1.5 h. The portion

containing ~5 mCi was used for the final dose preparation. The isolated yield (without decay correction) was 29.4%, with a radiochemical purity of >99% and specific activity of 2500 mCi/μmol (92.5 GBq/μmol).

**Radio-TLC of the radiofluorination of 6 with [$^{18}$F]fluoride ion after 10 minutes:**

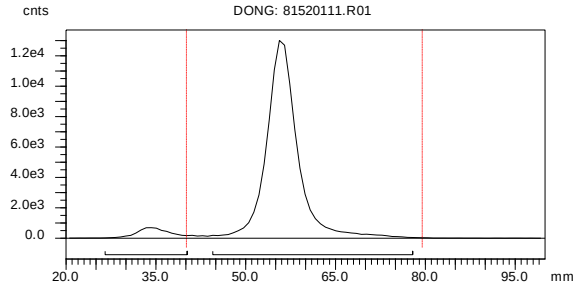


**TLC Eluting Conditions:** 100% EtOAc

**Region 1 (unreacted [$^{18}$F]fluoride; 35 mm):** 5.3%

**Region 2 ([$^{18}$F]fluoroproduct; 55 mm):** 94.7%

**Prep HPLC purification of crude material:**

**Conditions:** A: 80% ACN 20% $H_2O$ → B: 90% ACN 10% $H_2O$ over 15 mins, flow rate = 4 mL/ min, λ = 254 nm

**UV Trace:**

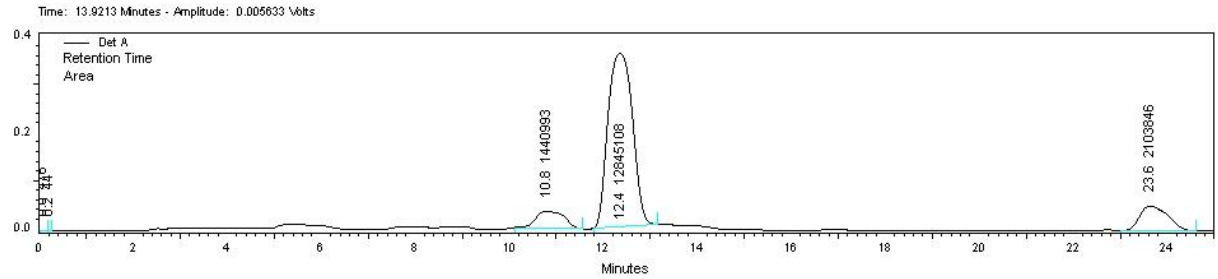


**Radioactivity Trace (Product: 15.2 min):**

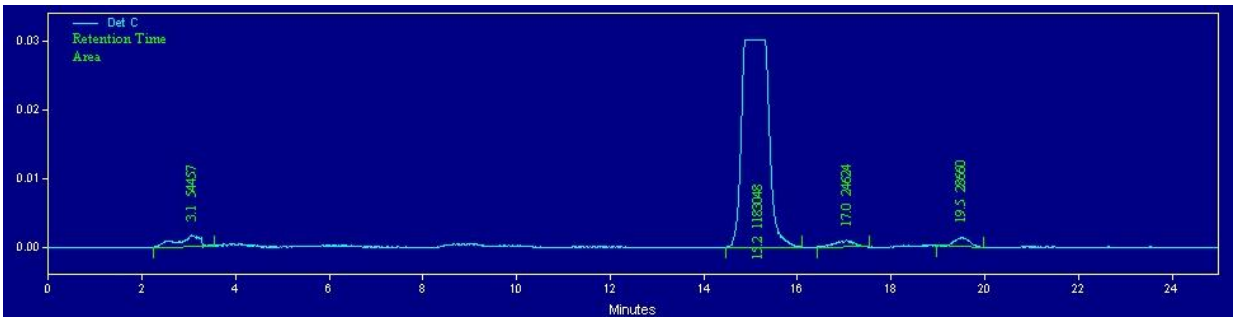

**Quality Control (QC) analysis after purification:**

**Conditions:** 80% ACN, 20% $H_2O$ flow rate = 2 mL/ min, λ = 254 nm

**UV trace used for specific activity determination (Product: 4.51 min):**

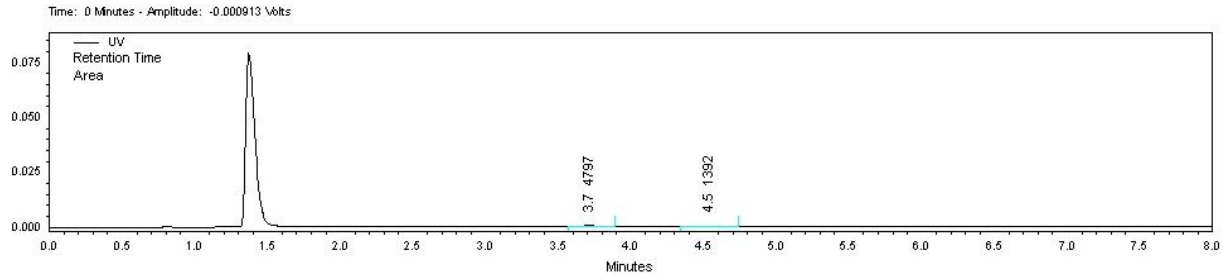


**UV trace of co-injection with cold standard for product (31) confirmation (Product: 4.56 min):**

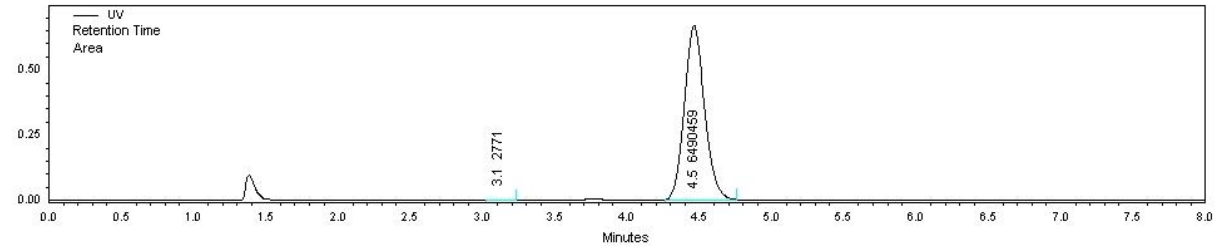


**Radioactivity trace of co-injection with cold standard for product (31) confirmation and radiochemical purity:**

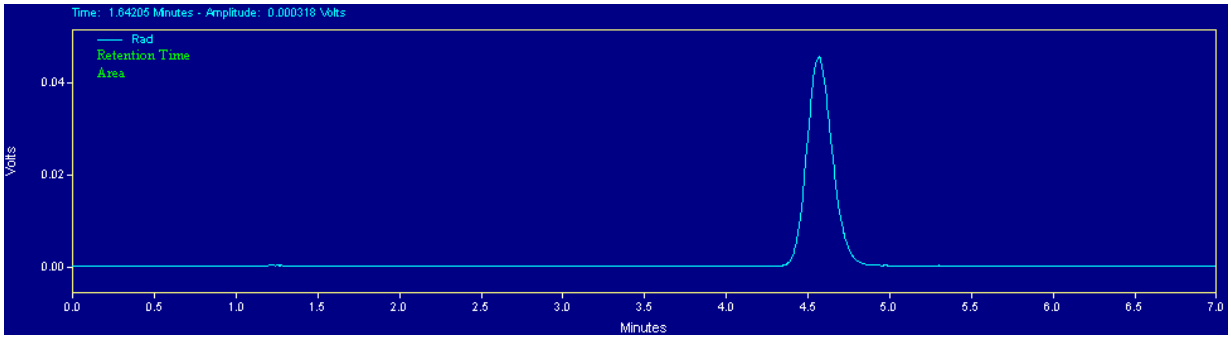

**[$^{18}$F]-EDC purity determined by radio-TLC:**

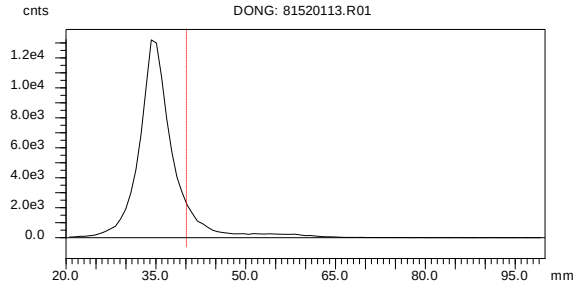


**TLC Eluting Conditions:** 100% MeOH

**Region 1 (35 mm; [$^{18}$F]-EDC):** 100%

**[$^{18}$F]-XDC (21):** By following procedure above, the radiochemical synthesis yielded 10.9 mCi of **21** in high radiochemical purity (>99%) and specific activity (1820 mCi/μmol, 67.3 GBq/μmol)) in 1.5 h. The portion containing 5.72 mCi was used for final dose preparation.

**[$^{18}$F]-XDC purity determined by radio-TLC:**

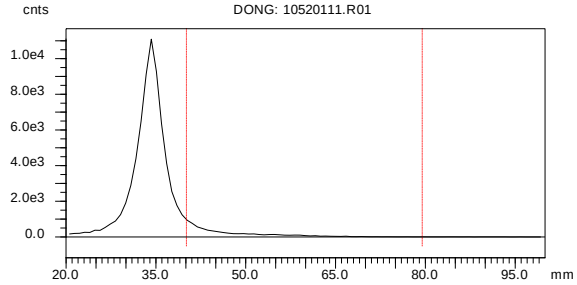


**TLC Eluting Conditions:** 100% MeOH

**Region 1 (35 mm):** 100%

**1-Azido-2-[$^{18}$F]fluoromethane (10):** [$^{18}$F]fluoride (62 mCi in 200 μL [$^{18}$O]water) was transferred to a BD vacutainer (13 × 75 mm, 5 mL, glass, no additives) containing $K_{222}$ (5.6 mg, 14.9 μmol) and $K_2CO_3$ (1 mg, 7.2 μmol), then the mixture was dried by azeotropic distillation at 105 ºC using ACN (3 × 1 mL) under a gentle flow of $N_2$ gas. When the drying was close to finish, the vacutainer was removed from the oil bath and the solvent residue (< 100 μL) was removed by a flow of $N_2$ at room temperature. The vacutainer was capped and connected to a dry ice trap (10 mL Pyrex tube with screw-cap) via Teflon tubing. After a solution of **9** (2 mg, 8.3 μmol) in ACN (200 μL) was added to the vacutainer, it was shaken and heated at 88 ºC for 5 min, directly followed by vacuum distillation which was achieved by a 50 mL syringe. The distillation lasted for 1 min, after which $N_2$ gas (10 mL) was released to the vacutainer. After this distillation procedure was repeated, the Pyrex tube was removed from the dry ice bath and warmed to

room temperature in a water bath for the subsequent click labeling (37 mCi). The processing time is about 10 min from the beginning of the labeling reaction, and the isolated yield is >80 %, determined by measuring the distilled activity (decay corrected).

**2,5-Dioxopyrrolidin-1-yl 4-((1-(2-[$^{18}$F]fluoroethyl)-1H-1,2,3-triazol-4-yl)methoxy)benzoate (12):** A solution of $CuSO_4 \cdot 5H_2O$ (1 mg, 4.0 µmol) in water (10 µL) and a solution of sodium ascorbate (3 mg, 15.1 µmol) in water (10 µL) were mixed; when the color of the mixture changed from black to yellow, the copper salt solution was mixed with a solution of BPDS (1.2 mg, 2.0 µmol) in 1 : 4 DMF/$H_2O$ (20 µL). A portion of above mixture (25 µL), along with **11** (1 mg, 3.66 µmol) in DMF (200 µL), was added to the distilled **10** in ACN (200 µL). After 5 min at room temperature, the reaction mixture was diluted with a solution of 10% ACN, 90% water, 0.1% TFA(3 mL) for reversed-phase HPLC purification using column A and mobile phase (32% ACN, 68% water, 0.1% TFA) at 4 mL/min, and UV at 240 nm. **12** was collected at 15 min in 90% yield (decay corrected). The HPLC fraction containing **12** was diluted in water (50 mL), then [$^{18}$F]**7** was isolated by solid-phase extraction using a C18 SepPak by passing the diluted sample through the SepPak. The SepPak was rinsed with water (10 mL), and dried under a stream of $N_2$ gas. **12** can be eluted from the SepPak in DMF for immediate conjugation, or in either dichloromethane or diethyl ether, to afford a dried form of **12** (15.71 mCi) after drying over $Na_2SO_4$ and removal of solvents.

**[$^{18}$F]-EDC-Click purity determined by radio-TLC:**

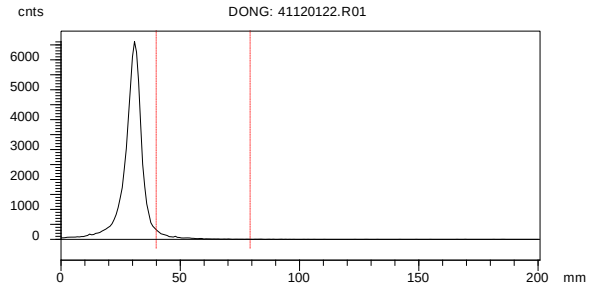


**TLC Eluting Conditions:** 100% MeOH
**Region 1 (35 mm):** 100%

**Biodistribution Experiments**

Female BALB/c mice were obtained from Charles River Laboratories and were housed in the Division of Comparative Animal Facility at Washington University Medical School. Animals were anesthetized in a Plexiglas induction chamber flowing with oxygen and 1-2% isoflurane. 15-20

µCi of **8**, **13** or **21** in 100 µL PBS buffer pre-weighed in a 0.300cc, 29 gauge x ½'' insulin syringe. The mouse was injected via the tail vein, and the syringe was post-counted to determine the total injected volume in grams. All injections were tolerated well. The mouse was weighed and returned to the cage to restore the animal to a normal, awake state. A spare, control dose was injected into a total volume of 100 mL of saline to disperse 1 mL aliquots into a vial for each animal that was counted along with each group of organs to create a standard. At 30 min and 2 h, the mice were sacrificed by cervical dislocation. Samples or whole organs were collected from blood, lung, liver, spleen, kidney, muscle, heart, abdominal aorta, uterus, bone and bone marrow. Organs were individually counted on a Beckmann gamma counter for 1 minute per sample. Calculations were then performed to determine % injected dose per gram and per organ. All measurements were properly corrected for decay.

**Blocking Experiments**

Animals were prepared and treated as discuss previously. Before injection of tracer, PBS solutions of cold EDC (**1**, 40 µg, 500-fold excess) or estradiol (20-60 µg, 100-500-fold excess) were introduced into the mice.

**Numerical Values of Biodistribution (Figure 3.9) for [$^{18}$F]-EDC-Si-$^{18}$F (Female; %ID/gram):**

| | 30 min | | 2 hour | | 2 hour Block ($E_2$) | |
|---|---|---|---|---|---|---|
| **Organ** | **%ID/gram** | **SD** | **%ID/gram** | **SD** | **%ID/gram** | **SD** |
| **Blood** | 11.5617 | 0.8457 | 3.0666 | 0.7052 | 2.2074 | 0.9256 |
| **Lung** | 26.0679 | 10.2063 | 13.5434 | 2.6317 | 22.0802 | 5.1329 |
| **Liver** | 39.6676 | 4.9527 | 68.0836 | 7.6045 | 61.4188 | 9.0476 |
| **Spleen** | 255.7602 | 37.0547 | 460.6485 | 72.375 | 388.6927 | 37.7974 |
| **Kidney** | 3.4063 | 0.3721 | 3.2370 | 0.7161 | 2.6122 | 0.5103 |
| **Muscle** | 0.9513 | 0.2086 | 0.6170 | 0.1296 | 0.6250 | 0.1477 |
| **Heart** | 19.6690 | 1.4342 | 16.2298 | 2.9426 | 10.9753 | 1.7948 |
| **Bone** | 5.7072 | 0.2562 | 8.3166 | 1.9434 | 7.6491 | 1.4159 |
| **Uterus** | 0.6049 | 0.3238 | 0.3358 | 0.1512 | 0.8235 | 0.4174 |
| **Abd. Aorta** | 8.1464 | 2.6876 | 6.5009 | 2.3213 | 5.2284 | 1.4757 |

**Numerical Values of Biodistribution for [$^{18}$F]-EDC-Si-$^{18}$F (Female; %ID/organ):**

| | 30 min | | 2 hour | | 2 hour Block ($E_2$) | |
|---|---|---|---|---|---|---|
| **Organ** | **%ID/organ** | **SD** | **%ID/organ** | **SD** | **%ID/organ** | **SD** |
| **Blood** | 16.2055 | 1.3237 | 4.1718 | 0.7856 | 2.9529 | 1.0425 |
| **Lung** | 3.6072 | 1.3777 | 2.0018 | 0.3391 | 3.0777 | 0.5913 |
| **Liver** | 34.5596 | 3.5457 | 55.3582 | 4.0014 | 48.1138 | 2.5438 |
| **Spleen** | 17.3475 | 3.0852 | 33.1527 | 4.1012 | 25.3507 | 3.7858 |
| **Kidney** | 0.4279 | 0.0803 | 0.3632 | 0.0598 | 0.3058 | 0.0896 |
| **Muscle** | 7.7454 | 1.2479 | 4.9146 | 0.7785 | 4.9174 | 0.8850 |
| **Heart** | 2.0643 | 0.1271 | 1.6251 | 0.2462 | 1.1555 | 0.1444 |
| **Bone** | 12.4810 | 1.1056 | 17.6862 | 3.7442 | 16.0541 | 2.1163 |
| **Uterus** | 0.0437 | 0.0231 | 0.0348 | 0.0179 | 0.0411 | 0.0172 |
| **Abd. Aorta** | 0.0805 | 0.0122 | 0.0819 | 0.0587 | 0.0595 | 0.0242 |

**Numerical Values of Biodistribution for [$^{18}$F]-EDC-Si-$^{18}$F (Male; %ID/gram):**

| | 30 min | | 2 hour | | 2 hour Block ($E_2$) | |
|---|---|---|---|---|---|---|
| **Organ** | **%ID/gram** | **SD** | **%ID/gram** | **SD** | **%ID/gram** | **SD** |
| **Blood** | 4.4978 | 1.7960 | 1.6116 | 0.3812 | 1.5946 | 0.2301 |
| **Lung** | 26.1280 | 11.5194 | 19.9430 | 3.6527 | 21.0828 | 4.0406 |
| **Liver** | 21.2623 | 7.3078 | 42.6931 | 3.7662 | 38.3988 | 3.2665 |
| **Spleen** | 84.8652 | 38.1032 | 230.5541 | 32.7841 | 237.2420 | 22.1027 |
| **Kidney** | 2.1468 | 0.7517 | 2.5679 | 0.4692 | 2.0270 | 0.1861 |
| **Muscle** | 0.7827 | 0.2846 | 0.7730 | 0.1641 | 0.7415 | 0.0916 |
| **Heart** | 17.2210 | 7.8135 | 15.6428 | 3.1304 | 16.1561 | 3.1632 |
| **Bone** | 6.8779 | 1.9062 | 10.1312 | 1.3382 | 8.3705 | 1.1216 |
| **Abd. Aorta** | 4.5541 | 1.6574 | 5.2080 | 2.4742 | 4.2915 | 0.8526 |

**Numerical Values of Biodistribution for [$^{18}$F]-EDC-Si-$^{18}$F (Male; %ID/organ):**

| | 30 min | | 2 hour | | 2 hour Block ($E_2$) | |
|---|---|---|---|---|---|---|
| **Organ** | **%ID/organ** | **SD** | **%ID/organ** | **SD** | **%ID/organ** | **SD** |
| **Blood** | 6.8814 | 2.5906 | 2.4177 | 0.6022 | 2.3815 | 0.2869 |
| **Lung** | 3.7986 | 1.6084 | 2.7518 | 0.5618 | 3.0157 | 0.7317 |
| **Liver** | 23.8014 | 8.0007 | 42.7630 | 4.5811 | 35.6260 | 1.8567 |
| **Spleen** | 6.4565 | 2.8316 | 14.0281 | 1.8753 | 14.0830 | 0.8566 |
| **Kidney** | 0.2980 | 0.0963 | 0.3693 | 0.0682 | 0.2783 | 0.0310 |
| **Muscle** | 7.0447 | 2.5373 | 6.7766 | 1.5213 | 6.4980 | 0.7727 |
| **Heart** | 2.0262 | 0.8755 | 1.7095 | 0.3545 | 1.7286 | 0.3618 |
| **Bone** | 16.4561 | 4.4628 | 23.6522 | 3.6493 | 19.4811 | 2.2915 |
| **Abd. Aorta** | 0.0294 | 0.0138 | 0.0269 | 0.0166 | 0.0279 | 0.0080 |

**Numerical Values of Biodistribution (Figure 3.10) for [$^{18}$F]-EDC-Click (Female; %ID/gram):**

| | 30 min | | 2 hour | |
|---|---|---|---|---|
| **Organ** | **%ID/gram** | **SD** | **%ID/gram** | **SD** |
| **Blood** | 13.2763 | 4.3466 | 2.4183 | 0.4952 |
| **Lung** | 21.6783 | 4.9191 | 12.0557 | 2.7106 |
| **Liver** | 39.9442 | 2.0635 | 53.9221 | 6.3387 |
| **Spleen** | 240.6968 | 38.1327 | 319.1434 | 78.3605 |
| **Kidney** | 4.3545 | 0.8784 | 3.5402 | 0.4672 |
| **Muscle** | 0.7859 | 0.2007 | 0.6593 | 0.1142 |
| **Heart** | 13.2138 | 1.9454 | 12.6973 | 2.1333 |
| **Brain** | 0.3379 | 0.1100 | 0.0961 | 0.0234 |
| **Bone** | 1.2983 | 0.2029 | 1.2563 | 0.1538 |
| **Marrow** | 1.8816 | 1.7191 | 3.7777 | 2.3665 |
| **Uterus** | 0.4777 | 0.5048 | 0.5607 | 0.3724 |
| **Abd. Aorta** | 7.8991 | 2.2757 | 6.7233 | 1.3971 |

**Numerical Values of Biodistribution for [$^{18}$F]-EDC-Click (Female; %ID/organ):**

| | 30 min | | 2 hour | |
|---|---|---|---|---|
| **Organ** | **%ID/organ** | **SD** | **%ID/organ** | **SD** |
| **Blood** | 18.3398 | 5.4995 | 3.2783 | 0.7466 |
| **Lung** | 3.2468 | 0.5963 | 1.8265 | 0.4122 |
| **Liver** | 37.0714 | 3.4032 | 47.7170 | 4.9140 |
| **Spleen** | 15.1994 | 2.1507 | 20.2292 | 4.2161 |
| **Kidney** | 0.5902 | 0.1007 | 0.4721 | 0.0588 |
| **Muscle** | 6.3973 | 1.5613 | 5.2131 | 0.8789 |
| **Heart** | 1.5091 | 0.1983 | 1.4633 | 0.1222 |
| **Brain** | 0.1302 | 0.0491 | 0.0376 | 0.0108 |
| **Bone** | 2.8123 | 0.4013 | 2.6456 | 0.3579 |
| **Marrow** | 0.0063 | 0.0036 | 0.0050 | 0.0015 |
| **Uterus** | 0.0284 | 0.0309 | 0.0296 | 0.0201 |
| **Abd. Aorta** | 0.0664 | 0.0209 | 0.0678 | 0.0249 |

**Numerical Values of Biodistribution (Figure 3.12) for [$^{18}$F]-XDC-Si-$^{18}$F (Female; %ID/gram):**

| | 30 min | | 2 hour | |
|---|---|---|---|---|
| **Organ** | **%ID/gram** | **SD** | **%ID/gram** | **SD** |
| **Blood** | 4.7034 | 0.5973 | 0.2027 | 0.1774 |
| **Lung** | 7.0214 | 2.4218 | 2.2039 | 1.0308 |
| **Liver** | 74.2952 | 8.9768 | 85.9090 | 7.4361 |
| **Spleen** | 84.8318 | 30.3325 | 76.0455 | 27.0040 |
| **Kidney** | 1.3145 | 0.2342 | 0.6222 | 0.0862 |
| **Muscle** | 0.1812 | 0.0241 | 0.0482 | 0.0148 |
| **Heart** | 1.5001 | 0.2845 | 0.2161 | 0.0493 |
| **Brain** | 0.1578 | 0.0175 | 0.0167 | 0.0101 |
| **Bone** | 1.4457 | 0.1795 | 1.6438 | 0.5637 |
| **Marrow** | 2.0014 | 0.6785 | 4.0009 | 3.4947 |
| **Uterus** | 0.3057 | 0.0526 | 0.1876 | 0.2002 |
| **Abd. Aorta** | 1.6118 | 0.3538 | 0.3590 | 0.4215 |

**Numerical Values of Biodistribution for [$^{18}$F]-XDC-Si-$^{18}$F (Female; %ID/organ):**

| | 30 min | | 2 hour | |
|---|---|---|---|---|
| **Organ** | **%ID/organ** | **SD** | **%ID/organ** | **SD** |
| **Blood** | 6.7759 | 0.6870 | 0.2913 | 0.2470 |
| **Lung** | 0.9492 | 0.2813 | 0.3287 | 0.1653 |
| **Liver** | 74.0380 | 6.6605 | 81.0654 | 2.7261 |
| **Spleen** | 7.0069 | 1.6299 | 6.5437 | 2.0763 |
| **Kidney** | 0.1649 | 0.0243 | 0.0856 | 0.0213 |
| **Muscle** | 1.5314 | 0.1956 | 0.4082 | 0.1146 |
| **Heart** | 0.1554 | 0.0246 | 0.0229 | 0.0038 |
| **Brain** | 0.0626 | 0.0047 | 0.0067 | 0.0039 |
| **Bone** | 3.2387 | 0.2428 | 3.7303 | 1.3515 |
| **Marrow** | 0.0024 | 0.0012 | 0.0045 | 0.0047 |
| **Uterus** | 0.0218 | 0.0080 | 0.0131 | 0.0171 |
| **Abd. Aorta** | 0.0087 | 0.0037 | 0.0020 | 0.0023 |

**Numerical Values of Biodistribution (Figure 3.11) for [$^{18}$F]-EDC-Click 30 min block (Female; %ID/gram):**

| | 30 min High Dose | | 30 min Low Dose | | 30 min $E_2$ Block | | 30 min EDC Block | |
|---|---|---|---|---|---|---|---|---|
| **Organ** | **%ID/gram** | **SD** | **%ID/gram** | **SD** | **%ID/gram** | **SD** | **%ID/gram** | **SD** |
| **Blood** | 14.4020 | 3.4107 | 5.2622 | 0.6678 | 6.9652 | 2.3877 | 0.4445 | 0.2580 |
| **Lung** | 13.6754 | 4.7922 | 5.7999 | 0.6310 | 9.2502 | 1.5521 | 6.4220 | 0.6113 |
| **Liver** | 27.9916 | 2.9665 | 38.3925 | 2.4497 | 39.7293 | 8.2372 | 78.0321 | 13.7196 |
| **Spleen** | 276.7966 | 39.2418 | 164.7847 | 10.0198 | 253.6580 | 30.9604 | 66.5555 | 14.2317 |
| **Kidney** | 3.4732 | 0.4287 | 3.6322 | 0.2811 | 3.4290 | 0.5995 | 20.5397 | 4.2353 |
| **Muscle** | 0.7231 | 0.1832 | 0.6095 | 0.1802 | 0.6947 | 0.1257 | 0.1923 | 0.1398 |
| **Heart** | 13.8879 | 2.2980 | 14.5021 | 2.6936 | 14.4835 | 2.6270 | 0.6416 | 0.1819 |
| **Bone** | 1.2921 | 0.3073 | 1.5970 | 0.3408 | 1.6274 | 0.2152 | 2.7976 | 0.4360 |
| **Uterus** | 0.3293 | 0.1173 | 0.3290 | 0.1495 | 0.4859 | 0.2145 | 1.1937 | 0.3873 |
| **Abd. Aorta** | 6.7090 | 1.7659 | 7.7939 | 0.5328 | 4.9989 | 0.8999 | 3.7690 | 2.4894 |

**Numerical Values of Biodistribution for [$^{18}$F]-EDC-Click 30 min block (Female; %ID/organ):**

| | 30 min High Dose | | 30 min Low Dose | | 30 min $E_2$ Block | | 30 min EDC Block | |
|---|---|---|---|---|---|---|---|---|
| **Organ** | **%ID/organ** | **SD** | **%ID/organ** | **SD** | **%ID/organ** | **SD** | **%ID/organ** | **SD** |
| **Blood** | 19.4566 | 4.3494 | 7.1185 | 0.9208 | 9.4879 | 3.4319 | 0.5902 | 0.3212 |
| **Lung** | 1.8661 | 0.6068 | 0.8495 | 0.1985 | 1.3660 | 0.3112 | 0.8691 | 0.1123 |
| **Liver** | 26.2894 | 2.9303 | 32.2982 | 1.9601 | 36.3072 | 7.9931 | 70.6540 | 8.5146 |
| **Spleen** | 20.5277 | 2.0437 | 12.2187 | 1.2697 | 19.8937 | 2.6393 | 4.9708 | 1.1179 |
| **Kidney** | 0.4215 | 0.0690 | 0.4678 | 0.0290 | 0.4022 | 0.0686 | 2.5734 | 0.5546 |
| **Muscle** | 5.7290 | 1.3983 | 4.8216 | 1.3871 | 5.5215 | 1.0177 | 1.5227 | 1.1391 |
| **Heart** | 1.2577 | 0.1584 | 1.2707 | 0.2567 | 1.2926 | 0.1979 | 0.0558 | 0.0163 |
| **Bone** | 2.7235 | 0.6398 | 3.3570 | 0.6668 | 3.4446 | 0.5358 | 5.8664 | 0.8290 |
| **Uterus** | 0.0318 | 0.0075 | 0.0365 | 0.0246 | 0.0401 | 0.0208 | 0.0941 | 0.0459 |
| **Abd. Aorta** | 0.0559 | 0.0068 | 0.0863 | 0.0068 | 0.0476 | 0.0193 | 0.0321 | 0.0363 |

**Numerical Values of Biodistribution (Figure 3.11) for [$^{18}$F]-EDC-Click 2 hr block (Female; %ID/gram):**

| | 2 hr High Dose | | 2 hr Low Dose | | 2 hr $E_2$ Block | | 2 hr EDC Block | |
|---|---|---|---|---|---|---|---|---|
| **Organ** | **%ID/gram** | **SD** | **%ID/gram** | **SD** | **%ID/gram** | **SD** | **%ID/gram** | **SD** |
| **Blood** | 3.3067 | 0.6453 | 1.0119 | 0.3471 | 1.2020 | 0.0434 | 0.1058 | 0.0255 |
| **Lung** | 9.3528 | 2.3708 | 6.9731 | 2.1549 | 4.4163 | 1.8373 | 3.4417 | 0.8115 |
| **Liver** | 44.9795 | 7.1587 | 41.4023 | 1.8900 | 45.8173 | 7.2316 | 79.5245 | 11.9594 |
| **Spleen** | 345.9963 | 27.7805 | 185.7553 | 24.4289 | 217.1845 | 82.3742 | 60.3171 | 9.3595 |
| **Kidney** | 2.9919 | 0.2015 | 2.7899 | 0.1400 | 2.6151 | 0.2209 | 20.3701 | 2.4284 |
| **Muscle** | 0.4642 | 0.1056 | 0.4559 | 0.1721 | 0.4622 | 0.2471 | 0.1488 | 0.0795 |
| **Heart** | 10.5887 | 1.9170 | 8.2754 | 1.0681 | 8.5800 | 0.8972 | 0.4593 | 0.1231 |
| **Bone** | 1.9091 | 0.3344 | 1.6217 | 0.3252 | 1.7204 | 0.0302 | 3.1844 | 0.6919 |
| **Uterus** | 0.2236 | 0.0392 | 0.2494 | 0.0451 | 0.1908 | 0.0111 | 1.3920 | 0.4801 |
| **Abd. Aorta** | 4.0470 | 1.0894 | 3.7275 | 1.7127 | 4.5092 | 0.5749 | 0.9734 | 0.7313 |

**Numerical Values of Biodistribution for [$^{18}$F]-EDC-Click 2 hr block (Female; %ID/organ):**

| | 2 hr High Dose | | 2 hr Low Dose | | 2 hr $E_2$ Block | | 2 hr EDC Block | |
|---|---|---|---|---|---|---|---|---|
| **Organ** | **%ID/organ** | **SD** | **%ID/organ** | **SD** | **%ID/organ** | **SD** | **%ID/organ** | **SD** |
| **Blood** | 4.4895 | 0.8347 | 1.3595 | 0.4803 | 1.6585 | 0.1075 | 0.1455 | 0.0340 |
| **Lung** | 1.4060 | 0.2169 | 0.9577 | 0.2775 | 0.6687 | 0.2699 | 0.4847 | 0.1154 |
| **Liver** | 38.3207 | 1.0643 | 38.0456 | 2.2391 | 41.7374 | 4.7256 | 66.1783 | 7.4003 |
| **Spleen** | 28.8584 | 4.3638 | 15.1268 | 1.0892 | 17.7193 | 4.1551 | 5.0899 | 0.7014 |
| **Kidney** | 0.3682 | 0.0494 | 0.3341 | 0.0593 | 0.3119 | 0.0291 | 2.5314 | 0.4036 |
| **Muscle** | 3.6879 | 0.7919 | 3.5982 | 1.4061 | 3.7620 | 2.1027 | 1.2092 | 0.6733 |
| **Heart** | 1.0314 | 0.1013 | 0.7345 | 0.0815 | 0.9260 | 0.2308 | 0.0440 | 0.0125 |
| **Bone** | 4.0443 | 0.7337 | 3.3923 | 0.7114 | 3.6951 | 0.1708 | 6.8252 | 1.4647 |
| **Uterus** | 0.0173 | 0.0061 | 0.0211 | 0.0041 | 0.0209 | 0.0085 | 0.1062 | 0.0242 |
| **Abd. Aorta** | 0.0173 | 0.0199 | 0.0344 | 0.0159 | 0.0448 | 0.0167 | 0.0074 | 0.0035 |

## VI. REFERENCES


(1) Barrett-Connor, E. Sex differences in coronary heart disease. Why are women so superior? The 1995 Ancel Keys Lecture. *Circulation* **1997**, *95*, 252.

(2) Stampfer, M. J.; Colditz, G. A.; Willett, W. C.; Manson, J. E.; Rosner, B.; Speizer, F. E.; Hennekens, C. H. Postmenopausal estrogen therapy and cardiovascular disease. Ten-year follow-up from the nurses' health study. *N. Engl. J. Med.* **1991**, *325*, 756.

(3) Mendelsohn, M. E.; Karas, R. H. Estrogen and the blood vessel wall. *Curr. Opin. Cardiol.* **1994**, *9*, 619.

(4) Effects of estrogen or estrogen/progestin regimens on heart disease risk factors in postmenopausal women. The Postmenopausal Estrogen/Progestin Interventions (PEPI) Trial. The Writing Group for the PEPI Trial. *JAMA* **1995**, *273*, 199.

(5) Blair, A.; Shaul, P. W.; Yuhanna, I. S.; Conrad, P. A.; Smart, E. J. Oxidized low density lipoprotein displaces endothelial nitric-oxide synthase (eNOS) from plasmalemmal caveolae and impairs eNOS activation. *J. Biol. Chem.* **1999**, *274*, 32512.

(6) Uittenbogaard, A.; Shaul, P. W.; Yuhanna, I. S.; Blair, A.; Smart, E. J. High density lipoprotein prevents oxidized low density lipoprotein-induced inhibition of endothelial nitric-oxide synthase localization and activation in caveolae. *J. Biol. Chem.* **2000**, *275*, 11278.

(7) Vane, J. R.; Anggard, E. E.; Botting, R. M. Regulatory functions of the vascular endothelium. *N. Engl. J. Med.* **1990**, *323*, 27.

(8) Nilsson, S.; Makela, S.; Treuter, E.; Tujague, M.; Thomsen, J.; Andersson, G.; Enmark, E.; Pettersson, K.; Warner, M.; Gustafsson, J.-A. Mechanisms of estrogen action. *Physiol. Rev.* **2001**, *81*, 1535.

(9) Rachez, C.; Freedman, L. P. Mediator complexes and transcription. *Curr. Opin. Cell Biol.* **2001**, *13*, 274.

(10) Paech, K.; Webb, P.; Kuiper, G. G. J. M.; Nilsson, S.; Gustafsson, J.-A.; Kushner, P. J.; Scanlan, T. S. Differential ligand activation of estrogen receptors ERα and ERβ at AP1 sites. *Science (Washington, D. C.)* **1997**, *277*, 1508.

(11) Power, R. F.; Mani, S. K.; Codina, J.; Conneely, O. M.; O'Malley, B. W. Dopaminergic and ligand-independent activation of steroid hormone receptors. *Science (Washington, D. C., 1883-)* **1991**, *254*, 1636.

(12) Matthews, J.; Gustafsson, J.-A. Estrogen signaling: a subtle balance between ERα and ERβ. *Mol. Interventions* **2003**, *3*, 281.

(13) Hammes, S. R.; Levin, E. R. Extranuclear steroid receptors: nature and actions. *Endocr. Rev.* **2007**, *28*, 726.

(14) Szego, C. M.; Davis, J. S. Adenosine 3',5'-monophosphate in rat uterus. Acute elevation by estrogen. *Proc. Natl. Acad. Sci. U. S. A.* **1967**, *58*, 1711.

(15) Pietras, R. J.; Szego, C. M. Endometrial cell calcium and estrogen action. *Nature (London)* **1975**, *253*, 357.

(16) Osborne, C. K.; Schiff, R. Estrogen-receptor biology: continuing progress and therapeutic implications. *J. Clin. Oncol.* **2005**, *23*, 1616.

(17) Levin, E. R. Integration of the extranuclear and nuclear actions of estrogen. *Mol. Endocrinol.* **2005**, *19*, 1951.

(18) Kelly, M. J.; Levin, E. R. Rapid actions of plasma membrane estrogen receptors. *Trends Endocrinol. Metab.* **2001**, *12*, 152.

(19) Deecher, D. C.; Swiggard, P.; Frail, D. E.; O'Connor, L. T. Characterization of a membrane-associated estrogen receptor in a rat hypothalamic cell line (D12). *Endocrine* **2003**, *22*, 211.

(20) Ho, K. J.; Liao, J. K. Nonnuclear actions of estrogen. *Arterioscler. Thromb. Vasc. Biol.* **2002**, *22*, 1952.

(21) Kim, H. P.; Lee, J. Y.; Jeong, J. K.; Bae, S. W.; Lee, H. K.; Jo, I. Nongenomic stimulation of nitric oxide release by estrogen is mediated by estrogen receptor alpha localized in caveolae. *Biochem. Biophys. Res. Commun*. **1999**, *263*, 257.

(22) Chambliss, K. L.; Yuhanna, I. S.; Anderson, R. G. W.; Mendelsohn, M. E.; Shaul, P. W. ERβ has nongenomic action in caveolae. *Mol. Endocrinol.* **2002**, *16*, 938.

(23) Norfleet, A. M.; Thomas, M. L.; Gametchu, B.; Watson, C. S. Estrogen receptor-α detected on the plasma membrane of aldehyde-fixed GH3/B6/F10 rat pituitary tumor cells by enzyme-linked immunocytochemistry. *Endocrinol.* **1999**, *140*, 3805.

(24) Razandi, M.; Pedram, A.; Greene, G. L.; Levin, E. R. Cell membrane and nuclear estrogen receptors (ERs) originate from a single transcript: studies of ERα and ERβ expressed in Chinese hamster ovary cells. *Mol. Endocrinol.* **1999**, *13*, 307.

(25) Razandi, M.; Pedram, A.; Merchenthaler, I.; Greene, G. L.; Levin, E. R. Plasma membrane estrogen receptors exist and functions as dimers. *Mol. Endocrinol.* **2004**, *18*, 2854.

(26) Marquez, D. C.; Chen, H.-W.; Curran, E. M.; Welshons, W. V.; Pietras, R. J. Estrogen receptors in membrane lipid rafts and signal transduction in breast cancer. *Mol. Cell. Endocrinol.* **2006**, *246*, 91.

(27) Pedram, A.; Razandi, M.; Levin, E. R. Nature of functional estrogen receptors at the plasma membrane. *Mol. Endocrinol.* **2006**, *20*, 1996.

(28) Krasinski, K.; Spyridopoulos, I.; Asahara, T.; Van, D. Z. R.; Isner, J. M.; Losordo, D. W. Estradiol accelerates functional endothelial recovery after arterial injury. *Circulation* **1997**, *95*, 1768.

(29) Sullivan, T. R., Jr.; Karas, R. H.; Aronovitz, M.; Faller, G. T.; Ziar, J. P.; Smith, J. J.; O'Donnell, T. F., Jr.; Mendelsohn, M. E. Estrogen inhibits the response-to-injury in a mouse carotid artery model. *J. Clin. Invest.* **1995**, *96*, 2482.

(30) Akishita, M.; Ouchi, Y.; Miyoshi, H.; Kozaki, K.; Inoue, S.; Ishikawa, M.; Eto, M.; Toba, K.; Orimo, H. Estrogen inhibits cuff-induced intimal thickening of rat femoral artery: effects on migration and proliferation of vascular smooth muscle cells. *Atherosclerosis (Shannon, Irel.)* **1997**, *130*, 1.

(31) Levine, R. L.; Shi-Juan, C.; Durand, J.; Chen, Y.-F.; Oparil, S. Medroxyprogesterone attenuates estrogen-mediated inhibition of neointima formation after balloon injury of the rat carotid artery. *Circulation* **1996**, *94*, 2221.

(32) Bourassa, P.-A. K.; Milos, P. M.; Gaynor, B. J.; Breslow, J. L.; Aiello, R. J. Estrogen reduces atherosclerotic lesion development in apolipoprotein E-deficient mice. *Proc. Natl. Acad. Sci. U. S. A.* **1996**, *93*, 10022.

(33) Cunningham, K. S.; Gotlieb, A. I. The role of shear stress in the pathogenesis of atherosclerosis. *Lab. Invest.* **2005**, *85*, 9.

(34) Chen, S.-J.; Li, H.; Durand, J.; Oparil, S.; Chen, Y.-F. Estrogen reduces myointimal proliferation after balloon injury of rat carotid artery. *Circulation* **1996**, *93*, 577.

(35) Hanke, H.; Hanke, S.; Finking, G.; Muhic-Lohrer, A.; Mueck, A. O.; Schmahl, F. W.; Haasis, R.; Hombach, V. Different effects of estrogen and progesterone on experimental atherosclerosis in female versus male rabbits: Quantification of cellular proliferation by bromodeoxyuridine. *Circulation* **1996**, *94*, 175.

(36) Mendelsohn, M. E.; Karas, R. H. The protective effects of estrogen on the cardiovascular system. *N. Engl. J. Med.* **1999**, *340*, 1801.

(37) Farhat, M. Y.; Lavigne, M. C.; Ramwell, P. W. The vascular protective effects of estrogen. *FASEB J.* **1996**, *10*, 615.

(38) Miller, V. M. Gender, estrogen, and NOS: cautions about generalizations. *Circ. Res.* **1999**, *85*, 979.

(39) Moncada, S.; Higgs, A. The L-arginine-nitric oxide pathway. *N. Engl. J. Med.* **1993**, *329*, 2002.

(40) Kolodgie, F. D.; Jacob, A.; Wilson, P. S.; Carlson, G. C.; Farb, A.; Verma, A.; Virmani, R. Estradiol attenuates directed migration of vascular smooth muscle cells in vitro. *Am. J. Pathol.* **1996**, *148*, 969.

(41) Caulin-Glaser, T.; Garcia-Cardena, G.; Sarrel, P.; Sessa, W. C.; Bender, J. R. 17β-Estradiol regulation of human endothelial cell basal nitric oxide release, independent of cytosolic Ca2+ mobilization. *Circ. Res.* **1997**, *81*, 885.

(42) Chen, Z.; Yuhanna, I. S.; Galcheva-Gargova, Z.; Karas, R. H.; Mendelsohn, M. E.; Shaul, P. W. Estrogen receptor α mediates the nongenomic activation of endothelial nitric oxide synthase by estrogen. *J. Clin. Invest.* **1999**, *103*, 401.

(43) Mendelsohn, M. E. Nongenomic, estrogen receptor-mediated activation of endothelial nitric oxide synthase. How does it work? What does it mean? *Circ. Res.* **2000**, *87*, 956.

(44) Mendelsohn, M. E. Mechanisms of estrogen action in the cardiovascular system. *J. Steroid Biochem. Mol. Biol.* **2000**, *74*, 337.

(45) Harman, S. M. Estrogen replacement in menopausal women: recent and current prospective studies, the WHI and the KEEPS. *Gend. Med.* **2006**, *3*, 254.

(46) Grady, D.; Gebretsadik, T.; Kerlikowske, K.; Ernster, V.; Petitti, D. Hormone replacement therapy and endometrial cancer risk: a meta-analysis. *Obstet. Gynecol.* **1995**, *85*, 304.

(47) Ullrich, J. W.; Miller, C. P. Estrogen receptor modulator review. *Expert Opin. Ther. Pat.* **2006**, *16*, 559.

(48) Silverman, S. L. New selective estrogen receptor modulators (SERMs) in development. *Curr. Osteoporos. Rep.* **2010**, *8*, 151.

(49) Vasudevan, N.; Kow, L.-M.; Pfaff, D. W. Early membrane estrogenic effects required for full expression of slower genomic actions in a nerve cell line. *Proc. Natl. Acad. Sci. U. S. A.* **2001**, *98*, 12267.

(50) Han, H.-J.; Lee, Y.-H.; Park, S.-H. Estradiol-17β-BSA stimulates Ca2+ uptake through nongenomic pathways in primary rabbit kidney proximal tubule cells: involvement of cAMP and PKC. *J. Cell. Physiol.* **2000**, *183*, 37.

(51) Temple, J. L.; Wray, S. Bovine serum albumin-estrogen compounds differentially alter gonadotropin-releasing hormone-1 neuronal activity. *Endocrinol.* **2005**, *146*, 558.

(52) Morales, A.; Diaz, M.; Ropero, A. B.; Nadal, A.; Alonso, R. Estradiol modulates acetylcholine-induced Ca2+ signals in LHRH-releasing GT1-7 cells through a membrane binding site. *Eur. J. Neurosci.* **2003**, *18*, 2505.

(53) Bulayeva, N. N.; Gametchu, B.; Watson, C. S. Quantitative measurement of estrogen-induced ERK 1 and 2 activation via multiple membrane-initiated signaling pathways. *Steroids* **2004**, *69*, 181.

(54) Marin, R.; Guerra, B.; Morales, A.; Diaz, M.; Alonso, R. An estrogen membrane receptor participates in estradiol actions for the prevention of amyloid-β peptide1-40-induced toxicity in septal-derived cholinergic SN56 cells. *J. Neurochem.* **2003**, *85*, 1180.

(55) Stevis, P. E.; Deecher, D. C.; Suhadolnik, L.; Mallis, L. M.; Frail, D. E. Differential effects of estradiol and estradiol-BSA conjugates. *Endocrinol.* **1999**, *140*, 5455.

(56) Kim, S. H.; Katzenellenbogen, J. A. Hormone-PAMAM dendrimer conjugates: polymer dynamics and tether structure affect ligand access to receptors. *Angew. Chem., Int. Ed.* **2006**, *45*, 7243.

(57) Anstead, G. M.; Carlson, K. E.; Katzenellenbogen, J. A. The estradiol pharmacophore: ligand structure-estrogen receptor binding affinity relationships and a model for the receptor binding site. *Steroids* **1997**, *62*, 268.

(58) Harrington, W. R.; Kim, S. H.; Funk, C. C.; Madak-Erdogan, Z.; Schiff, R.; Katzenellenbogen, J. A.; Katzenellenbogen, B. S. Estrogen dendrimer conjugates that preferentially activate extranuclear, nongenomic Versus genomic pathways of estrogen action. *Mol. Endocrinol.* **2006**, *20*, 491.

(59) Frasor, J.; Danes, J. M.; Komm, B.; Chang, K. C. N.; Lyttle, C. R.; Katzenellenbogen, B. S. Profiling of estrogen up- and down-regulated gene expression in human breast cancer cells: Insights into gene networks and pathways underlying estrogenic control of proliferation and cell phenotype. *Endocrinol.* **2003**, *144*, 4562.

(60) Kukowska-Latallo, J. F.; Candido, K. A.; Cao, Z.; Nigavekar, S. S.; Majoros, I. J.; Thomas, T. P.; Balogh, L. P.; Khan, M. K.; Baker, J. R., Jr. Nanoparticle targeting of

anticancer drug improves therapeutic response in animal model of human epithelial cancer. *Cancer Res.* **2005**, *65*, 5317.

(61) Wu, G.; Barth, R. F.; Yang, W.; Kawabata, S.; Zhang, L.; Green-Church, K. Targeted delivery of methotrexate to epidermal growth factor receptor-positive brain tumors by means of cetuximab (IMC-C225) dendrimer bioconjugates. *Mol. Cancer Ther.* **2006**, *5*, 52.

(62) Chambliss, K. L.; Wu, Q.; Oltmann, S.; Konaniah, E. S.; Umetani, M.; Korach, K. S.; Thomas, G. D.; Mineo, C.; Yuhanna, I. S.; Kim, S. H.; Madak-Erdogan, Z.; Maggi, A.; Dineen, S. P.; Roland, C. L.; Hui, D. Y.; Brekken, R. A.; Katzenellenbogen, J. A.; Katzenellenbogen, B. S.; Shaul, P. W. Non-nuclear estrogen receptor α signaling promotes cardiovascular protection but not uterine or breast cancer growth in mice. *J. Clin. Invest.* **2010**, *120*, 2319.

(63) Conner, P. Breast response to menopausal hormone therapy--aspects on proliferation, apoptosis and mammographic density. *Ann. Med.* **2007**, *39*, 28.

(64) Kousteni, S.; Chen, J. R.; Bellido, T.; Han, L.; Ali, A. A.; O'Brien, C. A.; Plotkin, L.; Fu, Q.; Mancino, A. T.; Wen, Y.; Vertino, A. M.; Powers, C. C.; Stewart, S. A.; Ebert, R.; Parfitt, A. M.; Weinstein, R. S.; Jilka, R. L.; Manolagas, S. C. Reversal of bone loss in mice by nongenotropic signaling of sex steroids. *Science (Washington, DC, U. S.)* **2002**, *298*, 843.

(65) Madak-Erdogan, Z.; Kieser, K. J.; Kim, S. H.; Komm, B.; Katzenellenbogen, J. A.; Katzenellenbogen, B. S. Nuclear and extranuclear pathway inputs in the regulation of global gene expression by estrogen receptors. *Mol. Endocrinol.* **2008**, *22*, 2116.

(66) Alyea, R. A.; Laurence, S. E.; Kim, S. H.; Katzenellenbogen, B. S.; Katzenellenbogen, J. A.; Watson, C. S. The roles of membrane estrogen receptor subtypes in modulating dopamine transporters in PC-12 cells. *J. Neurochem.* **2008**, *106*, 1525.

(67) Chakravarty, D.; Nair, S. S.; Santhamma, B.; Nair, B. C.; Wang, L.; Bandyopadhyay, A.; Agyin, J. K.; Brann, D.; Sun, L.-Z.; Yeh, I. T.; Lee, F. Y.; Tekmal, R. R.; Kumar, R.; Vadlamudi, R. K. Extranuclear functions of ER impact invasive migration and metastasis by breast cancer cells. *Cancer Res.* **2010**, *70*, 4092.

(68) Yang, L.-c.; Zhang, Q.-G.; Zhou, C.-f.; Yang, F.; Zhang, Y.-d.; Wang, R.-m.; Brann, D. W. Extranuclear estrogen receptors mediate the neuroprotective effects of estrogen in the rat hippocampus. *PLoS One* **2010**, *5*.

(69) Kousteni, S.; Almeida, M.; Han, L.; Bellido, T.; Jilka, R. L.; Manolagas, S. C. Induction of osteoblast differentiation by selective activation of kinase-mediated actions of the estrogen receptor. *Mol. Cell. Biol.* **2007**, *27*, 1516.

(70) Rostovtsev, V. V.; Green, L. G.; Fokin, V. V.; Sharpless, K. B. A stepwise Huisgen cycloaddition process: copper(I)-catalyzed regioselective "ligation" of azides and terminal alkynes. *Angew. Chem., Int. Ed.* **2002**, *41*, 2596.

(71) Liang, L.; Astruc, D. The copper(I)-catalyzed alkyne-azide cycloaddition (CuAAC) "click" reaction and its applications. An overview. *Coord. Chem. Rev.* **2011**, *255*, 2933.

(72) Marik, J.; Sutcliffe, J. L. Click for PET: rapid preparation of [$^{18}$F]fluoropeptides using CuI catalyzed 1,3-dipolar cycloaddition. *Tet. Lett.* **2006**, *47*, 6681.

(73) Li, S.-D.; Huang, L. Pharmacokinetics and Biodistribution of Nanoparticles. *Mol. Pharmaceutics* **2008**, *5*, 496.

(74) McManaway, M. E.; Jagoda, E. M.; Kasid, A.; Eckelman, W. C.; Francis, B. E.; Larson, S. M.; Gibson, R. E.; Reba, R. C.; Lippman, M. E. [$^{125}$I]17-α-Iodovinyl 11-β-methoxyestradiol interaction in vivo with estrogen receptors in hormone-independent MCF-7 human breast cancer transfected with the v-rasH oncogene. *Cancer Res.* **1987**, *47*, 2945.

(75) Opanasopit, P.; Nishikawa, M.; Hashida, M. Factors affecting drug and gene delivery: effects of interaction with blood components. *Crit. Rev. Ther. Drug Carrier Syst.* **2002**, *19*, 191.

(76) Owens, D. E.; Peppas, N. A. Opsonization, biodistribution, and pharmacokinetics of polymeric nanoparticles. *Int. J. Pharm.* **2006**, *307*, 93.

(77) Lee, C. C.; MacKay, J. A.; Frechet, J. M. J.; Szoka, F. C. Designing dendrimers for biological applications. *Nat. Biotechnol.* **2005**, *23*, 1517.

(78) Jiang, Y.-Y.; Tang, G.-T.; Zhang, L.-H.; Kong, S.-Y.; Zhu, S.-J.; Pei, Y.-Y. PEGylated PAMAM dendrimers as a potential drug delivery carrier: In vitro and in vivo comparative evaluation of covalently conjugated drug and noncovalent drug inclusion complex. *J. Drug Targeting* **2010**, *18*, 389.

(79) Nelson, H. D.; Humphrey, L. L.; Nygren, P.; Teutsch, S. M.; Allan, J. D. Postmenopausal hormone replacement therapy. *JAMA, J. Am. Med. Assoc.* **2002**, *288*, 872.

(80) Riggs, L.; Hartmann, L. C. Selective estrogen-receptor modulators - mechanisms of action and application to clinical practice. *N. Engl. J. Med.* **2003**, *348*, 618.

(81) Esfand, R.; Tomalia, D. A. Poly(amidoamine) (PAMAM) dendrimers: from biomimicry to drug delivery and biomedical applications. *Drug Discov. Today* **2001**, *6*, 427.

(82) Svenson, S.; Tomalia, D. A. Dendrimers in biomedical applications-reflections on the field. *Adv. Drug Delivery Rev.* **2005**, *57*, 2106.

CHAPTER 4

# SYNTHETIC APPROACHES TOWARDS THE $^{18}$F-LABELLING OF 2-[$^{18}$F]FLUOROESTRADIOL VIA COMPLEX DIARYLIODONIUM SALTS

## I. INTRODUCTION

### *A. Background*

Molecular imaging has become a key component in biomedical research and diagnostic clinical studies.[1] Imaging the presence and functionality of diseased states provides significant insight into the mechanisms leading to disease onset and progression.[2] Although similar information can be obtained through tumor biopsies and immunohistochemical evaluations, some tumor sites (i.e., brain) cannot be accessed for biopsy and thus, demand a less invasive approach. Additionally, tumor heterogeneity, biopsy sampling errors, and varying expression profiles between primary and metastatic sites further complicate matters and may not yield an accurate description of the diseased state.[3-7] Advances in medical imaging, however, can provide detailed biochemical information through minimally invasive procedures at the earliest stages of disease onset, before any observable symptoms are seen in the patient.

### *B. PET Imaging and the Estrogen Receptor*

The measurement of estrogen receptor (ER) levels in breast cancer by using PET imaging using the compound our group developed, 16α-[$^{18}$F]fluoroestradiol (**1**, Figure 4.1, [$^{18}$F]FES), appears to be a better predictor of benefit from endocrine therapies than are standard immunohistochemical assays of ER.[8-13] As a result, these [$^{18}$F]FES-PET studies can assist in the proper selection of patients to undergo less toxic endocrine therapies instead of the more costly and morbid cytotoxic therapy.[8,12] By individualizing treatment plans such as this one, the expectation is that patient outcomes will be greatly improved. However, despite the initial successes of FES, it is likely that PET measurements of ER in breast tumors can be vastly improved by developing other ER imaging agents having higher tumor-to-background-tissue activity, as this would extend the usefulness of the agent to detect smaller tumors and identify regions of lower ER concentrations.

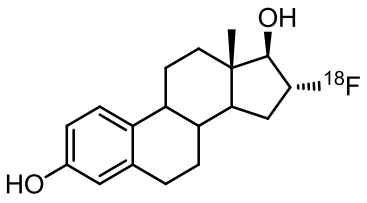


**1**, [$^{18}$F]FES

**Figure 4.1.** Structure of [$^{18}$F]FES (**1**), an agent used for ER-targeted PET imaging studies.

[$^{18}$F]FES (**1**) binds to ER as well as estradiol, but its affinity to an important serum protein, sex hormone binding globulin (SHBG), is less than 10% that of estradiol.[14] SHBG binding is thought to facilitate uptake into hormone target tissues and tumors in humans through a specific cell membrane receptor, megalin, which is distinct from ER.[15,16] Curiously, SHBG is not present in the blood of rats or mice, the species typically used for the development of PET imaging agents.[15,17] As further evidence of the importance of SHBG in target tissue uptake of F-18 labeled steroids in humans, we found some estrogens and androgens with high affinity for their receptor targets, but low affinity for SHBG, had high target tissue uptake in rodents, but very poor target tissue uptake in primates or humans.[14,18,19] Thus, we believe that F-18 labeled estrogens with high affinity for both ER and SHBG would be better ER imaging agents than [$^{18}$F]FES.

In this respect, 2-[$^{18}$F]fluoroestradiol ([$^{18}$F]2FES, **2**, Figure 4.2) appears promising: Its affinity for ER is 110% that of estradiol, similar to that of FES, but its affinity for SHBG is 3700%, whereas that for FES is only 9%.[14] It was originally thought that the design of agents with high affinity for SHBG was to be avoided since it might retard the release of these estrogens to the target tissue and restrict their bioavailability by excessive binding in blood.[20] However, recent evidence has indicated that binding to SHBG actually protects these agents from metabolism and subsequently, increases the bioavailability of estrogens to ER-rich target tissues.[16,21-23]

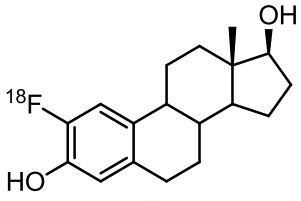


**2**, [$^{18}$F]2FES

**Figure 4.2.** Structure of [$^{18}$F]2FES (**2**), a potentially useful ER-targeted radiopharmaceutical.

*C. Radiosynthetic Challenges Associated with [$^{18}$F]2FES (**2**)*

The phenol function is ubiquitous in both naturally occurring and synthetic bioactive compounds.[24,25] In drugs, the phenolic function is often substituted with fluorine because fluorine substitution, particularly at the ortho position, enhances receptor target binding affinity, perhaps by adjusting the phenol pKa, and/or *in vivo* potency, by blocking the ortho-hydroxylation metabolism, extending drug clearance profile and increasing drug exposure.[24,25] In any case, fluorine substitution is either beneficial to bioactivity or, in the worst case, well-tolerated.

While there are many methods for labeling small molecules with F-18 at aliphatic positions and on electron-deficient aromatic rings, there are essentially no reliable and practical methods to label electron-rich aromatic rings, such as phenols, with F-18 at high specific activity. This is disappointing: Fluorine-labeled phenols are found in many drugs, because fluorine substitution often improves drug binding and pharmacokinetic properties; also, there are many interesting plant metabolites and hormones that contain either phenols or other electron-rich aromatic systems such as indoles, whose metabolism, transport, and distribution would be interesting to study if they could readily be prepared in F-18 labeled form (Figure 4.3).[24]

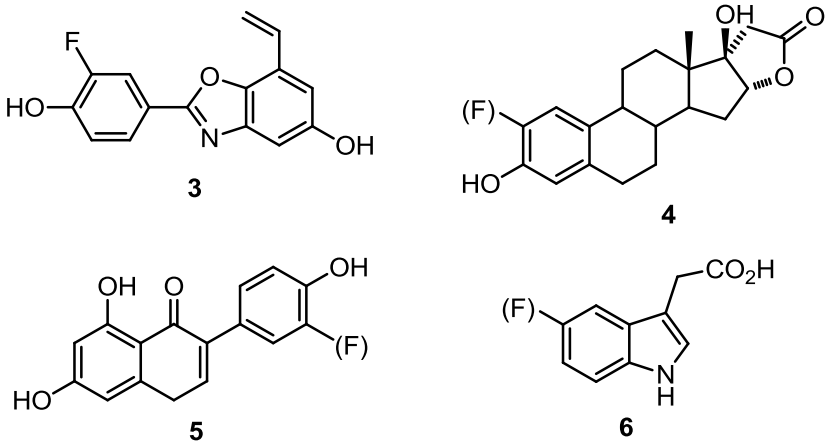


**Figure 4.3.** Phenolic and electron-rich molecules of interest for labeling with [$^{18}$F]fluoride ion. **3**: ERB-041, ERβ selective ligand; **4**: ERα selective ligand; **5**: Genistein, a plant isoflavone, **6**: Auxin, a plant hormone. F = already present on molecule; (F) = potential site of F-18 substitution.

Most approaches to label phenols with F-18 involve the labeling of electron-poor arenes by nucleophilic aromatic substitution, followed by subsequent conversion to phenols by oxidation or other multi-step sequences that are often inefficient and time consuming. Thus, the lack of good methods for labeling phenols and other electron-rich aromatics with F-18 at high specific activity represents a significant methodological gap in F-18 radiochemistry.

In our experience, preparing 2-[$^{18}$F]fluoroestradiol (**2**) is a prime example of the types of challenges present in the F-18 labeling of electron-rich aromatic systems.[26] We examined many A-ring estrogen precursors and after several trials, we were able to prepare 2-[$^{18}$F]fluoroestradiol by the three-step process shown in Scheme 4.1.[26] [$^{18}$F]Fluoride ion was introduced into the 2 position by displacement of a trimethylammonium group (**7**) that was activated by a carbonyl group introduced into the steroid system at C-6, para to the leaving group. Although the first radiofluorination step proceeded satisfactorily, the next two steps were time-consuming and inefficient, but mainly in the additional manipulations required to remove the activating group (**8**) and deprotection of the methyl ethers (**9**) to afford the diphenol **2**. Overall, the multistep transformations required to produce [$^{18}$F]2FES proved sufficiently awkward that further biological evaluations of this compound awaits improvements in the synthesis of F-18 labeled phenols.

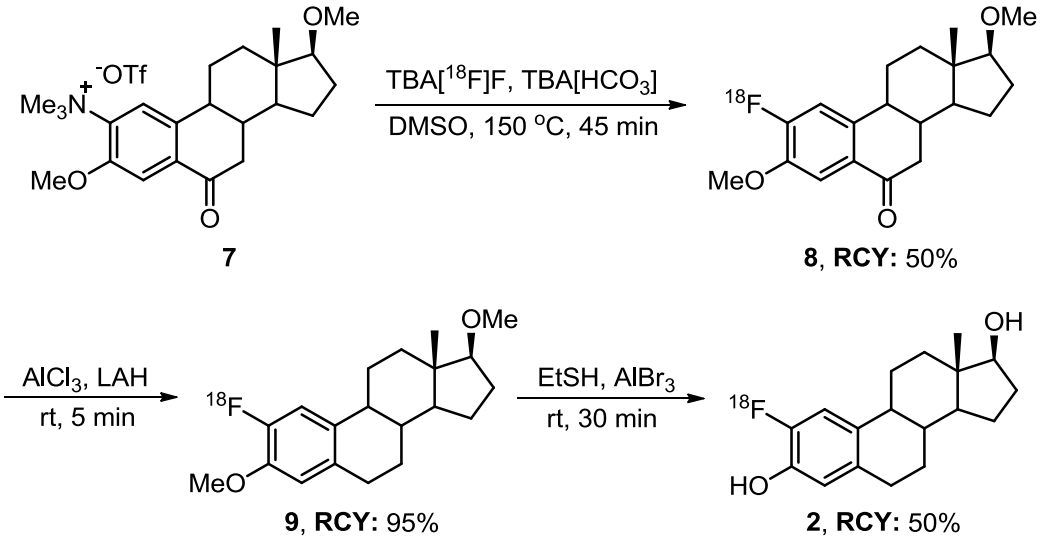


**Scheme 4.1.** Synthesis of [$^{18}$F]2FES (**2**) by nucleophilic aromatic substitution-reduction-deprotection sequence.[26]

*D. Radiofluorination of Electron-Rich Arenes with Diaryliodonium Salts*

The available methodology for the incorporation of [$^{18}$F]fluoride ion into electron-rich arenes is extremely limited, with only a few methods being reported. The Balz-Schiemann reaction, the classical method for aromatic fluorination, is unsuitable for $^{18}$F-labelling at high specific activity because the radiofluorine is extensively diluted by the large excess of unlabeled [$^{19}$F]fluoride in the counteranions. Although the use of other non-fluorine containing counteranions have been explored, the transition to tracer levels has been less than ideal.[27] The use of aryl triazenes as precursors for aromatic fluorination, known as the Wallach reaction,

actually predates the Balz-Schiemann reaction, and although it has been investigated as a method for radiofluorination, it is very inefficient at the tracer level, especially with electron-rich aromatic systems.[28,29]

A more recently described method for the preparation of [$^{18}$F]fluoroarenes is through the use of diaryliodonium salts. Hypervalent iodine compounds have tremendous utility in many aspects of mainstream organic chemistry as mild, nontoxic alternatives[30] to the commonly used oxidants and expensive organometallic catalysts. Although these agents have been known to exist since 1894, only recently have they been used for arene radiolabeling with [$^{18}$F]fluoride ion.[31] To date, the use of diaryliodonium salts represents the lone method by which electron-rich arenes can be radiofluorinated in sufficiently high RCYs and specific activities.

First reported by Pike,[31] the use of these salts has enabled reliable $^{18}$F-labelling of both unactivated or electron-rich [$^{18}$F]fluoroaromatic compounds, although most have been relatively simple substrates. Nucleophilic [$^{18}$F]fluoride attack occurs at the electrophilic iodine atom, and upon the release of one of the ligands, reductive elimination of the corresponding intermediate, Ar-I(Ar)($^{18}$F), affords the desired [$^{18}$F]fluoroarene.[32] [$^{18}$F]Fluorination tends to favor the more electron-deficient ring, and as a result, the use of unsymmetrical diaryliodonium salts where one aryl group is an electron-rich *p*-methoxyphenyl or 2-thienyl group results in selective fluorination to the other, less electronically rich arene.[33,34] Moreover, in the case of ortho-substituted diaryliodonium salts, the ortho-substituted arene is preferentially attacked by fluoride, even if it is more electron-rich, and this effect is further enhanced in the presence of doubly substituted arenes.[35] Initially, a "turnstile" mechanism[36] was proposed to account for the ortho effect, but subsequent theoretical studies have postulated other mechanisms and intermediates, including the formation of bridged dimers[37] or trimers,[38] before reductive elimination occurs. However, others have claimed a standard nucleophilic aromatic substitution mechanism based on Hammett plots.[33] Consequently, not all reactions show a correlation towards a presumed mechanism and are most likely dependent on the electronic and steric nature of the particular substrate for each reaction.

Access to diaryliodonium salts typically involves multi-step syntheses (Scheme 4.2) in which an aryl iodide (**10**) is oxidized to an aryliodine(III) (**11**) compound by treatment with an inorganic oxidant under acidic conditions. The diacetoxy reagents **11** are quite stable and can be isolated, and subsequent ligand exchange with arylstannanes, -silanes, or boronic acids (**12**) affords the desired salts (**13**). The anion ($X^-$) in these instances originates from the acid used

(typically from TsOH), and anion exchange with salts (i.e., KBr, KI) generates other variations in the final structure. Until now, this $^{18}$F-labelling approach has been largely applied to relatively simple diaryliodonium salts, and only a few complex examples have been reported.[34,39]

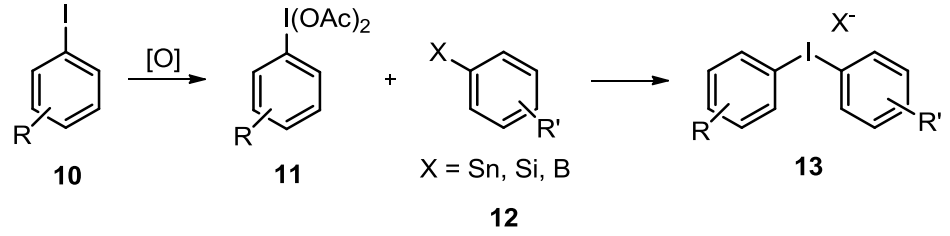


**Scheme 4.2.** Standard synthesis of unsymmetrical iodonium salts.

As part of our ongoing investigations in developing improved ER-targeted radiopharmaceuticals, we wished to explore facile approaches towards the radiosynthesis of 2-[$^{18}$F]fluoroestradiol. Herein, we describe a rapid strategy to access this promising ER imaging agent through diaryliodonium salts within 25 minutes with nucleophilic [$^{18}$F]fluoride ion in synthetically useful yields. This study demonstrates the critical dependence of multiple factors in the successful radiofluorination of unsymmetrical iodonium salts, and in our case, the bromide salt with K[$^{18}$F]F·$K_{222}$ in PhH was found to be the optimal conditions.

## II. RESULTS and DISCUSSION

*A. Synthesis of the Diaryliodonium Salts for [$^{18}$F]Fluorination*

The synthesis of the diaryliodonium salts (Scheme 4.3) commenced with a dimethylation of commercially available 17β-estradiol (**14**) with NaH and MeI in high yields. A subsequent regioselective bromination of **15** with NBS afforded bromide **16** in a 4:1 ratio of the desired regioisomer (2-position over the 4-position).[40] Two additional recrystallizations significantly increased the ratio to a synthetically useful proportion of 96:4 of the 2-position isomer over the 4-position one. Attempts to append the required tin moiety on the ring through palladium-mediated processes generated only the reduction product. However, dehalogenation of bromide **16** with *n*BuLi and subsequent capture of the lithium intermediate with trimethyltin chloride yielded **17** in good yields. Unfortunately, the tin species (**17**) was sensitive to protio-destannylation during purification and as a result, could not be obtained as a single product. Nevertheless, **17** was recovered in high crude chemical purity (>90%) after passing through a silica gel plug and could be used as it in the next step without any problems.

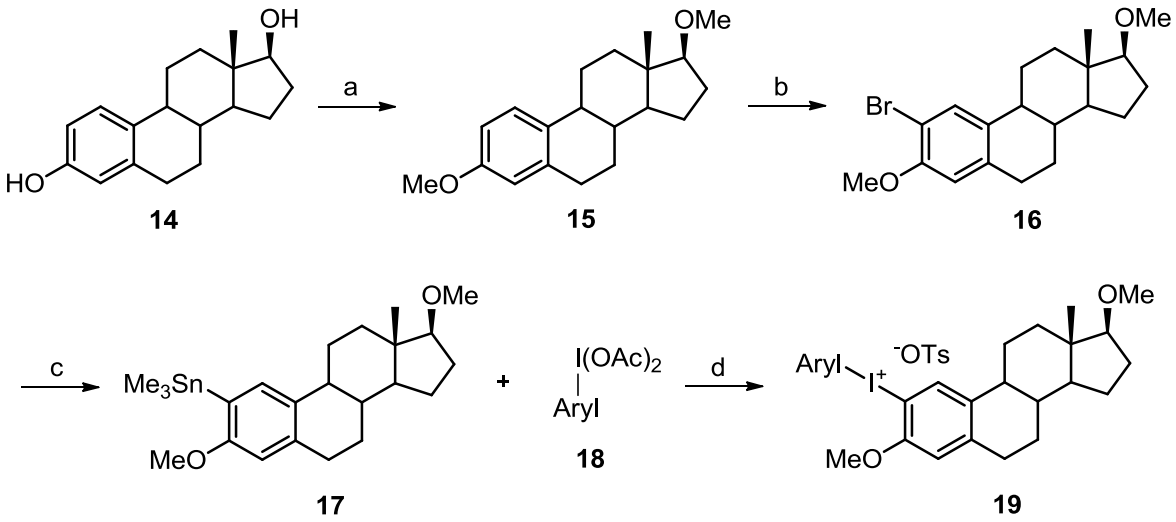


14 15 16 17 18 19

**Scheme 4.3.** Synthesis of the unsymmetrical diaryliodonium salts. (a) NaH, THF, 0 $^{o}$C→rt, 18 h; (b) NBS, DCM, ACN, rt, 18 h; (c) *n*BuLi, TMEDA, $Me_3SnCl$, THF, -78 $^{o}$C→rt, 2 h; (d) $RI(OAc)_2$, TsOH, ACN, rt, 18 h. (**18**) Aryl = 4-methoxyphenyl or 2-thiophene.

The required (diacetoxy)arenes (**18**) were prepared by oxidation of the corresponding iodoarenes with sodium perborate in acetic acid in synthetically useful yields.[41] The aryliodine(III) compounds are unreactive to the standard reaction conditions for the formation of iodonium salts, and only upon treatment of the diacetoxy derivatives to the Koser's reagent with tosylic acid monohydrate in acetonitrile can the salts (**19**) be formed.[40] These derivatives form readily with TsOH addition, but are difficult to isolate due to their instability; thus, they were used as is upon formation with the tin compound (**17**). We were interested in preparing salts containing one aryl ring that is electron-rich, such as a 4-methoxyphenyl or 2-thiophene groups, because fluorination tends to prefer the more electron-deficient ring. However, the exceptionally rich nature of the A-ring phenol of estradiol complicates fluorination onto the desired ring since it is difficult to synthesize iodonium salts that contain a more electron-rich second ring. Attempts to append additional electron donating groups such as methoxy groups onto these electron-rich rings were unsuccessful as these substrates were incompatible with the oxidizing conditions required to form the diacetoxy derivatives. As a result, the 4-methoxy and 2-thienyl arenes are two of the more commonly used dispensable arene rings for selective fluorination of unsymmetrical diaryliodonium salts and would serve as the basis of our precursors.[33]

The diaryliodonium tosylates (**19**) contained either a 4-methoxy or 2-thiophene aryl group and were readily converted into other salts ($PF_6^-$, $Br^-$, $I^-$) in moderate to high yields by anion exchange reactions, as shown in Figure 4.4.[40] In each case, metathesis was confirmed by the absence of the tosylate signals in the $^1$H NMR spectrum. The preparation of the salts was

simple and straightforward and each precipitated from solution under the metathesis conditions to afford bench stable solids. Preparation of other salts was attempted ($Cl^-$, $CF_3CO_2^-$, $BPh_4^-$) but yielded none of the desired material.

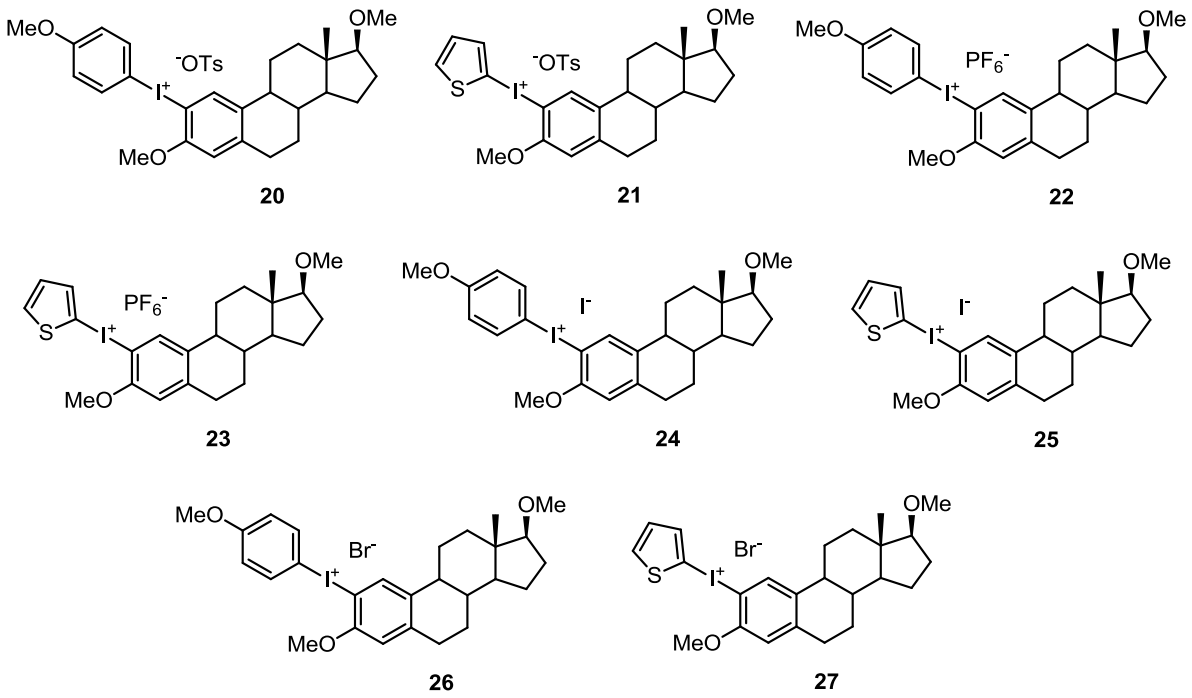


**Figure 4.4.** Representative structures of the prepared unsymmetrical diaryliodonium salts.

The reported diaryliodonium salts have involved relatively simple substrates, intended to investigate [$^{18}$F]fluorination selectivity, and of these, only a few have been applied to potential PET tracers.[39] Since this was relatively new territory for these substrates, we undertook an exhaustive screen of every potential factor in the fluorination of these salts (Figure 4.4), including the effect of fluoride source, temperature, solvent, anion, and aryl group.

*B. Influence of the Counteranion*

Counteranions in diaryliodonium salts can have a drastic effect on the radiochemical yields with [$^{18}$F]fluoride ion. This is mainly the result of how these anions contribute to the structures of the salt in solution during the reaction. At times, inorganic counterions induce an effective salt separation between the two, which results in a “naked” iodonium cation,[42] while other research suggests partially dimeric and trimeric structures of the iodonium salt.[37,38] Moreover, anions with high nucleophilicity also compete with [$^{18}$F]fluoride ion for the substitution reaction, which can significantly reduce the availability of precursor to undergo the desired reaction. Nonetheless, radiochemists tend to prefer the use conjugate bases of strong acids

($^{-}$OTs, $^{-}$OTf) due to their low nucleophilicity; however, recent evidence has suggested the use of the more nucleophilic bromides and chlorides as optimal counteranions.[43,44] The exact influence of the anions on these reactions is still unknown, but at least for the more nucleophilic examples, this may be related to the enhanced stability of these precursors, thus suppressing undesired decomposition reactions that reduce the availability of these substrates for reaction with [$^{18}$F]fluoride ion.

We initially studied the counterion effect more closely with our unsymmetrical diaryliodonium salts in which each substrate underwent the same reaction conditions with only the anion being varied. As shown in Scheme 4.4. (top half), the model reaction involved TBAF as the fluoride source and PhH as the solvent at 140 $^{o}$C for 20 minutes, and the yields were determined by integrating the ratios of the aromatic regions of the steroid products, the fluoro- (**29**) and iododimethoxyestradiol (**31**) in the $^{1}$H NMR spectrum. The use of benzene differs considerably from traditional [$^{18}$F]fluorination radiochemistry, which typically prefers the more polar, aprotic solvent, such as DMSO, ACN, DMF. However, recent reports have suggested the use of low polar, noncoordinating media, which can suppress side product formation, similar to those seen in transition metal complexes, is the preferred approach for improving the yields of fluorinated aromatic compounds.[40,45]

As shown in Scheme 4.4. (bottom two), the yields of the desired fluorinated compound (**29**) greatly depended on the counterion present, especially when the 4-methoxyphenyl group was used. Yields favor the use of the more nucleophilic ($Br^{-}$, $I^{-}$) over the non-nucleophilic counterions ($^{-}$OTs), which is consistent with previous examples,[33,35] but not with others,[46] and further supports the notion each substrate must be screened individually. By contrast, the yield of **29** from the thienyl compound (**32**) was surprisingly low. A recent report demonstrates the use of the 2-thiophene group as the preferred dispensable aryl group for the ortho-[$^{18}$F]fluorination of phenols[33] and yet, in our case, minimal or no yields of the desired compound were obtained with the 2-thiophene group. Consequently, our efforts on future reactions focused solely on the 4-methoxy derivative (**30**).

**Model Reaction:**

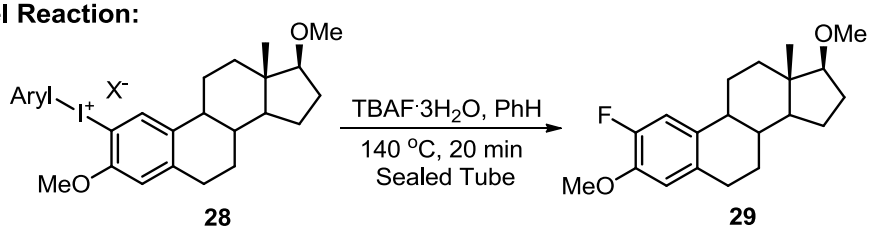


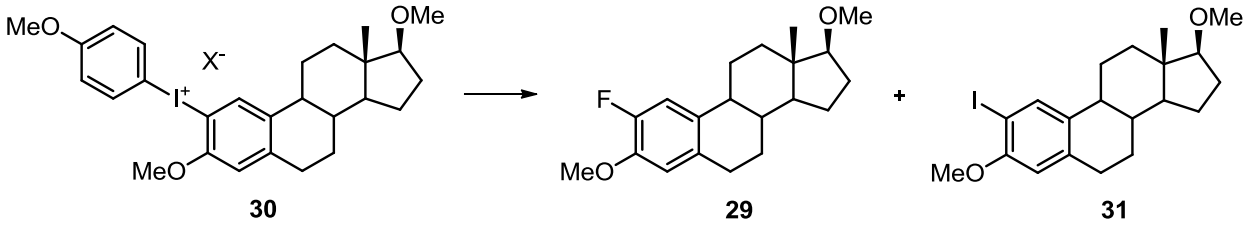


| X⁻ Counteranion | NMR Ratio of 29 | NMR Ratio of 31 |
|---|---|---|
| $PF_6^-$ | 50 | 50 |
| $Br^-$ | 35 | 65 |
| $I^-$ | 25 | 75 |
| $^-OTs$ | 0 | 100 |

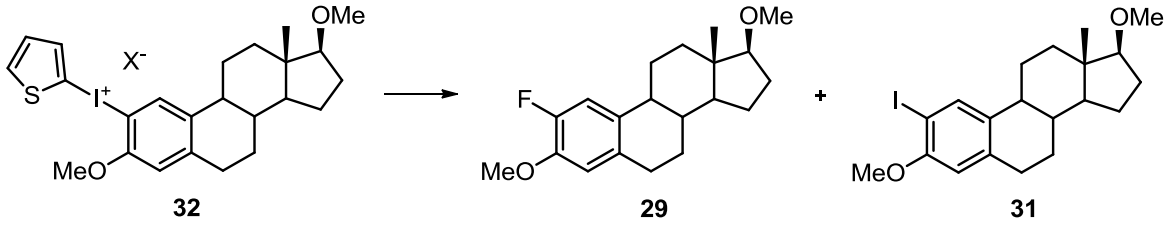


| X⁻ Counteranion | NMR Ratio of 29 | NMR Ratio of 31 |
|---|---|---|
| $PF_6^-$ | 10 | 90 |
| $Br^-$ | 0 | 100 |
| $I^-$ | 0 | 100 |
| $^-OTs$ | 0 | 100 |

**Scheme 4.4.** Investigations on the counterion effect on the different diaryliodonium salts. Yields are calculated from integration of the aromatic peaks of **29** to **31** in the $^1H$ NMR spectrum.

To further confirm PhH as the optimal solvent (data not shown), the same reactions were repeated with DMSO, DMF, ACN, $PhCH_3$, and cyclohexane. Again, PhH exhibited the highest yields of **29** and was used as the preferred solvent in all other reactions.

*C. Screening for the Fluoride Source*

We next studied the fluorination of diaryliodonium $PF_6^-$ (**22**) and bromide (**26**) salts with different fluoride sources. Of the available [$^{18}$F]fluorination sources, TMA[$^{18}$F]F, Cs[$^{18}$F]F, K[$^{18}$F]F·$K_{222}$, and TBA[$^{18}$F]F are four of the more well-known ones, with the latter two being the most commonly used. Overall, in both cases (Scheme 4.5), yields of **29** are fairly comparable with all fluoride sources, except for the use of TMAF and **22**. In contrast, TMAF afforded the highest yields of **29** with bromide derivative **26**. Nevertheless, the screen proved to be quite useful since it showed that these salts were reactive to a variety of fluoride sources; so, we were not constrained to a single source. This is significant especially since the transition to tracer level chemistry with [$^{18}$F]fluoride ion is highly unreliable, and variations in the original protocol are often required to achieve success.

Aside from the TMAF reaction, the $PF_6^-$ salt (**22**) showed slightly higher yields of **29** when compared to the bromide **26** yields. The increase is most likely attributed to the $PF_6^-$ anion, which can release fluoride anions from $PF_6^-$, and these ions can attack the iodine to form the desired compound (**29**). Since this side reaction would dilute the specific activity of the $^{18}$F-radiotracer, this substrate is not useful for us, and subsequently, all $^{18}$F-studies were conducted with bromide **26**.

Nevertheless, these findings proved significant since the fluorination can proceed to the unanticipated more electron-rich arene in sufficiently high yields, especially for $^{18}$F-chemistry and is most likely the result of the ortho effect.

**Model Reaction:**

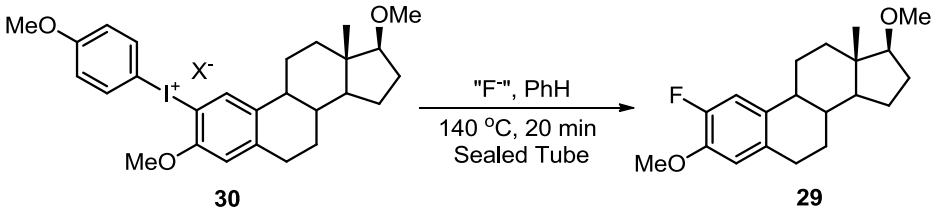


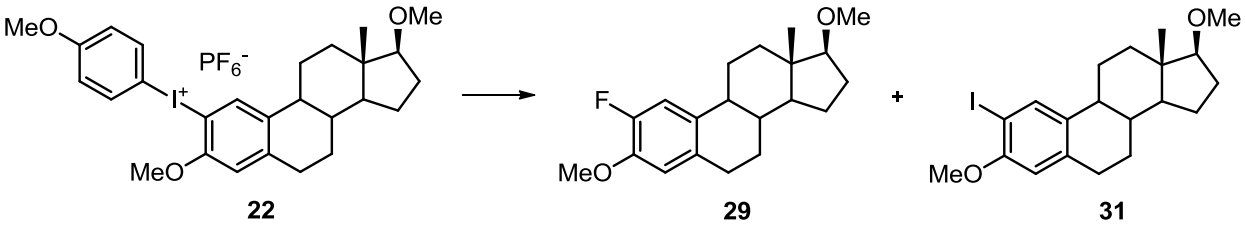


| Fluoride Source | NMR Ratio of 29 | NMR Ratio of 31 |
|---|---|---|
| TBAF | 50 | 50 |
| TMAF | 0 | 100 |
| KF, $K_{222}$ | 49 | 51 |
| CsF | 45 | 55 |

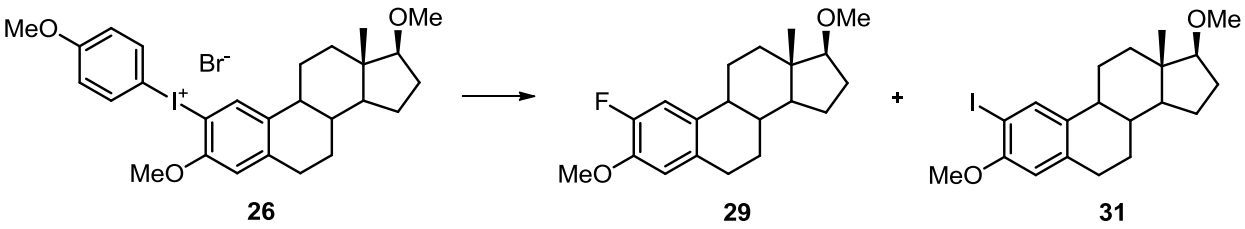


| Fluoride Source | NMR Ratio of 29 | NMR Ratio of 31 |
|---|---|---|
| TBAF | 35 | 65 |
| TMAF | 51 | 49 |
| KF, $K_{222}$ | 43 | 57 |
| CsF | 36 | 64 |

**Scheme 4.5.** Investigations of fluoride sources on the different diaryliodonium salts. Yields are calculated from integration of the aromatic peaks of **29** to **31** in the $^{1}$H NMR spectrum.

*D. Problems Associated with Methyl Ether Deprotection*

One of the main problems associated with C-$^{18}$F bond formation is the need for protecting groups, which adds to the technical difficulty in synthesizing short-lived isotope tracers through multistep sequences. The protecting groups are required due to the dual base/nucleophile nature of the fluoride, and the presence of acidic functionality can severely

affect the nucleophilicity of [$^{18}$F]fluoride ion and radiochemical yields. However, the rapid reaction times demanded by short-lived isotopes require fast deprotections and use of harsh conditions for their removal, which, in turn, causes additional problems in the process. In our case, methyl ethers are notorious in mainstream organic chemistry for the difficulty involved in their removal, and the difficulty is only further exacerbated with F-18 work. Initial deprotection attempts of the crude reaction mixture after fluorination with HCl and $AlCl_3$ proved to be futile. However, switching to pyridine·HCl revealed rapid removal of the methyl ethers within 10 minutes. Unfortunately, the harsh conditions required by the reaction (180-220 $^{o}$C) not only cleaved the iodine off the aryl ring, but strikingly, fluorine also proved sensitive, with the subsequent $^{1}$H NMR spectra showing only estradiol as the sole compound in the crude reaction mixture. After extensive screening and optimization, it was eventually discovered that $AlBr_3$ and dodecanethiol ($CH_3(CH_2)_{11}SH$) was the optimal combination for rapid and efficient deprotection of the methyl ethers (Scheme 4.6).

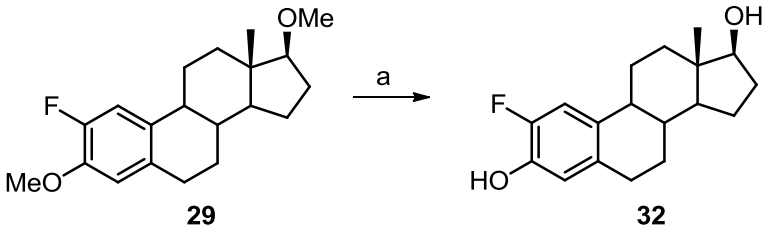


**29** **32**

**Scheme 4.6.** Deprotection of the methyl ethers to afford 2-fluoroestradiol (**32**). (a) $CH_3(CH_2)_{11}SH$, $AlBr_3$, rt, 5 min.

Overall, the cold chemistry revealed the following sequence for the synthesis of 2-[$^{18}$F]fluoroestradiol. The bromide salt **26** proved to be the best salt for the fluorination, and after passing through a silica gel plug, the crude material can be utilized in the deprotection step without the need for HPLC purification. This allows for **32** to be accessed rapidly within only 25 minutes of reaction time.

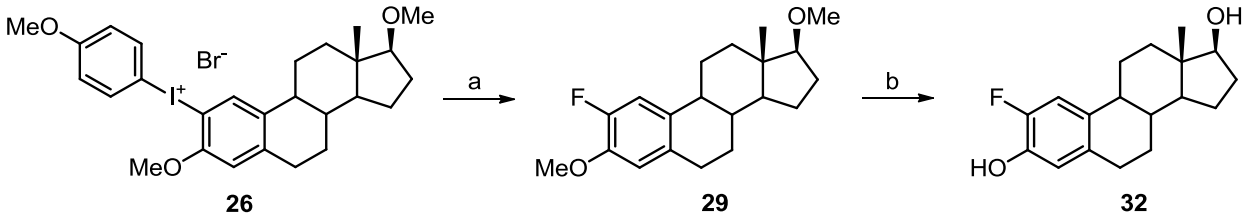


**26** **29** **32**

**Scheme 4.7.** Overall sequence for the synthesis of 2-fluoroestradiol (**32**). (a) KF, $K_{222}$, PhH, 120 $^{o}$C, 20 minutes; (b) $CH_3(CH_2)_{11}SH$, $AlBr_3$, rt, 5 minutes.

*E. Radiosynthesis of 2-[$^{18}$F]Fluoroestradiol (**2**)*

From our original cold screen, bromide **26** and PhH were the preferred substrate and solvent, respectively, with no considerable differences in yields with varying temperatures (80-140 $^{o}$C) or fluoride sources (Scheme 4.5). We next studied the application of these conditions to the synthesis of 2-[$^{18}$F]fluoroestradiol (**2**).

Since the [$^{18}$F]fluoride source is produced as an aqueous solution from the cyclotron, a drying step must be performed to remove the water in order to restore the nucleophilicity of the anion. Key to this drying step is the addition of an appropriate base to afford a reactive, organic soluble [$^{18}$F]fluoride source. Typically, alkali (i.e., K, Cs) or quaternary ammonium [$^{18}$F]fluoride salts are obtained from their respective carbonates, bicarbonates, or hydroxides, albeit with varying success. Overall, the appropriate choice of cation and base can have a critical role in the success of these reactions; however, definitive guidelines for the proper choice do not exist, and one must screen the reaction for the optimal base.

We initially investigated the use of quaternary ammonium salts, TMA[$^{18}$F]F and TBA[$^{18}$F]F, formed from TMA[$HCO_3$] and TBA[$HCO_3$], respectively, and our model reaction involved bromide **26** and PhH at 105 $^{o}$C for 20 minutes (Scheme 4.8). Not surprisingly, the successes seen previously in cold chemistry with these fluoride sources were not repeated, and no product (**33**) was formed. This was largely attributed to the low solubility of the [$^{18}$F]fluoride salts in PhH. After the drying step is performed and all the solvent is removed, the [$^{18}$F]fluoride source becomes adhered to the surface of the glass vial and must be resolubilized for the reaction to proceed. Polar, aprotic solvents (i.e., DMSO, DMF) tend to dissolve these salts quite readily, which explains their widespread use; however, these solvents were inferior to PhH in the original screen in terms of product formation. Attempts to use DMSO, instead of PhH, with TBA[$^{18}$F]F also yielded no success.

**Model Reaction:**

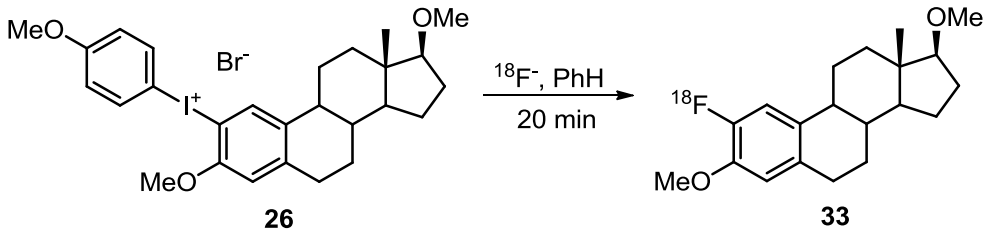


| Salt | Oil Bath (105 °C) | Microwave |
|---|---|---|
| $TMAHCO_3$ | 0 | 0 |
| $TBAHCO_3$ | 0 | 4 |
| $Cs_2CO_3$ | 0 | 14 |
| $CsHCO_3$ | 0 | 17 |
| $K_2CO_3/K_{222}$ | 19 | 10 |
| $KHCO_3/K_{222}$ | 0 | 7 |

**Scheme 4.8.** Evaluation of the effect of different salts on the radiofluorination of bromide **26**. Radiochemical yields were based on radio-TLCs and HPLC traces.

However, upon switching to $Cs_2CO_3$ and $CsHCO_3$ (Scheme 4.8), acceptable amounts of **33** were obtained through microwave heating. Unfortunately, a closer inspection of the reaction revealed similar solubility issues: after removal of the solvent, a majority of the Cs[$^{18}$F]F remained stuck to the vessel wall of the original vial. The minor, soluble amounts were sufficiently reactive to give the desired compound (**33**), but since over 85% of all of the original activity was retained on the vessel wall, Cs[$^{18}$F]F offers limited utility. This also demonstrates the dangers of interpreting reaction success based solely on radio-TLCs.

By far, the most commonly used [$^{18}$F]fluoride source is the K[$^{18}$F]F·$K_{222}$ cryptate, due to its superior organic solubility and fluoride nucleophilicity as compared to the other salts. K[$^{18}$F]F can be prepared from either the potassium carbonate or bicarbonate salt, but the presence of an additional protic hydrogen seems to have a critical effect on the reaction, since no product formed with $KHCO_3$. Nevertheless, acceptable RCYs of **33** were obtained with the $K_2CO_3/K_{222}$ approach in the preferred oil bath method. Further modification of the method with the addition of radical scavenger, TEMPO, afforded a 4-5% increase in yields. TEMPO is a common radical-scavenger additive for the radiofluorination of iodonium salts since these precursors are unstable to basic conditions and can generate aryl radicals by homolytic fragmentation of precursor. Although addition of TEMPO in the cold chemistry screen resulted in a significant

reduction in product formation, gratifyingly, its addition in the presence of F-18 increased the desired yields.

Additional investigations revealed that the reaction was complete within 10 minutes, and after elution through a silica gel plug, methyl ether deprotection proceeded rapidly with the original conditions ($AlBr_3$, $CH_3(CH_2)_{11}SH$) to generate 2-[$^{18}$F]fluoroestradiol (**2**) within 20 minutes. The overall sequence is shown in Scheme 4.9.

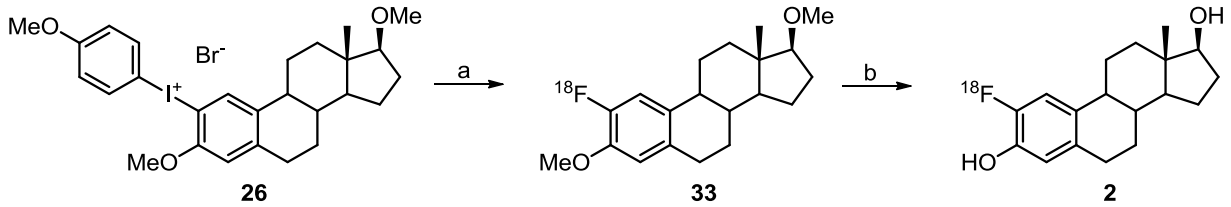


**Scheme 4.9.** Overall sequence for the radiosynthesis of 2-[$^{18}$F]fluoroestradiol (**2**). (a) K[$^{18}$F]F, $K_2CO_3$, $K_{222}$, TEMPO, PhH, 105 $^{o}$C, 10 min, RCY = 23%; (b) $CH_3(CH_2)_{11}SH$, $AlBr_3$, rt, 5 min.

Again, these findings are significant since we are obtaining [$^{18}$F]fluorination of the unanticipated more electron-rich ring, and although the yields are compared to mainstream organic chemistry, this is not unusual for F-18 chemistry (typically radiochemical yields range from 10-30%). Lower yields are not a significant problem for PET agent production since the sensitivity of PET imaging is extraordinarily high and only relatively low amounts of $^{18}$F-material are needed for biological evaluations. Although the yields are still not ideal, they are workable and sufficiently high to evaluate **2** in future animal studies.

## III. CONCLUSION

In summary, we have developed an experimentally simple method for the rapid and efficient preparation of a complex diaryliodonium bromide salt that can be used to afford 2-[$^{18}$F]fluoroestradiol within 20 minutes of reaction time in synthetically useful radiochemical yields. The reaction proved highly dependent on multiple factors (i.e., counteranion, solvent, fluoride source) and illustrates the lack of generality when utilizing these particular substrates to radiofluorinate electron-rich arenes. Current efforts have focused on scaling up the reaction with higher amounts of activity to generate sufficient amounts of the desired radiotracer for evaluation in the appropriate animal models.

## IV. METHODS

### Materials

All reactions were carried out under a nitrogen atmosphere with dry solvents using anhydrous conditions unless otherwise stated. Solvents used in the reactions were dried in a solvent delivery system (neutral alumina column). Reagents were purchased from Aldrich and used without further purification, unless otherwise stated. Yields refer to chromatographically and spectroscopically ($^1$H NMR) homogeneous materials, unless otherwise stated. Reactions were monitored by thin layer chromatography (TLC) carried out on Merck silica gel 60 F254 precoated plates (0.25 mm) using UV light as the visualizing agent and ceric ammonium molybdate and heat as developing agents. Flash column chromatography was performed on Silica P Flash silica gel (40-64 $\mu$M, 60 Å) from SiliCycle. $^1$H NMR spectra were recorded at 23 $^o$C on a Varian Unity-400, Varian Inova-500 or Varian Unity-500 spectrometers and are reported in ppm using residual protium as the internal standard ($CHCl_3$, δ = 7.26, $CD_2HCN$, δ = 1.94, center line, acetone-$d_6$, δ = 2.05, center line, DMSO-$d_6$, δ = 2.50, center line). The following abbreviations were used to explain the multiplicities: s = singlet, d = doublet, dd = doublet of doublets, t = triplet, q = quartet, m = multiplet and b = broad. Proton-decoupled $^{13}$C NMR spectra were recorded on a Varian Unity-500 (126 MHz) spectrometer and are reported in ppm using solvent as an internal standard ($CDCl_3$, δ = 77.16, $CD_3CN$, δ = 1.30, center line, acetone-$d_6$, δ = 29.80, center line, DMSO-$d_6$, δ = 40.1, center line). High resolution mass spectra were obtained at the University of Illinois Mass Spectrometry Laboratory. No-carrier added [$^{18}$F]fluoride was produced at Washington University Medical School by the $^{18}$O(p,n)$^{18}$F reaction through proton irradiation of enriched (95%) [$^{18}$O]$H_2O$ using a RDS111 cyclotron. Screw-cap test tubes used for drying fluoride and radiolabeling were purchased from Fisher Scientific (Pyrex No. 9825). Radiochemical purification utilized a reversed-phase semi-preparative HPLC column (HPLC: Thermo P2000, Column: Agilent Zorbax SB-C18, 5 µm, 9.4 X 250 mm, Product #: 880975-202, λ = 254 nm, ACN/$H_2O$). For quality control, the radiochemical purity was determined by analytical HPLC (HPLC: P4000, Column: Altima C18, 5 µm, 250 mm, Product #: 88056). C18 Sep-Pak cartridges were purchased from Waters Corporation (Milford, MA, USA). For the thin-layer chromatography (TLC) analyses, EM Science Silica Gel 60 F254 TLC plates were purchased from Fisher Scientific (Pittsburgh, PA, USA). Radio-TLC was accomplished using a Bioscan 200 imaging scanner (Bioscan, Inc., Washington, DC, USA). Radioactivity was counted with a Beckman Gamma 8000 counter containing a NaI crystal (Beckman Instruments, Inc., Irvine, CA, USA).

**(13S,17S)-3,17-Dimethoxy-13-methyl-7,8,9,11,12,13,14,15,16,17-decahydro-6H-cyclopenta-[a]phenanthrene (15):** To a solution of **14** (2.01 g, 7.38 mmol) in THF (100 mL) at 0 $^{o}$C was added NaH (1.35 g, 33.9 mmol, 60% dispersion in mineral oil) and left at this temperature for 15 minutes. MeI (4.59 mL, 73.8 mmol) was then added at 0 $^{o}$C and left to stir to room temperature overnight before being quenched with $H_2O$ (50 mL). The crude reaction was extracted with EtOAc (2 X 100 mL), and the combined organic extracts were dried over $MgSO_4$ and concentrated *in vacuo*. Purification by column chromatography (Hex:EtOAc, 10:1) afforded **15** (1.68 g, 75.7%) as a white solid; mp 154-155 $^{o}$C. $R_f$ = 0.85 (Hex:EtOAc, 5:1). $^{1}$H NMR (500 MHz, $CDCl_3$): $\delta$ 7.21 (d, *J* = 8.5 Hz, 1H), 6.72 (dd, *J* = 8.5, 2.7 Hz, 1H), 6.64 (d, *J* = 2.7 Hz, 1H), 3.79 (s, 3H), 3.39 (s, 3H), 3.32 (t, *J* = 8.3 Hz, 1H), 2.95-2.78 (m, 2H), 2.34-2.25 (m, 1H), 2.24-2.16 (m, 1H), 2.13-2.02 (m, 2H), 1.93-1.84 (m, 1H), 1.76-1.65 (m, 1H), 1.56-1.16 (m, 7H), 0.80 (s, 3H); $^{13}$C NMR (126 MHz, $CDCl_3$): $\delta$ 157.4, 138.0, 132.7, 126.3, 113.8, 111.4, 90.8, 57.9, 55.2, 50.3, 43.9, 43.2, 38.6, 38.1, 29.8, 27.8, 27.2, 26.4, 23.0, 11.5; HRMS (ESI) calc'd for $C_{20}H_{29}O_2$ [M + 1] 301.2168; found 301.2179.

**(13S,17S)-2-Bromo-3,17-dimethoxy-13-methyl-7,8,9,11,12,13,14,15,16,17-decahydro-6H-cyclopenta[a]phenanthrene (16):** To a solution of **15** (50.3 mg, 0.17 mmol) in DCM (1.5 mL) at room temperature was added NBS (32.5 mg, 0.18 mmol) in ACN (0.6 mL). The round bottom flask was wrapped in foil and left to stir at room temperature for 18 hours. The solvent was removed *in vacuo*, $CHCl_3$ was added and the suspension was filtered through a silica gel plug. The eluent was evaporated to afford a crude yellow oil. The oil was triturated with warm MeOH (30 mL) to yield an off-white solid; repeating the step with the crude solid with more MeOH (20 mL) yielded **16** (23.3 mg, 36.8%, 96:4) as an off-white solid; $R_f$ = 0.75 (Hex:EtOAc, 7:1). $^{1}$H NMR (500 MHz, $CDCl_3$): $\delta$ 7.44 (s, 1H), 6.62 (s, 1H), 3.86 (s, 3H), 3.39 (s, 3H), 3.32 (t, *J* = 8.4 Hz, 1H), 2.86-2.78 (m, 2H), 2.29-2.21 (m, 1H), 2.21-2.14 (m, 1H), 2.13-2.03 (m, 2H), 1.94-1.85 (m, 1H), 1.75-1.64 (m, 1H), 1.58-1.27 (m, 6H), 1.25-1.15 (m, 1H), 0.80 (s, 3H); $^{13}$C NMR (126 MHz, $CDCl_3$): $\delta$ 157.4, 138.0, 132.7, 126.3, 113.8, 111.4, 90.8, 57.9, 55.2, 50.3, 43.9, 43.2, 38.6, 38.1, 29.8, 27.8, 27.2, 26.4, 23.0, 11.5; HRMS (ESI) calc'd for $C_{20}H_{28}BrO_2$ [M + 1] 379.1273; found 379.1261.

**((13S,17S)-3,17-Dimethoxy-13-methyl-7,8,9,11,12,13,14,15,16,17-decahydro-6H-cyclo penta[a]phenanthren-2-yl)trimethylstannane (17):** To a solution of **16** (0.50 g, 1.32 mmol) and TMEDA (0.79 mL, 5.27 mmol) in $Et_2O$ (10 mL) at -78 $^{o}$C was added *n*BuLi (1.39 mL, 1.39

mmol, 1.6 M in hexanes) and left to stir at this temperature for 5 minutes. This solution was then cannulated into another flask containing $Me_3SnCl$ (1.32 mL, 1.32 mmol, 1.0 M in hexanes) and $Et_2O$ (10 mL), cooled to -78 $^oC$, and the resulting mixture was left to stir to room temperature over 2 hours. The solution was then passed through a silica gel plug (Hex:EtOAc, 1:1) and concentrated *in vacuo*. The crude product was used as is in the next step as this intermediate was prone to protio-destannylation during column chromatography and on the bench. $^1H$ NMR (500 MHz, $CDCl_3$): $\delta$ 7.30 (s, 1H), 6.56 (s, 1H), 3.76 (s, 3H), 3.39 (s, 3H), 3.33 (t, *J* = 8.3 Hz, 1H), 2.98-2.79 (m, 2H), 2.40-2.31 (m, 1H), 2.27-2.17 (m, 1H), 2.13-2.01 (m, 2H), 1.94-1.82 (m, 1H), 1.76-1.64 (m, 1H), 1.59-1.17 (m, 7H), 0.80 (s, 3H), 0.25 (s, 9H).

**General procedure for the formation of the diaryliodonium salts (20, 21):** To a partially dissolved solution of **18** (0.11 g, 0.32 mmol, 4-methoxyphenyl) in ACN (2 mL) was added TsOH (0.62 mg, 0.32 mmol) in ACN (2 mL) and the resulting solution was added to a flask containing **17** (0.15 g, 0.32 mmol) in THF (2 mL). The light yellow mixture was left stirring for 18 hours at room temperature in foil. The solution was evaporated to dryness to afford an oily product. The crude product was redissolved in EtOAc (1.5 mL) and MeOH (dropwise added until product dissolves fully) and the product was precipitated with hexanes (~3.0 mL). The mixture was left in a freezer for 3 hours until the mother liquor turned clear. The liquid was removed and the precipitation process was repeated once more to afford pure diaryliodonium salts. The procedure was repeated with the thiophene derivative the same way.

**20**: From **17** (0.15 g, 0.32 mmol), **20** (0.094 g, 40.9%) was obtained as an off-white solid. $^1H$ NMR (500 MHz, $CD_3CN$): $\delta$ 7.93 (d, *J* = 9.3 Hz, 2H), 7.83 (s, 1H), 7.53 (d, *J* = 8.3 Hz, 2H), 7.17 (d, *J* = 8.3 Hz, 2H), 6.98 (d, *J* = 9.0 Hz, 2H), 6.90 (s, 1H), 3.88 (s, 3H), 3.82 (s, 3H), 3.30 (s, 3H), 2.90 (dd, *J* = 8.5, 4.2 Hz, 2H), 2.42-2.33 (m, 4H), 2.26-2.18 (m, 1H), 2.11-1.95 (m, 2H), 1.91-1.81 (m, 1H), 1.72-1.62 (m, 1H), 1.52-1.13 (m, 8H), 0.74 (s, 3H); HRMS (ESI) calc'd for $C_{27}H_{34}IO_3$ 533.1553; found 533.1545.

**21**: From **17** (0.101 g, 0.22 mmol), **21** (0.123 g, 82.6%) was obtained as a light brown solid. $^1H$ NMR (500 MHz, $CD_3CN$): $\delta$ 7.89 (s, 1H), 7.84 (dd, *J* = 3.9, 1.2 Hz, 1H), 7.78 (dd, *J* = 5.4, 1.2 Hz, 1H), 7.51 (d, *J* = 8.3 Hz, 1H), 7.17 (d, *J* = 8.1 Hz, 1H), 7.10 (dd, *J* = 5.4, 3.9 Hz, 1H), 6.91 (s, 1H), 3.92 (s, 3H), 3.30 (s, 3H), 2.97-2.83 (m, 2H), 2.34 (s, 3H), 2.28-2.15 (m, 2H), 2.12-1.95

(m, 2H), 1.91-1.79 (m, 2H), 1.76-1.58 (m, 2H), 1.54-1.07 (m, 8H), 0.73 (s, 3H); HRMS (ESI) calc'd for $C_{24}H_{30}IO_2S$ 509.1011; found 509.1009.

**General procedure for anion exchange (22-27):** Salts (**20**, **21**) were dissolved in ACN (2 mL) and heated to 60 $^oC$. If the solid does not dissolve, a few drops of water were added until a clear solution forms. An aqueous solution of KBr ((or KI or $NaPF_6$) 120 mg in 1 mL $H_2O$) was added and left to cool in the dark to room temperature. The mother liquor was removed to afford a white solid. Impure salts were further recrystallized from EtOAc:MeOH:Hex as discussed previously.

**22**: From **17** (0.142 g, 0.31 mmol), **22** (0.072 g, 34.3%) was obtained as a light brown solid. $^1H$ NMR (500 MHz, $CD_3CN$): $\delta$ 7.93 (d, *J* = 9.0 Hz, 2H), 7.83 (s, 1H), 6.98 (d, *J* = 9.0 Hz, 2H), 6.89 (s, 1H), 3.88 (s, 3H), 3.81 (s, 3H), 3.30 (s, 3H), 2.90 (dd, *J* = 8.5, 4.0 Hz, 2H), 2.26-2.18 (m, 1H), 2.18-2.11 (m, 1H), 2.10-1.99 (m, 2H), 1.89-1.81 (m, 1H), 1.73-1.60 (m, 1H), 1.52-1.12 (m, 7H), 0.74 (s, 3H); HRMS (ESI) calc'd for $C_{27}H_{34}IO_3$ 533.1553; found 533.1543.

**23**: From **17** (0.150 g, 0.32 mmol), **23** (0.091 g, 43.3%) was obtained as a light brown solid. $^1H$ NMR (500 MHz, $CD_3CN$): $\delta$ 7.90 (s, 1H), 7.83 (dd, *J* = 3.8, 1.2 Hz, 1H), 7.77 (dd, *J* = 5.4, 1.3 Hz, 1H), 7.10 (dd, *J* = 4.9, 3.2 Hz, 1H), 6.90 (s, 1H), 3.92 (s, 3H), 3.30 (s, 3H), 2.90 (dd, *J* = 8.5, 4.0 Hz, 2H), 2.24-2.17 (m, 2H), 2.11-2.00 (m, 2H), 1.90-1.81 (m, 1H), 1.74-1.60 (m, 1H), 1.52-1.13 (m, 8H), 0.73 (s, 3H); HRMS (ESI) calc'd for $C_{24}H_{30}IO_2S$ 509.1011; found 509.1015.

**24**: From **17** (0.101 g, 0.22 mmol), **24** (0.054 g, 37.8%) was obtained as a off-white solid. $^1H$ NMR (500 MHz, DMSO-$d_6$): $\delta$ 8.10 (s, 1H), 8.01 (d, *J* = 9.0 Hz, 2H), 7.03 (d, *J* = 8.3 Hz, 2H), 6.96 (s, 1H), 3.87 (s, 3H), 3.78 (s, 3H), 3.26 (s, 3H), 2.91-2.82 (m, 2H), 2.41-2.32 (m, 1H), 2.23-2.09 (m, 1H), 2.05-1.91 (m, 2H), 1.85-1.75 (m, 1H), 1.68-1.56 (m, 1H), 1.48-1.12 (m, 8H), 0.70 (s, 3H); HRMS (ESI) calc'd for $C_{27}H_{34}IO_3$ 533.1553; found 533.1548.

**25**: From **17** (0.107 g, 0.22 mmol), **25** (0.041 g, 21.8%) was obtained as a light brown solid. $^1H$ NMR (500 MHz, DMSO-$d_6$): $\delta$ 8.12 (s, 1H), 8.03 (dd, *J* = 3.9, 1.3 Hz, 1H), 7.96 (dd, *J* = 5.4, 1.3 Hz, 1H), 7.31 (dd, *J* = 4.6, 3.4 Hz, 1H), 6.98 (s, 1H), 3.87 (s, 3H), 3.26 (s, 3H), 2.91-2.84 (m, 2H), 2.40-2.32 (m, 1H), 2.23-2.10 (m, 1H), 2.04-1.89 (m, 2H), 1.86-1.76 (m, 1H), 1.68-1.54 (m,

1H), 1.45-1.14 (m, 8H), 0.70 (s, 3H); HRMS (ESI) calc'd for $C_{24}H_{30}IO_2S$ 509.1011; found 509.1013.

**26**: From **17** (0.114 g, 0.25 mmol), **26** (0.087 g, 58.0%) was obtained as an off-white solid. $^1$H NMR (500 MHz, DMSO-$d_6$): $\delta$ 8.11 (s, 1H), 8.01 (d, *J* = 9.0 Hz, 2H), 7.03 (d, *J* = 9.3 Hz, 2H), 6.97 (s, 1H), 3.88 (s, 3H), 3.78 (s, 3H), 3.27 (s, 3H), 2.93-2.82 (m, 2H), 2.43-2.33 (m, 1H), 2.24-2.10 (m, 1H), 2.08-1.91 (m, 2H), 1.86-1.75 (m, 1H), 1.71-1.61 (m, 1H), 1.50-1.10 (m, 8H), 0.71 (s, 3H); HRMS (ESI) calc'd for $C_{27}H_{34}IO_3$ 533.1553; found 533.1544.

**27**: From **17** (0.114 g, 0.25 mmol), **27** (0.067 g, 46.7%) was obtained as a brown solid. $^1$H NMR (500 MHz, DMSO-$d_6$): $\delta$ 8.10 (s, 1H), 8.01 (dd, *J* = 3.9, 1.3 Hz, 1H), 7.95 (dd, *J* = 5.4, 1.3 Hz, 1H), 7.31 (dd, *J* = 4.6, 3.4 Hz, 1H), 6.99 (s, 1H), 3.87 (s, 3H), 3.26 (s, 3H), 2.91-2.84 (m, 2H), 2.40-2.32 (m, 1H), 2.23-2.10 (m, 1H), 2.03-1.89 (m, 2H), 1.86-1.75 (m, 1H), 1.69-1.54 (m, 1H), 1.47-1.13 (m, 8H), 0.70 (s, 3H); HRMS (ESI) calc'd for $C_{24}H_{30}IO_2S$ 509.1011; found 509.1014.

**General procedure for the investigations of fluoride sources on the different diaryliodonium salts.** To a heterogenous solution of salts (**22** or **26**, 1 mg) in PhH (0.3 mL) was added the fluoride source (1 equiv., $K_{222}$ = 3 equiv.) and then sealed and heated at 140 $^o$C for 20 minutes. After the allotted time, the vial was cooled to room temperature, passed through a silica gel plug and the combined organic solvents were concentrated *in vacuo*. Product ratios of **29**:**31** were analyzed through integrations of the A-ring aromatic peaks in the $^1$H NMR spectrum.

**General procedure for the investigations on the counterion effect on the different diaryliodonium salts.** To a heterogenous solution of salts (**20**-**27**, 1 mg) in PhH (0.3 mL) was added TBAF·3$H_2O$ (1 equiv.) and then sealed and heated at 140 $^o$C for 20 minutes. After the allotted time, the vial was cooled to room temperature, passed through a silica gel plug and the combined organic solvents were concentrated *in vacuo*. Product ratios of **29**:**31** were analyzed through integrations of the A-ring aromatic peaks in the $^1$H NMR spectrum.

**(Diacetoxy)-2-thiophene (18):** 4-Iodothiophene (1.1 mL, 10 mmol) was dissolved in AcOH (90 mL) and heated to 40 $^o$C. $NaBO_3$·4$H_2O$ was added portion wise over 1 hour and left to stir at this temperature for an additional 8 h. After the allotted time, the heterogeneous mixture was evaporated to approximately half the volume of the original AcOH and then the product was

extracted with DCM (2 X 100 mL) after adding $H_2O$ (50 mL). The combined organic extracts were dried over $MgSO_4$ and concentrated *in vacuo* to afford pure **18** (1.25 g, 38.1%) as a light yellow solid. $^1$H NMR (500 MHz, $CD_3CN$): $\delta$ 7.86 (dd, *J* = 3.9, 1.3 Hz, 1H), 7.79 (dd, *J* = 5.4, 1.3 Hz, 1H), 7.18 (dd, *J* = 5.5, 3.8 Hz, 1H), 1.93 (s, 6H); $^{13}$C NMR (126 MHz, $CD_3CN$): $\delta$ 219.8, 136.9, 130.7, 129.9, 120.9, 20.5.

**(Diacetoxy)-4-methoxybenzene (18):** 4-Iodoanisole (2.34 g, 9.99 mmol) was dissolved in AcOH (90 mL) and heated to 40 $^o$C. $NaBO_3{\cdot}4H_2O$ was added portion wise over 1 hour and left to stir at this temperature for an additional 8 h. After the allotted time, the heterogeneous mixture was evaporated to approximately half the volume of the original AcOH and then the product was extracted with DCM (2 X 100 mL) after adding $H_2O$ (50 mL). The combined organic extracts were dried over $MgSO_4$ and concentrated *in vacuo* to afford pure **18** (2.27 g, 64.5%) as a light yellow solid. $^1$H NMR (500 MHz, $CD_3CN$): $\delta$ 8.05 (d, *J* = 9.2 Hz, 2H), 7.06 (d, *J* = 9.2 Hz, 2H), 3.87 (s, 3H), 1.91 (s, 6H); $^{13}$C NMR (126 MHz, $CD_3CN$): $\delta$ 203.9, 139.4, 138.5, 130.7, 120.9, 56.6, 20.5.

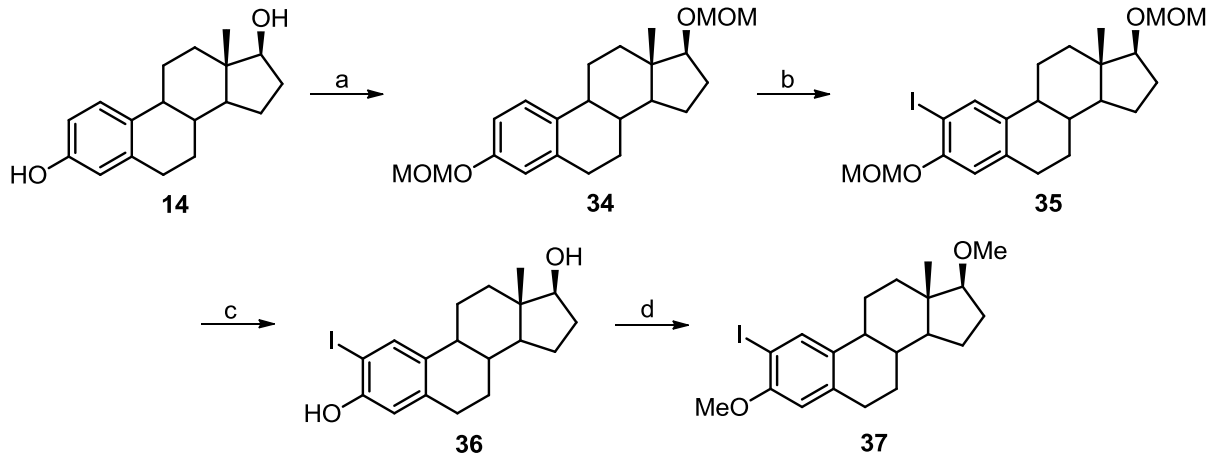


**Scheme 4.10.** Synthesis of the iodine standard for $^1$H NMR analysis. (a) MOMCl, Hunig's Base, THF, reflux, 16 h; (b) (i) *sec*-BuLi, THF, 30 min (ii) $I_2$, $Et_2O$, -78 $^o$C→rt, overnight; (c) HCl, THF, reflux, 12 h; (d) (i) NaH, DMF, 0 $^o$C, 10 min (ii) MeI, 0 $^o$C→rt, 5 h.

**(13S,17S)-3,17-Bis(methoxymethoxy)-13-methyl-7,8,9,11,12,13,14,15,16,17-decahydro-6H-cyclopenta[a]phenanthrene (34):** To a solution of 17β-estradiol (**14**, 2.01 g, 7.38 mmol) in THF (15 mL) was added Hunig's base (6.5 mL) and MOMCl (2.8 mL, 36.9 mmol) and left at reflux for 16 h before being quenched with $H_2O$ (50 mL) at room temperature. The crude reaction was extracted with EtOAc (2 X 100 mL), and the combined organic extracts were dried

over $MgSO_4$ and concentrated *in vacuo*. Purification by column chromatography (Hex:EtOAc, 4:1) afforded **34** (2.49 g, 93.6%) as a clear oil; $R_f$ = 0.95 (Hex:EtOAc, 2:1). $^1$H NMR (500 MHz, $CDCl_3$): $\delta$ 7.21 (d, *J* = 8.3 Hz, 1H), 6.84 (dd, *J* = 8.5, 2.9 Hz, 1H), 6.78 (d, *J* = 2.7 Hz, 1H), 5.15 (s, 2H), 4.71-4.64 (m, 2H), 3.63 (t, *J* = 8.4 Hz, 1H), 3.48 (s, 3H), 3.39 (s, 3H), 2.91-2.80 (m, 2H), 2.34-2.26 (m, 1H), 2.24-2.16 (m, 1H), 2.14-1.97 (m, 2H), 1.92-1.84 (m, 1H), 1.76-1.66 (m, 1H), 1.64-1.16 (m, 7H), 0.82 (s, 3H).

**(13S,17S)-2-Iodo-3,17-bis(methoxymethoxy)-13-methyl-7,8,9,11,12,13,14,15,16,17-decahydro-6H-cyclopenta[a]phenanthrene (35):** To a solution of **34** (1.01 g, 2.80 mmol) in THF (25 mL) at -78 $^o$C was added *sec*-BuLi (8 mL, 11.2 mmol, 1.4 M in cyclohexane) and left to stir for 30 min. This solution was cannulated into a solution of iodine (3.56 g, 14.01 mmol) in $Et_2O$ (25 mL) at -78 $^o$C and left to stir at room temperature overnight before being quenched with $H_2O$ (50 mL). The crude reaction was extracted with EtOAc (2 X 100 mL), and the combined organic extracts were dried over $MgSO_4$ and concentrated *in vacuo*. Purification by column chromatography (Hex:EtOAc, 6:1) afforded **35** (0.77 g, 56.3%) as a white solid; $R_f$ = 0.70 (Hex:EtOAc, 5:1). $^1$H NMR (500 MHz, $CDCl_3$): $\delta$ 7.66 (s, 1H), 6.79 (s, 1H), 5.20 (s, 2H), 4.71-4.56 (m, 2H), 3.62 (t, *J* = 8.4 Hz, 1H), 3.52 (s, 3H), 3.38 (s, 3H), 2.86-2.77 (m, 2H), 2.30-1.83 (m, 5H), 1.76-1.12 (m, 8H), 0.81 (s, 3H).

**(13S,17S)-2-Iodo-13-methyl-7,8,9,11,12,13,14,15,16,17-decahydro-6H cyclopenta[a]phenanthrene-3,17-diol (36):** To a solution of **35** (1.42 g, 2.92 mmol) in THF (30 mL) was added 12 M HCl (7 mL) and left to reflux for 12 h. The solution was cooled to room temperature and the crude reaction was extracted with EtOAc (2 X 100 mL), with the combined organic extracts were dried over $MgSO_4$ and concentrated *in vacuo*. Purification by column chromatography (Hex:EtOAc, 2:1) afforded **36** (1.07 g, 92.1%) as a white solid; $R_f$ = 0.19 (Hex:EtOAc, 4:1). $^1$H NMR (500 MHz, $CDCl_3$): $\delta$ 7.53 (s, 1H), 6.73 (s, 1H), 2.80 (dd, *J* = 8.9, 4.0 Hz, 2H), 2.30-2.08 (m, 2H), 2.00-1.83 (m, 3H), 1.75-1.65 (m, 1H), 1.56-1.13 (m, 7H), 0.79 (s, 3H).

**(13S,17S)-2-Iodo-3,17-dimethoxy-13-methyl-7,8,9,11,12,13,14,15,16,17-decahydro-6H-cyclopenta[a]phenanthrene (37):** To a solution of **36** (0.938 g, 2.36 mmol) in DMF (14 mL) at 0 $^o$C was NaH (0.44 g, 10.9 mmol, 60% oil dispersion) and left to stir at this temperature for 10 min. To this solution, MeI (1.47 mL, 23.6 mmol) was added and left to stir to room temperature for 5 h before being quenched with $H_2O$ (20 mL). The crude reaction was extracted with EtOAc

(2 X 100 mL), and the combined organic extracts were dried over $MgSO_4$ and concentrated *in vacuo*. Purification by column chromatography (Hex:EtOAc, 6:1) afforded **37** (2.49 g, 93.6%) as an off-white solid; $R_f$ = 0.87 (Hex:EtOAc, 4:1). $^1$H NMR (500 MHz, $CDCl_3$): $\delta$ 7.65 (s, 1H), 6.55 (s, 1H), 3.84 (s, 3H), 3.39 (s, 3H), 2.88-2.79 (m, 2H), 2.33-2.01 (m, 2H), 1.93-1.84 (m, 2H), 1.75-1.64 (m, 1H), 1.56-1.14 (m, 7H), 0.79 (s, 3H). $^{13}$C NMR (126 MHz, $CDCl_3$): $\delta$ 155.9, 138.4, 136.4, 135.0, 111.4, 90.4, 90.7, 57.9, 56.3, 50.2, 43.6, 43.2, 38.3, 37.9, 29.7, 27.7, 27.0, 26.4, 23.0, 11.5; HRMS (EI) calc'd for $C_{20}H_{27}IO_2$ 426.10561; found 426.10638.

**General procedure for the drying step:** To a glass vial was added the carbonate or bicarbonate of the respective alkali or tetralkylammonium salt (0.1-1 mg, $K_{222}$ = 1-5 mg) in water (25-200 µL). The vial was placed in an oil bath at 105 $^o$C and the water was removed by azeotropic distillation with ACN (1 mL) using a stream of nitrogen. This was repeated twice more with 1 mL increments of ACN until the [$^{18}$F]fluoride source was deemed dry. The corresponding diaryliodonium salt and PhH (0.3-0.5 mL) were added and then heated for the desired time period. The course of the reaction and yields were monitored by radio-TLC and -HPLC.

**Radio-TLC of the radiofluorination of 26 with [$^{18}$F]fluoride ion and Cs$^{18}$F (from $Cs_2CO_3$) after 20 minutes at 105 $^o$C (oil bath):**

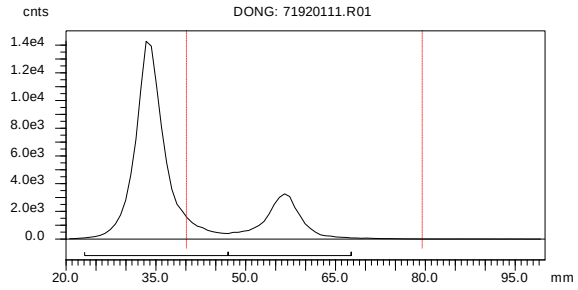


**TLC Eluting Conditions:** 100% EtOAc

**Region 1 (unreacted [$^{18}$F]fluoride; 35 mm):** 78.47%

**Region 2 ([$^{18}$F]fluoroproduct; 55 mm):** 21.53%

*Product did not co-elute with cold standard.

**Radio-TLC of the radiofluorination of 26 with [$^{18}$F]fluoride ion and Cs$^{18}$F (from $Cs_2CO_3$) after 5 minutes in the microwave:**

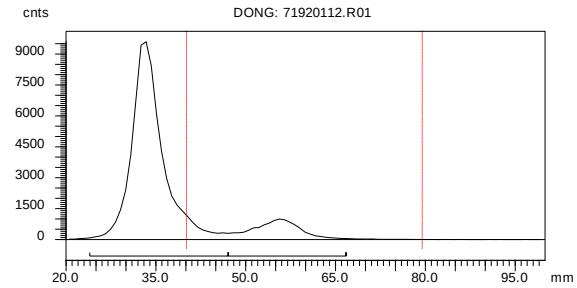


**TLC Eluting Conditions:** 100% EtOAc

**Region 1 (unreacted [$^{18}$F]fluoride; 35 mm):** 86.28%

**Region 2 ([$^{18}$F]fluoroproduct; 55 mm):** 13.72%

**Radio-TLC of the radiofluorination of 26 with [$^{18}$F]fluoride ion and Cs$^{18}$F (from $CsHCO_3$) after 20 minutes at 105 $^{o}$C (oil bath):**

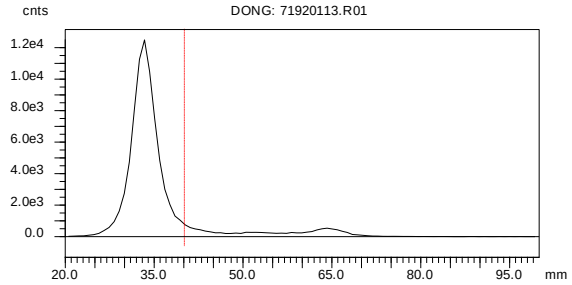


**TLC Eluting Conditions:** 100% EtOAc

**Region 1 (unreacted [$^{18}$F]fluoride; 35 mm):** 96.70%

**Region 2 ([$^{18}$F]fluoroproduct; 65 mm):** 3.30%

**Radio-TLC of the radiofluorination of 26 with [$^{18}$F]fluoride ion and Cs$^{18}$F (from $CsHCO_3$) after 5 minutes in the microwave:**

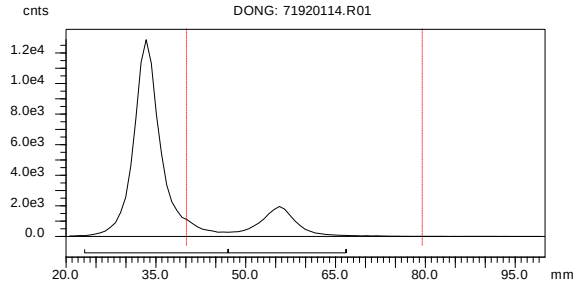


**TLC Eluting Conditions:** 100% EtOAc

**Region 1 (unreacted [$^{18}$F]fluoride; 35 mm):** 83.23%

**Region 2 ([$^{18}$F]fluoroproduct; 55 mm):** 16.77%

**Radio-TLC of the radiofluorination of 26 with [$^{18}$F]fluoride ion and K$^{18}$F (from $K_2CO_3$ and $K_{222}$) after 20 minutes at 105 $^{o}$C (oil bath):**

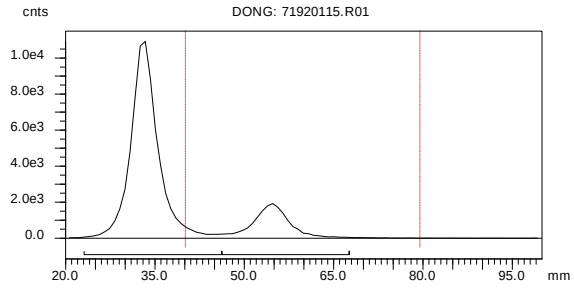


**TLC Eluting Conditions:** 100% EtOAc

**Region 1 (unreacted [$^{18}$F]fluoride; 35 mm):** 81.32%

**Region 2 ([$^{18}$F]fluoroproduct; 55 mm):** 18.68%

**Radio-TLC of the radiofluorination of 26 with [$^{18}$F]fluoride ion and K$^{18}$F (from $K_2CO_3$ and $K_{222}$) after 5 minutes in the microwave:**

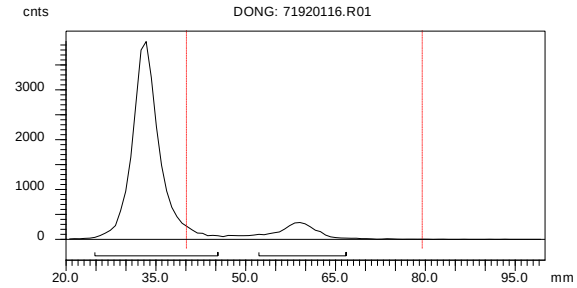


**TLC Eluting Conditions:** 100% EtOAc

**Region 1 (unreacted [$^{18}$F]fluoride; 35 mm):** 89.68%

**Region 2 ([$^{18}$F]fluoroproduct; 60 mm):** 10.32%

**Radio-TLC of the radiofluorination of 26 with [$^{18}$F]fluoride ion and K$^{18}$F (from $KHCO_3$ and $K_{222}$) after 20 minutes at 105 $^{o}$C (oil bath):**

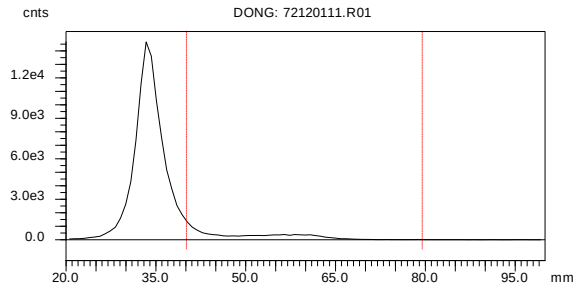


**TLC Eluting Conditions:** 100% EtOAc

**Region 1 (unreacted [$^{18}$F]fluoride; 35 mm):** 100%

**Region 2 ([$^{18}$F]fluoroproduct; 55 mm):** 0%

**Radio-TLC of the radiofluorination of 26 with [$^{18}$F]fluoride ion and K$^{18}$F (from $K_2CO_3$ and $K_{222}$) after 5 minutes in the microwave:**

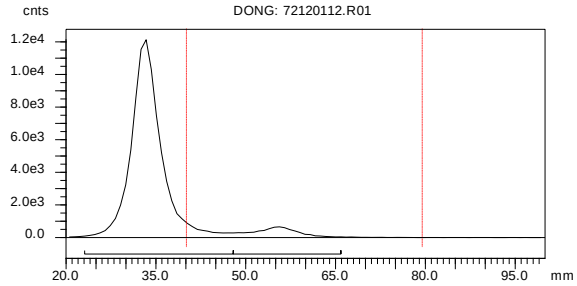


**TLC Eluting Conditions:** 100% EtOAc

**Region 1 (unreacted [$^{18}$F]fluoride; 35 mm):** 92.37%

**Region 2 ([$^{18}$F]fluoroproduct; 55 mm):** 7.63%

**Radio-TLC of the radiofluorination of 26 with [$^{18}$F]fluoride ion and K$^{18}$F (from $K_2CO_3$ and $K_{222}$) and TEMPO (95 µg) after 20 minutes at 105 $^{o}$C (oil bath):**

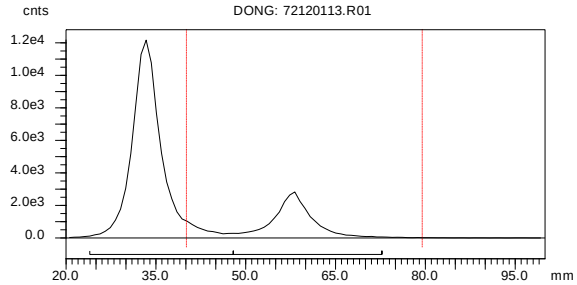


**TLC Eluting Conditions:** 100% EtOAc

**Region 1 (unreacted [$^{18}$F]fluoride; 35 mm):** 77.45%

**Region 2 ([$^{18}$F]fluoroproduct; 55 mm):** 22.55%

**Deprotection to 2-[$^{18}$F]fluoroestradiol (2):** After cooling to room temperature, the solution was passed through a silica gel plug and the solvent was blown down to dryness. The crude product was dissolved in dodecanethiol (0.2 mL) and $AlBr_3$ (10 mg) was added and left to stand at room temperature for 5 minutes. The reaction was quenched with 5% HCl and MeOH until the bubbling ceased and then passed through another silica gel plug.

**UV trace with injected cold standard (Product: 4.11 min):**

**Conditions:** 80% ACN 20% $H_2O$ 1.5 mL/min, λ = 254 nM

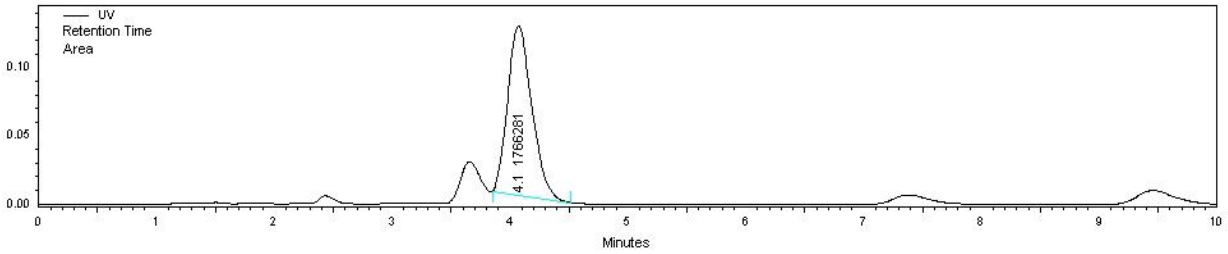


**Radioactivity trace (Product: 4.21 min):**

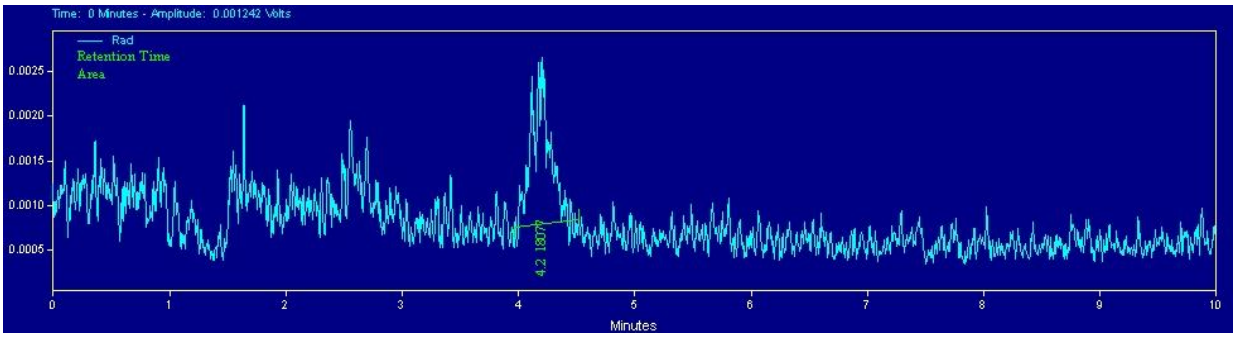


## V. REFERENCES


(1) Cassidy, P. J.; Radda, G. K. Molecular imaging perspectives. *J. R. Soc. Interface* **2005**, *2*, 133.

(2) James, M. L.; Gambhir, S. S. A molecular imaging primer: modalities, imaging agents, and applications. *Physiol. Rev.* **2012**, *92*, 897.

(3) Polyak, K. Heterogeneity in breast cancer. *J. Clin. Invest.* **2011**, *121*, 3786.

(4) Li, J.; Wang, K.; Jensen, T. D.; Li, S.; Bolund, L.; Wiuf, C. Tumor heterogeneity in neoplasms of breast, colon, and skin. *BMC Res. Notes* **2010**, *3*, 321.

(5) Regev, A.; Berho, M.; Jeffers, L. J.; Milikowski, C.; Molina, E. G.; Pyrsopoulos, N. T.; Feng, Z.-Z.; Reddy, K. R.; Schiff, E. R. Sampling error and intraobserver variation in liver biopsy in patients with chronic HCV infection. *Am. J. Gastroenterol.* **2002**, *97*, 2614.

(6) Chandran, U. R.; Ma, C.; Dhir, R.; Bisceglia, M.; Lyons-Weiler, M.; Liang, W.; Michalopoulos, G.; Becich, M.; Monzon, F. A. Gene expression profiles of prostate cancer reveal involvement of multiple molecular pathways in the metastatic process. *BMC Cancer* **2007**, *7*.

(7) Weigelt, B.; Peterse, J. L.; van't, V. L. J. Breast cancer metastasis: markers and models. *Nat. Rev. Cancer* **2005**, *5*, 591.

(8) Dehdashti, F.; Mortimer, J. E.; Siegel, B. A.; Griffeth, L. K.; Bonasera, T. J.; Fusselman, M. J.; Detert, D. D.; Cutler, P. D.; Katzenellenbogen, J. A.; Welch, M. J. Positron tomographic assessment of estrogen receptors in breast cancer: comparison with FDG-PET and in vitro receptor assays. *J. Nucl. Med.* **1995**, *36*, 1766.

(9) Dehdashti, F.; Flanagan, F. L.; Mortimer, J. E.; Katzenellenbogen, J. A.; Welch, M. J.; Siegel, B. A. Positron emission tomographic assessment of "metabolic flare" to predict response of metastatic breast cancer to antiestrogen therapy. *Eur. J. Nucl. Med.* **1999**, *26*, 51.

(10) Dehdashti, F.; Mortimer, J. E.; Trinkaus, K.; Naughton, M. J.; Ellis, M.; Katzenellenbogen, J. A.; Welch, M. J.; Siegel, B. A. PET-based estradiol challenge as a predictive biomarker of response to endocrine therapy in women with estrogen-receptor-positive breast cancer. *Breast Cancer Res. Treat.* **2009**, *113*, 509.

(11) Mortimer, J. E.; Dehdashti, F.; Siegel, B. A.; Trinkaus, K.; Katzenellenbogen, J. A.; Welch, M. J. Metabolic flare: indicator of hormone responsiveness in advanced breast cancer. *J. Clin. Oncol.* **2001**, *19*, 2797.

(12) Mortimer, J. E.; Dehdashti, F.; Siegel, B. A.; Katzenellenbogen, J. A.; Fracasso, P.; Welch, M. J. Positron emission tomography with 2-[$^{18}$F]fluoro-2-deoxy-D-glucose and 16α-[$^{18}$F]fluoro-17β-estradiol in breast cancer: Correlation with estrogen receptor status and response to systemic therapy. *Clin. Cancer Res.* **1996**, *2*, 933.

(13) McGuire, A. H.; Dehdashti, F.; Siegel, B. A.; Lyss, A. P.; Brodack, J. W.; Mathias, C. J.; Mintun, M. A.; Katzenellenbogen, J. A.; Welch, M. J. Positron tomographic assessment of 16 alpha-[$^{18}$F] fluoro-17 beta-estradiol uptake in metastatic breast carcinoma. *J. Nucl. Med.* **1991**, *32*, 1526.

(14) Pomper, M. G.; VanBrocklin, H.; Thieme, A. M.; Thomas, R. D.; Kiesewetter, D. O.; Carlson, K. E.; Mathias, C. J.; Welch, M. J.; Katzenellenbogen, J. A. 11β-Methoxy-, 11β-ethyl, and 17α-ethynyl-substituted 16α-fluoroestradiols: receptor-based imaging agents with enhanced uptake efficiency and selectivity. *J. Med. Chem.* **1990**, *33*, 3143.

(15) Fortunati, N. Sex Hormone-Binding Globulin: not only a transport protein. What news is around the corner? *J. Endocrinol. Invest.* **1999**, *22*, 223.

(16) Fortunati, N.; Fissore, F.; Fazzari, A.; Berta, L.; Benedusi-Pagliano, E.; Frairia, R. Biological relevance of the interaction between sex steroid binding protein and its specific receptor of MCF-7 cells: Effect on the estradiol-induced cell proliferation. *J. Steroid Biochem. Mol. Biol.* **1993**, *45*, 435.

(17) Fortunati, N.; Becchis, M.; Catalano, M. G.; Comba, A.; Ferrera, P.; Raineri, M.; Berta, L.; Frairia, R. Sex Hormone-Binding Globulin, its membrane receptor, and breast cancer: a new approach to the modulation of estradiol action in neoplastic cells. *J. Steroid Biochem. Mol. Biol.* **1999**, *69*, 473.

(18) Vanbrocklin, H. F.; Pomper, M. G.; Carlson, K. E.; Welch, M. J.; Katzenellenbogen, J. A. Preparation and evaluation of 17-ethynyl-substituted 16α-[$^{18}$F]fluoroestradiols: selective receptor-based PET imaging agents. *Nucl. Med. Biol.* **1992**, *19*, 363.

(19) Parent, E. E.; Dence, C. S.; Sharp, T. L.; Welch, M. J.; Katzenellenbogen, J. A. 7α-$^{18}$F-fluoromethyl-dihydrotestosterone and 7α-$^{18}$F-fluoromethyl-nortestosterone: ligands to

determine the role of sex hormone-binding globulin for steroidal radiopharmaceuticals. *J. Nucl. Med.* **2008**, *49*, 987.

(20) Katzenellenbogen, J. A.; Heiman, D. F.; Carlson, K. E.; Lloyd, J. E.; CRC: 1982; Vol. 1, p 93.

(21) Hobbs, C. J.; Jones, R. T.; Plymate, S. R. The effects of sex hormone binding globulin (SHBG) on testosterone transport into the cerebrospinal fluid. *J. Steroid Biochem. Mol. Biol.* **1992**, *42*, 629.

(22) Noe, G.; Cheng, Y. C.; Dabike, M.; Croxatto, H. B. Tissue uptake of human sex hormone-binding globulin and its influence on ligand kinetics in the adult female rat. *Biol. Reprod.* **1992**, *47*, 970.

(23) Tait, J. F.; Tait, S. A. S. The effect of plasma protein binding on the metabolism of steroid hormones. *J. Endocrinol.* **1991**, *131*, 339.

(24) Purser, S.; Moore, P. R.; Swallow, S.; Gouverneur, V. Fluorine in medicinal chemistry. *Chem. Soc. Rev.* **2008**, *37*, 320.

(25) Ismail, F. M. D. Important fluorinated drugs in experimental and clinical use. *J. Fluorine Chem.* **2002**, *118*, 27.

(26) Hostetler, E. D.; Jonson, S. D.; Welch, M. J.; Katzenellenbogen, J. A. Synthesis of 2-[$^{18}$F]Fluoroestradiol, a Potential Diagnostic Imaging Agent for Breast Cancer: Strategies to Achieve Nucleophilic Substitution of an Electron-Rich Aromatic Ring with [$^{18}$F]F. *J. Org. Chem.* **1999**, *64*, 178.

(27) Lal, G. S.; Pez, G. P.; Syvret, R. G. Electrophilic NF Fluorinating Agents. *Chem. Rev. (Washington, D. C.)* **1996**, *96*, 1737.

(28) Rosenfeld, M. N.; Widdowson, D. A. A mild and efficient method of aromatic fluorination. *J. Chem. Soc., Chem. Commun.* **1979**, 914.

(29) Tewson, T. J.; Welch, M. J. Preparation of fluorine-18 aryl fluorides: piperidyl triazenes as a source of diazonium salts. *J. Chem. Soc., Chem. Commun.* **1979**, 1149.

(30) Merritt, E. A.; Olofsson, B. Diaryliodonium Salts: A Journey from Obscurity to Fame. *Angew. Chem., Int. Ed.* **2009**, *48*, 9052.

(31) Pike, V. W.; Aigbirhio, F. I. Reactions of cyclotron-produced [$^{18}$F]fluoride with diaryliodonium salts - a novel single-step route to no-carrier-added [$^{18}$F]fluoroarenes. *J. Chem. Soc., Chem. Commun.* **1995**, 2215.

(32) Cai, L.; Lu, S.; Pike, V. W. Chemistry with [$^{18}$F]fluoride ion. *Eur. J. Org. Chem.* **2008**, 2853.

(33) Ross, T. L.; Ermert, J.; Hocke, C.; Coenen, H. H. Nucleophilic $^{18}$F-Fluorination of Heteroaromatic Iodonium Salts with No-Carrier-Added [$^{18}$F]Fluoride. *J. Am. Chem. Soc.* **2007**, *129*, 8018.

(34) Moon, B. S.; Kil, H. S.; Park, J. H.; Kim, J. S.; Park, J.; Chi, D. Y.; Lee, B. C.; Kim, S. E. Facile aromatic radiofluorination of [$^{18}$F]flumazenil from diaryliodonium salts with evaluation of their stability and selectivity. *Org. Biomol. Chem.* **2011**, *9*, 8346.

(35) Chun, J.-H.; Lu, S.; Lee, Y.-S.; Pike, V. W. Fast and High-Yield Microreactor Syntheses of ortho-Substituted [$^{18}$F]Fluoroarenes from Reactions of [$^{18}$F]Fluoride Ion with Diaryliodonium Salts. *J. Org. Chem.* **2010**, *75*, 3332.

(36) Grushin, V. V. Carboranylhalonium ions: from striking reactivity to a unified mechanistic analysis of polar reactions of diarylhalonium compounds. *Acc. Chem. Res.* **1992**, *25*, 529.

(37) Carroll, M. A.; Nairne, J.; Smith, G.; Widdowson, D. A. Radical scavengers: A practical solution to the reproducibility issue in the fluoridation of diaryliodonium salts. *J. Fluorine Chem.* **2007**, *128*, 127.

(38) Martin-Santamaria, S.; Carroll, M. A.; Pike, V. W.; Rzepa, H. S.; Widdowson, D. A. An ab initio and MNDO-d SCF-MO computational study of the extrusion reactions of R2I-F iodine(III) via dimeric, trimeric and tetrameric transition states. *J. Chem. Soc., Perkin Trans. 2* **2000**, 2158.

(39) Lee, B. C.; Lee, K. C.; Lee, H.; Mach, R. H.; Katzenellenbogen, J. A. Strategies for the Labeling of Halogen-Substituted Peroxisome Proliferator-Activated Receptor γ Ligands: Potential Positron Emission Tomography and Single Photon Emission Computed Tomography Imaging Agents. *Bioconjugate Chem.* **2007**, *18*, 514.

(40) Wang, B.; Qin, L.; Neumann, K. D.; Uppaluri, S.; Cerny, R. L.; DiMagno, S. G. Improved arene fluorination methodology for I(III) salts. *Org. Lett.* **2010**, *12*, 3352.

(41) Kryska, A.; Skulski, L. One-pot preparations of diaryliodonium bromides from iodoarenes and arenes, with sodium perborate as the oxidant. *Molecules* **2001**, *6*, 875.

(42) Ochiai, M.; Kida, M.; Sato, K.; Takino, T.; Goto, S.; Donkai, N.; Okuyama, T. Association and dissociation of (Z)-(β-bromoalkenyl)(phenyl)iodonium bromide in chloroform solution: detection of vinyl-λ3-iodane dimer in solution. *Tet. Lett.* **1999**, *40*, 1559.

(43) Boswell, C. A.; Sun, X.; Niu, W.; Weisman, G. R.; Wong, E. H.; Rheingold, A. L.; Anderson, C. J. Comparative in Vivo Stability of Copper-64-Labeled Cross-Bridged and Conventional Tetraazamacrocyclic Complexes. *J. Med. Chem.* **2004**, *47*, 1465.

(44) Chun, J.-H.; Lu, S.; Lee, Y.-S.; Pike, V. W. Fast and high-yield microreactor syntheses of ortho-substituted [$^{18}$F]fluoroarenes from reactions of [$^{18}$F]fluoride ion with diaryliodonium salts. *J. Org. Chem.* **2010**, *75*, 3332.

(45) Stang, P. J. Polyvalent Iodine in Organic Chemistry. *J. Org. Chem.* **2003**, *68*, 2997.

(46) Chun, J.-H.; Lu, S.; Pike, V. W. Rapid and Efficient Radiosyntheses of meta-Substituted [$^{18}$F]Fluoroarenes from [$^{18}$F]Fluoride Ion and Diaryliodonium Tosylates within a Microreactor. *Eur. J. Org. Chem.* **2011**, *2011*, 4439.